NASA CONTRACTOR REPORT

NASA CR-2567

NASA CR-25

TECH LIBRARY KAFB, NM

0061322

LOAN COPY: RETURN TO
AFWL TECHNICAL LIBRARY
KIRTLAND AFB, N. M.

AN INVESTIGATION OF TURBULENT TRANSPORT IN THE EXTREME LOWER ATMOSPHERE

Chester A. Koper, Jr., and Willy Z. Sadeh

Prepared by
COLORADO STATE UNIVERSITY FLUID DYNAMICS
Fort Collins, Colo. 80523 AND DIFFUSION LAB.
for George C. Marshall Space Flight Center

RECEIVED
18 SEP 975
Technical Library
AF Weapons
Laboratory

NATIONAL AERONAUTICS AND SPACE ADMINISTRATION • WASHINGTON, D. C. • AUGUST 1975

TECH LIBRARY KAFB, NM

0061322

TECHNICAL REPORT STANDARD TITLE PAGE

1. REPORT NO. NASA CR-2567	2. GOVERNMENT ACCESSION NO.	3. RECIPIENT'S CATALOG NO.
4. TITLE AND SUBTITLE An Investigation of Turbulent Transport in the Extreme Lower Atmosphere		5. REPORT DATE August 1975
		6. PERFORMING ORGANIZATION CODE M145
7. AUTHOR(S) Chester A. Koper, Jr. and Willy Z. Sadeh		8. PERFORMING ORGANIZATION REPORT # NAS-MSFC-2(CER74CAK-WZS34
9. PERFORMING ORGANIZATION NAME AND ADDRESS Fluid Dynamics and Diffusion Laboratory Colorado State University Fort Collins, Colorado 80523		10. WORK UNIT NO.
		11. CONTRACT OR GRANT NO. NAS8-28590
12. SPONSORING AGENCY NAME AND ADDRESS National Aeronautics and Space Administration Washington, D. C. 20546		13. TYPE OF REPORT & PERIOD COVERED Contractor
		14. SPONSORING AGENCY CODE

15. SUPPLEMENTARY NOTES Prepared under the sponsorship of the Aerospace Environment Division, Space Sciences Laboratory, Marshall Space Flight Center, Alabama 35812. Contract Monitor: R. E. Turner.

16. ABSTRACT

A model in which the Lagrangian autocorrelation is expressed by a domain integral over a set of usual Eulerian autocorrelations acquired concurrently at all points within a turbulence "box" was put forth. A method for ascertaining the statistical stationarity of turbulent velocity by creating an equivalent ensemble was developed. An experimental investigation of the flow in the extreme lower atmosphere was conducted using the wake flow generated by a large diameter fan installed on flat grassland. Simultaneous measurements of turbulent velocity on a turbulence "line" along the wake axis were carried out utilizing a longitudinal array of five hot-wire anemometers remotely operated.

The stationarity test revealed that the turbulent velocity can be approximated as a realization of a weakly self-stationary random process. The streamwise changing properties of turbulence were deduced from a set of five Eulerian autocorrelations. A first integral time scale, Eulerian reference-point autocorrelations and Eulerian autocorrelation envelopes were advanced. The longitudinal Lagrangian autocorrelation was estimated by a line integral over all the Eulerian autocorrelation envelopes for the turbulence line. Based on the Lagrangian autocorrelation it was found that: (1) large diffusion time predominated; (2) ratios of Lagrangian to Eulerian time and spatial scales were smaller than unity; and, (3) short and long diffusion time scales and diffusion spatial scales were constrained within their Eulerian counterparts. Concentration of diffusing material along the turbulence line was predicted employing the momentum exchange and the dispersion coefficients computed by means of the Lagrangian autocorrelation. A diffusion experiment utilizing sulfur hexaflouride was performed. A remarkable similar streamwise variation of predicted and measured concentrations along the turbulence line within a difference ranging from 4 to 13% was found.

17. KEY WORDS Turbulent Diffusion Heat Exchange Instrumentation Motion	18. DISTRIBUTION STATEMENT Unclassified - Unlimited CAT 47

19. SECURITY CLASSIF. (of this report)	20. SECURITY CLASSIF. (of this page)	21. NO. OF PAGES	22. PRICE
Unclassified	Unclassified	240	$7.50

*For sale by the National Technical Information Service, Springfield, Virginia 22161

FOREWORD

This report is one of several to be published from research conducted under, or supported in part by, NASA Contract NAS8-28590. This effort is sponsored by the NASA Office of Applications and Office of Manned Space Flight under the direction of Marshall Space Flight Center. Mr. Robert E. Turner, Aerospace Environment Division, Space Sciences Laboratory, was the contract monitor. A number of approaches have been, and continue to be, followed in the conduct of the research. The results presented in this report represent only a portion of the total research effort.

ACKNOWLEDGMENT

The support of this work by the National Aeronautics and Space Administration, George C. Marshall Space Flight Center (Contract No. NAS8-28590) is highly appreciated.

TABLE OF CONTENTS

LIST OF SYMBOLS

A	reference point in Sects. 3.2.1 and 3.2.2; constant in Sect. 5.2; calibration sine wave amplitude in Sect. 5.4
A_γ	reference point in the reference plane
A_o	area source cross section
a_ℓ	cartesian coordinates of point A
B	point on trajectory in Sects. 3.2.1 and 3.2.2; data bandwidth in Sects. 5.4, 5.5 and 6.2
B^k_γ	point in the B-point plane
b_ℓ	cartesian coordinates of point B
C	calibration constant in Eq. (5.8)
$C_{j,im}$, $C_{i,jn}$, $C_{im,jn}$	Eulerian space-time cross-correlation functions
$c_{j,im}$, $c_{i,jn}$	Eulerian two-point two-time velocity-velocity derivative cross products
$c_{im,jn}$	Eulerian two-point two-time double velocity derivative cross product
$\mathcal{D}$	dispersion coefficient
d	hot-wire diameter in Sect. 5.3
E	voltage
E_o	voltage in still air in Eq. (5.1)
$e(t)$	fluctuating voltage
$F(f)$	one-dimensional energy spectrum
f	frequency
f_c	center carrier frequency
f_m	data signal maximum frequency
f_p	peak frequency
f_s	sampling frequency
G	gain

G_c	CFA gain
G_F	filter attenuation
G_H	hot-wire anemometer gain
G_T	tape-recorder track gain
g	gravitational acceleration
h	sampling interval in Sect. 5.5; wake centerline height in Sects. 5.2, 6 and 6.3.
K	RC time constant
$\mathcal{K}$	turbulent exchange coefficient
$\mathcal{K}_C$	turbulent mass exchange coefficient
$\mathcal{K}_H$	turbulent heat exchange coefficient
$\mathcal{K}_M$	turbulent momentum exchange coefficient
k	k-th fluid particle in Sects. 3.2.1 and 3.2.2
L	turbulence measurement range
$\mathcal{L}_{ij}(a_\ell,\tau)$	single-reference-point Lagrangian autocorrelation
$L_{ij}(S,\tau)$	reference-plane Lagrangian autocorrelation
$L_{ij}(\tau)$	Lagrangian autocorrelation for homogeneous turbulence in Eq. (3.39)
$L(\tau)$	Lagrangian autocorrelation for isotropic turbulence in Eq. (3.40)
$L(x_o,\tau)$	Lagrangian autocorrelation of axial turbulent velocity for the turbulence line
ℓ	hot-wire length in Sect. 5.3
ℓ_m	largest eddy size
M	constant in Sect. 5.2; number of starting times in Sect. 6.2
m	flow factor in Sect. 5.2; counting index in Sect. 5.5
m_f	modulation index

N	number of sample records in Sects. 3.1 and 6.2; number of fluid particles in Sects. 3.2.1 and 3.3.2; resistance ratio in Sects. 5.2 and 5.3; rms noise in Sect. 5.5; angular fan speed in Sect. 6
γ	
n	n-th fluid particle in Sect. 3.2.1; counting index in Sect. 5.5
p^k	point on k-th trajectory
p	probability density function
Q	source strength
q_o	equivalent area source strength
R	fan radius
$R(t_o,t_o+\tau)$	autocorrelation in Sects. 3.1 and 6.2
$R(\tau)$	autocorrelation in Sects. 3.1, 5.5 and 6.2
$\check{R}(\tau)$	autocorrelation coefficient in Sects. 5.5 and 6.2; Eulerian autocorrelation coefficient in Sect. 6.3
$R(\tau)$	Eulerian autocorrelation
$\check{R}_o(\tau)$	Eulerian reference-point autocorrelation coefficient
$\mathcal{R}_{ij}(x_\ell;\tau)$	Eulerian autocorrelation at position x_ℓ in Sect. 3.2.2.
$\mathcal{R}_{ij}(\tau)$	Eulerian autocorrelation for homogeneous turbulence in Eq. (3.39)
$\mathcal{R}(\tau)$	Eulerian autocorrelation for isotropic turbulence in Eq. (3.40)
$\mathcal{R}(x;\tau)$	Eulerian autocorrelation of axial turbulent velocity at point x on the turbulence line
$\check{\mathcal{R}}_o(\tilde{x};\tau)$	envelope of Eulerian reference-point autocorrelation coefficients
Re	Reynolds number
Ri	Richardson number
R_w	heated hot-wire resistance

R_{wco}	cold hot-wire resistance
r_{ij}	Eulerian velocity product in Sect. 3.2.2
S	reference plane area in Sect. 3.2.2; tape recorder speed in Sect. 5.4
s	intrinsic coordinate
s^k	k-th fluid particle trajectory
s^k_B	intrinsic coordinates of point B on k-th particle trajectory
T	averaging time; time interval
T_B	observation time
T_p	computation period base time
T_r	sample record length
T_{ra}	available time history
T_s	analysis time
Tu	longitudinal turbulence intensity
$\mathcal{T}$	integral time scale
$\mathcal{T}_1$	first integral time scale
t	time
t_D	diffusion time
t_o	starting time
$\mathcal{t}$	micro time scale
U,V,W	longitudinal, lateral and vertical velocities
U_c	characteristic mean velocity scale for the turbulence line
U_t	rotor tip velocity
u(t)	longitudinal turbulent velocity
$\mathcal{V}$	turbulence box volume
v	Lagrangian turbulent velocity

$X_\ell(t)$	position vector
x, y, z	cartesian coordinates
x_B	point on turbulence line
x_ℓ	cartesian coordinates in tensor notation in Sects. 3.2.1 and 3.2.2.
x_o	reference point on turbulence line
x_o, y_s, z_s	point source centroid coordinates in Sect. 6.5
α	autocorrelation resolution coefficient
Γ	index for A_γ-reference point in the reference plane
Δ	increment
ε	rms error in Sect. 6.2; dissipation in Sect. 6.3
ε_R	autocorrelation normalized standard error
η	sample-record amplitude
θ	absolute temperature
Λ_1	first integral length scale
λ	micro length scale
ν	kinematic viscosity
ξ	turbulence line extent in Sects. 3.2.2, 6.4 and 6.5; sample-record amplitude in Sect. 6.2; point on turbulence line in Sects. 6.4 and 6.5
ρ	equivalent ensemble autocorrelation
σ	standard deviation
τ	time delay; time lapse; time displacement
τ_p	computation period time
τ_1	autocorrelation first zero crossing
ϕ^1_{ij}	particle-space average of the spatial mean value of the Eulerian velocity product

$\phi^2_{ij}, \phi^3_{ij}, \phi^4_{ij}$	particle-space averages of the spatial mean values of the Eulerian velocity cross products
X	concentration
Ψ^1_{ij}	reference-plane average of Eulerian velocity product
$\Psi^2_j, \Psi^3_{ij}, \Psi^4_{ij}$	reference-plane averages of Eulerian velocity cross products

Brackets

{ }	ensemble of sample records
< >	ensemble average

Superscripts

k,n	k-th and n-th fluid particles
~	means "dimensionless"
^	estimator
—	time averaged

Subscripts

A	reference point
B	point on particle trajectory in Sects. 3.2.1 and 3.2.2; observation time in Sect. 6.2; point on turbulence line in Sect. 6.4
C	mass in Sect. 5.6
c	correlation function analyzer (CFA) in Sect. 5.5; characteristic mean velocity in Sects. 3.2.2, 6.1.1, 6.1.2, 6.4 and 6.5
D	diffusion
eq	equivalent ensemble
f	frequency
H	heat in Sect. 5.6

i	counting index in Sect. 5.5
i,j,ℓ	cartesian tensor coordinates
i,k,m,n	summation index
k,m	sample records in Sects. 3.1 and 6.2
K	RC time constant
L	Lagrangian
M	momentum
max	maximum
p	PDF in Sect. 6.2; peak in Sect. 6.3
p1,p2	first-and second-order PDF's
R	autocorrelation
r	sample record
ra	available record
rms	root-mean-square value
y,z	lateral and vertical directions
γ	with respect to the A_γ-reference point; summation index in Sect. 3.2.2
Λ	first integral length scale
λ	micro length scale
ρ	equivalent ensemble autocorrelation
o	starting time in Sects. 3.1 and 6.2; reference point in Sects. 6.1.2., 6.3, 6.4 and 6.5
1	x_1-direction in Sect. 3.2.2; sample record in Sect. 6.2; first zero crossing and integral scale in Sects. 6.3, 6.4 and 6.5
2	sample record in Sect. 6.2
3	sample record in Sect. 6.2

Abbreviations

AC	alternating current
ADAS	Analog Data Acquisition System
CFA	correlation function analyzer
CSU	Colorado State University
DC	direct current
DPM	digital panel meter
ECD	electron capture detector
EEAC	equivalent ensemble autocorrelation
EEACC	EEAC coefficient
EFS	Environmental Field Station
FM	frequency modulation
IRIG	Inter Range Instrumentation Group
JPDF	joint probability density function
OD	outside diameter
PDF	probability density function
RC	resistor-capacitor network
RF	radio frequency
S/N	signal-to-noise ratio
STACC	starting time averaged EEACC

The International System (SI) of measurement was used throughout this work. Conversion from SI units to U.S. customary units was carried out to approximately three significant digits.

1. INTRODUCTION

Knowledge of turbulent transport properties in the extreme lower atmosphere is essential for determining water vapor mixing, evaporation rates, diffusion of pollutants and, generally, transport of any material. Turbulent transport can be analyzed by either the transfer theory or statistical description. In the transfer theory (or K-theory) the rate of turbulent transport of material is assumed locally proportional to the gradient of its concentration. The proportionality factors are expressed by turbulent exchange coefficients (or eddy diffusivities). Phenomenological models of this sort basically represent the turbulent transport as an enhanced or "speeded-up" molecular diffusion. Transfer theories provide hence an overall gross estimation of turbulent transport in terms of the K-coefficients. Initial development along this line is due to Boussinesq [1], G.I. Taylor [2] and Prandtl [3]. Comprehensive discussions of the transfer theory can be furthermore found in G.I. Taylor [4], Prandtl [5], von Kármán [6], Sutton [7], Monin [8], Priestley [9], Hinze [10], Pasquill [11] and numerous other references.

A fundamentally correct picture of the actual mechanism of turbulent-transport processes can be achieved by following the motions of the fluid elements as they wander through the flow field. Statistical description of turbulent transport accomplishes this by representing the movement of the fluid particles in terms of suitable average properties of the fluctuating velocity. In this approach the mean-square particle displacement, which is essentially a measure of turbulent diffusion, is estimated in terms of the Lagrangian (or material) turbulent velocity autocorrelation. The turbulent exchange coefficient is then the time rate of change of the mean-square particle displacement. Determination of turbulent exchange coefficients hinges therefore upon knowledge of the Lagrangian autocorrelation. Statistical analysis possesses inherently the potential to provide a complete description of turbulent motion and transport. The statistical approach was first suggested for homogeneous turbulence by G.I. Taylor in 1921 [12] and further extended by G.I. Taylor [13,14], Kampé de Fériet [15], Heisenberg [16] and many others. A collection of the classic papers on statistical theory by G.I. Taylor, von Kármán, Howarth, Kolmogoroff, C.C. Lin and others can be found in Friedlander and Topper [17]. Extensive reviews of the statistical treatment can be found in Frenkiel [18], Townsend [19], Hinze [10], Batchelor [20], C.C. Lin [21], Pasquill [11], Lumley and Panofsky [22], Lumley [23], Monin and Yaglom [24], Csanady [25] and a great number of other references.

Direct estimation of the Lagrangian autocorrelation is extremely difficult due to intrinsic problems associated with measuring the velocity of each moving fluid particle. Consequently, myriad attempts have been made to deduce the Lagrangian autocorrelation from the readily measurable Eulerian velocity. A thorough review of these methods will not be given here since the background literature is easily accessible. On the other hand, their main features pertinent to the work presented herein are briefly discussed. The available approaches for the estimation of the Lagrangian autocorrelation can be generally categorized into three broad groups based on their salient traits. These three classes are: (1) the linear correlation; (2) the moving-frame autocorrelation; and, (3) the probability method. All these three methods infer basically that the Lagrangian autocorrelation exhibits similarity to some particular Eulerian correlation function.

In the linear correlation approach it is proposed that the shape of the Lagrangian autocorrelation is similar to either an axial Eulerian cross-correlation [26] or a single Eulerian autocorrelation [27] provided that the turbulence is homogeneous and isotropic. The Lagrangian autocorrelation is then derived by simply contracting or stretching either of the foregoing Eulerian correlations by means of an empirical linear factor of proportionality. In neither case, however, does the coefficient of proportionality possess a unique value. The linear cross-correlation method was put forth by Mickelsen in 1955 [26] based on a mass diffusion experiment in the core of a pipe where the turbulence is isotropic. In this approach the time and space coordinates of the Lagrangian autocorrelation and the Eulerian longitudinal cross-correlation, respectively, are related by a single linear coefficient of proportionality. Values of this contracting proportionality factor varying from 0.55 to 0.725 (32% variation), depending on the mean and turbulent velocity levels, were reported. An average value for this factor of roughly 0.6 was further proposed throughout a turbulent velocity range from 0.55 to 4.27 m/s (1.8 to 14 ft/s).

It is postulated in the linear autocorrelation approach that the Lagrangian autocorrelation is identical in shape with a single Eulerian velocity autocorrelation at a fixed point in space but their time scales are different. The underlying hypothesis of this method, which was advanced by Hay and Pasquill in 1959 [27], is that in homogeneous turbulence the Lagrangian autocorrelation decays much more slowly than the Eulerian velocity autocorrelation measured at a fixed point. Consequently, it was suggested that the former can be obtained by linear stretching of the time coordinate of the latter. Values of the linear stretching factor changing randomly from 1.1 to 8.5 (87% variation) were inferred based on a diffusion experiment at ground level. Despite this considerable scattering an average Lagrangian time scale of four times the Eulerian time scale was suggested. This presumption was put forth in the light of lack of a systematic variation of the time scaling coefficient with the changing wind and stratification characteristics. It is important to remark that the autocorrelation linear extension yields basically a cross-correlation contraction factor equal to unity [11]. A similar linear stretching of the time coordinate in relating the Lagrangian and Eulerian autocorrelations was proposed by Angell in 1964 [28] based on monitoring the trajectories of tetroons at heights near 762 m (2500 ft). An average value of about 3.3 was put forward for the linear time coefficient. This average value was implied in spite of observing a strong tendency for this time scale to increase from 1 to 7 (86% variation) with decreasing turbulence intensity from 0.35 to 0.05. Although not explicitly stated it appears that homogeneous turbulence was insinuated. In addition, the time coefficient augmented with increasing stability. The similarity in shape of the Lagrangian autocorrelation and the Eulerian correlation measured at a fixed point (essentially the Eulerian autocorrelation) was further set forth in a quite indirect way by Snyder and Lumley in 1971 [29]. In this work the motion of single spherical beads of different weights in a vertical wind tunnel in homogeneous and isotropic turbulence was monitored photographically. The heavy particle correlations were interpreted as representative Eulerian correlations while the light particle correlations were construed as Lagrangian autocorrelations. Based on these far-reaching assumptions the ratio of Lagrangian to Eulerian autocorrelation integral time scales was crudely estimated to be about 3.

In the moving-frame autocorrelation approach it is implied that the Lagrangian autocorrelation can be estimated by the envelope of a set of Eulerian space-time cross-correlations of the longitudinal fluctuating velocity in homogeneous and isotropic turbulence. This envelope, which connects the peaks of the cross-correlations, is interpreted as a moving Eulerian autocorrelation which would be measured by a probe traveling steadily at the mean velocity. This scheme was put forward by Baldwin and Walsh in 1961 [30] and further explored by Baldwin and Mickelsen in 1963 [31] based on a pipe diffusion experiment in isotropic turbulence resembling that described in Ref. 26. It is basically implied in this method that the moving Eulerian autocorrelation and the Lagrangian autocorrelation are of similar shape but of different scales. Values of the factor relating the varying axial separation distance of the cross-correlations to the time coordinate of the Lagrangian autocorrelation ranging from 1.2 to 0.14 (88% variation) were reported for longitudinal turbulent velocity changing from 0.55 to 1.46 m/s (1.8 to 4.8 ft/s) [31]. It is interesting to note that the corresponding range of the linear autocorrelation stretching factor [27] would be 40 to 4.7.

A similar equivalence between the moving Eulerian time correlation and the Lagrangian autocorrelation was proposed by Deissler in

1961 [32] for decaying homogeneous turbulence. It was further shown that these two autocorrelations are approximately equal for low turbulence levels (large decay times) and small diffusion times. On the other hand, based on a heat dispersion experiment in approximately isotropic turbulence Shlien and Corrsin in 1974 [33] asserted that the Lagrangian autocorrelation is rather different in shape from the moving autocorrelation. In this work the Lagrangian autocorrelation was estimated by trial and error utilizing the Lagrangian micro and integral time scales which were computed from dispersion data.

The probability method is based on the conjecture that for very long time intervals the displacements of fluid particles become statistically independent of the velocity distribution in homogeneous turbulence. Then it was inferred that the Lagrangian autocorrelation approaches asymptotically the average weighted Eulerian space-time cross-correlation function. In other words, the Lagrangian autocorrelation is approximated asymptotically by a domain integral over the entire flow field (volume integral) of the Eulerian two-point two-time cross-correlation when the weight function is the particle displacement probability density function. Generally, this probability density function is unknown. This scheme was initially advanced by Corrsin in 1959 [34] for homogeneous turbulence and extended by Saffman in 1963 [35] for small time intervals in isotropic turbulence. In the latter case the Lagrangian autocorrelation is expressed by an integro-differential equation for the mean-square displacement of a fluid particle in terms of the spectrum function of the Eulerian space-time cross-correlation. Additionally, a normal probability density function for the displacement was assumed. The Lagrangian autocorrelation was then computed for isotropic turbulence assuming an exponential decaying spectrum and, subsequently, compared with the moving Eulerian autocorrelation. As a result it was found that the ratio of the integral time scales of the moving Eulerian autocorrelation and the Lagrangian autocorrelation is roughly 1.25 times the longitudinal turbulence intensity for small values of the latter [35]. As regards the linear autocorrelation approach the foregoing result yields a linear autocorrelation stretching factor of 5.6 for an axial turbulence intensity of about 0.14.

The probability approach was further explored by Kraichnan in 1964 [36] in isotropic turbulence without any time interval restrictions. In this analysis the Lagrangian and Eulerian velocity fields were expressed in terms of a passive scalar labeling field [37] and the direct-interaction approximation for this scalar field [38,39] was utilized. The Lagrangian time-covariance (autocorrelation) was then represented by an average of the Eulerian space-time covariance (cross-correlation) over the effective volume occupied by the particle displacement probability distribution function at any difference time (lag time). Basically, a similar domain integral representation was introduced as an asymptotic approximation in Ref. 34. The direct-interaction approximation predicts furthermore that the Lagrangian autocorrelation falls off more rapidly than the Eulerian autocorrelation at a fixed point [36]. This leads to a linear autocorrelation factor smaller than unity which is in opposition with the results presented in Ref. 27.

An additional attempt to relate the Lagrangian autocorrelation to the Eulerian correlation function using the probability approach was reported by Philip in 1967 [40]. In this paper it is proposed that the Lagrangian autocorrelation in isotropic turbulence can be estimated by a space-time integration of the weighted Eulerian correlation function of the longitudinal turbulent velocity in an arbitrary direction (space-time cross-correlation). The probability density distribution function governing the probability of finding at a given position after a certain time interval a particle released at some arbitrary point in space was introduced as the weight function. Although this hypothesis possesses some physical plausibility, its rigorous justification is not possible and, consequently, the pressing need for supplying experimental support was recognized by its own proponent [40]. The Lagrangian autocorrelation was then expressed by an integral equation assuming a Gaussian probability density distribution function and an exponential decaying Eulerian space-time cross-correlation. This integral was solved in terms of a parameter which depends on the Eulerian axial turbulent velocity, and Eulerian integral time and longitudinal length scales. Subsequently, it was found that the ratio of the integral time scales of the Lagrangian autocorrelation and the moving Eulerian autocorrelation increases with diminishing longitudinal turbulence intensity. The method suggested in this paper [40] is by and large similar in a number of respects to the analysis presented in Ref. 35. On the other hand, the values of the integral time scales ratio suggested in Ref. 35

are 2 to 3 times larger than their counterparts deduced in Ref. 40 for same longitudinal turbulence intensity.

This brief review of the various available methods for the estimation of the Lagrangian autocorrelation clearly reveals the wide disparities in both the basic approach and useful results. In the light of the significant discrepancies among these numerous attempts further investigation for the sake of putting forth a relationship between the Lagrangian autocorrelation and the readily measurable Eulerian correlation function is undoubtedly warranted. Evidently, the physical validity of such a relationship is entirely contingent upon adequate experimental substantiation.

2. OBJECTIVE

The present investigation focused on the turbulent transport properties in the extreme lower atmosphere which is defined as the layer extending up to about 5 m (≈16 ft) above earth's surface. Determination of turbulent transport of any transferable quantity depends basically upon knowledge of the turbulent exchange coefficients. The turbulent momentum eddy diffusivity is of prime interest since both mass and heat transport coefficients are commonly ascertained in terms of it. In this study the statistical analysis of turbulent transport was adopted in the light of its apparent superiority with respect to the transfer theory approach considering the random nature of turbulent flow. The turbulent exchange coefficient can be then assessed in terms of the Lagrangian turbulent velocity autocorrelation.

To start with, a method for approximating the statistical stationarity of turbulent velocity was developed as a necessary prerequisite for the statistical analysis. A relationship between the Lagrangian and Eulerian autocorrelations of turbulent velocity was sought. The underlying approach for this model was that the Lagrangian autocorrelation can be expressed by means of a space integral of a set of Eulerian autocorrelations which generally are readily measurable. The experimental work, which was strongly stressed, concentrated on estimating the turbulent momentum eddy diffusivity and mass exchange coefficient based on the foregoing method.

Simulation of the turbulent flow in the extreme lower atmosphere was achieved employing the wake flow of a 3.04 m (10 ft) diameter fan installed at the Colorado State University Environmental Field Station. Flow visualization by means of smoke and balloons was used to gain an overall picture of the flow pattern. The measurements concentrated solely on the longitudinal turbulent velocity since its energy is significantly greater than that of the other two velocity components. Detailed surveys of axial turbulent velocity at five fixed stations within the wake were carried out simultaneously under dry, stable conditions employing an array of five hot-wire anemometers. Such an array of probes is essential for obtaining a set of concurrent Eulerian autocorrelations necessary to estimate the Lagrangian autocorrelation. The turbulent momentum eddy diffusivity was then deduced from the Lagrangian autocorrelation. Subsequently, the diffusion of a gas was predicted assuming equal momentum and mass exchange coefficients. The computed gas concentration was further substantiated through a mass diffusion experiment utilizing sulfur hexaflouride emitted from a point source located within the wake. Similar results are expected for turbulent transport of water vapor, pollutants or any admixture.

3. ANALYSIS OF TURBULENT TRANSPORT

The turbulent transport of water vapor or pollutants and, generally, of any transferable quantity, e.g., momentum and energy, within the lower atmosphere is diffusive in nature. Due to the random character of turbulence, it is necessary to express the turbulent-transport rates, i.e., turbulent exchange coefficients or eddy diffusivities, of these quantities in terms of statistical functions of the turbulent velocity field and of boundary or initial conditions. Determination of turbulent mass transport depends upon knowledge of the turbulent momentum exchange coefficient. The latter can be estimated in terms of the turbulent velocity autocorrelation of moving fluid particles through the flow field, i.e., the Lagrangian autocorrelation [10,12,15]. Since the Lagrangian autocorrelation cannot be measured directly, it is of prime importance to adequately relate it to the readily measureable Eulerian autocorrelation, i.e., the autocorrelation at a fixed point in space. The analysis presented herein focuses on relating the Lagrangian and Eulerian autocorrelations.

3.1 Stationarity of a random process

Turbulent velocity is basically a random process and, hence, its properties are examined by statistical techniques. Random processes may be either stationary or nonstationary. In the former case the statistical average properties are time independent whereas in the latter case they are time varying. A totally satisfactory methodology for analyzing all classes of nonstationary random processes is not yet available due to their unique properties. On the other hand, adequate statistical methods are available for stationary random processes, i.e., statistically steady random processes. It is consequently imperative to assess the stationarity of the turbulent velocity field for ensuring the reliability of its computed statistical average properties. In regard to atmospheric turbulence this is of considerable significance since it possesses a greater likelihood to be nonstationary than, say, wind-tunnel turbulence. Its nonstationarity can result from effects induced by nonuniform terrain and varying mean wind which assist in generation of turbulence.

Determination of turbulence stationarity is contingent upon the availability of a sufficiently large number of turbulent velocity records. The collection of these sample records, which are in practice finite time histories of length T_r of the random turbulent velocity $u(t)$, form an ensemble. This is represented by the set $\{u(t)\}$, where the braces designate an ensemble of sample records. All sample records in the ensemble must be collected simultaneously in independent flows under exactly similar physical situations and utilizing identical measuring instruments. The statistical properties of the random turbulent velocity field are described by the ensemble second moment, i.e., the autocorrelation, and by ensemble higher order moments whenever necessary. In the light of the intrinsic definition of turbulence, the mean value of the turbulent velocity, i.e., the first order moment, is zero [10]. The ensemble moments are estimated by averaging over all sample records comprised in the ensemble. This ensemble averaging procedure is illustrated by employing a hypothetical ensemble of turbulent velocity sample records depicted in Fig. 3.1. In this figure each sample record of the N records in the set $\{u(t)\}$ is denoted by subscript k, i.e., $u_k(t)$. The ensemble autocorrelation is estimated by computing the product of instantaneous turbulent velocities at some starting time t_o and at time $t_o + \tau$ in each sample record, and then by calculating their average. Thus, the ensemble autocorrelation is [41]

$$\langle R(t_o,t_o+\tau)\rangle = \lim_{N \to \infty} \frac{1}{N} \sum_{k=1}^{N} u_k(t_o)u_k(t_o+\tau), \qquad (3.1)$$

where the bent brackets denote ensemble average and τ is the time displacement. If the ensemble autocorrelation is independent of the selected starting time t_o, i.e., the ensemble autocorrelation depends only upon the time delay $\langle R(t_o,t_o+\tau)\rangle = \langle R(\tau)\rangle$, the random turbulent velocity is called weakly stationary. The fluctuating velocity is strongly stationary when all possible ensemble higher order moments possess the very same time independence property.

Unfortunately, in practice an ensemble of turbulent velocity records cannot be obtained. Statistical description of turbulence is then based on the far-reaching assumption that turbulence is an ergodic random process. It is important to point out that an ergodic random process is necessarily stationary [41]. Consequently, adequate examination of turbulence stationarity is of considerable significance. Due to the insurmountable impediments in securing a true ensemble of turbulent velocity records, it is conjectured that it can be approximated by an equivalent ensemble. Such an equivalent ensemble can be formed by dividing a sufficiently long time history of turbulent velocity into a finite number of equal time length records. This partition into sample records depends upon assuring that the time history is obtained under unchanged flow conditions. Then, the length of each sample record is

$$T_r = T_{ra}/N, \tag{3.2}$$

in which T_{ra} is the available time history and N is the finite number of deduced sample records. Essentially, this suggested equivalent ensemble is similar to a true ensemble since the sample records in each are obtained by identical measuring instruments under same flow conditions. In a true ensemble each sample record is statistically independent of all other sample records in the set, i.e., all joint moments are zero. A similar criterion is to be employed for establishing the equivalent ensemble. Each segment T_r must be statistically independent from the other members of the equivalent ensemble. Additionally, the sample record length T_r must be longer than the largest turbulence time scale of interest for ensuring that all significant information is comprehended within it. Thereby, the number of segments N is uniquely determined. The sample records of the equivalent ensemble are defined in terms of the original time history $u(t)$ as

$$u_k(t) = u[t+(k-1)T_r], \tag{3.3}$$

where $(k-1)T_r < t \leq kT_r$ and $k = 1, 2, \ldots, N$. Generation of an equivalent ensemble $\{u(t)\}_{eq}$, where subscript eq designates equivalent ensemble, from an available time history T_{ra} is illustrated in Fig. 3.2. The sample records $u_k(t)$ obtained by the division of the available time history are arranged into the form characteristic to an ensemble as clearly depicted in this figure. Then, the equivalent ensemble autocorrelation $\langle R(t_o,t_o+\tau)\rangle_{eq}$ is computed in the very same manner as its true ensemble counterpart given by Eq. (3.1). The method by which this computation is performed is portrayed in Fig. 3.2 assuming five sample records (N = 5). When the equivalent ensemble autocorrelation is only a function of the time displacement $\langle R(t_o,t_o+\tau)\rangle_{eq} = \langle R(\tau)\rangle_{eq}$, i.e., independent of the starting time t_o, the fluctuating velocity can be approximated as a weakly stationary random process. In addition, the random turbulent velocity can be assumed as a strongly stationary random process provided that equivalent ensemble higher order moments are time invariant.

Based on the ergodic hypothesis the properties of a stationary random process are computed by simply taking time averages over any sample record in the ensemble. For an ergodic process these time-averaged properties are equal to their ensemble-averaged counterparts. The time-averaged autocorrelation of a single realization of turbulent velocity $u(t)$ is expressed by [41]

$$R(\tau) = \lim_{T \to \infty} \frac{1}{T} \int_0^T u(t)u(t+\tau)\, dt, \qquad (3.4)$$

where T stands for the averaging time. Illustration of the manner that this calculation is carried out is shown in Fig. 3.2. In practice the averaging time T is finite and is essentially the time required to account for the largest turbulent time scale of interest. For the special case when the autocorrelation change with augmenting averaging time is insignificant, the sample record can be viewed as a realization of a weakly self-stationary random process. When the very same condition is met for all possible higher order moments, the random process is said to be strongly self-stationary. In other words, the finite averaging time T is equal to the time length required for assuming that a random process is self-stationary. It is apparent that only an ergodic process can be self-stationary. It is, further, important to note that the length of the equivalent ensemble sample records T_r is necessarily greater than or at the least equal to the self-stationarity averaging time, i.e., $T_r \geq T$. Consequently, determination of the length of the sample records comprising an equivalent ensemble ensures simultaneously the validity of both equivalent ensemble techniques and self-stationarity time-averaging procedures. It is then hypothesized that the ergodic assumption is corroborated by the equality of the equivalent ensemble and time-averaged autocorrelations, i.e., $\langle R(\tau)\rangle_{eq} = R(\tau)$.

3.2 A relationship between the Lagrangian and Eulerian turbulent velocity autocorrelations

Turbulent diffusion is naturally described in a Lagrangian frame of reference (material coordinates) since in this moving frame it is possible to account for fluid particle displacement statistics. The turbulent momentum exchange coefficient, i.e., the turbulent momentum eddy diffusivity, can be effectively determined from the Lagrangian turbulent velocity autocorrelation. It is assumed hereafter that the turbulence is ergodic and, hence, necessarily stationary. All turbulent statistical properties can be therefore deduced from a single realization of the flow.

The Lagrangian autocorrelation (or the material autocorrelation) of turbulent velocity is obtained by, first, forming the velocity product of a tagged fluid particle at two instants in time. In other words, the product of a marked fluid element velocity at an arbitrary reference position and some other point along its path line after a certain time lapse is made up. Next, this product is averaged with similar products arising from all the particles which pass through the very same reference position during a selected time interval. This particle-space averaging yields the desired Lagrangian autocorrelation with respect to the selected reference point. To obtain the Lagrangian autocorrelation it is thus imperative to examine the trajectories (or path lines) and velocities of all tagged fluid particles that moved past the reference point in the course of time. Since this particle information is generally unmeasurable, the Lagrangian autocorrelation cannot be obtained directly. Estimation of the Lagrangian autocorrelation entails relating it to its readily accessible Eulerian (spatial) counterpart. The latter is the time-averaged product of turbulent velocities at the very same space location, i.e., in a fixed frame of reference (spatial coordinates). This autocorrelation is evaluated by measuring the fluctuating velocity at a fixed position in space, computing the velocity product at two instants in time, and time averaging over all possible products with an identical time delay over a chosen time interval.

3.2.1 *Lagrangian autocorrelation*

In the Lagrangian description the motion of a tagged fluid particle is described in the course of time in terms of its arbitrary reference position (or initial position). The coordinates of this initial point in a fixed frame of reference, i.e., an Eulerian frame or a spatial frame, and the time are the Lagrangian independent variables. Throughout this analysis cartesian tensor notation is utilized and, consequently, subscripts i, j and ℓ can take on only integer values 1, 2 or 3 unless specified otherwise.

The trajectory (or path line) of any k-th fluid particle which passes through a selected reference point A at some initial time t_A^k is denoted by $s^k[a_\ell, X_\ell(t^k)]$ (ℓ = 1, 2, 3). Superscripts are utilized in identifying the fluid particles which move past the reference point A during a certain time interval T. Path lines of several fluid particles which cross the same reference position A are portrayed in Fig. 3.3. With respect to a fixed frame of reference the coordinates of the arbitrary initial point A are $x_\ell = a_\ell$ and the k-th fluid particle instantaneous position vector is designated by $X_\ell(t^k)$. Hence, the k-th particle trajectory $s^k[a_\ell, X_\ell(t^k)]$ in the course of time in the spatial system of coordinates x_ℓ is described by the position vector $X_\ell(t^k)$. Each k-th marked particle that passes through the reference point A does so at an unique initial time t_A^k and, thus, for any two particles k and n, $t_A^k \neq t_A^n$. On the other hand, the position vectors of their initial point A are exactly the same, i.e., $X_\ell(t_A^k) = X_\ell(t_A^n)$. The initial times are related by

$$t_A^n = t_A^k + (n - k)\Delta t, \qquad (3.5)$$

where $n > k$ and Δt is the smallest increment of time required for two consecutive particles to leave and arrive at reference point A. This time increment is generally unknown.

The turbulent velocity of each k-th fluid element in the Lagrangian method is designated by $v_i(a_\ell, t^k)$ (i = 1, 2, 3) and it is depicted along the particle trajectory s^k in Fig. 3.3. In this analysis only the turbulent velocity is considered inasmuch as its autocorrelation is not affected by the mean velocity. On the other hand, the fluid particles are basically carried by the mean flow. The trajectories of the fluid elements ensue thus from the superposition of the mean and turbulent velocities. When the k-th tagged fluid particle is at the reference point A at initial time t_A^k it possesses a velocity $v_i(a_\ell, t_A^k)$. At a later time the very same k-th fluid particle is at some point B^k along its trajectory s^k as portrayed in Fig. 3.3. The elapse time needed for the k-th particle to travel from its initial point A to the new position B^k is τ and, hence, the particle arrives at this position at time $t_B^k = t_A^k + \tau$. At point B^k, whose coordinates are $x_\ell = b_\ell^k$, the particle position vector is $X_\ell(t_A^k+\tau)$ and its Lagrangian velocity is $v_j(a_\ell, t_A^k+\tau)$ $(j = 1, 2, 3)$. The Lagrangian turbulent velocity autocorrelation is then obtained by averaging the two-point velocity product (or the Lagrangian velocity product) over a large number of fluid particles N (k = 1 to N) that pass through the reference point A within a selected time interval T. This average can be essentially interpreted as a particle-space averaging with respect to these N fluid elements. Thus, the single-reference-point Lagrangian turbulent velocity autocorrelation is given by

$$L_{ij}(a_\ell, \tau) = \frac{1}{N} \sum_{k=1}^{N} v_i(a_\ell, t_A^k) v_j(a_\ell, t_A^k+\tau). \tag{3.6}$$

It is of prime importance to remark that the instantaneous Eulerian velocity $u_i(x_\ell, t)$ $(i = 1, 2, 3)$ at any position along the s^k path line is exactly equal to the Lagrangian velocity of the k-th tagged fluid particle at that instant in time when this particle passes the very same position. Thus, instantaneously at any point along a s^k trajectory defined by the position vector $X_\ell(t^k)$

$$u_i[X_\ell(t^k),t^k] = v_i(a_\ell,t^k), \qquad (3.7)$$

while when the fluid particle is at the initial position A

$$u_i[X_\ell(t_A^k),t_A^k] = v_i(a_\ell,t_A^k). \qquad (3.8)$$

Based on this instantaneous equality between the Eulerian and Lagrangian velocities, it is surmised that the time interval T required for carrying out the Lagrangian particle-space averaging is equal to the averaging time necessary to qualify the self-stationarity of the Eulerian velocity record (see Sect. 3.1). Essentially, it is conjectured that during this time interval T the number of fluid particles N moving past the reference point suffices to account for the largest Lagrangian time scale of turbulence.

3.2.2 *Lagrangian-Eulerian autocorrelation relationship*

It appears that a relationship between the Lagrangian and Eulerian correlation functions cannot yet be obtained through formal mathematics. The brief review in Sect. 1 of the attempts to set forth such a relationship clearly indicates the insurmountable difficulties related to a rigorous mathematical relationship. It is apparent, on the other hand, that in any attempt to obtain such a relation the physical features of the turbulent flow must be adequately incorporated. Any relationship thus would be inherently the outcome of blending the physics of the flow with a suitable mathematical formulation. Essentially, relating the Lagrangian and Eulerian autocorrelations consists of establishing a connection between the velocity products which comprise them. The Lagrangian velocity $v_i(a_\ell,t^k)$ of the k-th tagged fluid particle that moved past the reference point A is defined at any moment only at its particular location along its trajectory $s^k[a_\ell,X_\ell(t^k)]$. On the other hand, for the same instant in time t the Eulerian velocity $u_i(x_\ell,t)$ is basically specified at every position in space which all the fluid occupies since it is not related to any distinct fluid element. The change in position of the k-th marked fluid particle in the course of time can be expressed either in terms of its moving position vector $X_\ell(t^k)$ or in terms of the distance which it moved along its trajectory s^k as portrayed in Fig. 3.4. In a fixed frame reference (or spatial frame) x_ℓ, the position vectors of the k-th fluid particle at times t^k and $t^k + dt^k$ are $X_\ell(t^k)$ and $X_\ell(t^k+dt^k)$. The change in the position vector of this element is thus $dX_\ell(t^k)$. Concurrently, with respect to the fluid particle natural (or intrinsic) coordinate, viz., the fluid particle trajectory s^k, the incremental distance traveled by the k-th fluid element is ds^k. This incremental distance is related to the change in position vector by

$$(ds^k)^2 = dX_\ell(t^k)dX_\ell(t^k), \tag{3.9}$$

in which the usual summation convention holds in regard to repeated subscripts. Then, the distance traveled by the k-th fluid particle along its trajectory from its reference position A to a point B^k is

$$s_B^k = \int_{a_\ell}^{b_\ell^k} [dX_\ell(t^k)dX_\ell(t^k)]^{\frac{1}{2}}, \tag{3.10}$$

where the coordinates of the positions A and B^k are $x_\ell = a_\ell$ and b_ℓ^k in the spatial frame or $s^k = 0$ and s_B^k in the intrinsic frame, respectively. This distance s_B^k, which is traveled by the fluid element in time $\tau = t_B^k - t_A^k$, is depicted in Fig. 3.4. The Eulerian velocity along a path line can be therefore expressed as $u_i(s^k,t)$ in terms of the intrinsic coordinate. It is evident that the properties of the Eulerian velocity, viz., a continuous differentiable function, are preserved in both the spatial and natural systems of coordinates.

The Eulerian velocity at any point P^k on the k-th fluid element trajectory s^k can be evaluated at any instant in time by means of Taylor series expansions of its corresponding velocities at reference point A and at point B^k. In the intrinsic system of coordinates the Eulerian velocities at points A and B^k are $u_i(0,t)$ and $u_j(s_B^k,t)$, and the coordinate of point P^k is s^k where $0 < s^k < s_B^k$. The Eulerian velocity at point P^k in terms of a Taylor series expansion about point A when the time is held at t_A^k is

$$u_i(s^k;t_A^k) = u_i(0,t_A^k) + \sum_{m=1}^{\infty} \frac{(s^k)^m}{m!} \left[\frac{d^m u_i(s^k;t_A^k)}{d(s^k)^m} \right]_{s^k=0} . \tag{3.11}$$

Similarly, at time $t_B^k = t_A^k + \tau$ the Eulerian velocity at the very same point P^k estimated by a Taylor series expansion about point B^k is

$$u_j(s^k;t_A^k+\tau) = u_j(s_B^k,t_A^k+\tau) + \sum_{n=1}^{\infty} \frac{(s^k - s_B^k)^n}{n!} \left[\frac{d^n u_j(s^k;t_A^k+\tau)}{d(s^k)^n} \right]_{s^k=s_B^k} . \tag{3.12}$$

In the preceding two equations the semicolon indicates that the series expansions about the points A and B^k were carried out at two specific instants in time, i.e., when in each case the time is held constant at t_A^k and t_B^k, respectively. This semicolon is used only with respect to any point P^k on the trajectory whose coordinate is s^k. The foregoing two Taylor series expansions are illustrated in Fig. 3.4. It is, furthermore, important to remark that the first terms in the series expansions in Eqs. (3.11) and (3.12) are exactly the Lagrangian particle velocities at times t_A^k and $t_A^k + \tau$ at point P^k. This results from the instantaneous equality between the Eulerian and Lagrangian velocities. In other words, $u_i(0,t_A^k) = v_i(a_\ell,t_A^k)$ and $u_j(s_B^k,t_A^k+\tau) = v_j(a_\ell,t_A^k+\tau)$ in accordance to Eq. (3.7), whence

$$u_i(0,t_A^k)u_j(s_B^k,t_A^k+\tau) = v_i(a_\ell,t_A^k)v_j(a_\ell,t_A^k+\tau). \tag{3.13}$$

At any point the Lagrangian velocity is tangent to the path line. The Eulerian velocity, on the other hand, is generally unknown with respect to the particular trajectory s^k except at that instant when it equals its Lagrangian counterpart as shown in Fig. 3.4. In other words, the Eulerian velocity is not necessarily tangent to any single path line at all times since it arises from all fluid particles.

The Eulerian velocity product $r_{ij}(s^k;t_A^k,\tau)$ at any point P^k is formed by simply multiplying the velocities prevailing at this position at times t_A^k and $t_A^k + \tau$ which are given by Eqs. (3.11) and (3.12). This product yields

$$
\begin{aligned}
r_{ij}(s^k;t_A^k,\tau) &= u_i(s^k;t_A^k)u_j(s^k;t_A^k+\tau) \\
&= v_i(a_\ell,t_A^k)v_j(a_\ell,t_A^k+\tau) + \sum_{m=1}^{\infty} \frac{(s^k)^m}{m!} c_{j,im}(s_B^k,0,t_A^k+\tau,t_A^k) \\
&+ \sum_{n=1}^{\infty} \frac{(s^k - s_B^k)^n}{n!} c_{i,jn}(0,s_B^k,t_A^k,t_A^k+\tau) \\
&+ \sum_{m=1}^{\infty}\sum_{n=1}^{\infty} \frac{(s^k)^m(s^k - s_B^k)^n}{m!n!} c_{im,jn}(0,s_B^k,t_A^k,t_A^k+\tau),
\end{aligned} \tag{3.14}
$$

in which the Lagrangian velocity product is substituted for the product of the first terms in the series expansions of the Eulerian velocity in view of Eq. (3.13). The last three terms in Eq. (3.14) stand for the Eulerian velocity cross products since the Eulerian two-point two-time velocity-velocity derivative cross products are

$$
c_{j,im}(s_B^k,0,t_A^k+\tau,t_A^k) = u_j(s_B^k,t_A^k+\tau)\left[\frac{d^m u_i(s^k;t_A^k)}{d(s^k)^m}\right]_{s^k=0}, \tag{3.15}
$$

$$
c_{i,jn}(0,s_B^k,t_A^k,t_A^k+\tau) = u_i(0,t_A^k)\left[\frac{d^n u_j(s^k;t_A^k+\tau)}{d(s^k)^n}\right]_{s^k=s_B^k}, \tag{3.16}
$$

and the Eulerian two-point two-time double velocity derivative cross product is

$$
c_{im,jn}(0,s_B^k,t_A^k,t_A^k+\tau) = \left[\frac{d^m u_i(s^k;t_A^k)}{d(s^k)^m}\right]_{s^k=0}\left[\frac{d^n u_j(s^k;t_A^k+\tau)}{d(s^k)^n}\right]_{s^k=s_B^k}. \tag{3.17}
$$

A relationship between the Lagrangian and Eulerian velocity products of the k-th fluid particle at any point P^k on its trajectory is hence supplied by Eq. (3.14). An illustration of how the Eulerian velocity product is obtained for a single velocity component at any point P^k on the trajectory s^k is provided by Fig. 3.5. At time t_A^k the instantaneous Eulerian velocity along the k-th path line $u_i(s^k;t_A^k)$ is depicted in Fig. 3.5(a). A hypothetical variation of, say, the $u_1(s^k;t_A^k)$ component is also displayed. Similarly, the instantaneous Eulerian velocity at time $t_A^k + \tau$ along the very same trajectory and the assumed change of the same $u_1(s^k;t_A^k+\tau)$ component are shown in Fig. 3.5(b). The product of these two velocity components formed at any point P^k is finally portrayed in Fig. 3.5(c).

It is conceivable to express the Eulerian velocity product and velocity cross products in Eq. (3.14) at all possible points P^k on the k-th trajectory in terms of single characteristic values. In other words, these Eulerian quantities are represented by their spatial mean values on the k-th path line between reference point A and position B^k. This averaging involves basically line integration along the k-th trajectory from initial point $s^k = 0$ to point s_B^k, i.e., trajectory averaging in the natural frame. Since the k-th fluid particle reaches point s_B^k on its path line after some time lapse τ the trajectory averaging is applied for each position s_B^k. The Lagrangian velocity product, on the other hand, is not affected by this trajectory averaging inasmuch as it is independent of the intrinsic coordinate s^k. As a result of this trajectory averaging the Lagrangian velocity product for the k-th fluid particle is expressed by the spatial mean values of the Eulerian velocity product and velocity cross products along the path line segment traveled by this fluid element during time τ.

Throughout time interval T a large number of fluid particles N moved past the reference point A as illustrated in Fig. 3.3. The Lagrangian velocity autocorrelation for all these N fluid elements is obtained according to Eq. (3.6) by particle-space averaging of their Lagrangian velocity products. Then the single-reference-point Lagrangian turbulent velocity autocorrelation is supplied by particle-space averaging of the spatial mean values of the Eulerian velocity product and velocity cross products considering Eq. (3.14). This particle-space averaging yields basically unique mean values for the trajectory averages of the Eulerian velocity product and the three Eulerian velocity cross products for all the path lines traced by these N fluid particles. Hence, the single-reference-point Lagrangian autocorrelation, is

$$L_{ij}(a_\ell,\tau) = \phi^1_{ij}(a_\ell,\tau) - [\phi^2_{ji}(a_\ell,\tau) + \phi^3_{ij}(a_\ell,\tau) + \phi^4_{ij}(a_\ell,\tau)], \quad (3.18)$$

where the elapse time (or time delay) τ can take on any value. In this equation the first ϕ-term

$$\phi^1_{ij}(a_\ell,\tau) = \frac{1}{N}\sum_{k=1}^{N}\frac{1}{s^k_B}\int_0^{s^k_B} r_{ij}(s^k;t^k_A,\tau)\, ds^k \quad (3.19)$$

is the particle-space average of the spatial mean value of the Eulerian velocity product, and the other three ϕ-terms

$$\phi_{ji}^{2}(a_{\ell},\tau) = \frac{1}{N}\sum_{k=1}^{N}\left[\sum_{m=1}^{\infty}\frac{(s_B^k)^m}{(m+1)!}\,c_{j,im}(s_B^k,0,t_A^k+\tau,t_A^k)\right], \tag{3.20}$$

$$\phi_{ij}^{3}(a_{\ell},\tau) = \frac{1}{N}\sum_{k=1}^{N}\left[\sum_{n=1}^{\infty}\frac{(-1)^n(s_B^k)^n}{(n+1)!}\,c_{i,jn}(0,s_B^k,t_A^k,t_A^k+\tau)\right], \tag{3.21}$$

and

$$\phi_{ij}^{4}(a_{\ell},\tau) = \frac{1}{N}\sum_{k=1}^{N}\left[\sum_{m=1}^{\infty}\sum_{n=1}^{\infty}\frac{(-1)^n(s_B^k)^{n+m}}{(m+n+1)!}\,c_{im,jn}(0,s_B^k,t_A^k,t_A^k+\tau)\right] \tag{3.22}$$

are the particle-space averages of the spatial mean values of the Eulerian velocity cross products. In Eqs. (3.19) to (3.22) the terms in the brackets are the results of the trajectory averaging whereas the summation over k designates the particle-space averaging. With regard to the trajectory averaging, the terms $c_{j,im}$, $c_{i,jn}$ and $c_{im,jn}$ are constants since they are evaluated at fixed positions on the trajectory as indicated in Eqs. (3.15), (3.16) and (3.17). The trajectory averaging of the Eulerian velocity product and velocity cross products is outlined in Appendix I.

The single-reference-point Lagrangian autocorrelation given by Eq. (3.18) expresses the average characteristics of the turbulence along the fluid particles trajectories which originated at the selected reference point A. For any flow situation it is possible to generally choose innumerable reference points. It is conceivable, however, to restrict the selection of these points within a particular finite plane. The most convenient and practical choice is apparently a plane normal to the main flow direction. Then the intrinsic nature of all the single-reference-point Lagrangian autocorrelations defined with respect to all possible reference points in this plane is the specification of the downstream average turbulence properties. This control surface, which is the locus of all the A-reference points, can be thus viewed as a reference plane or an A-point plane. In either confined and/or unconfined flows such a reference plane can be readily envisioned. For wind-tunnel and/or pipe flows this reference plane is basically their cross sections at any desired streamwise position. All fluid particles must move past such a plane. In the case of atmospheric and/or wake flows, it is always feasible and, moreover, desirable to adequately delineate the flow region of interest by means of suitable imaginary boundaries.

As a result a finite reference plane, which includes all the Γ relevant A-reference points, viz., A_γ where $\gamma = 1$ to Γ, can be introduced for any flow situation. The picture of the path lines traced by the N fluid particles that pass through a single reference point A portrayed in Fig. 3.3 applies thereby to all the A_γ-reference points in the reference plane. It can be further theorized that all the $\Gamma \times N$ trajectories, which arise from the N fluid particles that pass each of the Γ reference points in the A-point plane during a time interval T, describe a continuous expanding or contracting control volume with increasing time lapse τ. In other words, this control volume encompasses all the path lines originated within the reference plane which extends over the elapse time τ. Each of the $\Gamma \times N$ fluid particles crosses its particular A_γ-reference point at some initial time $(t_A^k)_\gamma$ and in moving along its trajectory reaches some new position B_γ^k after a time lapse τ. It is thus possible to consider a bounded control volume which encloses all the $\Gamma \times N$ trajectory segments traced throughout the time displacement τ. The locus of all B^k_γ points which contains all the locations of the $\Gamma \times N$ fluid particles at times $(t^k_A)_\gamma + \tau$ is the B-point plane. This finite control volume is thus demarcated by the A- and B-point planes. Apparently, this control volume can be interpreted as a turbulence "box". In the limiting case when $\tau = 0$, the turbulence "box" reduces to a turbulence "plane" which is the reference plane (the A-point plane) since the B-point plane collapses on it. The turbulence "box" becomes moreover the entire flow field downstream of the reference plane, i.e., a flow field extending to infinity, as $\tau \to \infty$.

The turbulence "box" can be visualized by the following hypothetical flow situation: (1) mean flow in only x_1-direction; (2) an arbitrary control surface, i.e., reference plane, normal to the x_1-axis which is defined by $x_1 = S =$ constant; (3) all $\Gamma \times N$ fluid particles entering the control volume V, i.e., the turbulence "box", pass through this A-point plane; (4) the envelope of the control volume (all lateral surfaces) are impermeable; and, (5) all $\Gamma \times N$ fluid particles arrive after some time lapse τ at a plane B, i.e., the B-point plane. This hypothetical flow situation is illustrated in Fig. 3.6. A cut through the turbulence "box" is also shown in Fig. 3.6 to provide a better view of the A-point plane and several trajectories. The separation ξ between the reference and B-point planes, which is shown in this figure, can be approximated using a characteristic mean velocity scale U_c and the time lapse τ according to

$$\xi = U_c \tau. \qquad (3.23)$$

Practically, this streamwise length ξ can be viewed as representative of the final position $(s_B^k)_\gamma$ for all the $\Gamma \times N$ fluid particles. This longitudinal extent ξ can be furthermore interpreted as a turbulence "line" within the turbulence box.

The problem of interest is now to estimate the overall properties of the turbulence within this box. A plausible description of these properties can be supplied by the average of all single-reference-point Lagrangian autocorrelations over all A_γ-reference points in the reference plane S. To this end, the coordinates of the single reference point a_ℓ, the natural coordinate of any position s^k along the trajectories originated at this point and the initial time t_A^k are superseded in Eqs. (3.18) through (3.22) by $a_{\ell\gamma}$, s_γ^k and $(t_A^k)_\gamma$, respectively. This replacement accounts for the A_γ-reference points. Average of the single-reference-point Lagrangian autocorrelations $\mathcal{L}_{ij}(a_{\ell\gamma},\tau)$ with respect to all corresponding A_γ-reference points, i.e., reference-plane averaging, is simply achieved by summing Eq. (3.18) over $\gamma = 1$ to Γ. The reference-plane average Lagrangian autocorrelation is therefore expressed by

$$L_{ij}(S,\tau) = \frac{1}{\Gamma} \sum_{\gamma=1}^{\Gamma} \mathcal{L}_{ij}(a_{\ell\gamma},\tau), \tag{3.24}$$

where S is the A-point plane or the reference plane. Next, the reference-plane Lagrangian autocorrelation can be expressed in terms of the representative Eulerian quantities for the turbulence box by substituting Eq. (3.18) into Eq. (3.24). This substitution yields

$$L_{ij}(S,\tau) = \Psi_{ij}^1(S,\tau) - [\Psi_{ji}^2(S,\tau) + \Psi_{ij}^3(S,\tau) + \Psi_{ij}^4(S,\tau)], \tag{3.25}$$

in which the reference-plane average of the Eulerian velocity product is

$$\Psi^1_{ij}(S,\tau) = \frac{1}{\Gamma}\sum_{\gamma=1}^{\Gamma} \phi^1_{ij}(a_{\ell\gamma},\tau) \ , \tag{3.26}$$

and the reference-plane averages of the three Eulerian velocity cross products are

$$\Psi^2_{ji}(S,\tau) = \frac{1}{\Gamma}\sum_{\gamma=1}^{\Gamma} \phi^2_{ji}(a_{\ell\gamma},\tau), \tag{3.27}$$

$$\Psi^3_{ij}(S,\tau) = \frac{1}{\Gamma}\sum_{\gamma=1}^{\Gamma} \phi^3_{ij}(a_{\ell\gamma},\tau), \tag{3.28}$$

and

$$\Psi^4_{ij}(S,\tau) = \frac{1}{\Gamma}\sum_{\gamma=1}^{\Gamma} \phi^4_{ij}(a_{\ell\gamma},\tau), \tag{3.29}$$

and where Eqs. (3.19), (3.20), (3.21) and (3.22) are expressed in terms of $a_{\ell\gamma}$, s^k_γ and $(t^k_A)_\gamma$. The foregoing four Ψ-terms are essentially the characteristic values of the Eulerian velocity product and velocity cross products for the entire turbulence box. They resulted from trajectory, particle-space and, finally, reference-plane averaging procedures. It is of considerable significance to point out that these three average processes represent basically an interweaving of space and time averagings within the turbulence box. These intrinsic features lead naturally to the inference that these Ψ-terms can be estimated by ordinary space-time averaging. The space under consideration is the volume V of the turbulence box whereas the time during which these averages are undertaken is the time interval T necessary for the $\Gamma \times N$ fluid particles to pass through the reference plane.

The elements constituting the $\Psi^1_{ij}(S,\tau)$ term, which is given by Eq. (3.26), are the Eulerian velocity products $r_{ij}[s^k_\gamma;(t^k_A)_\gamma,\tau]$ at all points within the turbulence box. These products can be arranged in time sequences at every point x_ℓ (or s^k_γ) in this box. Such a typical position is shown in Fig. 3.6. Due to this grouping the Eulerian velocity product at each point x_ℓ can be expressed for all time t by $r_{ij}(x_\ell,t,\tau)$. Each time sequence comprises all successive velocity products during the time interval T at any point. Subsequent time averaging of such a time sequence furnishes exactly the local ordinary Eulerian autocorrelation

$$R_{ij}(x_\ell;\tau) = \frac{1}{T}\int_0^T r_{ij}(x_\ell;t,\tau)\ dt, \tag{3.30}$$

at position x_ℓ. Then the domain integral over the volume V of the turbulence box of all the common Eulerian autocorrelations supplies the equivalent space-time average representation of the reference-plane average value of $\Psi^1_{ij}(S,\tau)$, viz.,

$$\Psi^1_{ij}(S,\tau) = \frac{1}{V}\int_V R_{ij}(x_\ell;\tau)\ dV. \tag{3.31}$$

Next, the constitutents of the remaining three Eulerian Ψ-terms in Eq. (3.25) consist of velocity-velocity derivative (Eqs. (3.27) and (3.28)) and double velocity derivative (Eq. (3.29)) cross products at positions located solely in the A- and B-point planes along the same trajectory s^k_γ. The coordinates of such a pair of points are $a_{\ell\gamma} = x_\ell$ and $b^k_{\ell\gamma} = b_\ell$ or $s^k_\gamma = 0$ and $(s^k_B)_\gamma$ in the spatial and natural frames, respectively. These coordinates are portrayed in Fig. 3.6. In a similar manner as for $\Psi^1_{ij}(S,\tau)$, the various cross products composing these three Ψ-terms can be rearranged into time sequences for every pair of points. As a result of this sorting the velocity-velocity derivative cross products can be represented at all time t by $c_{j,im}(b_\ell,x_\ell,t+\tau,t)$ and $c_{i,jn}(x_\ell,b_\ell,t,t+\tau)$. Similarly, the double velocity derivative cross product can be expressed at all time t by $c_{im,jn}(x_\ell,b_\ell,t,t+\tau)$. Time averaging over time sequences of the foregoing cross products during time interval T yields the Eulerian space-time cross-correlation functions

$$C_{j,im}(b_\ell,x_\ell,\tau) = \frac{1}{T}\int_0^T c_{j,im}(b_\ell,x_\ell,t+\tau,t)\,dt, \tag{3.32}$$

$$C_{i,jn}(x_\ell,b_\ell,\tau) = \frac{1}{T}\int_0^T c_{i,jn}(x_\ell,b_\ell,t,t+\tau)\,dt, \tag{3.33}$$

and

$$C_{im,jn}(x_\ell,b_\ell,\tau) = \frac{1}{T}\int_0^T c_{im,jn}(x_\ell,b_\ell,t,t+\tau)\,dt. \tag{3.34}$$

The space-time average values for these three Ψ-terms are subsequently estimated by simple area integration over the reference plane S of the above three space-time cross-correlations. Hence, the equivalent space-time average representations of the reference-plane averages of the last three Ψ-terms in Eq. (3.25) are

$$\Psi^2_{ji}(S,\tau) = \sum_{m=1}^{\infty} \frac{(U_c\tau)^m}{(m+1)!}\,\frac{1}{S}\int_S C_{j,im}(b_\ell,x_\ell,\tau)\,dS, \tag{3.35}$$

$$\Psi_{ij}^{3}(S,\tau) = \sum_{n=1}^{\infty} \frac{(-1)^n (U_c\tau)^n}{(n+1)!} \frac{1}{S}\int_S C_{i,jn}(x_\ell,b_\ell,\tau)\, dS, \tag{3.36}$$

and

$$\Psi_{ij}^{4}(S,\tau) = \sum_{m=1}^{\infty} \sum_{n=1}^{\infty} \frac{(-1)^n (U_c\tau)^{m+n}}{(m+n+1)!} \frac{1}{S}\int_S C_{im,jn}(x_\ell,b_\ell,\tau)\, dS. \tag{3.37}$$

In these three foregoing equations the distance along each trajectory $(s_B^k)_\gamma$ was approximated by the length ξ of the turbulence line in accordance to Eq. (3.24). Computation of all these four Eulerian Ψ-terms is evidently contingent upon simultaneous knowledge of the Eulerian autocorrelations $R_{ij}(x_\ell;\tau)$ at all points in the turbulence box and of the Eulerian cross-correlations $C_{j,im}(b_\ell,x_\ell,\tau)$, $C_{i,jn}(x_\ell,b_\ell,\tau)$ and $C_{im,jn}(x_\ell,b_\ell,\tau)$ at all positions in the A- and B-point planes. This involves in practice the use of an array of probes which monitor concurrently the turbulent velocity at all points of interest within a flow field.

It is plausible that the last three Ψ-terms in Eq. (3.25) can be disregarded since they are composed of correlations between velocity and/or velocity derivatives. The interrelation between the turbulent velocity and its derivatives is progressively weakened with increasing order of differentiation. As a result correlations between a turbulent velocity and the derivative of another turbulent velocity or between two turbulent velocity derivatives basically cannot be expected to take on values even as large as the correlation between the actual velocities. With augmenting streamwise distance ξ of the turbulence box, and hence with time lapse τ, the correlation between two velocities in the A- and B-point planes generally decreases. Then in all likelihood, the three Eulerian space-time cross-correlations vanish rapidly with increasing space and time separations. Therefore, the Lagrangian autocorrelation can be practically approximated in terms of the usual Eulerian autocorrelations by the relationship

$$L_{ij}(S,\tau) \approx \frac{1}{V}\int_V R_{ij}(x_\ell;\tau)\, dV \tag{3.38}$$

whenever the last three Eulerian Ψ-terms, i.e., the Eulerian velocity cross products, can be neglected. Experimental examination of the cross-correlations given by Eqs. (3.32), (3.33) and (3.34) is however imperative to ascertain whether these terms can be satisfactorily disregarded.

The foregoing relationship for the Lagrangian autocorrelation is not constrained to either homogeneous and/or isotropic turbulence. Such ideal flows, on the other hand, enable considerable simplification of the former expression. If the flow is homogeneous the Eulerian autocorrelation is independent of its position x_ℓ within the turbulence box, i.e., $R_{ij}(x_\ell,\tau) = R_{ij}(\tau)$. Then it follows formally from Eq. (3.38) that

$$L_{ij}(S,\tau) = L_{ij}(\tau) \approx R_{ij}(\tau). \tag{3.39}$$

In isotropic turbulence the Eulerian autocorrelation is moreover independent of direction, i.e., $R_{ij}(\tau) = R(\tau)$. The corresponding Lagrangian autocorrelation can be then deduced from a single Eulerian autocorrelation since Eq. (3.39) becomes

$$L_{ij}(\tau) = L(\tau) \approx R(\tau). \tag{3.40}$$

It is important to point out that truly homogeneous and/or isotropic turbulence are not realizable particularly in the atmosphere. Hence, Eq. (3.38) is to be utilized for estimation of the Lagrangian autocorrelation for any flow.

It is interesting to mention that the Lagrangian autocorrelation expression for homogeneous turbulence given by Eq. (3.39) is intrinsically similar to the linear autocorrelation model set forth by Hay and Pasquill [21] when the stretching factor equals one. In addition, the equality of the Lagrangian and Eulerian autocorrelations in isotropic turbulence with zero mean flow was put forward by Deissler [32] in the moving-frame autocorrelation approach. The concept of a turbulence box was indirectly advanced in the the probability method inasmuch as a domain integral was employed in estimating the Lagrangian autocorrelation.

4. EXPERIMENTAL APPARATUS

The objective of the experimental program was to investigate the turbulent transport properties in the extreme lower atmosphere under dry conditions. Specifically, the estimation of the momentum exchange coefficient, i.e., the eddy diffusivity, was sought. The extreme lower atmosphere was defined as the earth-atmosphere interface which was assumed to extend up to about 5 m (16.4 ft) above the earth's surface. Such a study could not be accomplished by measuring the features of naturally occurring turbulence due to the continuous changing weather conditions. Moreover, it was desired to obtain such a flow that could be further utilized for studies of water vapor and/or contaminant (pollutant) turbulent mixing under controlled circumstances. Laboratory simulation of atmospheric flows is, to a large extent, disputable since exact dynamic similarity, i.e., Reynolds-number equality, is not readily achievable. In the lower atmosphere the Reynolds number based on the largest possible eddy size and the ambient wind is of the order of 10^6 or greater (using the kinematic viscosity). Within this layer the maximum eddy size which can be sustained is at most equal to its thickness, viz., 5 m. Such high Reynolds numbers cannot be obtained in the laboratory, e.g., in wind-tunnel flows, and, consequently, under the assumption that the atmospheric flow is inertia dominated the requirement of dynamic similitude is commonly relaxed.

For these reasons, the atmospheric flow was simulated using the wake flow generated by a 3.04 m (10 ft) diameter, 6-blade fan of variable pitch (Hartzell Propeller Fan Co., Model A120-6) installed at a field site. Generally, the prevailing wind at this field site is approximately 3.6 m/s (8 mph). The fan, which was driven by an internal combustion engine, could produce air speeds up to about 15 m/s (49 ft/s). Turbulent eddies within the wake were expected to possess a maximum size at the least equal to the fan diameter. The Reynolds number within the wake was roughly of the order of 10^6 and, therefore, the condition of dynamic similitude was met.

The fan constitutes the core of the Colorado State University Environmental Field Station (EFS). This fan and its anchored supporting structure are located on flat grassland. Its wake is free of immediate downwind natural and/or man-made obstructions to about 300 m (984 ft). The geometric centerline of the fan is positioned 3.04 m (one fan diameter) above the surface. The EFS is equipped with an Analog Data Acquisition System (ADAS) installed in a mobile trailer. This trailer is located outside the wake at a distance larger than 20 m ($\approx$66 ft) from the fan's centerline and about 60 m (197 ft) downstream of the fan. The ADAS is capable of collecting, recording, preparing, qualifying and preliminary on-line analysis of the data. Measurement probes were mounted on stands 3 and/or 4.5 m high placed in the wake at selected positions. Guys prevented the stands from swaying.

The experiment was conducted under calm or near calm conditions with winds not exceeding about 1 m/s ($\approx$2 mph). These conditions occur frequently at the field site since base temperature inversions prevail almost daily in early morning and at twilight. The Richardson number in this experiment, which indicates the flow stability, was about 0.002 (see Sect. 6.1.1). Under an inversion, i.e., stable conditions, turbulence is sustained when the Richardson number is positive and less than 0.2 [7,22]. Ambient wind was measured by means of a cup anemometer (Belfort Instrument Co., Wind Speed Transmitter, Type M) placed outside of the wake. Its signal was continuously monitored utilizing a digital voltmeter (Hewlett-Packard Co., Model 3440A). The vertical variation of the ambient temperature was measured by means of four shielded mercury thermometers (Van Waters & Rogers, Type 61001-044) mounted on an 18 m (59 ft) tower located near the ADAS. The field station layout and all important dimensions are depicted in Fig. 4.1. A picture of the fan and the field site is provided by Fig. 4.2.

5. EXPERIMENTAL TECHNIQUE AND INSTRUMENTATION

5.1 Flow visualization

Flow visualization was extensively conducted to provide an overall qualitative view of the flow pattern within the wake. It was especially important for ascertaining the predominant sizes of the turbulent eddies and to observe their streamwise behavior. Two visualization methods were employed, smoke and balloons. Smoke grenades were attached to stands located at selected positions in the wake at several heights. These grenades emitted a continuous relatively dense red smoke for a duration of about 2 min. The turbulent eddies entrained the smoke and, thereby, the streamwise turbulent transport and diffusion became clearly visible.

Ordinary rubber balloons were inflated with helium to a neutrally buoyant size. Five balloons were attached to one stand symmetrically about the fan's geometric centerline at vertical increments of 0.5R (fan radius R = 1.52 m (5 ft)). When the stand was placed in wake, the balloons were captured by the eddies indicating their relative strength and size at that particular position. Subsequent simultaneous release of the balloons yielded further visualization of the turbulent flow patterns and the downstream change of the eddies' sizes and strengths. Two color movies were produced showing the smoke and balloon patterns within the wake. The movies were made using a 16 mm movie camera (Paillard Inc., Model Bolex H-16 Rex).

5.2 Mean velocity and turbulence measurement

The wake was expected to stretch at least 68 m (223 ft) longitudinally and 6 m (20 ft) laterally. This extent was estimated by similitude based on a preliminary investigation of a wake produced by a small indoor fan [42]. Longitudinal mean velocity $\overline{U}$ along the fan centerline was measured by means of a single hot-wire anemometer. To obtain a clear picture of the axial mean velocity variation the hot-wire probe was initially placed 5R (7.6 m (25 ft)) downstream of the fan and, subsequently, moved in steps of 1R (1.52 m (5 ft)) up to 14R (21.28 m (70 ft)). The turbulence characteristics within the field flow were measured by the simultaneous use of an array of five hot-wire anemometers. To avoid perturbations generated by the fan supporting structure, the hot-wire probes were positioned at distances greater than 7R (10.64 m (35 ft)) downstream of the fan [42]. All hot-wire probes were positioned along the fan centerline, i.e., at a height $h = 3.04$ m (10 ft) above the ground, 1R apart, with the first probe located 10R (15.2 m (50 ft)) from the fan. The turbulence measurement range thus extended from $x = 15.2$ to 21.28 m (50 to 70 ft), and the hot-wire probes were located at $x = 15.2$, 16.72, 18.24, 19.76 and 21.28 m (50, 55, 60, 65 and 70 ft). In this region the lateral and vertical mean velocity components, i.e., $\overline{V}$ and $\overline{W}$, were anticipated to be much less than 10% of the longitudinal mean velocity $\overline{U}$ [42]. Since a hot wire is most sensitive to the velocity's normal component according to the cosine law [43], the sensors were aligned normal to the longitudinal component of the mean velocity $\overline{U}$. In terms of the system of coordinates utilized, the probe axis was parallel to the z-direction (vertically) and the sensor axis was parallel to the y-direction (laterally). The probes' arrangement and the system of coordinates used are portrayed in Fig. 5.1.

Basically, a hot-wire anemometer measures the cooling due to the flow of an electrically heated fine wire. Previous experiments clearly indicate that there is a power dependence of the heat transfer, i.e., Nusselt number, on the Reynolds number (based on the undisturbed mean velocity and the wire diameter). The value of the exponent varies from 0.45 to 0.52 [43,44,45] but, generally, a square-root law, i.e., the so-called King's law, is employed [43,45,46]. Whenever the fluctuating velocities in the y- and z-directions are negligible with respect to the instantaneous velocity normal to the wire $(\overline{U} + u)$, the relationship between the total voltage drop across the wire and the velocity is

$$(\overline{E} + e)^2 = E_o^2 + A(\overline{U} + u)^{\frac{1}{2}}, \tag{5.1}$$

where u is the velocity fluctuation parallel to the mean velocity $\overline{U}$, and the overbar denotes time-averaged (mean) value. The voltage in still air (at zero velocity or shielded sensor), which is a constant under the selected operating conditions, is designated by E_o. In Eq. (5.1) $\overline{E}$ stands for the time-averaged voltage (DC) necessary to balance the bridge under steady conditions which is proportional to the mean velocity $\overline{U}$. The instantaneous voltage (AC) arising from the fluctuating velocity u is denoted by e. The constant A is experimentally determined from the calibration of each particular wire. Its value depends on wire configuration and material and is affected by air properties. Furthermore, both E_o and A depend upon the resistance ratio of the bridge $N = R_w/R_{wco}$, viz., the ratio of the heated wire resistance under working condition R_w to its cold resistance in still air R_{wco}.

Under the assumption of small fluctuations, i.e., $u/\overline{U} << 1$ and, hence, $e/\overline{E} << 1$, the higher order terms in the binomial expansion of

$(\overline{E} + e)^2$ and $(\overline{U} + u)^{\frac{1}{2}}$ can be neglected. Next, after some manipulations, the turbulence intensity, which is commonly defined as $u_{rms}/\overline{U}$, is given by

$$\frac{u_{rms}}{\overline{U}} = 4M \frac{e_{rms}}{\overline{E}} , \tag{5.2}$$

where [46]

$$M = 1/[1 - 1/(1 + m)^2]. \tag{5.3}$$

The flow factor due to the voltage drop is

$$m = \Delta\overline{E}/E_o, \tag{5.4}$$

in which the DC voltage drop $\Delta\overline{E} = (\overline{E} - E_o)$. The subscript rms designates square-root of mean (time-averaged) square values, i.e., $(\overline{u^2})^{\frac{1}{2}}$ and $(\overline{e^2})^{\frac{1}{2}}$. In addition to the condition of small fluctuations, the mean velocity must be high enough such that $m \geq 0.2$ for Eq. (5.2) to be valid [46]. Otherwise the coefficient M becomes very large since $M \to \infty$ as $m \to 0$. In this experiment the velocity range of interest was up to about 10.1 m/s (≈33.1 ft/s), the value of m ranged from 0.22 to 0.39, and the longitudinal turbulence intensity varied up to about 30%. The level of fluctuating signal (AC) was consistently about ten times smaller than the DC component $(\Delta\overline{E})$ throughout all measurements. Representative values for all five probes are listed in Appendix II.

5.3 Hot-wire anemometer measuring system

The hot-wire anemometer utilized in this work is a novel constant-temperature system conceived, designed and built at the Fluid Dynamics and Diffusion Laboratory, Colorado State University [47]. Commercially available hot-wire anemometer units could not be employed since they are commonly designed for a specific length of the cables connecting the sensor to the bridge of the system. This results from the need to account for the leads' resistance when measuring the wire resistance and balancing the Wheatstone bridge of the anemometer under both cold and hot conditions. The cables' length is usually limited to about 6 to 9 m (20 to 30 ft). Moreover, the noise level of available units is relatively high, viz., more than a few millivolts rms, and increases significantly with the leads' length. In addition, the frequency response is drastically affected and reduced by long cables.

To overcome the shortcomings of limited cables' length a three-lead bridge system was devised for the CSU hot-wire anemometer [48]. In this system the sensor, which is an arm of the bridge, is connected to the bridge by means of three leads. This new design permits efficient remote use of a hot-wire anemometer, which is of prime importance in atmospheric measurements. The length of the leads connecting the sensor to the unit can be in excess of 150 m (492 ft). The three-lead bridge balance is independent of the cables' length and, thus, of their resistance. Consequently, the balance of the bridge and the noise level of the unit are unaffected by the leads. The frequency response is only slightly affected by the cables' length, viz., it is diminished by about 20 to 30%.

The CSU constant-temperature hot-wire anemometer is based on a new dual-amplifier concept [47]. In addition to the commonly used feedback amplifier, a second operational amplifier is employed to control the current through the bridge. This current amplifier insures a high stability and extremely low noise. The drift in the value of the output signal is less than 1% over about 100 h of continuous operation. In this experiment the noise of the anemometer with cables of 150 m length ranged from 350 to 750 μV rms. The AC signal proportional to the fluctuating velocity was of the order of 40 to 60 mV rms and thus, the signal-to-noise ratio (S/N) varied from 53 to 171. The fluctuating velocity can be measured with a resolution better than 0.5% of the mean velocity. With 150 m length of cables the frequency response of the unit is about 70 to 80 kHz.

Furthermore, the CSU hot-wire anemometer unit is a versatile system with several important built-in signal conditioning capabilities. Two ranges of wire resistance R_{wco}, up to 10 Ω and from 10 to 50 Ω are provided. This permits the use of a great variety of sensors and a wide range of resistance ratios. Within the 10 Ω range the wire resistance can be measured with a resolution of 0.005 Ω, whereas beyond 10 Ω the resolution is 0.025 Ω. To control the hot-wire sensitivity, the bridge resistance ratio N (or overheat ratio) can be set at any desired value within the foregoing two resistance ranges. Either the voltage across the bridge or the current flowing through it are displayed on the unit's digital panel meter (DPM) with an accuracy of 1 mV and 0.1 mA, respectively. The value of the signal displayed on the DPM is proportional to the instantaneous velocity and can be held at any instant to permit easier reading. Moreover, the displayed voltage can be time integrated over periods of 5, 10 and 20 s supplying a better value for $\overline{E} \sim \overline{U}$.

The hot-wire anemometer unit possesses identical front and rear output channels, each capable of operating independently of the other. This allows different operations to be performed simultaneously on the output signal. Each output channel is equipped with identical variable low-pass filter and amplifier. Both can be varied in steps from 1 to 50 kHz for the former and from 1 to a gain of 100 for the latter. Time averaging of the rear output signal can be performed over periods of 10, 20 and 30 s by means of a built-in averaging circuit. Thereby, on-line recording of the DC signal proportional to the mean velocity can be carried out. By means of independent suppression networks the DC level of both output channels can be adjusted to any desired value between the zero-velocity voltage E_o and the total output voltage $E = E_o + \Delta E$. It is generally efficient to suppress the still-air voltage E_o and, hence, measure the voltage drop caused by the flow, i.e., $\Delta E = E - E_o = \Delta\overline{E} + e$. Consequently, the resolution and accuracy of the measurement of the output voltage are greatly improved. Higher amplifications of the suppressed signals are readily achievable. This feature is of particular significance when the output signals are recorded on magnetic tape and analyzed employing other instrumentation. All the performances of the hot-wire anemometer system, i.e., frequency response, filter cutoff, gain, time averaging, S/N, can be easily checked on-line using a sine wave and DC test signals. A general view of the CSU constant-temperature hot-wire anemometer unit is provided by Fig. 5.2.

The signals ΔE generated by the array of five hot-wire anemometers used in this experiment were recorded simultaneously on magnetic tape. A threefold amplification, i.e., a gain $G_H = 3$, was applied to all signals. Additionally, a 1 kHz low-pass filter was continuously employed to cut off extraneous RF waves which were occasionally inducted into the long cables. In connection with the hot-wire anemometer measuring system, an Analog Data Acquisition System (ADAS) was employed for data collection, recording, preparation, qualification, reduction and analysis. This ADAS consisted of the following equipment:

(1) An FM magnetic tape recording system (Ampex Corp., Portable Magnetic Tape Recorder/Reproducer, Model CP-100, see Sect. 5.4) for simultaneous recording of signals from the five hot-wire array for future analysis;

(2) An analog correlator system (Princeton Applied Research Corp., Correlation Function Computer, Model 101A, see Sect. 5.5) for preliminary on-line and subsequent detailed autocorrelation analysis of the output signals;

(3) A wave analyzer (General Radio Corp., Sound and Vibration Analyzer, Type 1564-A) for on-line frequency spectral analysis;

(4) Four dual-beam oscilloscopes (Tektronix Inc., Model 502A) for quick assessment of the output signals from the array of five hot wires and for monitoring their simultaneous recording on magnetic tape;

(5) Two oscilloscope cameras (Tektronix Inc., Model C-12) for obtaining oscillograms of the turbulent signals;

(6) Two true root-mean-square meters (Ballantine Laboratories Inc., Model 320A) for measurement of rms values;

(7) A digital DC voltmeter (Hewlett-Packard Co., Model 3440A) for monitoring the DC output voltages;

(8) A function generator (Hewlett-Packard Co., Variable Phase Function Generator, Model 203A) for check-out of the hot-wire anemometer unit;

(9) A DC voltage supply (Electronic Development Corp., Precision DC Voltage Standard, Model VS-11-R) for check-out of the hot-wire anemometer unit.

A block diagram of the hot-wire anemometer measuring system, i.e., the hot-wire anemometer unit and the ADAS, is portrayed in Fig. 5.3. An overall view of the ADAS is provided by Fig. 5.4.

A copper-plated tungsten wire of 0.0089 mm (0.00035 in) diameter and of about 1 mm (0.04 in) length was used (Flow Corp., Hot-Wire Filament, Type W3). Its aspect ratio, the ratio of its length to diameter ℓ/d, was approximately 110. Single wire probes were used throughout the experiment, with the sensor mounted normal to the probe axis (Flow Corp., Probe, Type B-1-C).

Calibration of the hot wire was performed utilizing a standard calibrator (Thermo-Systems Inc., Calibrator, Model 1125). Before every run the wire was cleaned using a concentrated cleaning solution of potassium chromate and sulfuric acid ($K_3CrO_4 + H_2SO_4$). A bottle of compressed dry air maintained at ambient temperature was available at the field site to permit calibration before and after each run. The auxiliary calibration system is included in the block diagram shown in Fig. 5.3. The pressure drop across the calibrator nozzle was measured using an electronic pressure meter (Trans-Sonic Inc., Equibar Pressure Meter, Type 120A). In connection with the calibration, the ambient temperature and barometric pressure were continuously monitored by means of a mercury thermometer (Van Waters & Rogers, Type 61001-044) and an aneroid barometer (Friez Instruments Div., Bendix Aviation Corp., Cat. No. 620). A sample of the kind of calibration curves obtained is displayed in Fig. 5.5. Within the velocity range of interest it was found that the ½-power law was reasonably satisfied.

5.4 Data recording

In this experiment, as previously mentioned, the signals from the array of five hot-wire anemometers were continuously and simultaneously recorded and stored on magnetic tape. The recording was imperative to enable further reduction of the data and, particularly, to permit the autocorrelation analysis. A versatile analog tape recorder (Ampex Corp., Portable Instrumentation Magnetic Tape Recorder/Reproducer, Model CP-100) was utilized to record the total instantaneous voltage drop $\Delta E = \Delta\overline{E} + e$ generated by each of the five hot-wire anemometers. The recording was performed using a 1 in wide tape, i.e., 14-track tape. Frequency modulation (FM) recording was employed since this procedure is particularly adequate for low-speed turbulence data. The FM process is characterized by its capability to record low frequency signals, by its low noise, viz., S/N greater than 40 dB, and, moreover, possesses the ability to record DC voltages.

In FM recording procedure the frequency of a constant amplitude carrier wave is varied (or modulated) in accordance with variations of the input data signal (the modulating or information-bearing signal). The carrier is commonly a square wave of a frequency f_c, called the center carrier frequency, larger than the maximum frequency of the data signal f_m. In response to the instantaneous voltage value of the modulating signal, the instantaneous frequency of the modulated signal deviates linearly about the center carrier frequency within a deviation frequency range Δf. A DC input signal augments or diminishes the center carrier frequency depending upon its polarity and directly proportional to its magnitude. A zero input signal yields a modulated signal of exactly same frequency as of the carrier. An AC modulating signal alternately increases and decreases the center carrier frequency at a rate equal to its frequency. Commonly, a modulated signal bandwidth extending from 0.6 to 1.4 f_c, i.e., $\mp 40\%$ maximum deviation of the center carrier frequency f_c, is used [49]. The rms value of the input signal amplitude yielding a peak 40% frequency deviation, i.e., the 40% deviation voltage, can be adjusted to any desired value within a range from 0.7 to 10 V rms [49]. Thus, the modulated signal is a square wave of continuous varying width. Its amplitude is exactly equal to that of the carrier since the frequency-modulated signal is recorded at saturation.

Determination of the FM recording center carrier frequency f_c and tape speed S depends upon knowledge of the maximum frequency of interest of the input data signal f_m. The center carrier frequency f_c and the nominal data bandwidth B, i.e., the bandwidth of the information-bearing signal which is recorded and reproduced, are interrelated according to the specified IRIG standards [49,50]. Elimination of undesired interferences between the highest frequency of the data signal f_m and the lowest deviation frequency $0.6f_c$ is achieved when a frequency interval greater than about 1.5 octaves ($0.6f_c/f_m > 2.83$) is provided [49,50,51]. Furthermore, faithful demodulation, i.e., reproduction of the input signal, is ensured when the bandwidth of the modulated signal $2\Delta f$ is, at the least, four times larger than the bandwidth of the data signal f_m [51].

A preliminary discrete spectral analysis of the signals generated by the array of hot-wire anemometers was conducted using a wave analyzer (General Radio Corp., Sound and Vibration Analyzer, Type 1564-A) to ascertain their maximum frequencies of interest. It was found that the turbulent energy for all the signals at frequencies beyond 500 Hz was insignificant, viz., less than 1% of the total energy. Moreover, the energy spectrum up to 250 Hz contained, in all cases, more than 95% of the total energy, i.e., $f_m = 250$ Hz. Consequently, a nominal data bandwidth $B = 625$ Hz was selected to warrant reliable recording. The recording was carried out using the standard narrow band mode and, hence, the corresponding center carrier frequency f_c was 3375 Hz [49,50]. Once f_c is determined, the tape speed S is uniquely established. The former in kHz is equal to 0.9 of the latter in ips (inches per second) for the narrow band FM recording employed [49,50, 51] and, hence, a tape speed $S = 3\text{-}3/4$ ips was used. Since the tape speed of the recorder can be varied in six steps from 1-7/8 to 60 ips, playback at higher speeds allows analysis of very-low frequency signals. Note that the frequency transformation is directly proportional to the change in tape speed. The center carrier frequency was 2.44 octaves higher than the nominal data bandwidth, i.e., $f_c/B = 5.4$, and the bandwidth of the modulated signal extended from 2025 to 4725 Hz, i.e., $\mp$ 40% deviation frequencies. Thus, the lowest frequency deviation was 1.7 octaves larger than B, viz., $0.6f_c/B = 3.24$. Moreover, the bandwidth of the modulated signal $2\Delta f$ was 4.32 times the nominal data bandwidth. The modulation index, i.e., the ratio of the maximum deviation frequency to the highest modulating frequency $m_f = \Delta f/B$, was 2.16. For this particular value the S/N is greater than for other values of m_f [41]. The recorder was adjusted for a 40% deviation of 1 V rms. Thus, an instantaneous input amplitude of 1.414 V yielded a maximum frequency deviation of either $1.4f_c$ or $0.6f_c$ depending upon its polarity. A check of the linear dependence of both modulation and demodulation upon the data signal amplitude revealed that it was within 1.5% up to 1.414 V rms, i.e., 56% deviation frequency. Consequently, the input voltage was maintained at a level lower than or equal to 1.414 V rms which corresponds to an instantaneous 2 V peak.

To efficiently carry out the recording, it was necessary to consistently suppress the hot-wire anemometer output signal at zero velocity E_o which varied from 1.5 to 2 V. This suppression was performed by means of the anemometer unit's built-in suppression network. Subsequently, the total voltage drop due to the flow ΔE, which generally ranged from 0.4 to 0.65 V, was continuously amplified three times, as previously mentioned, using the anemometers built-in output amplifier ($G_H = 3$). Thus, the instantaneous amplitude of the conditioned input signal ranged from 1.2 to 1.95 V, and its rms value varied roughly from 0.85 to 1.38 V. In most cases the input signal was of same polarity and, hence, frequency deviation above the center carrier resulted. The level of the hot-wire anemometers' fluctuating signals (AC) was generally between 40 and 60 mV rms. Due to the threefold amplification ($G_H = 3$) and since the noise level of the recorder was about 350 μV rms, the recording S/N was greater than 50 dB, i.e., larger than 340 times.

It was important to record the voltage time history of the signals produced by the hot-wire anemometers over sufficiently long time interval to permit data editing, preparation, qualification and, particularly, adequate analysis. Data editing refers to pre-analysis procedures designed to detect and eliminate spurious and/or degraded signals. Such signals may result from acquisition and recording problems, e.g., excessive noise, signal dropout and malfunctions of the transducers. Data preparation involves conversion of the electrical signal into engineering units, i.e., calibration, and formation of data loops for continuous analog display.

The record length is of considerable significance in relation to data qualifications and subsequent analysis. Evaluation of the stationarity of the random data and generation of an equivalent ensemble are strongly affected by the available sample record length T_{ra}. The data analysis and interpretation of the results depend upon the averaging time T required to compute the various statistical parameter estimates. Usually the averaging time is smaller than or equal to the sample record length. It is desirable to select a sample record length such that the computed statistical averaged parameters are within acceptable confidence levels. The formulas relating their normalized standard errors (rms errors) to the averaging time T and the finite bandwidth of the data include factors which are unknown prior to data collection [41]. Furthermore, these error equations are based on the assumption of Gaussian (normal) data with zero mean. Consequently, they provide solely a first order rough approximation for the averaging time. Since the autocorrelation analysis was of primary interest, the normalized mean-square error for the autocorrelation was employed to obtain a guideline for estimating the necessary averaging time. This error is given by [41]

$$\varepsilon_R^2 = (1 + \alpha^{-2})/2BT, \tag{5.5}$$

in which B is the nominal bandwidth and T stands for the averaging time. The ratio of the smallest amplitude of the autocorrelation $R(\tau)$ to be resolved (τ is the time delay) to its maximum value $R(0)$ (the mean-square value) is designated by the resolution coefficient α, i.e., $\alpha = R(\tau)/R(0)$. Notice that the error equation for the autocorrelation involves only a random error term since the bias error vanishes whenever the record length $T_r \geq T + \tau$. Assuming a desired resolution coefficient $\alpha = 0.02$ and a normalized standard error $\varepsilon_R = 0.1$, the required averaging time $T = 200$ and 500 s when $B = 625$ and 250 Hz, respectively. To account for the uncertainties in the estimation of the averaging time, since it is not feasible to assume a priori a normal distribution, a longer sample record is desirable. In addition, a relatively long record is necessary to permit the generation of an equivalent ensemble. As a result, sample records of $T_{ra} = 1$ h were employed.

The signal on each track was identified by means of voice and frequency coded headers. The pertinent information, i.e., date, probe position and test conditions, was recorded utilizing a microphone and function generator (Hewlett-Packard Co., Variable Phase Function Generator Model 203A). A 100 Hz frequency sine wave of 1 V peak (0.707 V rms) was recorded on each track to be used as an amplitude calibration signal. Additionally, the sine wave was also recorded continuously throughout each run on a separate track to supply a time base signal. The gain of each track $G_T = 1/A$, where A is the amplitude of the calibration sine wave after reproduction. The values of G_T which varied slightly with the track being used from 0.83 to 1.03 are presented in Appendix II.

In conjunction with the calibration of the tape recorder and subsequent data recording and analysis, the following additional equipment was employed:

(1) A standard tape recorder calibrator (Ampex Corp., FM Calibration Unit, Model (TC-10) for calibrating the recording and reproducing amplifiers of the tape recorder;

(2) A digital DC voltmeter (Hewlett-Packard Co., Model 3440A) for measuring DC voltages;

(3) A frequency counter (Computer Measurements Co., Universal Counter-Timer, Model 726C) for measuring calibration frequencies;

(4) A microphone for voice recording of an identification header;

(5) A DC voltage supply (Electronic Development Corp., Precision DC Voltage Standard, Model VS-11-R) for checking the linearity of the recording and reproducing amplifiers;

(6) Four dual-beam oscilloscopes (Tektronix Inc., Model 502A) for calibration and for data monitoring during recording and reproducing;

(7) An analog correlator system (Princeton Applied Research Corp., Correlation Function Computer, Model 101A, see Sect. 5.5) for extensive autocorrelation analysis;

(8) Five strip chart recorders (F. L. Moseley Co., Autograf Strip Chart Recorder, Model 680) for hard-copy recording of mean and mean-square values;

(9) Two true root-mean-square meters (Ballantine Laboratories Inc., Model 320A) for measuring rms and mean-square values;

(10) An integrator (Princeton Applied Research Corp., Operational Amplifier Unit, Model 215) for time integration of mean and mean-square values.

A block diagram of the tape recorder system, incorporating its calibration system, is depicted in Fig. 5.6.

5.5 Autocorrelation computation

The autocorrelations of the signals generated by the array of five hot-wire anemometers were computed employing a hybrid correlation function analyzer, which will be called a CFA for convenience (Princeton Applied Research Corp., Correlation Function Computer, Model 101A [52]). Under the assumption of small velocity fluctuations, i.e., $u \sim e$, the turbulent velocity autocorrelation coefficient (or the normalized autocorrelation function) is

$$\tilde{R}(\tau) = \overline{e(t)e(t-\tau)}/\overline{e^2(t)}, \tag{5.6}$$

in which $e(t)$ is the instantaneous fluctuating AC voltage arising from the fluctuating velocity $u(t)$, and the overbar designates time-averaged values. The fluctuating signal delayed by time τ is $e(t-\tau)$, and $\overline{e^2(t)}$ stands for the mean-square value of the signal which is proportional to the autocorrelation at zero-time delay. Note that $\overline{e(t)e(t-\tau)} = \overline{e(t)e(t+\tau)}$ whenever $e(t)$ is a stationary signal [41]. It is further, important to remark that the autocorrelation is equal to the autocovariance since the turbulent velocity possesses zero mean.

Computation of the autocorrelations were performed using the signals recorded on FM magnetic tape. Since the anemometer total voltage drop $\Delta E = \Delta\overline{E} + e$ was recorded, it was necessary to suppress its DC component $\Delta\overline{E}$ proportional to the mean velocity $\overline{U}$. This suppression was achieved by utilizing the CFA in its AC coupling mode, which is equipped with a high-pass filter whose cutoff frequency is 0.32 Hz. Any smaller frequency components were assumed to pertain to the DC signal and, therefore, were disregarded. Moreover, since the AC component was roughly ten times smaller than the DC signal, the suppression of the latter allowed the use of the full dynamic range of the CFA input amplifier.

Estimation of the autocorrelation was accomplished by digitally sampling the input signal which is to be delayed, delaying the samples within a computation period time, multiplying the delayed samples by the original input signal and averaging the lagged products in an RC integrator. The signal to be delayed was fed to channel A of the CFA where it underwent adequate digitization. Simultaneously, the input signal was supplied to channel B for further multiplication. An identical gain $G_C = 5$ was applied to both channels to ensure a high S/N. The output noise N (rms) of the CFA is constant at fixed values of the computation period time and RC time constant. Thus, the CFA output signal $E_c(\tau)$ can be readily corrected for the noise by simply subtracting it. At the completion of the computation the output signal

$E_c(\tau)$ is directly proportional to the turbulent velocity autocorrelation since

$$E_c(\tau) = G\ \overline{e(t)e(t-\tau)}, \tag{5.7}$$

in which the overall gain

$$G = \frac{1}{C}\ (G_C\ G_F\ G_T\ G_H)^2\ , \tag{5.8}$$

where $G_C = 5$ and $G_H = 3$ are the CFA and hot-wire anemometer gains, respectively. The values of the tape recorder gain G_T, which varied slightly with the track being used, are listed in Appendix II, as previously mentioned. A low-pass filter (Spencer Kennedy Laboratories Inc., Variable Electronic Filter, Model 308A) was employed to cut off undesired high frequency components of the signal prior to supplying it to the CFA. The filter attenuation $G_F = 0.61$. The CFA internally derived calibration constant whose value is 1 V is designated by C. A flow diagram of the signal in accordance with Eq. (5.7) is provided by Fig. 5.7. Substitution of Eq. (5.7) into Eq. (5.6) yields the autocorrelation coefficient in terms of the CFA output signal

$$\tilde{R}(\tau) = E_c(\tau)/E_c(0), \tag{5.9}$$

where at $\tau = 0$ the output signal of the CFA is

$$E_c(0) = G\ \overline{e^2(t)}, \tag{5.10}$$

in which G is the overall gain.

The sampling interval h provided by the CFA is

$$h = T_p/100, \tag{5.11}$$

where T_p is the computation period base time which is adjustable in steps from 50 μs to 10 s in 1, 2, 5 sequence. Then, the sampling frequency (sampling rate) is

$$f_s = 100/T_p, \qquad (5.12)$$

which can be varied from 10 Hz to 2 MHz. Proper sampling is ensured when the samples contain all the information of the original signal up to its highest frequency of interest f_m. In other words, it is imperative to avoid aliasing (folding). This was achieved by selecting a sampling frequency twice the maximum frequency of interest of the signal [41,53]. The latter, which is the cutoff frequency, is called Nyquist or folding frequency. A sampling frequency $f_s = 500$ Hz was employed since for all signals the maximum significant frequency f_m was 250 Hz. Then, from Eqs. (5.12) and (5.11) the computation period base time and the sampling interval were 200 and 2 ms, respectively. The nominal data bandwidth B of the recorded signals was 625 Hz. Cutoff of information above the maximum frequency of significant data, i.e., at frequencies $f > f_m = 250$ Hz, was performed by filtering the input signals utilizing the previously mentioned low-pass filter.

Calculation of the output signal $E_c(\tau) \sim R(\tau)$ over averaging time T

$$E_c(\tau) = \frac{G}{T}\int_0^T e(t)e(t-\tau)\,dt \qquad (5.13)$$

was carried out in the continuous scan lag time method [41]. This procedure produces a continuous autocorrelogram when RC averaging is employed. The scan rate is automatically adjusted for a lag time resolution (or increment) $\Delta\tau$ equal to the sampling interval h. For this purpose the channel A digitized signal is time shifted in the computer shift register throughout 100 incrementally increasing time delays τ with same resolution $\Delta\tau$, i.e., $\tau_i = i\Delta\tau$ where $i = 0$ to 99 and $\Delta\tau = 2$ ms. In other words, each digitized sample is consecutively shifted in real time from the initial zero lag time to the final time delay. Thus, the computation extends from $\tau = 0$ to $\tau_p = 0.99T_p$. The total time displacement is equal to the computation period base time T_p. At all 100 time delays the autocorrelation is computed concurrently since the CFA is a multiple lag time correlator. As a result, the analysis time T_s required to obtain the autocorrelation within a computation base time is effectively equal to the averaging time T.

It is, further, important to obtain the autocorrelation over a sufficiently long time delay to observe its rate of decrease and, particularly, how its value approaches zero asymptotically. This is of considerable significance for the computation of the exchange coefficient. The time delay range was stretched beyond one single computation period time, i.e., beyond $\tau_p = 0.99T_p$, utilizing the pre-computation period mode of the CFA. In this mode time displacements varying from T_p to a maximum of $19T_p$ can be piecewise added to the computation period base time T_p. This is accomplished by using an additional shift register inserted between the sampler and computer shift register. The computation, moreover, can be started at any fractional delay $T_p/4$ within a computation period base. These fractional time delays can be added to any computation period base. Therefore, the computation can be extended from zero lag time up to a time delay $\tau = \tau_p + (n + 0.25m)T_p$ where n and m vary in steps from 0 to 19 and 0 to 3, respectively. The piecewise computation of the autocorrelation is then achieved by adequate matching of the resulting segments. The matching is further facilitated by the availability of the fractional time delays. It was found that an acceptable picture of the autocorrelation variation including its vanishing behavior was obtained using a total time delay of 3 s. Hence, the piecewise computation was carried out employing 15 equal computation periods T_p of 200 ms each. The estimation of the autocorrelation for each piece was performed in the very same manner.

At all 100 lag times (or points) within each segment the autocorrelation integrand, i.e., $e(t)e(t-i\Delta\tau)$ where $i = 0$ to 99, was evaluated in the same way. Multiplication of the time delayed signal (digitized channel A signal) with the original undelayed input signal (channel B signal) is carried out automatically. Due to quantizer and sampler circuitries the digitized signal is consistently delayed by additional 15 ns to provide the necessary isolation between them. Practically, this built-in delay is completely negligible since the sampling interval (or lag time increment) was 2 ms. The lagged products are averaged in the 100 RC integrators of same time constant K, i.e., $K = RC$. Simultaneously, the RC networks act as low-pass filters with a time constant K smoothing out fluctuations in the instantaneous value of the output signal $E_c(\tau)$.

All the operations involved in computing the autocorrelation at all 100 points within each computation period T_p are performed concurrently in real time. Consequently, the averaging time T, the analysis time T_s and the needed sample record length T_r depend upon the time constant K of the RC integrator. The analysis time, as mentioned earlier, is equal to the averaging time utilized for each computation period (or segment). Since the complete autocorrelation was obtained by piecewise addition of 15 segments, the total analysis time $T_s = 15T$.

An RC averaging network responds fully yielding an unbiased estimation of the integrated signal when the averaging time $T = 4$ to 5 K and $T_r > K$ [41]. Basically, the averaging time T indicates the required time length over which the signal can be assumed self-stationary. Whenever the autocorrelation of a single sample record of a random process does not exhibit significant changes with increasing averaging time, it can be inferred that the signal is weakly self-stationary. Such a signal can be only a realization of an ergodic process and, thus, necessarily of a stationary process.

To start with, an averaging time of 500 s was estimated using Eq. (5.5) when $f_m = 250$ Hz. Then, the minimum value of K was 100 s. The normalized rms error ε_R, which is given by Eq. (5.5), decreases with increasing averaging time T and, hence, with larger K. The former is simply a multiple of the latter, i.e., $T = nK$. On the other hand, the largest possible value of K is affected by the used sample record length T_r. To a first approximation, the sample record length T_r was assumed to be equal to the averaging time T. Thus, $T/5 \leq K < T_r = T$ which yields $100 \text{ s} \leq K < 500 \text{ s}$. Since no optimum value of K can be readily assessed, it was imperative to estimate it empirically within the foregoing bounds. This was effectively attained by examining the variation of the CFA output signal at selected time delays τ_i as a function of the time constant and continuously increasing averaging time T, i.e., $E_c(\tau_i,K,T)$. At a specified value of lag time τ the fluctuations in the output signal diminished with augmenting time constant K. The elapsed averaging time corresponding to negligible fluctuations was, then, the time required to assume self-stationarity.

The output signal $E_c(\tau_i,K,T)$ was surveyed at two significant time delays for increasing averaging time T up to about 1800 s by recording it on a strip chart recorder. Note that the available record length T_{ra} was 3600 s. This survey was conducted at three selected values of time constant K within the previously mentioned limits, viz., at $K = 100$, 200 and 300 s. The time constant K of the CFA can be easily varied in steps from 0.1 to 400 s by simply changing the resistors of the RC networks. The autocorrelation at zero time delay is highly sensitive to the RC integrator time constant since it is proportional to the total turbulent kinetic energy $\overline{u^2}$. Consequently, the output signal at zero lag time $E_c(0,K,T)$ was examined. The variations of this signal with increasing averaging time at the three values of K are depicted in Fig. 5.8(a). It is, further, natural to inspect the output signal change, which is proportional to the autocorrelation variation, at relatively large values of the time delay. With increasing time delay the amplitude of the autocorrelation coefficient $\tilde{R}(\tau,K,T) = E_c(\tau,K,T)/\overline{E}_c(K)$, which is exactly the autocorrelation running resolution coefficient $\alpha(\tau,K,T)$ (see Sect. 5.4), diminishes. The fluctuations in amplitude of $\alpha(\tau,K,T)$ are proportional to the changes of the output signal at the particular time delay τ_i being considered $E_c(\tau_i,K,T)$ since $\overline{E}_c(K)$ is the mean value of the signal at zero time delay. It was found that $\alpha(\tau,K,T) < 0.02$ when $\tau = 184$ ms. This time delay corresponds to $0.9T_p$. Recall that for $\varepsilon_R = 0.1$ the required resolution coefficient is 0.02. The variations of the running resolution coefficient at this time delay $\alpha(184,K,T) = E_c(184,K,T)/\overline{E}_c(K)$ with augmenting averaging time at the same three time constants are portrayed in Fig. 5.8(b). In both Figs. 5.8(a) and 5.8(b) the averaging time in terms of multiples of the time constant K, i.e., $T/K = n$, is also shown.

To assess the best estimate for the time constant K and corresponding averaging time T a continuous standard deviation test was applied to the two representative signals, viz., $E_c(0,K,T)$ and $E_c(184,K,T)$. This check was performed for all three values of the time constant K with continuous increasing averaging time. The standard deviation test, practically, permits evaluation of the elapsing averaging time necessary to qualify the self-stationarity of the sample record. The normalized standard deviation is given by

$$\tilde{\sigma}_K(\tau,K) = \left\{ \frac{1}{N-1} \sum_{i=1}^{N} \left[\frac{E_c(\tau,K,T_i)}{\overline{E}_c(K)} - \frac{\overline{E}_c(\tau,K)}{\overline{E}_c(K)} \right]^2 \right\}^{\frac{1}{2}} , \tag{5.14}$$

where the mean value is

$$\overline{E}_c(\tau,K) = \frac{1}{N} \sum_{i=1}^{N} E_c(\tau,K,T_i) , \tag{5.15}$$

and $\overline{E}_c(K)$ is the mean value at zero time delay. The latter was utilized as the normalizing scale since it represents the total energy of the signal. Variations of the signal are of importance only when they are referred to its total energy. In Eq. (5.14) the terms $E_c(\tau,K,T)/\overline{E}_c(K)$ and $\overline{E}_c(\tau,K)/\overline{E}_c(K)$ are the running resolution coefficient $\alpha(\tau,K,T)$ and its mean value $\overline{\alpha}(\tau,K)$, respectively. It is, further, worthwhile to point out that Eq. (5.14) is an unbiased, efficient and consistent estimator for $\tilde{\sigma}_K(\tau,K)$ [41]. The computation of the normalized standard deviation was carried out employing 18 equally spaced values, i.e., N = 18, within continuous increasing averaging time in the confidence interval $4K \leq T \leq 6K$. In all cases, changes in the value of $\tilde{\sigma}_K(\tau,K)$ were completely negligible for $T > 6K$. Thus, in this averaging time range the RC network responded fully. Essentially, the $\tilde{\sigma}_K(\tau,K)$ must be smaller than the normalized standard error ε_R, which was assumed to be, at the most, 0.1 (see Sect. 5.4). The results of the normalized standard deviation test, for the sake of comparison, are summarized below:

τ (ms)		0	184	
K	$\overline{E}_c(K)$	$\tilde{\sigma}_K$	$\alpha(184,K)$	$\tilde{\sigma}_K$
(s)	(mV)			
100	223	0.041	0.010	0.024
200	223	0.036	0.004	0.014
300	194	0.022	0.016	0.009

A time constant $K = 300$ s was selected for the computation of the autocorrelation since the standard deviation was the smallest in this case. The confidence interval for the averaging time to meet the condition of self-stationarity ranged then from 1200 to 1800 s. An averaging time $T = 1200$ s ($T = 4K$) sufficed inasmuch as the level of significance of the autocorrelation measurement was not affected by its further increase. Then, the necessary sample record length $T_r = 1200$ s based on the assumption that it is equal to the averaging time T. The total analysis time required to obtain the entire autocorrelation, which extended over a time delay interval of 3 s was 18,000 s since 15 segments were needed. Recall that for each piece the analysis time is equal to the averaging time. It is worth mentioning that this averaging time enhances the goodness of the autocorrelation estimate. The normalized rms error based on Eq. (5.5) when $T =$ 1200 s, $B = 250$ Hz and for $\alpha = 0.02$ is 0.065. On the other hand, the standard deviation is only 0.022. Hence, both the efficiency and consistency of the estimator are significantly improved. In addition, the bias error is completely negligible for $T \geq 4K$ [41].

With the completion of the time averaging the output signal for each segment $E_c(\tau)$, whose time displacement stretched up to $T_p =$ 200 ms, is stored in the CFA 100-channel capacitive analog memory which is shown in Fig. 5.7. Each memory channel corresponds to a lag time (or a point) of the autocorrelation. Then, the signal is read out by sequential scanning of the memory. The read-out can be performed at three scanning rates, viz., fast, medium and slow, in either continuous or single sweep display modes. Within several sweeps the memory read-out is nondegrading permitting repetitive scanning of the signal. In addition, the scan can be stopped at any lag time τ_i to allow read-out of the output signal $E_c(\tau_i,K,T)$ of the corresponding memory channel as the averaging time increases. In this stop read-out mode the degradation of the signal is compensated for since the CFA is correlating continuously.

The output signal was read out in the following four modes: (1) displayed on an oscilloscope (Tektronix Inc., Model 502A) for on-line preliminary monitoring; (2) supplied to an X-Y recorder (Hewlett-Packard Co., Model 7035B) for obtaining hard copy of the autocorrelogram; (3) fed to a digital voltmeter (Hewlett-Packard Co., Model 3440A) for further digital recording; and, (4) furnished to a strip chart recorder (F.L. Moseley Co., Autograf Strip Chart Recorder, Model 680) for recording the signal at selected time delays with continuous increasing averaging time. These four read-out modes are illustrated in Fig. 5.9.

When the signal was monitored on the oscilloscope, the fast read-out rate in the continuous display mode was utilized. The time required to scan the entire memory was 50 ms since in the fast scan rate 2 points/ms are read out. Additional 10 ms are required to perform the built-in internal read-out logic.

To obtain hard copy of the autocorrelogram using an X-Y recorder, the slow read-out rate in the single sweep display mode was employed. The entire memory was scanned in 50 s since 2 points/s are read out in the slow rate. To carry out the read-out logic functions additional 10 s are needed. The X-Y recorder enabled immediate normalization of the output signal by its zero lag time value yielding directly the autocorrelation coefficient, viz., $\tilde{R}(\tau) = E_c(\tau)/E_c(0)$. This was accomplished by adjusting the recorder's vertical sensitivity for a full scale pen deflection when the first channel of the memory was scanned, i.e., at $\tau = 0$. Then, the 15 segments of the autocorrelation coefficient were pieced together. Since the output noise N of the CFA is constant for all lag times, it was easily subtracted prior to normalization and subsequent recording of the autocorrelogram. During the computation it was found that $E_c(0)/N$ was greater than 33.

Further analyses using the autocorrelation were contingent upon securing a listing of its amplitude at each time delay. For this purpose the signal was fed to a digital voltmeter. Subsequently, the digital output of the digital voltmeter was supplied to a digital recorder equipped with a paper tape (Hewlett-Packard Co., Model 562A). This digital read-out was carried out concurrently with the autocorrelogram recording. For a single autocorrelation 1500 values of its amplitude were printed on the paper tape since the autocorrelation, which extended over a time displacement of 3 s, consisted of 15 segments of 100 points (or lag times) each. In other words, the digital read-out of the entire autocorrelation was performed at a rate of 500 points/s. The values of the amplitude were obtained with an accuracy of four significant digits. In this case, similarly to the X-Y recording, the noise was accounted for by simply subtracting it from the value of the signal $E_c(\tau)$. The signals at $\tau = 0$ and 184 ms, which were employed in the standard deviation test, were obtained by reading them out in the stop mode and subsequent recording utilizing a strip chart recorder.

In connection with the autocorrelation computation system in addition to the previously mentioned instruments, the following auxiliary equipment was used:

(1) A FM magnetic tape recorder (Ampex Corp., Portable Magnetic Tape Recorder/Reproducer, Model CP-100) to provide the signals to the CFA;

(2) A dual beam oscilloscope (Tektronix Inc., Model 502A) for monitoring the reproduced signals from the tape recorder, and for CFA checkout and alignment;

(3) An oscilloscope camera (Tektronix Inc., Model C-12) to obtain oscillograms of the autocorrelograms;

(4) A function generator (Hewlett-Packard Co., Variable Phase Function Generator, Model 203A) to provide a calibration signal to the CFA;

(5) A frequency counter (Computer Measurements Co., Universal Counter-Timer, Model 726C) for CFA calibration and check-out;

(6) A digital DC voltmeter (Hewlett-Packard Co., Model 3440A) for CFA check-out and alignment.

A block diagram of the autocorrelation computation system, including its calibration system, is provided by Fig. 5.9.

5.6 Diffusion measurement

Computation of the turbulent momentum exchange coefficient K_M (eddy diffusivity) depends basically upon knowledge of the Lagrangian autocorrelation. The turbulent exchange coefficients (eddy transport or diffusivity coefficients) for other transferable quantities, e.g., K_C for mass and K_H for heat, can be subsequently deduced from the momentum eddy diffusivity K_M. These three turbulent exchange coefficients are generally different depending upon the stratification conditions. On the other hand, $K_M \approx K_C \approx K_H$ when the Richardson number of the flow is less than 0.1 [22,54]. Then the turbulent momentum exchange coefficient K_M is employed to evalute both mass and heat eddy diffusivity coefficients.

A diffusion experiment was carried out to substantiate the predicted concentrations of a gas based on the momentum eddy diffusivity. The gas diffusion experiment was accomplished by continuously emitting sulfur hexaflouride SF_6 from a point source located in the wake. Dosages of the tracer-air mixtures were collected simultaneously at five stations downstream of the gas release point. This experiment was performed under identical flow conditions and approximately same Richardson number (about 0.002) as those during the turbulence and mean velocity survey.

A sketch of the mass diffusion experiment arrangement is portrayed in Fig. 5.10. Five dosage collection points located at exactly same positions as the hot-wire probes were utilized (see Fig. 5.1). To avoid perturbations generated by the fan supporting structure and to minimize disturbances caused by the release of a gas tracer, the source was positioned midway between the fan and the first collection point. Thus, the source point was located on the fan centerline at x = 5R (7.6 m (25 ft)) from the fan. Along the centerline (mean wind direction or x-axis) of a continuous point-source generated plume, the downstream concentration χ is [7,10]

$$\chi \sim \frac{Q}{x(K_{Cy}K_{Cz})^{\frac{1}{2}}}, \tag{5.16}$$

in which Q is the source strength (or emission rate), x denotes the downwind distance, and K_{Cy}, K_{Cz} designate the turbulent mass exchange coefficients in the lateral and vertical direction. It is important to remark that Eq. (5.16) is based on assuming constant eddy diffusivities and, thus, provides only a rough representation of the concentration. The continuous point source strength Q of SF_6 necessary to produce an arbitrary concentration along the fan centerline was evaluated, to a first approximation, using the data on its diffusion reported Ref. 55. This approximation relied on the assumption that the eddy diffusivities are the same in both cases. This is supported, to some extent, inasmuch as the prevailing meteorological conditions were almost similar during these two experiments. The emission rate is then estimated by

$$Q_1 = Q_2 \frac{x_1}{x_2} \frac{\chi_1}{\chi_2} \quad , \tag{5.17}$$

where the subscripts 1 and 2 designate this experiment and the data presented in Ref. 55, respectively. For an assumed concentration χ_1 = 100 ppb (parts per billion) at x_1 = 7.6 m (25 ft) downwind of the source, and utilizing Q_2 = 2200 cm^3/s (0.0777 ft^3/s), x_2 = 650 m (2132 ft) and χ_2 = 14.2 ppb [55], an emission rate Q_1 = 182 cm^3/s (0.00643 ft^3/s) was approximated. In the light of the discrepancies between the predicted concentration by means of Eq. (5.17) and its measured value [7,55], it was decided to select a slightly larger emission rate. For convenience, a source strength Q_1 = 250 cm^3/s (0.0088 ft^3/s) was employed.

Sulfur hexaflouride SF_6 was selected as the gas tracer since it is easily separated by gas chromatography from other constituents of moist air and is highly sensitive to electron-capture detection [55]. Its background concentration, except near electrical power transformers, is generally smaller than 0.01 ppb [55] and, hence, it was negligible with respect to the expected concentration in the wake, viz., 100 ppb. Furthermore, SF_6 meets the characteristics sought for a gas tracer [56]. It is nontoxic, odorless, colorless even in relatively high concentrations, chemically and thermally stable, convenient to handle and dispense into air, and samples are readily collected. A bottle of compressed SF_6 maintained at ambient temperature was utilized for the continuous point source supply. Its emission rate Q was monitored by means of a flow meter (Fischer and Porter Co., Flowrator, Tube-B4-21-10, Float-BSVT-45). Polyethylene tubing (Imperial Eastman Corp., Poly Flow Thermoplastic Tubing, OD = 6.25 mm) was used for all connections of the point source and dosage collection points since its retention of SF_6 is insignificant. The dosages were collected by drawing in the tracer-air mixtures from the collection points through equal lengths of tubing into 4 ℓ (244 in^3) saran bags (Ansepec Co., Saran Plastic Sampling Bag). This was achieved by placing the saran bags in a vacuum chamber located outside of the wake. At a constant vacuum of 25.4 mm Hg (1 in Hg) applied to the chamber, the saran bags sucked the air mixture at a filling rate of about 2 mℓ/s (0.12 in^3/s). The vacuum was measured throughout the run by a pressure meter (Trans-Sonic Inc., Equibar Pressure Meter, Type 120A).

The SF_6 in each collection bag was essentially the mean concentration over the used filling time, i.e., time-averaged dosage. Since the collection of SF_6 was conducted under flow conditions similar to those during the turbulence measurement, a filling-averaging time equal to that utilized to meet the self-stationarity condition of the fluctuating velocity (see Sect. 5.5) was desired. Based on the autocorrelation measurement this averaging time was estimated to amount to 1200 s. Additional 125 s was required to draw in about 250 mℓ (15.25 in^3) of uncontaminated air initially present in the tubing. For convenience, a collection time of 1500 s was selected. During this time the volume of gas tracer-air mixture, i.e., contaminated air, sucked into the collection bags was 2750 mℓ (≈168 in^3). An additional volume of uncontaminated air of 250 mℓ (the tubing volume) was also drawn in. As a result, the sulfur hexaflouride concentration in the mixture was further diluted by 8%. To account for this dilution of the tracer-air mixture the SF_6 measured concentration was multiplied by a dilution correction factor of 1.09 (1/0.92).

The SF_6-air samples were analyzed by means of a gas-solid chromatograph (Hewlett-Packard Co., Research Chromatograph, Model 7620A [57]). This instrument separates the SF_6 from other constituents in the moist air and then detects its concentration. A small volume of the dosage was introduced into the chromatograph injection port where it was entrained by a carrier gas, i.e., the so-called mobile phase [57,58]. This phase consisted of a 5% methane and 95% argon mixture flowing at a rate of about 1 mℓ/s (≈0.06 in^3/s) [55,57]. Then the effluent, i.e., dosage and carrier gas, passes through two tubular columns in series which are 1 m (39.37 in) long and 3.175 mm (0.125 in) in diameter. These columns constitute the stationary phase. The first column, packed with silica gel, removed any moisture from the effluent [58,59]. Moreover, due to the adsorption of the carbon dioxide CO_2 and SF_6 onto the silica gel, their passage through the column is delayed with respect to the other sample constituents, viz., nitrogen N_2 and oxygen O_2. The second column, which was packed with activated charcoal, separated the SF_6 and the N_2 from the CO_2 and O_2, respectively. By means of this differential adsorption process, it was found that the SF_6 emerged from the columns well separated from the other constituents after about 300 s.

A pulsed electron capture detector ECD (Hewlett-Packard Co., Tritium Electron Capture Detector, Model 7623A) was employed to measure the relative concentrations of the gases eluted from the columns. This ECD utilized a radioactive tritium foil emitting electrons (beta-radiations) as an electron source. When the sample constituent molecules pass between the ECD anode and cathode, they absorb (capture) free electrons from the system and, thereby, reduce the current flow. Both the ECD and stationary phase were maintained at a constant 150°C (302°F) temperature. A representative response of the electron capture detector to the constituent gases in the dosage is provided by Fig. 5.11. In the response curve the peaks indicate the detection of the eluted O_2, CO_2 and SF_6, respectively. Although nitrogen emerges from the stationary phase after O_2, it is not detected since N_2 cannot absorb additional electrons. A nitrogen atom possesses three unpaired electrons among the five in its outmost shell which form a very stable triple bond (three electron pairs) with a second nitrogen atom [60]. The area under the peaks in the response curve is proportional to each constituent concentration in ppm (parts per million). This area was computed on-line by employing a digital integrator (Infrotronics, Automatic Digital Integrator, Model CRS-208). The chromatograph was calibrated with known samples of SF_6. These samples were prepared employing a certified standard mixture of SF_6 in balanced air (Matheson Gas Products). This standard mixture which consisted of 103 ppm SF_6 concentration was further diluted in 1 ℓ (61 in^3) glass bottles down to the dosage levels obtained in the wake. A typical calibration curve of the ECD response to known SF_6 concentrations χ (in ppm) in air mixtures is displayed in Fig. 5.12.

6. EXPERIMENTAL RESULTS

The experimental investigation of the wake flow had the following main purposes:

(1) To substantiate the simulation of atmospheric turbulent flow under dry, stable conditions;

(2) To estimate the stationarity of a random turbulent velocity signal;

(3) To obtain an insight into the properties of the turbulence along a turbulence line based on a set of Eulerian autocorrelations;

(4) To deduce the Lagrangian autocorrelation from an Eulerian autocorrelation set;

(5) To estimate the turbulent momentum exchange coefficient and the mass diffusion of a gas tracer.

The system of coordinates used in the presentation of the results is portrayed in Fig. 5.1. Its origin is at the geometrical center of the fan. Whenever suitable the results are presented in dimensionless form for generality. Dimensionless variables are denoted by a tilde. The dimensionless x- and z-coordinates are defined by

$$\tilde{x}, \tilde{z} = x/R, z/R, \tag{6.1}$$

where $R = 1.52$ m (5 ft) is the fan radius. Under all conditions the longitudinal turbulent velocity possesses generally considerable more energy than the other two components [22]. Consequently, the turbulence measurement concentrated on the axial turbulent velocity $u(t)$. All measurements were performed along the fan wake centerline within the turbulence measurement range which extended from $\tilde{x} = 10$ to 14 (15.20 to 21.28 m (50 to 70 ft)) as shown in Fig. 5.1. This centerline, whose elevation above the ground was $h = 3.04$ m (10 ft), defined the x-axis of the wake. Basically, the turbulence measurement range can be viewed as a turbulence "line" within the turbulence box outlined in Fig. 3.6. The angular speed N of the fan was maintained at 315 rpm and, hence, the corresponding constant rotor tip velocity $U_t = (2\pi N/60)R$ was 50.1 m/s (164 ft/s). As the experimental results are presented below, relevant discussions are interspersed whenever it is deemed helpful for the proper interpretation of the results.

6.1 Simulation of atmospheric flow

Turbulent atmospheric flow in the extreme lower layer of the atmosphere, which extends roughly up to about 5 m (16.4 ft) above the ground, was simulated by utilizing the wake flow produced by an adequate fan as described in Sect. 4. The simulation depends essentially upon fulfillment of dynamic similarity. In other words the wake flow bulk turbulent Reynolds number must be of the order of 10^6. This characteristic turbulent Reynolds number is based on mean wind velocity and size (or scale) of the largest eddy which can be sustained within the extreme lower atmosphere. In addition, the subsistence of turbulence under stable conditions is ensured when the Richardson number is positive and less than 0.2 [7,22].

Measurements were conducted during autumn and winter seasons in early morning under dry and almost calm conditions, i.e., ambient wind not exceeding about 1 m/s (≈2 mph). In all cases, the surface was either grassland or approximately 0.3 m (1 ft) of snow packed cover. The roughness effect of both these surfaces are nearly the same [61]. A morning base temperature inversion prevailed daily at the field site and, thus, the runs were carried out under stable conditions. The ambient temperature θ at wake centerline height was 7.7°C (18°F). A sample of the monitored vertical temperature distribution is provided by Fig. 6.1.

6.1.1 *Mean velocity survey*

The axial mean velocity $\overline{U}$ along the wake x-axis was measured up to $\tilde{x} = 14$ downstream of the fan. During the measurements the hot wires were aligned normal to the longitudinal velocity for maximum sensitivity (see Sect. 5.2). Hereafter, the axial mean velocity is referred to the fan constant rotor tip velocity U_t used in this experiment. Thus, the dimensionless axial mean velocity is

$$\overline{U} = \tilde{\overline{U}}/U_t, \tag{6.2}$$

in which, as previously mentioned, $U_t = 50.1$ m/s (164 ft/s). The measured axial mean velocity distribution along the wake centerline, i.e., the turbulence line, is displayed in Fig. 6.2. Within the turbulence measurement range, which stretched from $\tilde{x} = 10$ to 14, $\tilde{\overline{U}}$ exhibited a decrease of about 18%. The fluctuations in the axial mean velocity are due to the unconfined wake of the fan. The space average of the mean velocity in this region was used to compute the bulk Reynolds and Richardson numbers. This characteristic mean velocity scale which accounted for the streamwise variation of the axial mean velocity is

$$U_c = \frac{1}{L} \int_{x_o}^{x_o+L} \overline{U}\, dx, \tag{6.3}$$

where $x_o = 10R$ and the turbulence measurement range is denoted by $L = (14\text{-}10)R$. It was found that $U_c = 7.12$ m/s (23.4 ft/s).

The bulk turbulent Reynolds number is defined as

$$Re = U_c \ell_m / \nu, \tag{6.4}$$

in which ℓ_m designates the largest turbulent eddy size (or scale) that can be sustained and the kinematic viscosity $\nu = 1.51 \times 10^{-5}$ m^2/s (1.63×10^{-4} ft^2/s). Within the wake the expected maximum eddy scale is at the least equal to the fan diameter and at the most of same magnitude as the thickness of the extreme lower atmospheric layer (see Sect. 4). In other words, it was assumed that ℓ_m ranged from about 3 to 5 m (9.84 to 16.4 ft). The bulk turbulent Reynolds number varied then from 1.41×10^6 to 2.35×10^6. It is thus apparent that *simulation of turbulent flow in the extreme lower layer of the atmosphere by means of the wake flow met the required dynamic similitude criterion.*

The bulk Richardson number, which is the ratio of buoyancy to inertia forces, is an index of flow stability and, moreover, indicates whether turbulence can be maintained. It is expressed by [22]

$$Ri = \frac{g}{\theta} \, \frac{d\theta}{dz} \Bigg/ \left(\frac{d\bar{U}}{dz}\right)^2, \tag{6.5}$$

where $\theta = 265°K$ ($\approx -8°C$) is the absolute ambient temperature and g denotes the gravitational acceleration (9.81 m/s^2(32.2 ft/s^2)). In the above equation, $d\theta/dz$ designates the vertical temperature gradient and $d\bar{U}/dz$ is the mean velocity shear. The vertical temperature and mean velocity gradients were approximated by their incremental forms $\Delta\theta/\Delta z$ and $\Delta\bar{U}/\Delta z$, respectively. Based on the vertical temperature distribution shown in Fig. 6.1, $\Delta\theta/\Delta z = 0.321°C/m$ (0.176°F/ft), where

Δz = 3.04 m (9.97 ft). The vertical mean velocity gradient was estimated using the mean velocity scale U_c and assuming a linear velocity shear with height. Hence, $\Delta\overline{U}/\Delta z = U_c/h = 2.34\ s^{-1}$, where h = 3.04 m (10 ft) is the height of the wake centerline above the ground. Consequently, Ri = 0.002. Since the bulk Richardson number was smaller than 0.2, *the turbulence can be sustained within the wake under the prevailing stable conditions.*

6.1.2 *Turbulence intensity survey*

Concurrently, with axial mean velocity survey the longitudinal fluctuating velocity was measured within the turbulence measurement range. i.e., along the turbulence line. An array of five hot-wire probes installed along the wake x-axis at $\tilde{x}$ = 10, 11, 12, 13 and 14 were utilized simultaneously (see Sect. 5.2). The turbulence intensity based on local mean velocity $\overline{U}$

$$Tu = u_{rms}/\overline{U} \ , \tag{6.6}$$

was calculated according to Eq. (5.2). In addition, the turbulence intensity referred to the characteristic mean velocity in this region

$$Tu_c = u_{rms}/U_c \ , \tag{6.7}$$

U_c = 7.12 m/s (23.4 ft/s) was also computed. The results are displayed in Fig. 6.3. A similar axial change is clearly discerned for both turbulence intensities. They exhibit relatively large values of 0.3 and 0.35, respectively, at the first station. These turbulence intensities gradually decrease around $\tilde{x}$ = 12 and they very slightly intensify as the other end of the turbulence measurement range is approached. The levels of the turbulence intensities for $\tilde{x}$ = 11 to 14 varies between 0.16 and 0.21. Next, the mean-square value of the longitudinal fluctuating velocity was computed from the turbulence-intensity data. Its axial variation is also portrayed in Fig. 6.3. The mean-square value of the fluctuating velocity is basically the local total turbulent kinetic energy (per unit mass). In this figure the mean-square value of the turbulent velocity was made dimensionless with respect to its value at the first station $\tilde{x}_o = 10$ in the turbulence measurement range

$$\overline{\tilde{u}^2} = \overline{u^2}/\overline{u_o^2} , \tag{6.8}$$

in which $\overline{u_o^2} = 6.25\ m^2/s^2$ ($67.2\ ft^2/s^2$). When $\overline{u^2}$ is normalized in this manner its relative changes can be easily discerned. The mean-square value of fluctuating velocity reveals a longitudinal behavior similar to those of the turbulence intensities. Essentially, the observed axial variation of the turbulence intensities and turbulent velocity are attributed to the unconfined nature of the fan wake flow. The distinct streamwise variation of the mean-square value (turbulent kinetic energy) of the axial turbulent velocity clearly indicates that *the nonhomogeneous nature of the turbulence along the turbulence line.* A similar change was found in a preliminary study using a small indoor fan [42]. The local turbulence intensity remained nearly constant beyond $\tilde{x} = 14$ up to about $\tilde{x} = 30$ based on this earlier study.

6.1.3 *Flow visualization*

Extensive flow visualization was performed for substantiating the subsistence of turbulence under the aforementioned conditions.

Additionally, the visualization provided a qualitative picture of the turbulent eddy scales and their streamwise diffusion. The flow visualization was accomplished by utilizing smoke and balloons under a variety of ambient conditions and at different fan speeds. Several frames from a movie showing smoke plume circulation, entrainment, and dispersion are given in Fig. 6.4. The fan is also shown in Fig. 6.4(a). Powerful and relatively large scale vortices, even greater than the vertical extent of the wake, were clearly discerned when unstable conditions (superadiabatic lapse rates) prevailed. The photographs provided by Figs. 6.4(a) and 6.4(b) were taken under such conditions. Without a temperature inversion the vortices quickly dispersed the smoke plume at higher altitudes. Under a temperature inversion, on the other hand, the restriction of the smoke plume within the wake was distinctly perceived. The vortices revealed a remarkable streamwise persistence accompanied by a slight downwind diminution of their scales. Even at downwind distances greater than 30R (45.6 m (150 ft)) from the fan their subsistence was prominent as illustrated by the photograph shown in Fig. 6.4(c). *The visualization clearly indicated that turbulent eddies of scales commensurate with the wake size and, hence, within the extreme lower atmosphere thickness were sustained when a temperature inversion prevailed.*

6.2 <u>Stationarity of turbulent velocity</u>

The stationarity of the turbulent velocity $u(t)$ was ascertained by forming an equivalent ensemble of the fluctuating voltage $e(t)$ and subsequent computation of the equivalent ensemble autocorrelation as proposed in Sect. 3.1. In accordance to Eq. (5.2) the fluctuating voltage $e(t)$ is proportional to the turbulent velocity $u(t)$. Adequate establishment of an equivalent ensemble $\{e(t)\}_{eq}$ is contingent upon fulfilling the following three criteria: (1) satisfactory unchanged flow conditions throughout the entire recorded time history T_{ra} of the turbulent velocity signal $e(t)$; (2) each sample record of the equivalent ensemble is sufficiently long so that it contains all the information up to the largest turbulent time scale of significance; and, (3) the sample records are statistically independent among themselves. The available recorded time history of the turbulent velocity signal $e(t)$ extended over a period $T_{ra} = 3600$ s (see Sect. 5.4). The first condition was suitably satisfied since during this time length no perceivable changes in the overall flow conditions were discerned. In line with the second requirement, the sample record time length T_r was estimated to equal the averaging time T necessary to confidently warrant the self-stationarity of the turbulent velocity. Based on the autocorrelation computation (see Sect. 5.5) an averaging time $T = 1200$ s sufficed to encompass all the significant information concerning the turbulent velocity signal. Therefore, an equivalent ensemble $\{e(t)\}_{eq}$ comprising three sample records, i.e., $N = 3$, of time length $T_r = 1200$ s each was formed by using Eq. (3.2). These three sample records consist of segments of the original time history $e(t)$ as stipulated by Eq. (3.3), and they are:

$$e_1(t) = e(0 < t \leq 1200 \text{ s}), \tag{6.9a}$$

$$e_2(t) = e(1200 \text{ s} < t \leq 2400 \text{ s}), \tag{6.9b}$$

$$e_3(t) = e(2400 \text{ s} < t \leq 3600 \text{ s}). \tag{6.9c}$$

This equivalent ensemble is illustrated in Fig. 6.5.

Estimate of the statistical independence of the sample records $e_k(t)$ composing the equivalent ensemble $\{e(t)\}_{eq}$, i.e., the third criterion, entails satisfying the relationship [41]

$$p_{k,m}(\xi,\eta) = p_k(\xi)p_m(\eta), \tag{6.10}$$

in which $p_{k,m}(\xi,\eta)$ is the joint probability density function (JPDF) of any two different sample records $e_k(t)$ and $e_m(t)$. Hence, the subscripts k and m, which designate the sample records within the equivalent ensemble, take on different integer values from 1 to N, i.e., k, $m = 1, 2, 3$ and $k \neq m$. The variables ξ and η denote the amplitudes of the aforementioned sample records. In the foregoing equation $p_k(\xi)$ and $p_m(\eta)$ are the individual probability density functions (PDF) of the very same two sample records $e_k(t)$ and $e_m(t)$, respectively. Basically, the JPDF describes the probability that $e_k(t)$ and $e_m(t)$ assume simultaneously values within some defined pair of ranges, i.e., the probability that $\xi < e_k(t) \leq \xi + \Delta\xi$ and $\eta < e_m(t) \leq \eta + \Delta\eta$ occurs concurrently during an observation time T_B. Similarly, the PDF defines this probability for a single sample record $e_k(t)$, viz., the probability that $e_k(t)$ assumes a value $\xi < e_k(t) \leq \xi + \Delta\xi$ during an observation time T_B. Estimates for both JPDF and PDF are provided by the relationships [41]

$$\hat{p}_{k,m}(\xi,\eta) = \frac{1}{\Delta\xi\Delta\eta}\,\frac{T_{k,m}}{T_B}\ , \tag{6.11}$$

and

$$\hat{p}_k(\xi) = \frac{1}{\Delta\xi}\,\frac{T_k}{T_B}\ . \tag{6.12}$$

The total amount of time that $e_k(t)$ and $e_m(t)$ simultaneously fall inside the previously stated ranges is denoted by $T_{k,m}$. Its counterpart for a single sample record $e_k(t)$ is designated by T_k. The observation time T_B required to compute the JPDF and PDF was estimated based on the maximum significant time delay employed in calculating the equivalent ensemble autocorrelation. This maximum time delay τ_{max} was assumed to equal, at the least, that used in computing the single record time-averaged autocorrelation $R(\tau)$, viz., $\tau_{max} = 3$ s (see Sect. 5.5). Since it was necessary to compute the equivalent ensemble autocorrelation at several different starting times t_o, segments of length $T_B = 5$ s were utilized. These portions consist of the parts of the sample records which lie between two 5 s spaced vertical cuts across the equivalent ensemble $\{e(t)\}_{eq}$ as shown in Fig. 6.5. Oscillograms of the leading 5 s pieces of each sample record are illustrated in Fig. 6.6. The amplitude windows defined by the ranges $(\xi, \xi + \Delta\xi)$ and $(\eta, \eta + \Delta\eta)$ are depicted for $e_1(t)$ and $e_2(t)$ segments portrayed in this figure.

To carry out efficiently the computation of the JPDF's and individual PDF's and the three segments of $T_B = 5$ s length each were digitized. A stereocomparator (Wild-Heerbrugg Instruments Inc., Model Wild Stk-2702) was employed together with a digitizer (Auto-Trol Corp., 3800/4D) and a card punch (International Business Machines Co., Model 29), were employed for this purpose. The sterocomparator stepwise magnification permitted sampling frequencies in increments of 440 Hz due to the oscillogram size. Since the highest frequency of interest of the signal was about 250 Hz (see Sect. 5.4) a sampling rate of $f_s = 880$ Hz was utilized. As a result 4400 discrete values were obtained for each sample record. In computing the JPDF's and PDF's their amplitudes ξ and η were made dimensionless employing the absolute value of the maximum instantaneous fluctuating voltage e_{max}. Thus, the dimensionless amplitudes are

$$\tilde{\xi},\ \tilde{\eta} = \xi/e_{max},\ \eta/e_{max}, \tag{6.13}$$

in which e_{max} = 400 mV for all three segments. An amplitude window $\Delta\tilde{\xi} = \Delta\tilde{\eta} = 0.2$ ($\Delta\xi = \Delta\eta$ = 80 mV) was utilized throughout the computation of the probability density functions.

The JPDF's and product of individual PDF's define surfaces in the coordinate space $(\tilde{\xi},\tilde{\eta},\hat{p})$. A total of six surfaces were obtained, viz., $\hat{p}_{1,2}$, $\hat{p}_{1,3}$, $\hat{p}_{2,3}$, $\hat{p}_1\hat{p}_2$, $\hat{p}_1\hat{p}_3$ and $\hat{p}_2\hat{p}_3$, since three segments were utilized. These surfaces are portrayed in Fig. 6.7. In calculating the estimates for JPDF and PDF the bias error was completely negligible compared to the variance of the estimator, i.e., the random error [41]. For a given window size the bias error is proportional to the square of the curvature of the probability function. This error was neglected since the curvature was sufficiently small. The normalized mean-square error for the second- and first-order probability density functions are then approximated by standard errors [41]

$$\varepsilon^2_{p2} \approx \frac{c^2}{BT_B\Delta\tilde{\xi}\Delta\tilde{\eta}}\,\frac{1}{\hat{p}_{k,m}(\tilde{\xi},\tilde{\eta})}\ , \tag{6.14}$$

and

$$\varepsilon^2_{p1} \approx \frac{c^2}{2BT_B\Delta\tilde{\xi}}\ \frac{1}{\hat{p}_k(\tilde{\xi})}\ , \tag{6.15}$$

respectively. In these two expressions $T_B = 5$ s while the signal bandwidth $B = 250$ Hz. The value of the constant c is generally unknown. On the other hand, it can be assumed that $c = 1$ whenever the signal is digitized into, at the least, $2BT_B$ discrete values [41]. In this case the signal was digitized into 4400 discrete values whereas $2BT_B = 2500$. The normalized mean-square errors depend upon the window widths and values of the probability density functions. Their validity is restricted to values of $\hat{p}_{k,m}(\tilde{\xi},\tilde{\eta})$ and $\hat{p}_k(\tilde{\xi})$ different from zero inasmuch as a finite observation time T_B was employed. It was found that the normalized mean-square errors for the second- and first-order probability density functions, under the foregoing conditions, are $\varepsilon_{p2}^2 \approx 0.02/\hat{p}_{k,m}(\tilde{\xi},\tilde{\eta})$ and $\varepsilon_{p1}^2 \approx 0.002/\hat{p}_k(\tilde{\xi})$, respectively. The peak values of both JPDF's and products of PDF's were about 2 as observed in Fig. 6.7. With increasing values of $\hat{p}_{k,m}(\tilde{\xi},\tilde{\eta})$ from 0.1 to 2, the ε_{p2}^2 decreased from 0.4 to 0.01. Similarly, the ε_{p1}^2 diminished from 0.04 to 0.001 for augmenting $\hat{p}_k(\tilde{\xi})$ from 0.1 to 2. Hence, the computed estimators of the probability density functions were within reasonable levels of confidence.

The JPDF's and the respective products of individual PDF's for all three segments portrayed in Fig. 6.7 exhibit a striking qualitative congruent variation. This overall similarity is further substantiated by the isoprobability curves of the JPDF's and the products of individual PDF's depicted in Fig. 6.8. To quantitatively ascertain the extent to which the statistical independence criterion set forth by Eq. (6.10) is satisfied, the variations of both $\hat{p}_{k,m}(\tilde{\xi},\tilde{\eta})$ and $\hat{p}_k(\tilde{\xi})\hat{p}_m(\tilde{\eta})$ along the surfaces $\tilde{\xi} = \tilde{\eta}$ and $\tilde{\xi} = -\tilde{\eta}$ were examined. The projections of these surfaces are indicated by the diagonals AA and BB in the $\tilde{\xi}$-$\tilde{\eta}$ plane in Fig. 6.8. The changes of the JPDF's and corresponding products of PDF's along these diagonals are depicted in Fig. 6.9. A remarkable agreement in their variations is clearly discerned. The degree of statistical independence was evaluated by computing the normalized standard deviation between $\hat{p}_k(\tilde{\xi})\hat{p}_m(\tilde{\eta})$ and $\hat{p}_{k,m}(\tilde{\xi},\tilde{\eta})$. In this case, the normalized standard deviation $(\tilde{\sigma}_p)_{k,m}$ is defined by

$$(\tilde{\sigma}_p)_{k,m} = \left\{ \frac{\int_{-1}^{1}\int_{-1}^{1} [\hat{p}_k(\tilde{\xi})\hat{p}_m(\tilde{\eta}) - \hat{p}_{k,m}(\tilde{\xi},\tilde{\eta})]^2 \, d\tilde{\xi}d\tilde{\eta}}{\int_{-1}^{1}\int_{-1}^{1} [\hat{p}_{k,m}(\tilde{\xi},\tilde{\eta})]^2 \, d\tilde{\xi}d\tilde{\eta}} \right\}^{\frac{1}{2}} . \qquad (6.16)$$

It basically expresses the relative amount of volume that lies between the two surfaces $\hat{p}_{k,m}(\tilde{\xi},\tilde{\eta})$ and $\hat{p}_k(\tilde{\xi})\hat{p}_m(\tilde{\eta})$. The results of this computation with increasing observation time are tabulated below:

T_B (s)	$(\tilde{\sigma}_p)_{1,2}$	$(\tilde{\sigma}_p)_{1,3}$	$(\tilde{\sigma}_p)_{2,3}$
3	0.17	0.22	0.17
4	0.16	0.15	0.15
5	0.12	0.13	0.13

These results clearly show that the degree of statistical independence is enhanced with increasing observation time. For the entire length of the segments used, viz., $T_B = 5$ s, $(\tilde{\sigma}_p)_{k,m} \leq 0.13$. Based on the trend in the variation of the normalized standard deviation $(\tilde{\sigma}_p)_{k,m}$ it can be inferred that the three sample records constituting the equivalent ensemble are satisfactorily statistically independent. *An acceptable equivalent ensemble* $\{e(t)\}_{eq}$ *was thus generated since all of the* *necessary three conditions were reasonably met.* Consequently, the autocorrelation analysis for ascertaining the stationarity of the equivalent ensemble can be performed.

The test for stationarity of the fluctuating voltage consisted of (1) computation of the equivalent ensemble autocorrelation, called hereafter the EEAC; and (2) examination of the EEAC variation as the starting time t_o assumed different values within a specified range. In the equivalent ensemble the starting time t_o is the instant of time at which the computation of the EEAC is initiated. For $\{e(t)\}_{eq}$ the EEAC is defined by

$$<\rho(t_o,t_o+\tau)>_{eq} = \frac{1}{N} \sum_{k=1}^{N} e_k(t_o)e_k(t_o+\tau), \qquad (6.17)$$

where τ stands for the time delay and the number of sample records in the equivalent ensemble $N = 3$. The EEAC coefficient (or normalized EEAC) is obtained by dividing the foregoing equation by the equivalent ensemble mean-square value, i.e., the EEAC at $\tau = 0$. Hence, the EEAC coefficient, called hereinafter EEACC for convenience, is

$$<\tilde{\rho}(t_o,t_o+\tau)>_{eq} = \frac{<\rho(t_o,t_o+\tau)>_{eq}}{<\rho(t_o)>_{eq}} \qquad (6.18)$$

It is worth mentioning that its turbulent velocity counterpart $<\tilde{R}(t_o,t_o+\tau)>_{eq} = <\tilde{\rho}(t_o,t_o+\tau)>_{eq}$ since $u \sim e$. The normalized EEAC's were computed employing the very same 5 s segment of the equivalent ensemble $\{e(t)\}_{eq}$ used in the statistical independence test. In computing the EEACC's the starting time t_o varied between 0 and 2 s since a maximum delay $\tau_{max} = 3$ s was required based on the single record time-averaged autocorrelation. Inasmuch as a sampling frequency f_s = 880 Hz was utilized in the digitization of $e(t)$, 1760 EEACC's were obtained within the aforementioned starting time range. Editing of the EEACC's was necessary to insure a consistent variation in their values since the normalized EEAC's exhibited random fluctuations. It was surmised that these fluctuations were due to the small number of sample records, viz., 3 records, used in calculating EEACC's. A bandpass smoothing scheme was employed to remove these irregular fluctuations. This smoothing procedure consisted, first, of obtaining the Fourier transform of the EEACC for identifying any inconsistencies in the frequency domain, i.e., to discern any pronounced extraneous peaks in its variation. Next, central averaging was carried out to eliminate these spurious peaks. Afterwards, an inverse Fourier transform was utilized to recover the EEACC. Final editing was then accomplished by central averaging of the partially smoothed EEACC. This smoothing procedure is described by the block diagram provided by Fig. 6.10. Representative samples of the normalized EEAC's at five selected starting times viz., at t_o = 0.2, 0.7, 1.2, 1.4 and 1.9 s are portrayed in Fig. 6.11. Generally, these five representative EEAC coefficients reveal a satisfactory similar change with augmenting time delay. For the sake of a closer comparison, the EEACC's during the 1 s lag time are provided by the accompanying insert in Fig. 6.11.

Essentially, assessment of the equivalent ensemble stationarity consists of determining the effect of varying the starting time upon the EEACC's. A standard deviation test was conducted for ascertaining to what degree the EEACC's were independent of the changing starting time. This test was performed by calculating the normalized incremental standard deviation of each EEACC about the starting-time-averaged EEACC. The latter is basically representative of all the EEACC's since it is averaged over all possible starting times, i.e., over all equivalent ensemble autocorrelation coefficients. This particular EEACC is consequently a characteristic property of the equivalent ensemble. The normalized incremental standard deviation within any lag time range $\tau_1 \leq \tau < \tau_2$ is defined by

$$\tilde{\sigma}_\rho(t_o,\tau_1,\tau_2) = \left\{ \frac{\int_{\tau_1}^{\tau_2} [<\tilde{\rho}(t_o,t_o+\tau)>_{eq} - <\tilde{\rho}(\tau)>_{eq}]^2 \, d\tau}{\int_0^{\tau_{max}} [<\tilde{\rho}(\tau)>_{eq}]^2 \, d\tau} \right\}^{\frac{1}{2}}, \qquad (6.19)$$

in which the starting-time-averaged EEACC, called hereafter the STACC, is

$$<\tilde{\rho}(\tau)>_{eq} = \frac{1}{M} \sum_{i=1}^{M} < \tilde{\rho}(t_{oi},t_{oi}+\tau)>_{eq}, \qquad (6.20)$$

where M designates the total number of starting times utilized and the maximum time delay $\tau_{max} = 3$ s. This incremental standard deviation measures the contribution to the relative amount of area between the EEACC and the STACC during any time delay interval $\tau_1 \leq \tau < \tau_2$. Thus, the incremental standard deviation readily permits estimation of the EEACC's independence of the starting time. Results of the standard deviation test for the five representative EEACC's depicted in Fig. 6.11 at several lag time increments are summarized below:

t_o(s)		0.2	0.7	1.2	1.4	1.9
τ_1	τ_2	$\tilde{\sigma}_\rho$	$\tilde{\sigma}_\rho$	$\tilde{\sigma}_\rho$	$\tilde{\sigma}_\rho$	$\tilde{\sigma}_\rho$
(s)	(s)					
0	0.1	0.10	0.01	0.07	0.03	0.01
0.1	0.2	0.04	0.10	0.11	0.07	0.06
0.2	0.3	0.01	0.08	0.08	0.13	0.14
0.3	0.4	0.04	0.03	0.08	0.04	0.09
0.4	0.5	0.11	0.02	0.04	0.06	0.13
0.8	0.9	0.02	0.03	0.03	0.01	0.01
1.2	1.3	0	0	0.01	0	0
0	1	0.20	0.16	0.23	0.18	0.28
0	2	0.20	0.16	0.23	0.18	0.28
0	3	0.20	0.16	0.23	0.18	0.28

Generally, for time delay increments of 0.1 s the normalized standard deviation varied from 0.01 to about 0.14. Values of the normalized incremental standard deviation larger than about 0.1 occurred randomly at a few lag time gaps. The relatively high value of the overall normalized standard deviation, viz., $\tilde{\sigma}_\rho(t_o,0,3)$, arises primarily from several isolated discrepencies between $\langle\tilde{\rho}(t_o,t_o+\tau)\rangle_{eq}$ and $\langle\tilde{\rho}(\tau)\rangle_{eq}$. In the light of the approximations associated with the computations of the EEACC's and the STACC even an overall standard deviation of 0.28 is acceptable. Based on these results it can be assumed that the equivalent ensemble is statistically steady. Consequently, *the fluctuating voltage* e(t) *and corresponding turbulent velocity* u(t) *are approximately weakly stationary*. This result is of considerable significance in view of the small number of sample records employed, viz., 3 sample records. It is conjectured that the consistency of the EEACC's would be considerably enhanced with increasing number of sample records of the equivalent ensemble. Essentially, this analysis clearly indicates that the stationarity of a random signal can be reasonably estimated using an equivalent ensemble.

The acquirement of a stationary equivalent ensemble and knowledge of the EEACC naturally suggests a heuristic test of the ergodic assumption. Under this assumption the statistical properties of the ensemble are estimated by taking time averages over any single representative sample record in the ensemble, i.e., the respective ensemble and time-average moments are equal. At present time no theoretical foundation relating the equivalent ensemble averaged moments to their time-averaged counterparts is available. Then, the test for ergodicity simply entails comparison of the equivalent ensemble autocorrelation coefficient with its counterpart obtained by time averaging over a single selected sample record. In carrying out this comparison the STACC, which is a basic feature of the entire equivalent ensemble, was utilized.

The equivalent ensemble autocorrelation coefficient averaged over all starting times (STACC) $<\tilde{\rho}(\tau)>_{eq}$ and time-averaged autocorrelation coefficient over a single sample record $\tilde{R}(\tau)$ (see Sect. 5.5) are depicted together in Fig. 6.12. An enlargement of the autocorrelations during the initial 1 s lag time is provided by the insert in this figure. A striking overall similarity in the variation of these two autocorrelations is clearly discerned. A standard deviation test was further performed to quantitatively determine the variation of the former about the latter. This standard deviation test can be thus employed to approximately indicate the validity of the ergodic assumption. A normalized incremental standard deviation $\tilde{\sigma}_R(\tau_1,\tau_2)$ formally similar to that used for the equivalent ensemble stationarity test,

$$\tilde{\sigma}_R(\tau_1,\tau_2) = \left\{ \frac{\int_{\tau_1}^{\tau_2} [\langle\tilde{\rho}(\tau)\rangle_{eq} - \tilde{R}(\tau)]^2 \, d\tau}{\int_0^{\tau_{max}} \tilde{R}^2(\tau) \, d\tau} \right\}^{\frac{1}{2}}, \tag{6.21}$$

was utilized to carry out the ergodicity test. Its value for several lag time increments are tabulated below:

τ_1 (s)	τ_2 (s)	$\tilde{\sigma}_R$
0	0.1	0.08
0.1	0.2	0.11
0.2	0.3	0.11
0.3	0.4	0.10
0.4	0.5	0.09
1.5	1.6	0.08
2.5	2.6	0.02
0	1.0	0.30
0	2.0	0.35
0	3.0	0.37

Values of the normalized incremental standard deviation larger than or equal to 0.10 occurred for several time delay intervals. The overall standard deviation over the entire time delay range, viz., $\tau = 0$ to 3 s reached a relatively high value of about 0.37. A better agreement cannot be basically expected considering the numerous approximations involved in this computation and, particularly, the limited number of sample records forming the equivalent ensemble, viz., 3 sample records.

On the other hand, it is quite remarkable that for most of the time delay intervals the normalized incremental standard deviation was less than about 0.10. *It is hypothesized that even this limited agreement provides acceptable support for the claim of ergodicity. Since both the stationarity and ergodicity criteria were reasonably met the turbulent velocity can be considered as a realization of a weakly self-stationary random process.* The foregoing analysis clearly demonstrates that the stationarity and, to some extent, the ergodicity of a random process can be practically ascertained, employing an equivalent ensemble. It further indicates that 3 sample records is, in all likelihood, the minimum number which can be effectively used to generate an equivalent ensemble.

6.3 Eulerian autocorrelation

The Eulerian autocorrelation coefficient of the longitudinal turbulent velocity $u(t)$ is expressed by

$$\tilde{R}(\tau) = \overline{u(t)u(t+\tau)}/\overline{u^2} \ , \tag{6.22}$$

in which τ is the lag time and $\overline{u^2}$ designates the autocorrelation at zero time delay, i.e., the local mean-square value of the fluctuating velocity which is exactly the total turbulent kinetic energy per unit mass. This normalized autocorrelation function equals the autocorrelation coefficient of the hot-wire anemomenter output voltage defined by Eq. (5.6) since $u \sim e$. A set of five autocorrelation coefficients were obtained simultaneously by means of the array of five hot-wire anemometers installed within the turbulence measurement range, i.e., along the turbulence line. The autocorrelations were computed using the tape recorded voltage time histories e(t) (see Sect. 5.5). Variations of the five autocorrélation coefficients up to a time delay of 3 s are displayed in Fig. 6.13(a). The same autocorrelation coefficients are portrayed in Fig. 6.13(b) over a lag time interval $\tau = 0$ to 1 s to permit a closer comparison of their decreasing trend. A consistent similar change in amplitude is exhibited by all five autocorrelations with augmenting time displacement. *Each of the five autocorrelation coefficients reveal distinctly a cusp at zero lag time.* All five autocorrelations decay to their first zero crossing of the time axis at time delays ranging from $\tau_1 = 0.2$ to 0.5 s with increasing streamwise distance as shown in Figs. 6.13. Thereafter, they take on negative values and asymptotically approach zero level.

Usually, the autocorrelation is employed to deduce two characteristic time scales of turbulence: (1) the micro time scale and (2) the integral time scale. The former is a measure of the most rapid changes that can occur in the fluctuating velocity. In addition it provides an insight into the smaller dissipation scale of turbulence. The micro time scale is proportional to the inverse of the curvature of the autocorrelation coefficient at $\tau = 0$ [10]. Whenever the autocorrelation possesses a cusp at zero lag time, it is anticipated that the micro time scale would be, at the least, one order of magnitude smaller than the integral time scale. This is generally a common occurrence for large-scale turbulence such as encountered in atmospheric flows [22]. The micro time scale t was estimated by fitting an osculating parabola to the peak of each autocorrelation coefficient and finding out the lag time at which this parabola intersects the time axis. This time delay then equals the micro time scale. Subsequently, a characteristic micro length scale was computed according to

$$\lambda = \overline{U}t \ , \tag{6.23}$$

where $\overline{U}$ is the local mean velocity. This micro length scale λ can be viewed as representative of the small-scale eddies at each position. The micro time and length scales were made dimensionless using their values at the first station on the turbulence line which can be basically considered a reference point. Thus,

$$\tilde{t} = t/t_o, \tag{6.24}$$

and

$$\tilde{\lambda} = \lambda/\lambda_o, \tag{6.25}$$

where t_o = 5.77 ms and λ_o = 4.82 cm (0.158 ft) are the micro time and length scales at $\tilde{x}_o$= 10. Their variations with augmenting streamwise distance $\tilde{x}$ are shown in Fig. 6.14. Both micro time and length scales display a continuous increase followed by a leveling off trend around $\tilde{x}$ = 13. They attain their largest values of 2.15 (12.4 ms) and 1.77 (8.53 cm (0.230 ft)) at $\tilde{x}$ = 14 and 13, respectively. The streamwise augmentation of the micro scales suggests a similar behavior for the integral scales.

The integral time scale T represents the average duration time of the turbulent velocity, and this scale is ordinarily defined by [10]

$$T = \int_0^\infty \tilde{R}(\tau)\, d\tau \ , \tag{6.26}$$

where $\tilde{R}(\tau)$ is the autocorrelation coefficient. For stationary turbulence the integral time scale is proportional to the value of the turbulent energy spectrum at zero frequency. This results from the Fourier transform of the autocorrelation coefficient [10]. Since turbulence is nonexisting at zero frequency considering its intrinsic nature, it appears that the integral scale should also vanish. This possible nonmaterialization of the integral time scale is suggested in Ref. 62. The autocorrelation coefficient should consist of equal positive and negative portions when the integral time scale becomes zero in the light of its definition given by Eq. (6.26). This situation is approximately met by the five autocorrelation coefficient set displayed in Fig. 6.13(a). On the other hand, it is conceivable to introduce a characteristic time scale of the turbulence by considering only the positive autocorrelation. Such a time scale can be interpreted as the largest time scale since it decreases gradually as the negative autocorrelation is accounted for. This largest time scale, which is defined by

$$T_1 = \int_0^{\tau_1} \tilde{R}(\tau)\, d\tau , \qquad (6.27)$$

can be viewed as the first integral time scale of the turbulence. In the above equation, τ_1 is the particular lag time when the autocorrelation coefficient becomes firstly zero, i.e., the first zero crossing. A similar definition was advanced in Ref. 63 for a so-called apparent integral length scale of the longitudinal space cross-correlation. This apparent length scale was obtained by a space integral of the cross-correlation up to the particular separation gap where the cross-correlation became zero for the first time. Basically, this implies disregarding the negative portion of the space cross-correlation function.

The first integral time scale for the autocorrelation set was computed using Eq. (6.27). In this computation the first zero crossings τ_1 = 0.21, 0.34, 0.40, 0.50 and 0.47 s for the five autocorrelations with augmenting $\tilde{x}$ from 10 to 14. Normalization of the first integral time scale was performed in the same manner as for the micro time scale. Hence,

$$\tilde{T}_1 = T_1/T_{10} , \tag{6.28}$$

where T_{10} = 54.5 ms is the value of this integral time scale at the first station (or the reference point) on the turbulence line, i.e., at $\tilde{x}_o$ = 10. Results of this computation are portrayed in Fig. 6.15. The first integral time scale $\tilde{T}_1$ exhibits a monotonical streamwise increase. It levels off around $\tilde{x}$ = 12 and reaches its largest value of 2.24 (123 ms) at $\tilde{x}$ = 14. The observed systematic increase of the first integral time scale indicates that the peak in the turbulence energy spectrum is gradually shifting to lower frequencies. *This behavior can occur due to the energy dissipation at high frequencies and concurrent energy extraction from the mean flow at low frequencies.* It is further interesting to examine the ratio of the integral to micro time scales inasmuch as it was presupposed that the latter is significantly smaller than the former based on the observed cusp of the autocorrelation coefficient curves. This ratio for the autocorrelation set is tabulated below:

$\tilde{x}$	10	11	12	13	14
T_1/t	9.44	9.90	10.32	10.00	9.88

Thus, the first integral time scale is about tenfold larger than the micro time scale.

In a similar manner as for the micro length scale, a characteristic length scale corresponding to the first integral time scale was defined by

$$\Lambda_1 = \bar{U}T_1 \ , \qquad (6.29)$$

where $\bar{U}$ is the local axial mean velocity. This first integral length scale can be considered representative of the predominant turbulent eddy sizes at a given location. It was further made dimensionless by its value at the reference position $\tilde{x}_o = 10$ according to

$$\tilde{\Lambda}_1 = \Lambda_1/\Lambda_{10} \ , \qquad (6.30)$$

where $\Lambda_{10} = 45.4$ cm (1.49 ft). The streamwise change of the first integral length scale $\tilde{\Lambda}_1$ is depicted also in Fig. 6.15. Its variation basically resembles that of the integral time scale with its largest value of 1.88 (83.5 cm (2.74 ft)) at $\tilde{x} = 13$. *The streamwise trend of the first integral length scale implies that the turbulence structure is apparently dominated by relatively large-scale eddies. This is attributed to a continuous accumulation of energy at large scales.* This increase in eddy size was expected based on the similar trend of the micro length scale. Since both the integral and micro length scales are defined in terms of the very same local mean velocity, their ratio is exactly equal to the ratio of their corresponding time scales. *The streamwise variations of both micro* *and integral time and length scales underscore moreover the nonhomogeneous nature of the turbulence.*

Additional significant insight into the intrinsic character of the turbulence can be obtained by examining the streamwise variation of the Reynolds numbers based on the micro and/or first integral length scales and the local turbulent velocity (rms). The micro length scale Reynolds number is expressed by [10]

$$Re_\lambda = \lambda(\overline{u^2})^{\frac{1}{2}}/\nu \ , \tag{6.31}$$

while the first integral length scale Reynolds number is given by

$$Re_\Lambda = \Lambda_1(\overline{u^2})^{\frac{1}{2}}/\nu \ , \tag{6.32}$$

where $(\overline{u^2})^{\frac{1}{2}}$ designates the rms value of the turbulent velocity and the air kinematic viscosity $\nu = 1.51 \times 10^{-5}$ m^2/s (1.63×10^{-4} ft^2/s). The former Reynolds number is indicative of the small-eddy dissipation range whereas the latter Reynolds number is characteristic of the energy-containing eddy domain. Practically, the ratio of these two Reynolds numbers is exactly the ratio of integral and micro length and/or time scales. Both micro and integral scale Reynolds numbers for the five stations on the turbulence line are depicted in Fig. 6.16. The two Reynolds numbers exhibit a relative minimum value around $\tilde{x} = 11$, whereas their values at either end of the turbulence line are roughly the same in each case. This change is attributed to the varying turbulent kinetic energy along the turbulence measurement range which is displayed in Fig. 6.3. The micro and integral scale Reynolds numbers ranged from about 5.8×10^3 to 8.0×10^3 and 5.8×10^4 to 7.8×10^4, respectively. In addition, the ratio of these two

Reynolds numbers is of the order of 10. It is important to point out that in atmospheric turbulence values of the micro scale Reynolds number of the order of 10^3 or even 10^4 can be encountered and, generally, the integral length scale Reynolds number is at the least ten times larger [22]. *The structure of the turbulence from the large to the small eddy sizes within the wake is consequently in acceptable agreement with its atmospheric counterpart.* This further qualifies the present simulation of the turbulence in the extreme lower atmosphere.

It is, furthermore, relevant to inspect the turbulence dissipation for approximately ascertaining the relative significance of the small eddies. To a first approximation the dissipation ε was estimated using its relation defined for ideal isotropic turbulence. In this very restrictive case, the dissipation expressed in terms of the local mean-square value of turbulent velocity $\overline{u^2}$ and the longitudinal micro length scale λ is [10]

$$\varepsilon = 30\nu\ \overline{u^2}/\lambda^2 \ , \tag{6.33}$$

where ν is the kinematic viscosity. It basically represents the dissipation in the small-eddy range and/or the work done by the energy-containing eddies in supplying energy to smaller eddies. The dissipation was normalized according to

$$\tilde{\varepsilon} = \varepsilon/\varepsilon_o \ , \tag{6.34}$$

in which $\varepsilon_o = 1.22\ m^2/s^3$ ($13\ ft^2/s^3$) is the dissipation at the first station on the turbulence line, i.e., at $\tilde{x}_o = 10$. Its change in the streamwise direction is displayed in Fig. 6.17. The dissipation exhibits initially a decrease larger than about 80% up to $\tilde{x} = 11$.

Subsequently, it remains at a nearly constant level of about 0.09 (0.11 m^2/s^3 (1.18 ft^2/s^3)) throughout the turbulence line. *This drastic reduction is indicative of the lessening role of the small-scale eddies and, hence, the predominance of the large-scale structure.*

In computing the integral time scale the negative autocorrelation was disregarded since the former vanishes as the latter is accounted for. The integral time and length scales are basically representative of the large-scale turbulence structure. Then their gradual decrease induced by the negative autocorrelation can be apparently interpreted as a measure of turbulent kinetic energy transfer from larger to smaller scales. In general, two different trends of the autocorrelation coefficients with regard to their negative portions can be distinctly perceived based on the autocorrelation coefficients variations shown in Figs. 6.13. In one case, the autocorrelation quickly attains relatively large negative values after its first zero crossing τ_1 and, subsequently, asymptotically approaches zero. This trend is clearly observed at $\tilde{x}$ = 11, 12, 13 and 14 where the maximum negative autocorrelation coefficient $\tilde{R}(\tau)$ ranges from -0.101 to -0.155. The second tendency is characterized by a shallower negative autocorrelation where the asymptotic approach to zero begins almost immediately after the first zero crossing τ_1. This behavior is particularly prominent at the reference station, viz., at $\tilde{x}$ = 10. A higher degree of negative autocorrelation at larger time displacements suggests sustenance of larger-scale eddies. This necessarily leads to a slower rate of energy transfer to smaller eddies and, hence, to accumulation of energy at large-scale eddies. On the other hand, a shallower negative autocorrelation represents exactly the opposite situation. Then the turbulent energy is transferred more rapidly from larger to smaller scales. The five autocorrelation coefficients displayed in Fig. 6.13(a) exhibit generally larger negative values with augmenting axial distance $\tilde{x}$. This indicates *the increasing significance of the large-scale turbulence structure in the streamwise direction.* The longitudinal large-scale eddy structure is substantiated by the axial augmentation of the micro and integral length scales and accompanying diminution of the dissipation. Further confirmation for this eddy structure comes from the fact that large-scale eddies usually undergo elongation in the mean flow direction [22,64]. *Such a streamwise stretching of the large eddies is supported by the axial increase of the first integral length scale.*

The energy spectrum (or the frequency-density function) $F(f)$ of the longitudinal turbulent velocity $u(t)$ was computed for all five autocorrelation coefficients $\tilde{R}(\tau)$ by means of a Fourier transform since the turbulence is stationary (see Sect. 6.2). Hence, the one-dimensional spectrum is expressed by [41]

$$F(f) = 4\overline{u^2} \int_0^{\infty} \tilde{R}(\tau) \cos 2\pi f\tau \, d\tau \ , \qquad (6.35)$$

where $\overline{u^2}$ is the local mean-square value of the turbulent velocity (the total turbulent kinetic energy) and f designates the frequency. The resulting spectra in terms of $F(f)/\overline{u^2}$ vs. f are displayed in Fig. 6.18. All five spectra exhibit a peak around 0.7 to 1.0 Hz. A continuous shift of the peak to lower frequencies is clearly discerned as the axial distance $\tilde{x}$ becomes larger. For the sake of closer comparison, the peak frequency-density function $F_p/\overline{u^2}$ and corresponding peak frequency f_p including their dimensionless values computed in accordance to the universal spectral function

$$\tilde{F}_p = F_p f_p/\overline{u^2} , \tag{6.36}$$

and dimensionless peak frequency

$$\tilde{f}_p = f_p h/\overline{U} , \tag{6.37}$$

where $h = 3.04$ m (10 ft) is the height of the turbulence line above the ground and $\overline{U}$ is the local mean velocity, are tabulated below:

$\tilde{x}$	10	11	12	13	14
$F_p/\overline{u^2}$ (s)	0.203	0.335	0.345	0.352	0.386
$\tilde{F}_p$	0.222	0.265	0.253	0.258	0.283
f_p (Hz)	1.098	0.793	0.732	0.732	0.732
$\tilde{f}_p$	0.400	0.369	0.327	0.315	0.327

With increasing streamwise distance $\tilde{x}$ the proportion of turbulent kinetic energy concentrated at the peak frequency augments by about 90%. This is in agreement with the axial increase of the integral length scale and, moreover, *attests to the accumulation of energy at large-scales*. An inertial subrange, where $F(f) \sim f^{-5/3}$, is distinguished in all five cases for a frequency bandwidth extending roughly from 2 to 10 Hz. The energy-containing range of the spectrum which occurs at large scales is hence separated from the dissipation range. This further confirms the predominance of the large-scale eddies.

It is worthwhile to compare the peak frequency-density functions with those obtained in the atmosphere for roughly similar flat terrain. The spectral peaks are of interest since they are indicative of the maximum concentration of turbulent energy. This comparison was carried out using the longitudinal spectra measured at Round Hill [65], Kennedy Space Center [66] and in the Air Force Cambridge Research Laboratories experiment in Kansas [67,68]. At Round Hill the peak spectra under stable conditions was found for peak reduced frequency $\tilde{f}_p$ varying from 0.04 to 0.20. The peak reduced frequency observed at the Kennedy Space Center under neutral conditions ranged from 0.04 to 0.4. In the Kansas experiment, which was conducted under a variety of degree of stability, the peak reduced frequency took on values between about 0.08 and 0.34. In the present experiment, the peak reduced frequency varies from 0.315 to 0.400 and, therefore, *it is in acceptable agreement with their atmospheric counterparts.*

Generally, an autocorrelation is normalized with respect to the local mean-square value of the turbulent velocity according to Eq. (6.22). For nonhomogeneous turbulence, on the other hand, it is of considerable significance to examine the behavior of the autocorrelations when they are all referred to the same characteristic turbulent energy. Such a normalization depicts the relative changes in the autocorrelations which are due to the turbulence nonhomogeneity. It is natural to render the autocorrelation set dimensionless by using the mean-square value of fluctuating velocity at the reference position on the turbulence line. These reference-point autocorrelation coefficients are expressed by

$$\tilde{R}_o(\tau) = \overline{u(t)u(t+\tau)}/\overline{u_o^2} \qquad (6.38)$$

in which $\overline{u_o^2} = 6.25\ m^2/s^2$ ($67.4\ ft^2/s^2$) is the mean-square value of fluctuating velocity at the first station on the turbulence line, i.e., at the reference point $\tilde{x}_o = 10$. The set of five reference-point autocorrelation coefficients is displayed in Fig. 6.19. *This representation provides an unified insight into the variation of the autocorrelations along the turbulence line and, hence, into the streamwise changing turbulence properties.* The value of the autocorrelation at any point on the turbulence line can be readily supplied by the envelope of the reference-point autocorrelation set. At any time delay τ the envelope is furnished by the curve connecting the corresponding amplitudes of the five reference-point autocorrelations. Such an envelope is denoted by $\tilde{R}_o(\tilde{x};\tau)$, where the semicolon indicates that it represents the axial variation of the reference-point autocorrelation at any desired time displacement τ. For instance, the curve joining the peaks $\tilde{R}_o(0)$ of the reference-point autocorrelation coefficient set, which is depicted by a dashed line in Fig. 6.19, is the envelope $\tilde{R}_o(\tilde{x};0)$. It is important to note that this envelope describes exactly the streamwise variation of the dimensionless turbulent kinetic energy $\overline{u^2}$. Thus, *the reference-point autocorrelation set comprehends essentially the evolution of the turbulence along the turbulence line.*

6.4 Lagrangian autocorrelation

The Lagrangian autocorrelation can be computed according to Eq. (3.38) provided that the Eulerian autocorrelations are concurrently secured at all points within the flow domain of interest. This domain represents essentially the so-called turbulence "box" depicted in Fig. 3.6. In this experiment the turbulence box was established by the extent of the wake in the turbulence measurement region. The lateral stretch of the wake was roughly 6 m (20 ft) (see Sect. 5.2).

In the vertical direction the wake extended up to about the depth of the extreme lower atmospheric layer, viz., up to 5 m (16.4 ft) (see Sect. 4). The longitudinal fetch of the box was demarcated by the axial reach of the turbulence measurement range. This span, which extended from $\tilde{x} = 10$ to 14 along the centerline of the wake (x-axis) as shown in Fig. 5.1, delineated the turbulence line within the box. The first station on this turbulence line, i.e., $\tilde{x}_o = 10$, can be thus viewed as a point in the reference plane (or A-point plane) whereas the other four stations, viz., $\tilde{x}_B = 11$, 12, 13 and 14, can be interpreted as positions in four different B-point planes considering the turbulence box depiction portrayed in Fig. 3.6. Basically, the reference plane is the plane $\tilde{x}_o = 10 =$ constant since it is, by definition, normal to the mean flow direction, as further shown in Fig. 3.6. The separation ξ between the reference and B-point planes is the distance traveled during a time lapse τ by fluid particles that moved past the former plane. This distance is essentially the axial extent of the turbulence line measured from the reference point x_o, i.e., $\xi = x_B - x_o$.

Within the turbulence box the longitudinal turbulent velocity was of primary interest since its energy is substantially larger than that of the other two components. Moreover, changes in the structure of the turbulence entail mainly streamwise stretching of the turbulent eddies [22]. The Eulerian autocorrelations of the axial velocity along the turbulence line can be thus considered representative of the turbulence within the entire box. Furthermore, the minimum number of these autocorrelations necessary to reasonably describe the turbulence along this line can be based on the changes in their first integral time scales. It was deduced that the five autocorrelation set sufficed in this regard inasmuch as their first integral time scales displayed a consistent variation as shown in Fig. 6.15. Estimation of the longitudinal Lagrangian autocorrelation for the turbulence box, i.e., i = j = 1 in Eq. (3.38), was consequently of prime concern. This reference-point Lagrangian autocorrelation is simply obtained by reducing the domain integral in Eq. (3.38) to a line integral along the turbulence line. The Lagrangian autocorrelation of the axial turbulent velocity is thus given by

$$L(x_o,\tau) = \frac{1}{\xi}\int_{x_o}^{x_o+\xi} R(x;\tau)\ dx, \tag{6.39}$$

where x_o = 10R (15.2m (50 ft)) denotes the reference point on the turbulence line whose axial extent is ξ. In the foregoing equation the integrand $R(x;\tau)$ designates the usual Eulerian autocorrelation at all points on the turbulence line, i.e., at all x-positions ranging from x_o to $x_o + \xi$, for any time displacement τ.

It is essential to phrase Eq. (6.39) in a dimensionless form by means of an unique value of turbulent energy for the entire turbulence line at all time delays. At the reference point $\tilde{x}_o = 10$ (or $\tilde{\xi} = 0$) the Lagrangian axial turbulent velocity v_o is instantaneously equal to its measured Eulerian counterpart u_o in accordance to Eq. (3.8). Consequently, at the reference point $\overline{v_o^2} = \overline{u_o^2}$. This reference-point Lagrangian turbulent velocity v_o can be furthermore viewed as a characteristic velocity for the entire turbulence line considering the nonhomogeneous nature of the turbulence. In the light of the foregoing instantaneous velocity equality it is apparent that the

Lagrangian and Eulerian autocorrelation coefficients can be defined as follows:

$$\tilde{L}_o(\tilde{x}_o,\tau) = L(x_o,\tau)/\overline{v_o^2}, \tag{6.40}$$

and

$$\tilde{R}_o(\tilde{x};\tau) = R(x;\tau)/\overline{u_o^2}, \tag{6.41}$$

where $\overline{v_o^2} = \overline{u_o^2} = 6.25\ m^2/s^2$ ($67.2\ ft^2/s^2$; see Sect. 6.1.2) and $\tilde{x},\tilde{x}_o = x/R, x_o/R$. The latter equation describes the dimensionless envelope at any time delay τ of the Eulerian reference-point autocorrelation coefficient set shown in Fig. 6.19. A picture of such envelopes is provided by Fig. 6.20 at three time delays, viz., at $\tau = 0$, c_1 and c_2. Then substitution of Eqs. (6.40) and (6.41) into Eq. (6.39) yields the Lagrangian autocorrelation coefficient

$$\tilde{L}_o(\tilde{x}_o,\tau) = \frac{1}{\tilde{\xi}} \int_{\tilde{x}_o}^{\tilde{x}_o+\tilde{\xi}} \tilde{R}_o(\tilde{x};\tau)\ d\tilde{x}, \tag{6.42}$$

where the dimensionless extent of the turbulence line is defined in the same manner as the axial distance, i.e, $\tilde{\xi} = \xi/R$. Illustration of how the integral in Eq. (6.42) is evaluated at a particular lag time τ is portrayed in Fig. 6.20. The shaded area in this figure depicts the result of the integration when $\tau = c_2$ and, thus, it equals $\tilde{\xi}\tilde{L}_o(\tilde{x}_o,\tau = c_2)$.

In computing the Lagrangian autocorrelation coefficient by means of Eq. (6.42), it was necessary to estimate the maximum time delay τ_{max} which corresponded to the longest axial reach of the turbulence line ξ_{max}. These two parameters are related through the characteristic mean velocity U_c for the turbulence line in accordance to

Eq. (3.23), viz., $\tau_{max} = \xi_{max}/U_c$. Since the turbulence line extended from $\tilde{x}_o = 10$ to $\tilde{x}_B = 14$, its maximum axial extent $\tilde{\xi}_{max} = 4$ (6.08 m (20 ft)). The corresponding maximum time displacement $\tau_{max} = 0.85$ s inasmuch as the characteristic mean velocity scale $U_c = 7.12$ m/s (23.4 ft/s)(see Sect. 6.1.1). Evaluation of the integral in Eq. (6.42) was performed numerically for time delay intervals of 2 ms in the manner manner portrayed in Fig. 6.20. Insofar as the time displacement $\tau = 0$ to 0.85 s, 426 envelopes $\tilde{R}_o(\tilde{x};\tau)$ were employed. These envelopes were obtained by interpolation from the five Eulerian reference-point autocorrelation coefficients shown in Fig. 6.19. The variation of the resulting Lagrangian autocorrelation coefficient $\tilde{L}_o(\tilde{x}_o,\tau)$ with increasing time delay τ is displayed in Fig. 6.21. An enlargement of its positive portion is further depicted in the insert included ir this figure. The Lagrangian autocorrelation coefficient exhibits distinctly a cusp at zero time delay. A similar cusp was revealed by all five Eulerian autocorrelations. The first zero crossing of the time axis τ_1 occurs at about 0.26 s. This value of τ_1 lies within the range of the Eulerian autocorrelation set first zero crossings which varied from about 0.2 to 0.5 s. After the time axis crossing the Lagrangian autocorrelation displays relatively shallow negative values. Essentially, this Lagrangian autocorrelation can be viewed representative for the entire turbulence box. This ensues from the nature of the Eulerian autocorrelation set employed to compute it.

Simultaneous examination of the variations in time and space of the set of five Eulerian reference-point autocorrelation coefficients $\tilde{R}_o(\tau)$, of several selected envelopes $\tilde{R}_o(\tilde{x};\tau)$ and of the Lagrangian autocorrelation coefficient $\tilde{L}_o(\tilde{x}_o,\tau)$ can supply a significant insight into the turbulence development along the turbulence line. Such an overall display is provided by Fig. 6.22. Both the axial position $\tilde{x}$ and the axial distance $\tilde{\xi}$ from the reference point $\tilde{x}_o$ along the turbulence line are shown in this figure. The time axis τ extends up to 1 s since the maximum time displacement of interest for the Lagrangian autocorrelation was 0.85 s. A complete picture of the time variation of the five Eulerian reference-point autocorrelation coefficients at each position and of the spatial change of their envelopes at any time delay is essentially furnished by Fig. 6.22. This dual representation permit's immediate estimation of the Eulerian autocorrelation everywhere on the turbulence line. The contribution of each envelope $\tilde{R}_o(\tilde{x};\tau)$ to the Lagrangian autocorrelation can be moreover identified by means of this representation. For instance, the shaded areas in Fig. 6.22 denote those portions of the envelopes which were utilized in computing the Lagrangian autocorrelation coefficient. It is evident according to Eq. (6.42) that *the Lagrangian autocorrelation represents basically an average over all Eulerian reference-point autocorrelations on the turbulence line.* The evolution of the Lagrangian autocorrelation with augmenting time displacement τ and/or its corresponding axial distance $\tilde{\xi}$ from the reference point depicted in Fig. 6.22 *clearly indicates this notable property.* This is due to the fact that the Lagrangian autocorrelation expresses the interconnection between velocities at two instants in time which accounts inherently for two positions in space. One of these spatial locations is the reference point $\tilde{\xi} = 0$ whereas the second position is approximated by the distance $\tilde{\xi}$ along the turbulence line. Therefore, the projection of the Lagrangian autocorrelation onto the $\tilde{\xi}$-τ plane traces a line $\tau = \xi/U_c$. *The concurrent representation of these three autocorrelation functions describes consequently the turbulence properties for the entire turbulence line in terms of both Eulerian and Lagrangian variables.*

The Lagrangian autocorrelation was computed by means of Eq. (6.39) which is basically the axial component of Eq. (3.38). This latter equation was obtained by neglecting in Eq. (3.25) the three Eulerian velocity cross products given by Eqs. (3.35), (3.36) and (3.37). The first two cross products are comprised of sums of two-point two-time velocity-velocity derivative cross-correlations while the last cross product consists of a sum of two-point two-time double velocity derivative cross-correlations. These cross-correlations are significantly lessened with augmenting order of differentiation (see Sect. 3.2.2). As a result, the three sums are apparently dominated by their respective first-order space-time cross-correlation terms. To justify the disregarding of the three Eulerian velocity cross products the magnitudes of their first-order terms were estimated. The method by which these cross-correlations were evaluated is described in Appendix III. Their variations with increasing time delay up to 1 s and for a fixed correlation length $\tilde{\xi} = 1$ are displayed in Fig. A.III.1. All three first-order cross-correlations are vanishingly small at almost all time delays. Their amplitudes reached at most values of about 0.015 to 0.02 at only several time displacements. Consequently, it is reasonable to infer that the three Eulerian velocity cross products can be disregarded.

The Lagrangian autocorrelation coefficient can be further utilized to estimate the Lagrangian micro and integral time scales.

These two time scales are representative of short and long diffusion times, respectively. It is significant to point out that the Lagrangian autocorrelation yields unique values for these two characteristic time scales for the entire turbulence line. Formally, the Lagrangian time scales are defined in exactly the same manner as their Eulerian counterparts. The Lagrangian micro time scale or small diffusion time scale t_L was thus approximated by the intersection of the osculating parabola of the autocorrelation coefficient at zero lag time with the time axis [10]. It was found that t_L = 5.45 ms. A small value for this time scale was anticipated in the light of the distinctive cusp displayed by the Lagrangian autocorrelation at zero time delay as clearly revealed in Fig. 6.21.

The Lagrangian integral time scale or large diffusion time scale is given by [10]

$$T_L = \int_0^\infty \tilde{L}_o(\tilde{x}_o,\tau)\, d\tau. \tag{6.43}$$

This integral time is expected to equal zero based on its analogy to its Eulerian counterpart. It is therefore natural to advance a Lagrangian first integral time scale or first long diffusion time scale

$$T_{L1} = \int_0^{\tau_1} \tilde{L}_o(\tilde{x}_o,\tau)\, d\tau, \tag{6.44}$$

where τ_1 = 0.26 s is the first zero crossing of the Lagrangian autocorrelation. Essentially, the first integral time scale accounts solely for the positive portion of the Lagrangian autocorrelation shown in Fig. 6.21. A value of T_{L1} = 51.5 ms was obtained. This yields a Lagrangian time scales ratio T_{L1}/t_L = 9.45

which *clearly suggests the predominance of large diffusion times.* The ratios of the Eulerian time scales are exactly of same order of magnitude.

It is worthwhile to further inspect the streamwise changes of the Lagrangian to Eulerian micro time scale and first integral time scale ratios. These ratios are denoted by t_L/t and T_{L1}/T_1, respectively. The variations of these two ratios along the turbulence line are shown in Fig. 6.23. Both ratios exhibit a similar continuous decrease with increasing axial extent $\tilde{\xi}$ of the turbulence line. Their values diminish from about 0.96 at the reference point $\tilde{\xi} = 0$ (or $\tilde{x}_o = 10$) to roughly 0.42 at the downstream end of the turbulence line $\tilde{\xi}_{max} = 4$ (or $\tilde{x}_B = 14$). This persistent streamwise diminution of the time scale ratios can be attributed to the accompanying continuous change of the turbulence time scales. It is apparent that the use of unique values for these ratios is precluded considering the increase of the Eulerian time scales along the turbulence line. Moreover, the Lagrangian or diffusion time scales are consistently smaller than their Eulerian equivalents. Since the turbulence is the agent effecting the diffusion, the Lagrangian time scales reflect, in all likelihood, the restrictions imposed by the turbulence or Eulerian time scales. The diffusing material is basically entrained and conveyed by the existing turbulent eddies. With increasing Eulerian time scales the diffusion is consequently enhanced and, as a result, smaller diffusion time scales prevail. *Then both short and long diffusion time scales are constrained within the micro and first integral time scales of the turbulence, i.e.,*

$t_L < t$ and $T_{L1} < T_1$. If the Eulerian time scales would decrease in the streamwise direction, the opposite situation is anticipated.

Comparison of the foregoing results with available data is quite difficult due to the considerable scattering of the latter. Ratios of the Lagrangian to Eulerian integral time scales ranging from 1.1 to 8.5 were proposed by Hay and Pasquill [27] for atmospheric flow. Furthermore, constant value of 4 for this ratio was suggested in this reference. For large-scale atmospheric motion Kao [69] reported that the Lagrangian to Eulerian integral time scale ratio is generally smaller than unity. Values of about 0.43 to 0.45 for this ratio are further presented in Ref. 69. In pipe and/or wind-tunnel flows, values of the integral time scales ratio usually larger than or equal to unity are reported. For pipe diffusion Baldwin and Mickelsen [31] found that this ratio can change from 4.7 to 40. Constant values of 3, 1 and 1.3 for the integral time scales ratio were proposed by Snyder and Lumley [29], Deissler [32] and Shlien and Corrsin [33], respectively. An analysis of some existing data led Philip [40] to the inference that this ratio can change from 0.3 to beyond 14 depending upon the flow situation. The smaller values refer to large-scale atmospheric turbulence. It is thus apparent that the results given in Fig. 6.23 are corroborated to a reasonable extent by previous findings.

The Lagrangian or diffusion first integral length scale Λ_{L1} was furthermore examined since it is representative of the longitudinal displacement traveled by diffusing particles [10]. This spatial scale is formally similar to its Eulerian counterpart Λ_1 inasmuch as both are based on their respective first integral time scales. The differences between the Lagrangian and Eulerian first integral length scales stem from the fact that the fomer is expressed in terms of the Lagrangian turbulent velocity whereas the latter is defined by the Eulerian mean velocity. In computing this Lagrangian spatial scale the characteristic Lagrangian turbulent velocity v_o, i.e., the velocity at the reference point $\tilde{\xi} = 0$, was utilized. Thus, the Lagrangian first integral length scale is

$$\Lambda_{L1} = (\overline{v_o^2})^{\frac{1}{2}} T_{L1}, \tag{6.45}$$

where $(\overline{v_o^2})^{\frac{1}{2}} = 2.5$ m/s (8.22 ft/s) and $T_{L1} = 51.5$ ms. It was found that $\Lambda_{L1} = 12.9$ cm (0.424 ft). This diffusion spatial scale was further compared to the Eulerian first integral length scale Λ_1. The latter represents the large scale structure of the turbulence along the turbulence line. Variation of the ratio of the Lagrangian to Eulerian first integral length scales Λ_{L1}/Λ_1 with increasing axial separation $\tilde{\xi}$ is depicted in Fig. 6.24. Its value ranges from about 0.28 to 0.15. These relatively small values of this ratio indicate that the spatial scales of the turbulence are larger than the displacement scales of diffusing particles. In other words, *the diffusion spatial scales are restricted within the space scales of the prevalent turbulence.* Generally, the values of the length scale ratio portrayed in Fig. 6.24 are in reasonable agreement with the limited available previous data. For changing turbulent velocity from 0.55 to 1.46 m/s (1.8 to 4.8 ft/s) Baldwin and Mickelsen [31] found values of this ratio varying from 1.2 to 0.14. A value of 0.34 for this length scale ratio is implied by Snyder and Lumley [29] for a turbulent velocity of 13 cm/s (0.426 ft/s).

Computation of the turbulent momentum exchange coefficient for very long diffusion times hinges upon knowledge of the Lagrangian autocorrelation up to its final asymptotic zero trend. It is anticipated that the Lagrangian autocorrelation would approach zero level in a comparable manner as the Eulerian autocorrelation since they possess similar properties [10]. The stipulation that the Lagrangian integral time scale would finally become zero with increasing time displacement was employed in extrapolating the Lagrangian autocorrelation beyond the lag time $\tau = 0.85$ s. This condition was fulfilled at a time delay around 4.2 s. The axial extent corresponding to this extended time lapse was estimated based on Eq. (3.23) and using same characteristic mean velocity scale as for the turbulence line, viz., $\xi = U_c \tau$. An extended longitudinal reach of about 30 m (100 ft) was obtained since $U_c = 7.12$ (23.4 ft/s) (see Sect. 6.1.1). Thus, the extending time displacement yielded roughly a turbulence line of an axial fetch $\tilde{\xi} = 20$. This axial separation can be viewed as the largest distance traveled by diffusing material before the autocorrelation of their turbulent velocity completely vanishes. Such a long distance can be attributed to the convection of material by the mean flow. The variation of this extended Lagrangian autocorrelation coefficient with increasing time delay is depicted in Fig. 6.25.

6.5 Turbulent diffusion

Generally, under stable conditions at Richardson numbers smaller than about 0.1 the turbulent momentum, mass and heat exchange coefficients are approximately equal [22,54]. Then estimation of the momentum exchange coefficient suffices to ascertain the features of turbulent diffusion processes. This approach was explored in this experiment since the Richardson number of the wake flow was roughly 0.002 (see Sect. 6.1.1). Computation of the turbulent momentum exchange coefficient (or eddy diffusivity) is basically contingent upon knowledge of the Lagrangian autocorrelation within the flow domain of interest.

In this work the axial Lagrangian autocorrelation coefficient $\tilde{L}_o(\tilde{x}_o,\tau)$ was obtained from a set of Eulerian autocorrelations on the turbulence line as described in Sect. 6.4. The axial turbulent momentum exchange coefficient $K_M(\tilde{x}_o,t_D)$ can be then evaluated by means of the relationship [10,12]

$$K_M(\tilde{x}_o,t_D) = \overline{v_o^2} \int_o^{t_D} \tilde{L}_o(\tilde{x}_o,\tau)\, d\tau, \tag{6.46}$$

in which the characteristic mean-square value of the Lagrangian velocity for the turbulence line $\overline{v_o^2} = 6.25\ m^2/s^2$ $(67.2\ ft^2/s^2)$ and $\tilde{x}_o = x_o/R$. This characteristic velocity was utilized considering the nonhomogeneous nature of the turbulence along the turbulence line. In the foregoing equation the elapsed diffusion time since the starting of a diffusion process is denoted by t_D for convenience. The eddy diffusivity is ascertained with respect to the reference point $\tilde{x}_o = 10$ (or $\tilde{\xi} = 0$) on the turbulence line due to the intrinsic definition of the reference-point Lagrangian autocorrelation. Consequently, it can be viewed as representative for the entire turbulence box. The longitudinal eddy diffusivity was made dimensionless, for the sake of generality, using $\overline{v_o^2}$ and the Lagrangian first integral time scale $T_{L1} = 51.5$ ms (see Sect. 6.4) according to

$$\tilde{K}_M(\tilde{x}_o,\tilde{t}_D) = K_M(\tilde{x}_o,t_D)/\overline{v_o^2}\, T_{L1}, \tag{6.47}$$

where the dimensionless diffusion time is defined by

$$\tilde{t}_D = t_D/T_{L1}, \tag{6.48}$$

where T_{L1} = 51.5 ms. The first integral time scale was utilized inasmuch as it is indicative of the long diffusion times.

To obtain a complete picture of the eddy diffusivity variation at very large diffusion times it is imperative to account for the final asymptotic decay of the Lagrangian autocorrelation coefficient. The dimensionless turbulent momentum exchange coefficient $\tilde{K}_M(\tilde{x}_o,\tilde{t}_D)$ was hence computed by means of Eq. (6.47) employing the extended Lagrangian autocorrelation coefficient. The resulting axial eddy diffusivity change with augmenting diffusion time from $\tilde{t}_D$ = 0 to 82 (0 to 4.2 s) is portrayed in Fig. 6.26. A closer examination of its variation for short diffusion times ranging from $\tilde{t}_D$ = 0 to 0.2 (0 to 103 ms) is provided by the insert incorporated in this figure. For very short diffusion times, viz., from 0 to about 0.1 (5.15 ms), the momentum exchange coefficient can be approximated by $\tilde{K}_M(\tilde{x}_o,\tilde{t}_D) \approx \tilde{t}_D$ within about 10% difference as clearly shown in Fig. 6.26. This time range is practically equal to the Lagrangian micro time scale t_L = 5.45 ms (see Sect. 6.4).

The momentum exchange coefficient attains its maximum value at a diffusion time equal to the first zero crossing of the Lagrangian autocorrelation, viz., at $t_D = \tau_1$ = 0.26 s (see Sect. 6.4). Then $K_M(\tilde{x}_o,t_D$ = 0.26 s) = 3219 cm²/s (3.46 ft²/s) or $\tilde{K}_M(\tilde{x}_o,\tilde{t}_D$ = 5.05) = 1.0 as indicated in Fig. 6.26. *This value of the eddy diffusivity accounts* *solely for the positive autocorrelation.* It is worthwhile to remark that the normalizing scale $\overline{v_o^2}\, T_{L1}$ is basically the largest value that the momentum exchange coefficient can attain in view of the definition of the Lagrangian first integral time scale. The eddy diffusivity peak value of 3219 cm^2/s is in reasonable agreement with reported available results for similar stability conditions in the extreme lower atmosphere. In a study at Round Hill, peak values of the momentum exchange coefficient varying from 2400 to 5600 cm^2/s (2.58 to 6.03 ft^2/s) for heights from 2.3 to 6.4 m (7.5 to 21 ft) and wind speeds of 2.52 to 3.13 m/s (8.27 to 10.27 ft/s) were found by Cramer in 1953 [70]. At a height of 2 m (6.6 ft) over grass ranging from 1 to 60 cm (0.0328 to 1.97 ft) high and for a wind speed of 5 m/s (16.4 ft/s), typical maximum values for the eddy diffusivity varying from 2200 to 4800 cm^2/s (2.37 to 5.16 ft^2/s) were reported by Pasquill in 1962 [11].

After its peak value the turbulent momentum exchange coefficient displays a consistent decrease with increasing diffusion time as shown in Fig. 6.26. This continuous diminishing trend results from accounting for the negative Lagrangian autocorrelation. It is natural to furthermore expect that the turbulent momentum exchange coefficient will vanish at very long diffusion times inasmuch as a turbulent flow within a finite axial extent was investigated. Zero eddy diffusivity was obtained at about $\tilde{t}_D = 82$. This long diffusion time corresponds to the time delay $\tau = 4.2$ s which yielded the final asymptotic zero decay of the extended Lagrangian autocorrelation coefficient. In other words, the turbulent exchange coefficient with respect to the reference point $\tilde{x}_o = 10$ vanishes within an axial reach of roughly $\tilde{\xi} = 20$.

The axial turbulent momentum exchange coefficient $K_M(\tilde{x}_o, t_D)$ and the dispersion coefficient (or mean-square displacement) $D(\tilde{x}_o, t_D)$ are related by [10,15]

$$K_M(\tilde{x}_o, t_D) = \frac{1}{2}\frac{d}{dt_D} D(\tilde{x}_o, t_D), \tag{6.49}$$

since the former is the time rate change of the latter. In terms of the Lagrangian autocorrelation coefficient $\tilde{L}_o(\tilde{x}_o, \tau)$, the longitudinal mean-square displacement is expressed by [10,15]

$$D(\tilde{x}_o, t_D) = 2\,\overline{v_o^2} \int_o^{t_D} (t_D - \tau)\, \tilde{L}_o(\tilde{x}_o, \tau)\, d\tau. \tag{6.50}$$

Often the mean-square displacement is designated by either $\overline{Y^2}$ or $\overline{X^2}$. The dispersion coefficient was made dimensionless employing the same characteristic Lagrangian velocity and first integral time scale used in normalizing the eddy diffusivity, viz.,

$$\tilde{D}(\tilde{x}_o, \tilde{t}_D) = D(\tilde{x}_o, t_D)/\overline{v_o^2}\, T_{L1}^2. \tag{6.51}$$

It is important to note that this axial dispersion coefficient is essentially defined with respect to the reference point $\tilde{x}_o = 10$ (or $\tilde{\xi} = 0$) on the turbulence line in a similar manner as for both the eddy diffusivity and Lagrangian autocorrelation. As a result, it is representative for the entire turbulence box.

The dimensionless axial dispersion coefficient was computed using Eq. (6.51) and its variation with increasing diffusion time $\tilde{t}_D$ is portrayed in Fig. 6.27. For very short diffusion times up to the Lagrangian micro time scale, viz., for $\tilde{t}_D$ up to roughly 0.1, the dispersion coefficient can be approximated by $\tilde{D}(\tilde{x}_o,\tilde{t}_D) \approx \tilde{t}_D^2$ within a difference of about 8%. This behavior is clearly revealed in the insert included in Fig. 6.27. Generally, the axial dispersion coefficient exhibits a monotonical increase with augmenting diffusion time. At very long diffusion times the mean-square displacement approaches asymptotically a constant level $D(\tilde{x}_o,t_D = 4.2 \text{ s}) = 1.06 \text{ m}^2(11.5 \text{ ft}^2)$ or $\tilde{D}(\tilde{x}_o,\tilde{t}_D = 81.6) = 64.2$. This constant value is obtained as the eddy diffusivity vanishes considering Eq. (6.49). Essentially, *this upper bound indicates the largest longitudinal mean-square displacement of diffusing material.*

To substantiate the estimation of the dispersion coefficient and its use in predicting the concentration of transportable material along the turbulence line a gas diffusion experiment was performed. Sulfur hexaflouride was continuously emitted at a constant rate $Q = 250 \text{ cm}^3/\text{s}$ ($0.0088 \text{ ft}^3/\text{s}$) at a point source located 7.60 m (25 ft) upstream of the turbulence-line reference point, i.e., at $\tilde{x} = 5$, as shown in Fig. 5.10. The features of this experiment and the concentration measurements are described in Sect. 5.6. In the presentation of the results, the measured concentration is referred to its monitored level at the reference point $\tilde{\xi} = 0$ (or $\tilde{x}_o = 10$). Thus, the normalized concentrations

$$\tilde{\chi}(\xi) = \chi(\xi)/\chi_o, \tag{6.52}$$

where $\chi_o = 5.8$ ppm (parts per million). Variation of the normalized measured concentration with increasing axial distance $\tilde{\xi}$ along the turbulence line is depicted in Fig. 6.29. This concentration exhibits a continuous decrease to about 0.74 (4.3 ppm) as $\tilde{\xi}$ increases to 4.

The dispersion coefficient computed in accordance to Eq. (6.50) in terms of the Lagrangian autocorrelation was used to predict the concentration along the turbulence line in terms of a known concentration at the reference point. Essentially, the gas emitted a flow rate Q by the point source located at $\tilde{x} = 5$ was entrained by the turbulent flow forming a spreading plume. Then at the reference point the gas tracer was distributed within a finite area A_o which is basically the local cross section of the growing plume. The flow visualization clearly revealed this situation. This finite area A_o is interpreted as a hypothetical area source of finite concentration contained within the reference plane defined by $\tilde{x}_o = 10$ = constant with regard to the turbulence box. It is further reasonable to assume that the gas is uniformly distributed within the area. Then the concentration everywhere in the area source A_o equals the measured value χ_o at the reference point. The cross section of this area source based on mass continuity is

$$A_o = Q/\chi_o U_c, \tag{6.53}$$

and the equivalent area source strength is

$$q_o = Q/A_o, \tag{6.54}$$

where Q is the point source emission rate and the characteristic mean velocity scale $U_c = 7.12$ m/s (23.4 ft/s) (see Sect. 6.1.1). It was found that the cross section of the area source $A_o = 6.05\ m^2$ (65 ft^2) and its strength $q_o = 4.13 \times 10^{-3}$ cm/s (1.36×10^{-4} ft/s) since $Q = 250\ cm^3/s$ and $\chi_o = 5.8$ ppm.

The area source A_o consists essentially of numerous differential area sources of flow rate $q_o dA_o$. Each differential area source

dA_o can be approximated by a hypothetical point source located at its centroid (x_o, y_s, z_s). Consequently, the differential concentration $d\chi$ induced by an area source element dA_o at a point ξ along the turbulence line is estimated by the point-source concentration equation [10]

$$d\chi(\xi, x_o, y_s, z_s) = \frac{q_o dA_o}{(2\pi)^{3/2}} \int_0^\infty \frac{1}{[D(\tilde{x}_o, t_D)]^{3/2}}$$

$$\cdot \exp\left[-\frac{(\xi - U_c t_D - x_o)^2 + y_s^2 + z_s^2}{2D(\tilde{x}_o, t_D)}\right] dt_D, \tag{6.55}$$

where $D(\tilde{x}_o, t_D)$ is the dispersion coefficient. This equation is for uniform flow in isotropic turbulence. It implies furthermore that the displacement probability density distribution of diffusing material is Gaussian [10]. As a result, Eq. (6.55) provides solely a first order approximation for the concentration. Computation of the gas differential concentration $d\chi$ on the turbulence line was carried out using the dispersion coefficient given by Eq. (6.50). The contribution of the integrand in Eq. (6.55) is negligibly small at very long diffusion times due to the exponential decay. It suffices then to compute the concentration up to the diffusion time corresponding to the upper bound of the dispersion coefficient, viz., up to $t_o = 4.2$ s. The total concentration at a point ξ on the turbulence line caused by the entire area source is simply obtained by integrating the foregoing point-source concentration equation over its cross section A_o. Thus,

$$\tilde{\chi}(\tilde{\xi}, \tilde{x}_o) = \int_{A_o} d\chi(\xi, x_o, y_s, z_s)/\chi_o, \tag{6.56}$$

where the total concentration was referred to the measured level $X_o = 5.8$ ppm at the reference point $\tilde{x}_o = 10$.

Variation of the normalized computed concentration $\tilde{X}(\tilde{\xi},\tilde{x}_o)$ with increasing axial separation $\tilde{\xi}$ from the reference point. $\tilde{x}_o$ is portrayed together with its measured counterpart in Fig. 6.28. A striking congruent behavior of the computed and measured concentrations is clearly observed. Both concentrations exhibit a similar gradual decrease in the streamwise direction. The predicted concentrations. revealed slightly larger values than the measured levels. Their differences varied from about 4% at $\tilde{\xi} = 1$ to roughly 13 and 12% at $\tilde{\xi} = 3$ and 4, respectively. These results are in a remarkable agreement considering the assumptions involved in employing the point source-concentration approximation. *It is thus apparent that the notable congruence of the predicted and measured concentrations corroborates the deduced dispersion coefficient. Moreover, this result attests to the validity of the model utilized in computing the Lagrangian autocorrelation.*

7. SUMMARY AND CONCLUSIONS

The main goals of this work were the development of a model for the evaluation of the Lagrangian turbulent velocity autocorrelation and its experimental substantiation in the extreme lower atmosphere. Knowledge of the Lagrangian autocorrelation is indispensable for the estimation of the turbulent momentum exchange coefficient, the dispersion coefficient and, finally, the spatial concentration of transportable material. In this work, the statistical treatment of turbulence was utilized due to its recognized superiority with respect to the transfer theory approach.

A method for assessing the statistical stationarity of turbulent velocity was put forth as a prerequisite for the statistical analysis. In this method an equivalent ensemble was created by dividing a sufficiently long time history of turbulent velocity into a finite number of equal time length records. The establishment of an equivalent ensemble was based upon fulfilling the following three criteria: (1) unchanged flow conditions throughout the time history; (2) each sample record contains all the information up to the largest turbulent time scale of interest; and, (3) the sample records are statistically independent among themselves.

A relationship between the Lagrangian and Eulerian autocorrelations was developed based on trajectory, particle-space and reference-plane averagings of Eulerian velocity products. The Lagrangian autocorrelation is expressed in this model by a domain integral over a set of ordinary Eulerian autocorrelations which are to be obtained concurrently at all positions in the flow field of interest. Such a flow field is viewed as a turbulence "box." The relationship for the

Lagrangian autocorrelation is not constrained to either homogeneous and/or isotropic turbulence.

An experimental investigation was primarily conducted for the purpose of verifying the proposed model for computing the Lagrangian autocorrelation and its application to predicting turbulent diffusion. Turbulent flow within the extreme lower atmospheric layer, i.e., the layer up to about 5 m depth was simulated using the wake flow generated by a 3.04 m diameter fan installed on flat grassland at the Colorado State University Environmental Field Station. Both dynamic and thermal similitude criteria were satisfactorily fulfilled by this simulated flow. Detailed velocity surveys were carried out under calm wind, dry and stable conditions over an axial fetch of 6.08 m along the wake axis. This stretch was considered a turbulence "line" within its box, viz., within the wake. All the measurements were performed simultaneously at five stations on the turblence line using a longitudinal array of five hot-wire anemometers. These hot-wire anemometer systems were remotely operated. The measurements concentrated on the longitudinal turbulent velocity since its energy is substantially larger than those of the other two components.

The stationarity test of the turbulent velocity clearly indicated that it was approximately weakly stationary in a statistical sense. Substantiation of the ergodic assumption was furthermore roughly accomplished through a heuristic checkup. As a result, the turbulent velocity was considered a realization of a weakly self-stationary random process. The streamwise changing turbulence properties along the turbulence line was deduced from a set of five Eulerian autocorrelations which were obtained concurrently. The autocorrelations displayed a consistent similar change in amplitude with augmenting time displacement including their negative portions and final zero decay. A first integral time scale was introduced as a characteristic large time scale of the turbulence. This time scale was defined by considering only the positive autocorrelation. The micro and first integral time and length scales of the turbulence revealed a continuous streamwise increase along the turbulence line. This behavior attested to the nonhomogeneous nature of the turbulence. It was attributed to the energy dissipation at high frequencies and concomitant energy extraction from the mean flow at low frequencies. The turbulence structure was clearly dominated by relatively large-scale eddies inasmuch as the first integral time and length scales were about tenfold larger than their micro scale counterparts. Moreover, the structure of the turbulence from large to small eddy sizes was in acceptable agreement with atmospheric flows based on the micro and integral scale Reynolds numbers and the peak reduced frequency of the axial turbulent velocity energy spectrum. Further substantiation of the large-scale structure predominance was furnished by the drastic reduction in the dissipation along the turbulence line. The negative autocorrelation was interpreted as a measure of turbulent kinetic energy transfer from larger to smaller scales. A higher degree of negative autocorrelation at greater time displacements indicated sustenance of larger-scale eddies and, hence, a slower rate of energy transfer to smaller eddies.

A simultaneous unified insight into the continuous time and space changes of the Eulerian autocorrelations along the turbulence line was procured by introducing Eulerian reference-point autocorrelations and Eulerian autocorrelation envelopes. The Eulerian reference-point autocorrelations supplied the time change of the autocorrelation with respect to the turbulent kinetic energy at the reference point on the turbulence line, i.e., the first station on this line. This representation was put forth in the light of the turbulence non-homogeneity. The spatial variations of the autocorrelations was furnished by the Eulerian autocorrelation envelopes. These envelopes were obtained by connecting the simplitudes of the reference-point autocorrelations at selected time displacements.

The longitudinal Lagrangian autocorrelation was estimated by means of a line integral over all the Eulerian autocorrelation envelopes for the turbulence line. Basically, the Lagrangian autocorrelation variation with augmenting time delay including its negative asymptotic zero approach was qualitatively similar to the Eulerian autocorrelation. Large diffusion times predominated since the Lagrangian first integral time scale was about ten times larger than the micro time scale. The integral scale accounted solely for the positive Lagrangian autocorrelation. Ratios of the Lagrangian to Eulerian time and length scales smaller than unity were found. These ratios are in reasonable agreement with previous findings. The Lagrangian time and length scales reflected the restrictions imposed by the Eulerian scales since the turbulence is the agent effecting the diffusion. Both short and long diffusion time and length scales were constrained within the Eulerian scales of turbulence.

Turbulent momentum exchange coefficient (or eddy diffusivity) and dispersion coefficient (or mean-square displacement of diffusing material) variations with augmenting diffusion time were ascertained using the known Lagrangian autocorrelation. The eddy diffusivity attained its maximum value at a diffusion time equal to the first zero crossing of the Lagrangian autocorrelation. This peak value is in reasonable agreement with available results in the extreme lower atmosphere. At very long diffusion time the momentum exchange coefficient vanished inasmuch as a turbulent flow within a finite axial extent was investigated. Concentration of diffusing material along the turbulence line was predicted employing the deduced dispersion coefficent. The computed concentration distribution along the turbulence line was compared with measured concentrations of sulfur hexaflouride which was utilized as a gas tracer in a diffusion experiment. Both concentrations exhibited a striking congruent variation with increasing axial distance along the turbulence line. They differed by 4 to 13% at the most. This result clearly substantiates the model utilized for computing the Lagrangian autocorrelation and, hence, the deduced turbulent momentum exchange and dispersion coefficient.

REFERENCES

1. Boussinesq, J., "Essai Sur la Théorie des Eaux Courantes," Mém. prés. par div. savants à l' Académie des Sciences, Paris, Vol. 23, No. 1, 1877, pp. 1-680.

2. Taylor, G.I., "Eddy Motion in the Atmosphere," Philosophical Transactions of the Royal Society, Vol. 215, 1915, pp. 1-26.

3. Prandtl, L., "Über die ausgebildete Turbulenz," Zeitschrift für angewandte Mathematik und Mechanik, Vol. 5, 1925, pp. 136-139.

4. Taylor, G.I., "The Transport of Vorticity and Heat through Fluids in Turbulent Motion," Proceedings of the Royal Society, A, 135, 1932, pp. 685-705.

5. Prandtl, L., "The Mechanisms of Viscous Fluids," Aerodynamic Theory, ed. Durand, W.F., Vol. 3, Dover Publications, Inc., New York, N.Y., 1963, pp. 34-208.

6. von Kármán, T., "Mechanical Similitude and Turbulence," NACA TM 611, March 1931, Washington, D.C.

7. Sutton, O.G., Micrometeorology, McGraw-Hill Book Company, Inc., New York, N.Y. 1953.

8. Monin, A.S., "Turbulent Diffusion in the Ground Layer of the Atmosphere," Szvestiya AN SSR Seriya Geofizicheskaya, No. 12, 1956, pp. 1461-1473.

9. Priestley, C.H.B., Turbulent Transfer in the Lower Atmosphere, The University of Chicago Press, Chicago, Ill., 1959.

10. Hinze, J.O., Turbulence: An Introduction to Its Mechanism and Theory, McGraw-Hill Book Co., New York, N.Y., 1959.

11. Pasquill, F., Atmospheric Diffusion, D. Van Nostrand Co. Ltd., London, England, 1968.

12. Taylor, G.I., "Diffusion by Continuous Movements," Proceedings of the London Mathematical Society, Vol. 20, 1921, pp. 196-212.

13. Taylor, G.I., "Statistical Theory of Turbulence, Parts I-IV," Proceedings of the Royal Society, A, Vol. 151, 1935, pp. 421-478.

14. Taylor, G.I., "The Spectrum of Turbulence," Proceedings of the Royal Society, A, Vol. 164, 1938, pp. 476-490.

15. Kampé de Fériet, J., "Les Fonctions Aléatorires Stationnaires et la Theorie Statistique de la Turbulence Homogène, "Annales Société Scientifique de Bruxelles, Vol. 59, Ser. 1, 1939, pp. 145-194.

16. Heisenberg, W., "On the Statistical Theory of Turbulence," NACA TM 1431, January 1958, Washington, D.C.

17. Friedlander, S.K. and Topper, L.,eds., Turbulence *Classic Papers on Statistical Theory*, Interscience Publishers, Inc., New York, N.Y., 1961.

18. Frenkiel, F.N., "Turbulent Diffusion: Mean Concentration Distribution in a Flow Field of Homogeneous Turbulence," Advances in Applied Mechanics, Vol. 3, eds. von Mises, R. and von Kármán, T., Academic Press, New York, N.Y., 1953, pp. 61-107.

19. Townsend, A.A., The Structure of Turbulent Shear Flow, Cambridge University Press, London, 1956.

20. Batchelor, R.K., The Theory of Homogeneous Turbulence, Cambridge University Press, London, 1959.

21. Lin, C.C., "Statistical Theories of Turbulence," Turbulent Flows and Heat Transfer, ed. Lin, C.C., High Speed Aerodynamics and Jet Propulsion, Vol. 5, Princeton University Press, Princeton, N.J., 1959, pp. 196-253.

22. Lumley, J.L. and Panofsky, H.A., The Structure of Atmospheric Turbulence, Interscience Publishers, New York, N.Y., 1964.

23. Lumley, J.L., Stochastic Tools in Turbulence, Applied Mathematics and Mechanics, eds. Frenkiel, F.N. and Temple, G., Vol. 12, Academic Press, New York, N.Y., 1970.

24. Monin, A.S. and Yaglom, A.M., Statistical Fluid Mechanics: Mechanics of Turbulence, Vol. 1, The MIT Press, Cambridge, Mass., 1971.

25. Csanady, G.T., Turbulent Diffusion in the Environment, D. Reidel Publishing Co., Boston, Mass., 1973.

26. Mickelsen, W.R., "An Experimental Comparison of the Lagrangian and Eulerian Correlation Coefficients in Homogeneous Isotropic Turbulence, NACA TN 3570, 1955, Washington, D.C.

27. Hay, J.S. and Pasquill, F.,"Diffusion From a Continuous Source in Relation to the Spectrum and Scale of Turbulence," Advances in Geophysics, Vol. 6, eds. Frenkiel, F.N. and Sheppard, P.A., Academic Press, New York, N.Y., 1959, pp. 345-365.

28. Angell, J.K., "Measurements of Lagrangian and Eulerian Properties of Turbulence at a Height of 2,500 ft," Royal Meterological Society Quarterly Journal, Vol. 90, 1964, pp. 57-71.

29. Snyder, W.H. and Lumley, J.L., "Some Measurements of Particle Velocity Autocorrelation Functions in a Turbulent Flow," Journal of Fluid Mechanics, Vol. 48, Pt. 1, 1971, pp. 41-71.

30. Baldwin, L.V. and Walsh, T.J., "Turbulent Diffusion in the Core of Fully Developed Pipe Flow," American Institute of Chemical Engineers Journal, Vol. 7, 1961, pp. 53-61.

31. Baldwin, L.V. and Mickelsen, W.R., "Turbulent Diffusion and Anemometer Measurements," American Society of Civil Engineers Transactions, Vol. 128, No. 1, 1963, pp. 1595-1631.

32. Deissler, R.G., "Analysis of Multipoint-Multitime Correlations and Diffusion in Decaying Homogeneous Turbulence," NASA TR-R-96, 1961, Washington, D.C.

33. Shlien, D.J. and Corrsin, S., "A Measurement of Lagrangian Velocity Autocorrelation in Approximately Isotropic Turbulence," Journal of Fluid Mechanics, Vol. 62, Pt. 2, 1974, pp. 255-271.

34. Corrsin, S., "Progress Report on Some Turbulent Diffusion Research," Advances in Geophysics, Vol. 6, eds. Frenkiel, F.N. and Sheppard, P.A., Academic Press, New York, N.Y., 1959, pp. 161-164.

35. Saffman, P.G., "An Approximate Calculation of the Lagrangian Auto-covariance Coefficient for Stationary Homogeneous Turbulence," Journal of Applied Science Research, Sect. A, Vol. 11, 1963, pp. 245-255.

36. Kraichnan, R.H., "Relation between Lagrangian and Eulerian Correlation Times of a Turbulent Velocity Field," The Physics of Fluids, Vol. 7, No. 1, January 1964, pp. 142-143.

37. Batchelor, G.K., "The Effect of Homogeneous Turbulence on Material Lines and Surfaces," Proceedings of the Royal Society of London, Mathematical and Physical Sciences, Ser. A, Vol. 213, No. 1114, July 1952, pp. 349-366.

38. Roberts, P.H., "Analytical Theory of Turbulent Diffusion," Journal of Fluid Mechanics, Vol. 11, Pt. 2, September 1961, pp. 257-283.

39. Kraichnan, R.H., "The Closure Problem of Turbulence Theory," Hydrodynamic Instability, Proceedings of Symposia in Applied Mathematics, Vol. 13, eds. Burkhoff, G., Bellman, R. and Lin, C.C., American Mathematical Society, Providence, R.I., 1962, pp. 199-255.

40. Philip, J.R., "Relation between Eulerian and Lagrangian Statistics," The Physics of Fluid Supplement, 1967, pp. S69-S71.

41. Bendat, J.S. and Piersol, A.G., Random Data: Analysis and Measurement Procedures, Wiley-Interscience, New York, N.Y., 1971.

42. Koper, Jr., C.A. and Sadeh, W.Z., "A Preliminary Study of a Fan Wake," RM23 (PGD-FF/1)/CEM70-71CAK-WZS23, March 1971, College of Engineering, Colorado State University, Fort Collins, Colo.

43. Kovasznay, L.S.G., "Hot-Wire Method," Physical Measurements in Gas Dynamics and Combustion, ed. Landenburg, R.W., et al., University Press, Princeton, N.J., 1954, Pt. 2, Art. F, pp. 219-285.

44. Collins, D.C. and Williams, M.J., "Two-Dimensional Convection from Heated Wires at Low Reynolds Numbers," Journal of Fluid Mechanics, Vol. 6, Pt. 3, 1959, pp. 357-384.

45. Sandborn, V.A., Resistance Temperature Transducers, Meterology Press, Fort Collins, Colo., 1972.

46. Sadeh, W.Z., Maeder, P.F., and Sutera, S.P., "A Hot-Wire Method for low Velocity with Large Fluctuations," The Review of Scientific Instruments, Vol. 41, No. 9, 1970, pp. 1295-1298.

47. Sadeh, W.Z. and Finn, C.L., "A Novel Hot-Wire Anemometer System," to be published.

48. Sadeh, W.Z. and Finn, C.L., "A Method for Remote Use of Hot-Wire Anemometer," The Review of Scientific Instruments, Vol. 42, No. 9, 1971, pp. 1376-1377.

49. Ampex Corp., "Portable Instrumentation Magnetic Tape Recorder/Reproducer," 1964, Redwood City, Calif.

50. Pear, Jr., C.B., Magnetic Recording in Science and Industry, Reinhold Publishing Corp., New York, N.Y., 1967.

51. Magrab, E.B. and Blomquist, D.S., The Measurement of Time-Varying Phenomena: Fundamentals and Applications, Wiley-Interscience, New York, N.Y., 1971.

52. Princeton Applied Research Corp., "Instruction Manual Correlation Function Computers Models 100A & 101A," 1969, Princeton, N.J.

53. Otnes, R.K. and Enochson, L., Digital Time Series Analysis, Wiley-Interscience, New York, N.Y., 1972.

54. Merritt, G. and Rudinger, G., "Thermal and Momentum Diffusivity Measurements in a Turbulent Stratified Flow," AIAA Journal, Vol. 11, No. 11, November 1973, pp. 1465-1470.

55. Turk, A., Edmonds, S.M., and Mark, H.L., "Sulfur Hexaflouride as a Gas-Air Tracer," Environmental Science & Technology, Vol. 2, No. 1, January 1968, pp. 44-48.

56. Collins, G.F., et al., "A Preliminary Evaluation of Gas Air Tracers," Journal of the Air Pollution Control Association, Vol. 15, No. 3, March 1965, pp. 109-112.

57. Hewlett-Packard Co., "Gas Chromatograph 7620A Operating and Service Manual, Vol. III and IV," 1972 and 1970, Avondale, Penn.

58. Burchfield, H.P. and Storrs, E.E., Biochemical Applications of Gas Chromatography, Academic Press, New York, N.Y., 1962.

59. Saltzman, B.E., Coleman, A.I., and Clemons, C.A., "Halogenated Compounds as Gaseous Meteorological Tracers," Analytical Chemistry, Vol. 38, No. 6, May 1966, pp. 753-758.

60. Pauling, L., General Chemistry, W.H. Freeman and Co., San Francisco, Calif., 1956.

61. Geiger, R., The Climate near the Ground, Harvard University Press, Cambridge, Mass., 1966.

62. Comte-Bellot, G. and Corrsin, S., "Simple Eulerian Time Correlation of Full- and Narrow-Band Velocity Signals in Grid-Generated, 'Isotropic' Turbulence," Journal of Fluid Mechanics, Vol. 48, Pt. 2, 1971, pp. 273-337.

63. Frenkiel, F.N., "Statical Study of Turbulence-Spectral Functions and Correlation Coefficients," NACA TM 1436, Washington, D.C., 1948.

64. Panofsky, H.A. and Press, H., "Meteorological and Aeronautical Aspects of Atmospheric Turbulence," Progress in Aeronautical Sciences, Vol. 3, eds. Ferri, A., Küchemann, D. and Sterne, L.H.G., Macmillan Co., 1962, pp. 179-232.

65. Busch, N.E. and Panofsky, H.A., "Recent Spectra of Atmospheric Turbulence, "Quarterly Journal of the Royal Meteorological Society, Vol. 94, No. 400, April 1968, pp. 132-148.

66. Fichtl, G.H. and McVehil, G.E., "Longitudinal and Lateral Spectra of Turbulence in the Atmospheric Boundary Layer at the Kennedy Space Center," Journal of Applied Meteorology, Vol. 9, No. 1, February 1970, pp. 51-63.

67. Kaimal, J.C., Wyngaard, J.C., Izumi, Y., and Coté, O.R., "Spectral Characteristics of Surface-Layer Turbulence," Quarterly Journal of the Royal Meteorological Society, Vol. 98, No. 417, July 1972, pp. 563-589.

68. Kaimal, J.C., "Turbulence Spectra, Length Scales and Structure Parameters in the Stable Surface Layer," Boundary-Layer Meteorology, Vol. 4, 1973, pp. 289-309.

69. Kao, S.K., "Basic Characteristics of Global Scale Diffusion in the Troposphere," Advances in Geophysics, Vol. 18B, eds. Frenkiel, F.N. and Munn, R.E., Academic Press, New York, N.Y., 1974, pp. 15-32.

70. Cramer, H.E. and Record, F.A., "The Variation with Height of the Vertical Flux of Heat and Momentum," Journal of Meteorology, Vol. 10, June 1953, pp. 219-226.

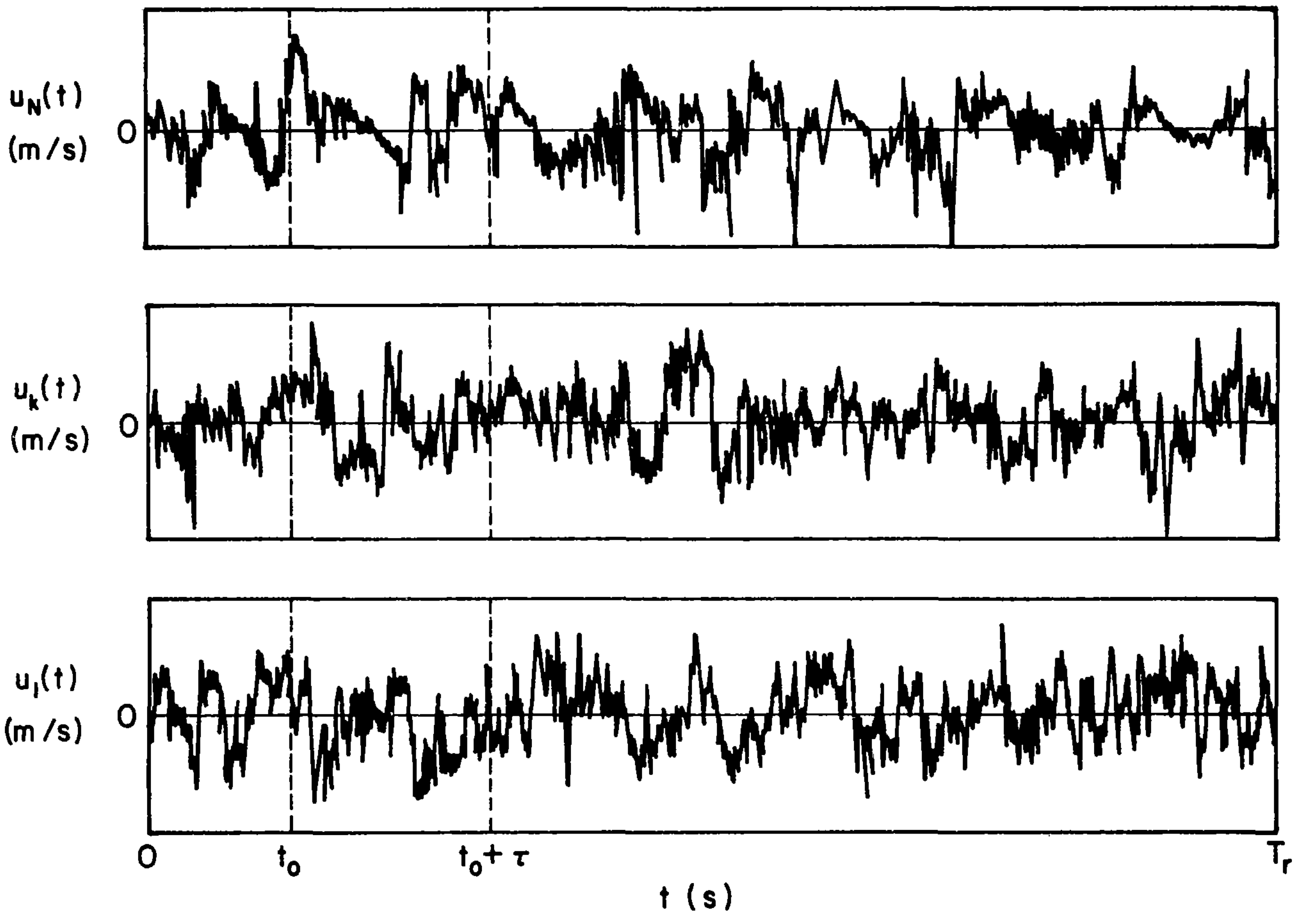

Fig. 3.1 Hypothetical ensemble of turbulent velocity sample records {u(t)}.

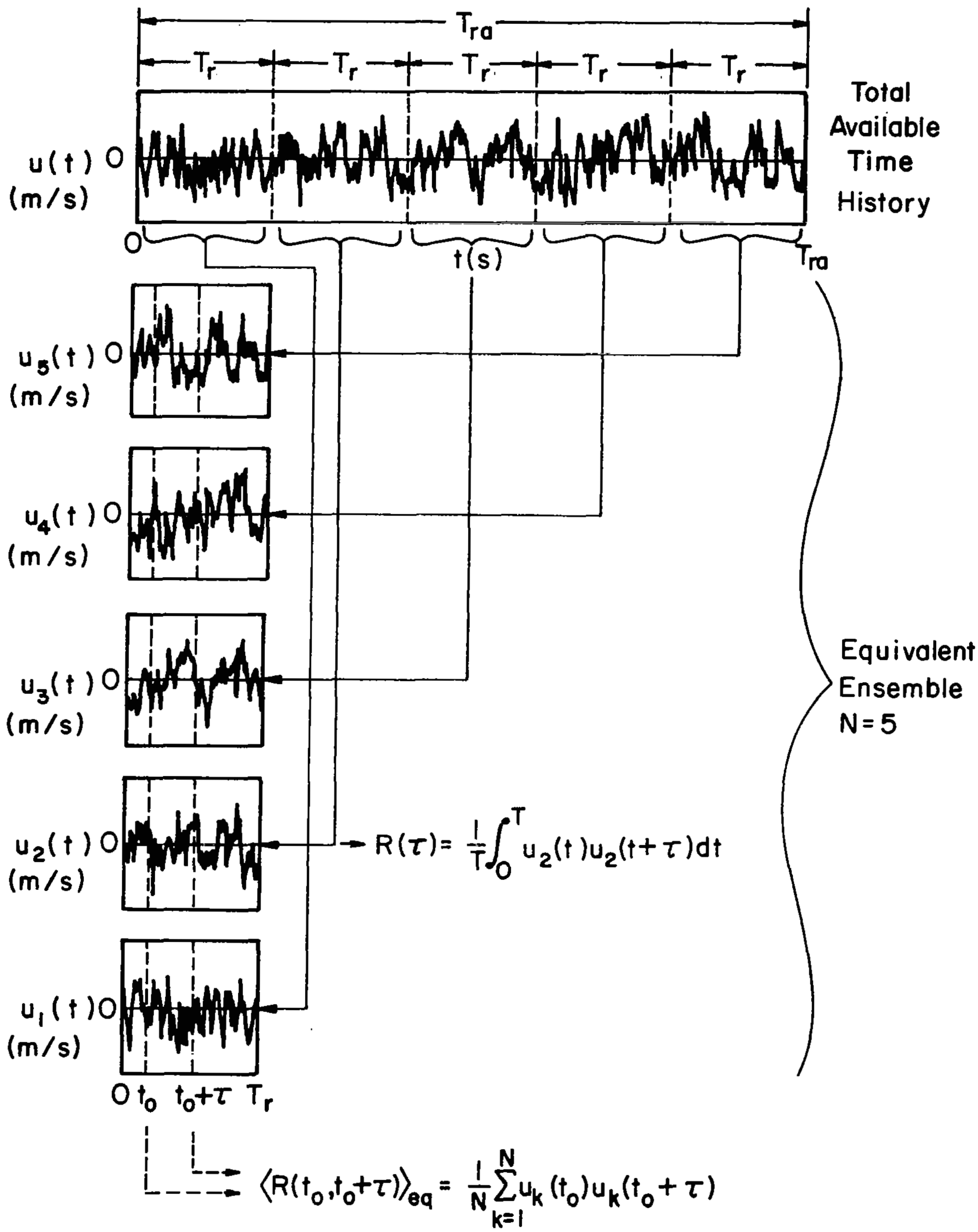

Fig. 3.2 Illustration of the generation of an equivalent ensemble $\{u(t)\}_{eq}$ from an available time history T_{ra}.

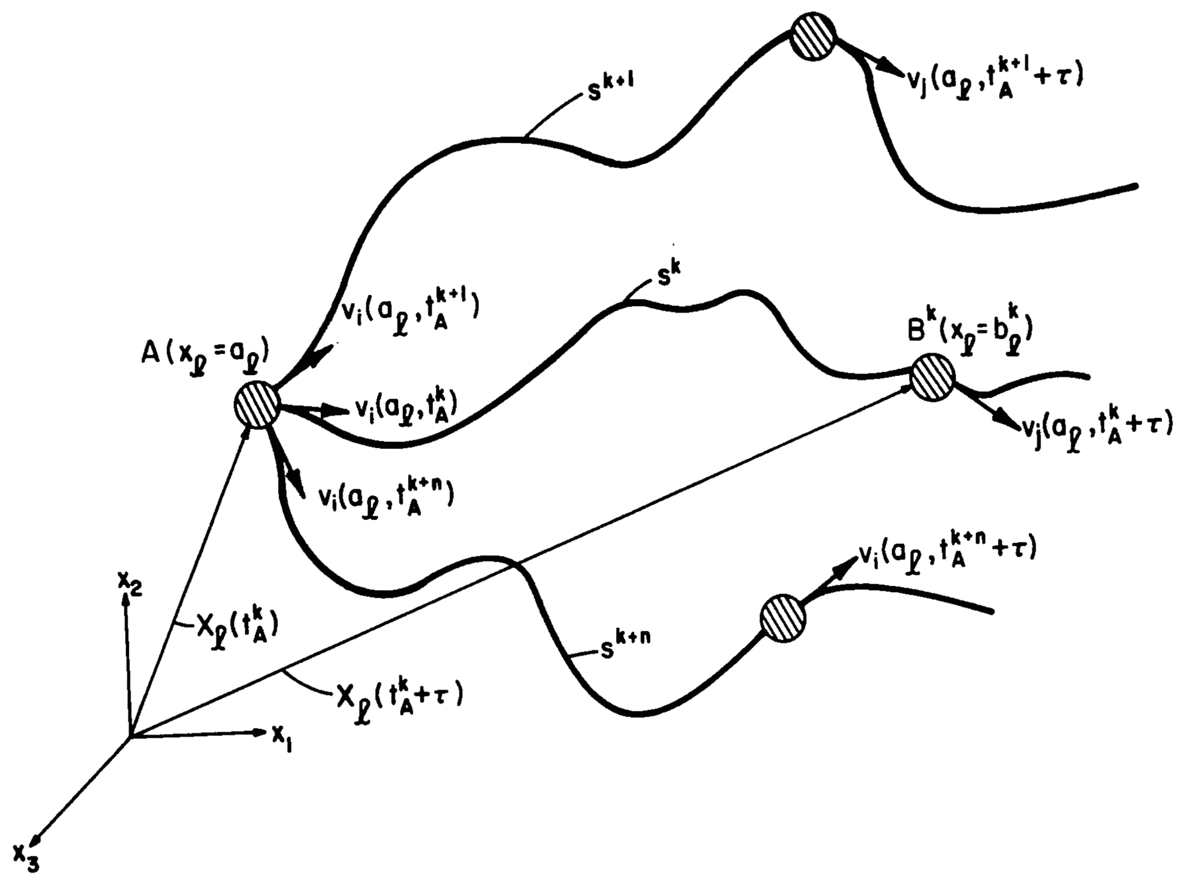

Fig. 3.3 Path lines of several fluid particles which cross the same reference position A.

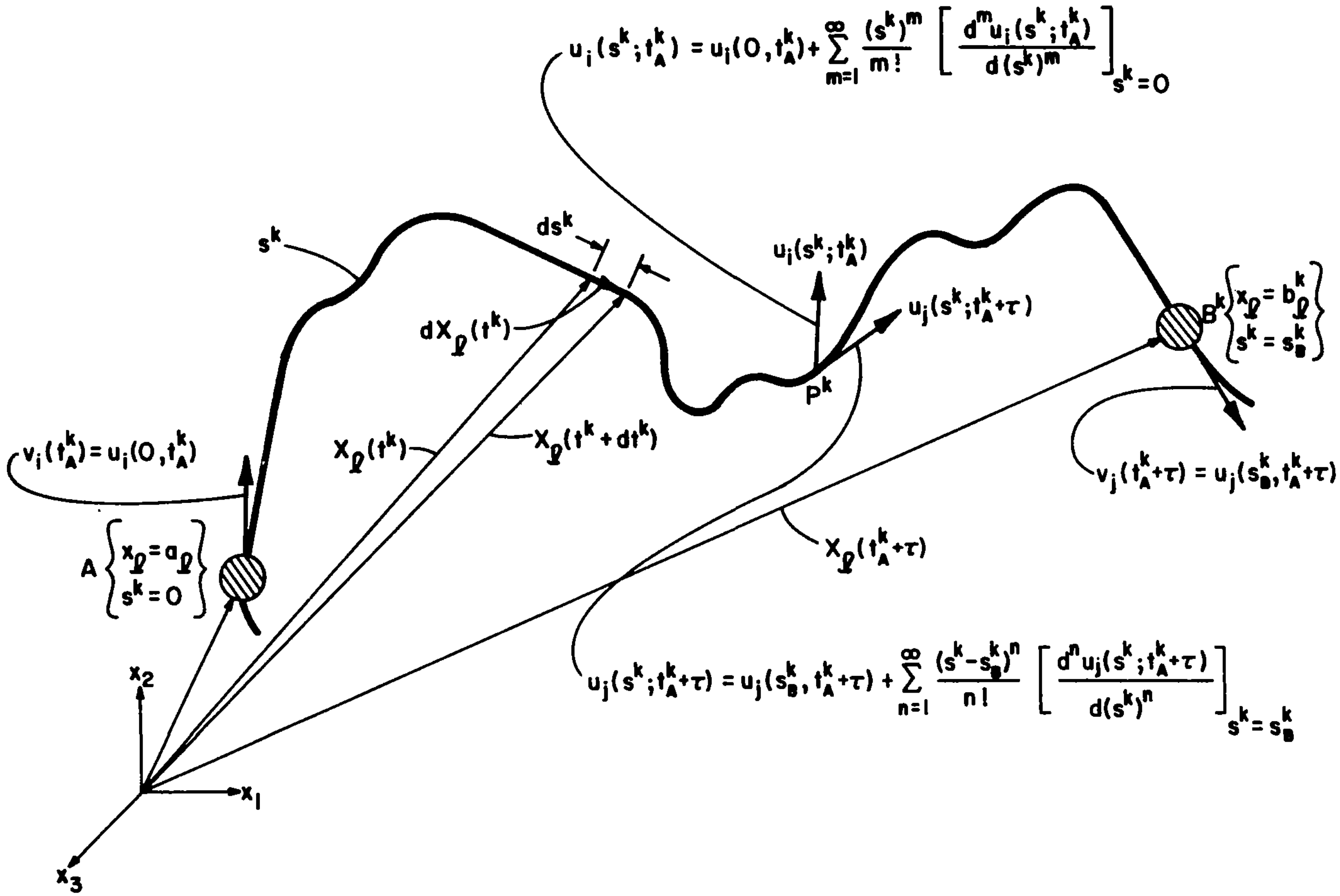

Fig. 3.4 Illustration of the distance s^k_B traveled by a fluid particle along its trajectory and of the Taylor series expansions of the Eulerian velocities at a point P^k on a path line.

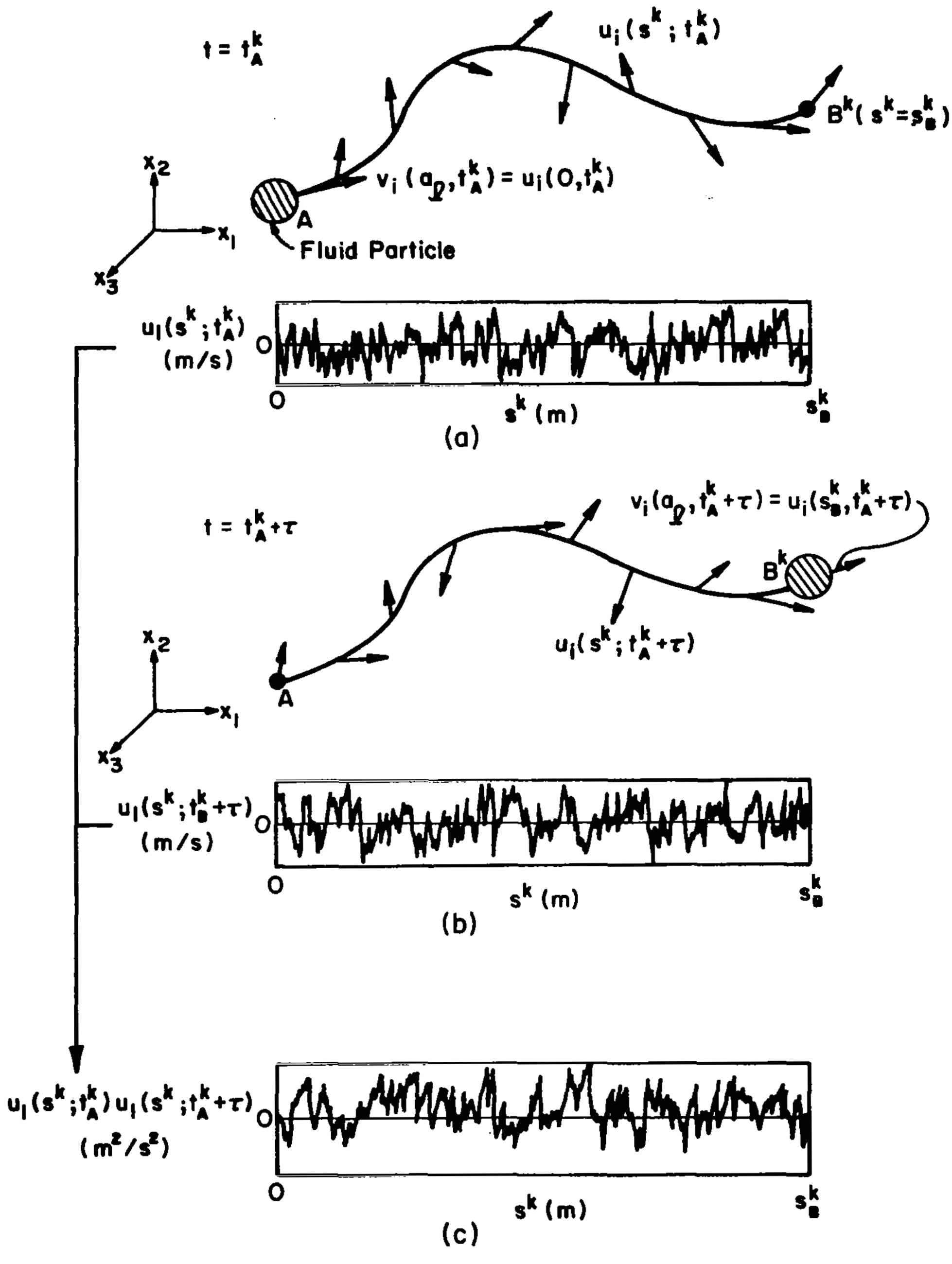

Fig. 3.5 Illustration of the Eulerian velocity product formatioı for a single velocity component at a point on a trajectory.

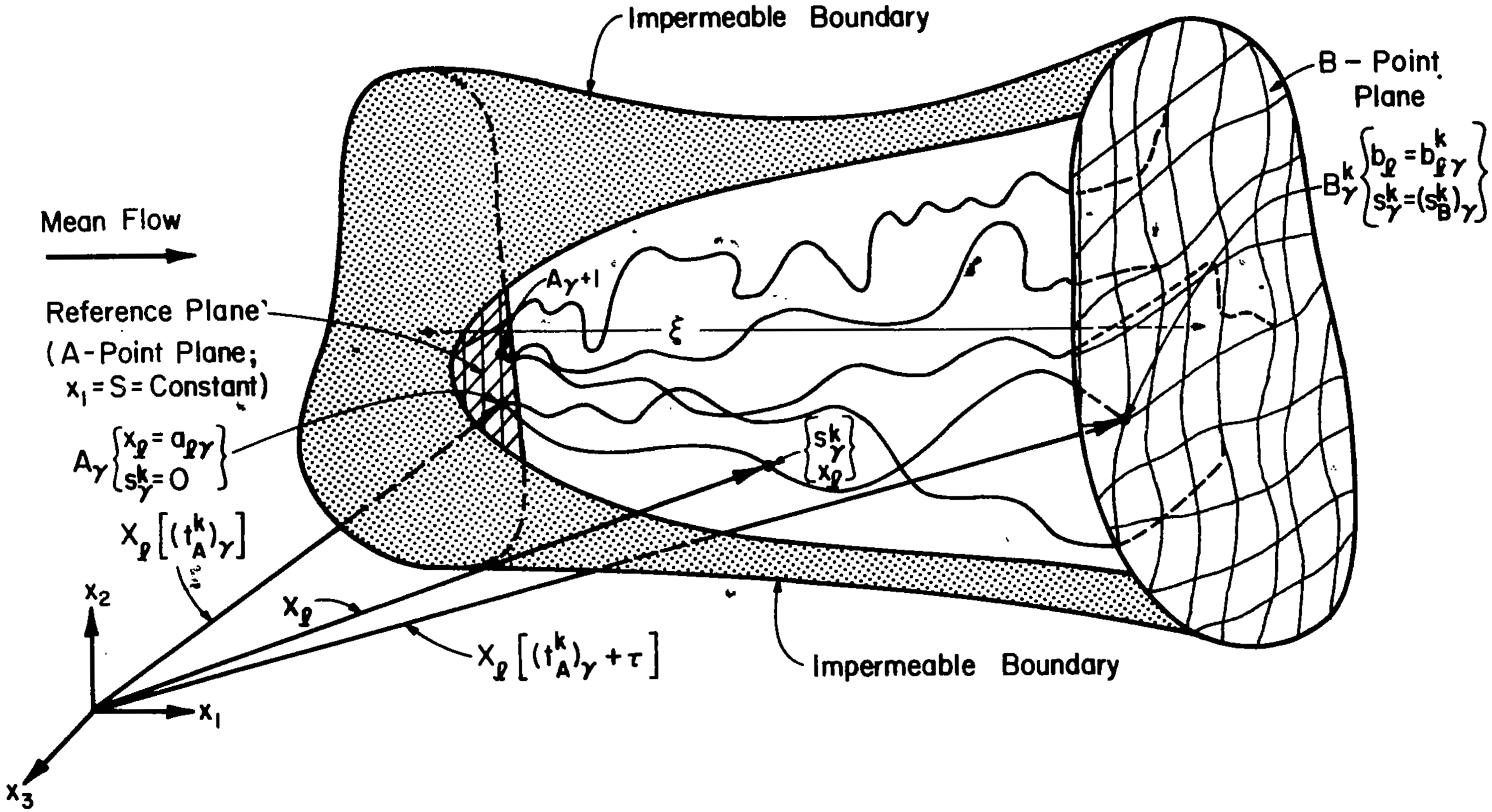

Fig. 3.6 Illustration of a hypothetical turbulence "box."

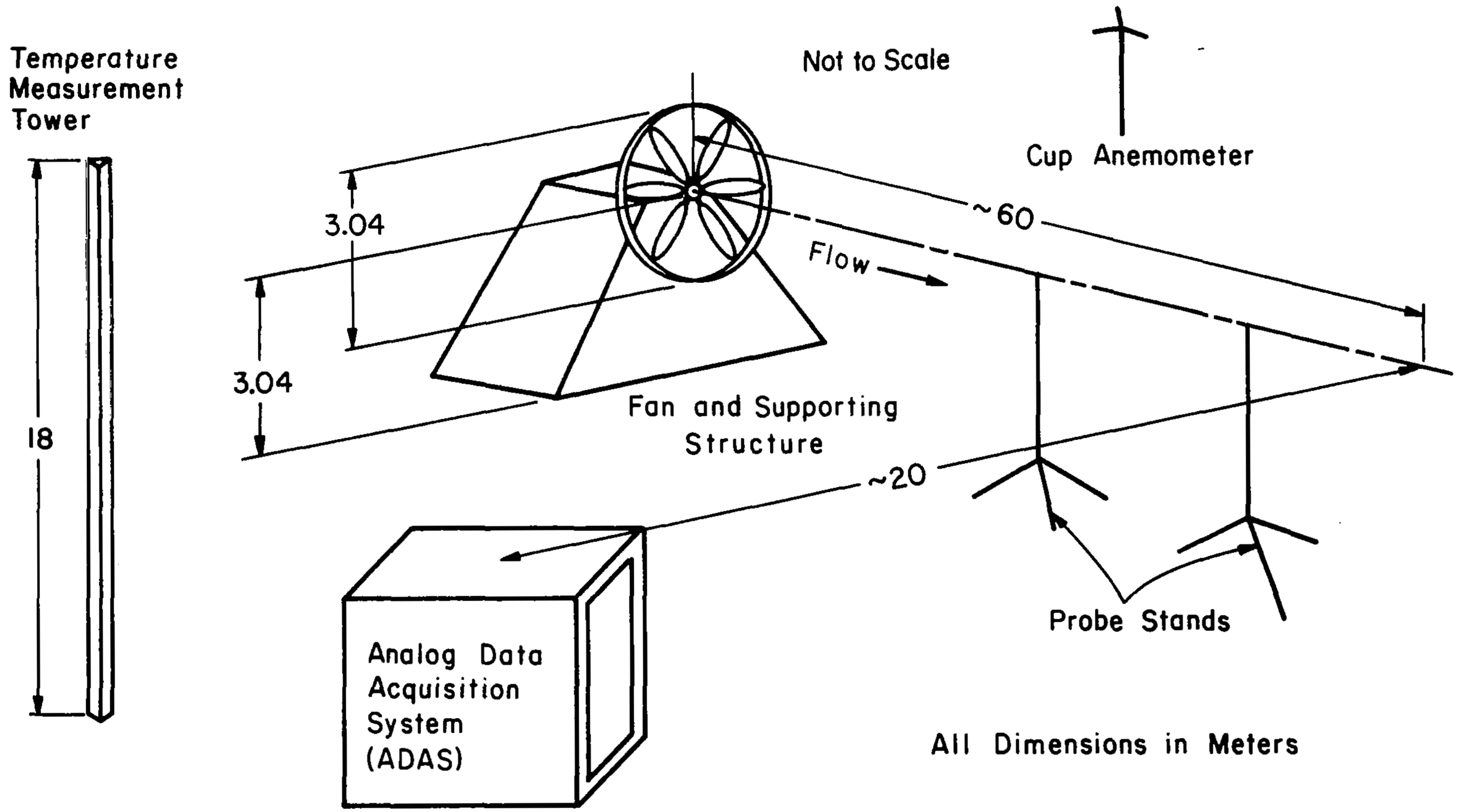

Fig. 4.1. Sketch of the Environmental Field Station (EFS).

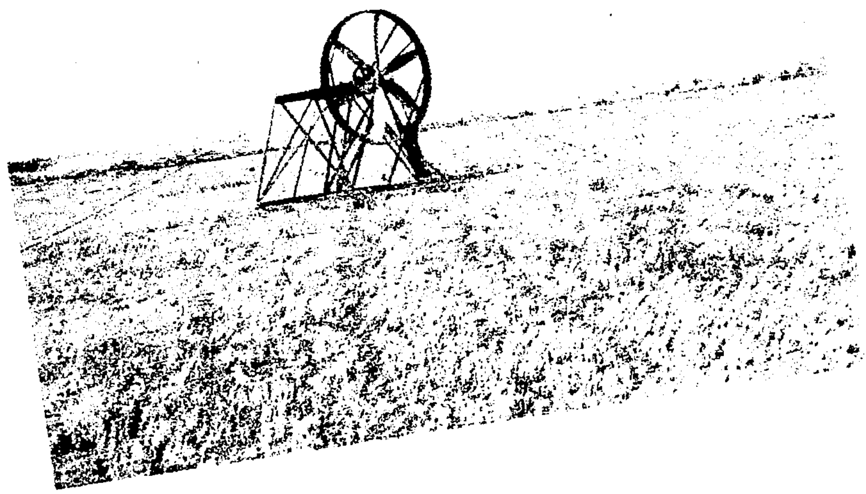

Fig. 4.2 View of the fan and field site.

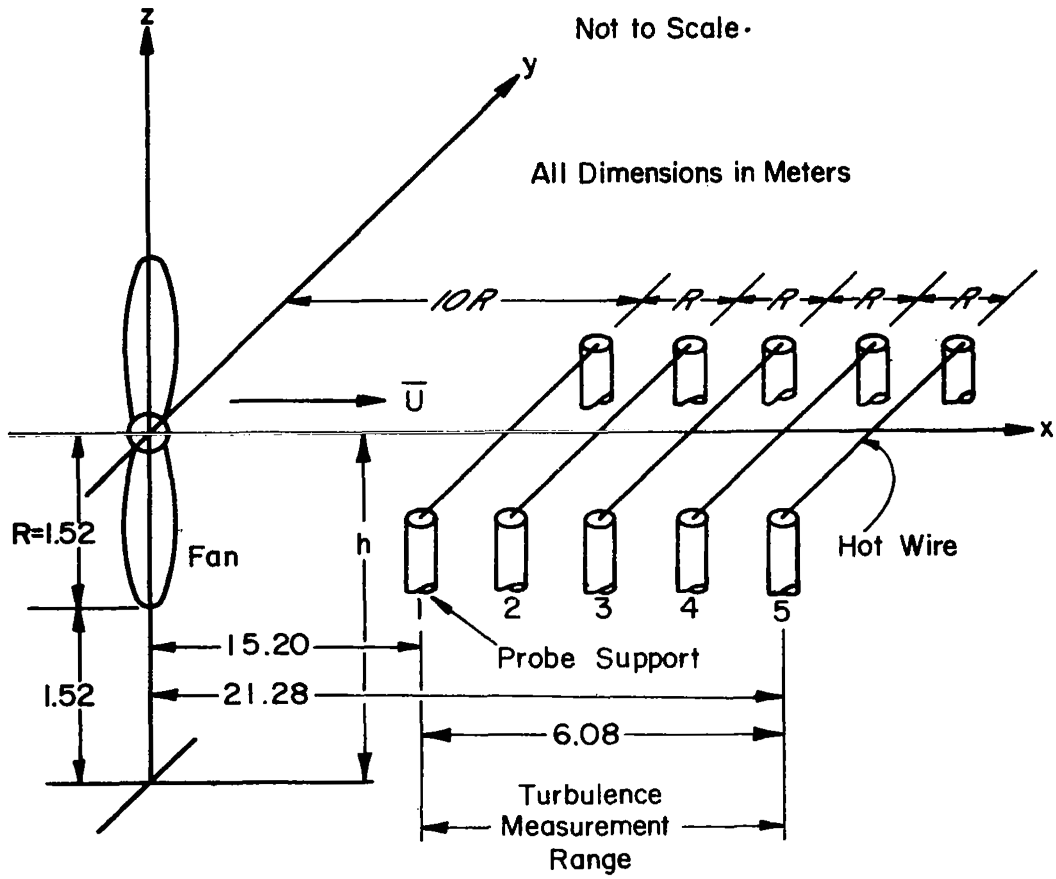

Fig. 5.1. Sketch of the array of five hot wires and the system of coordinates.

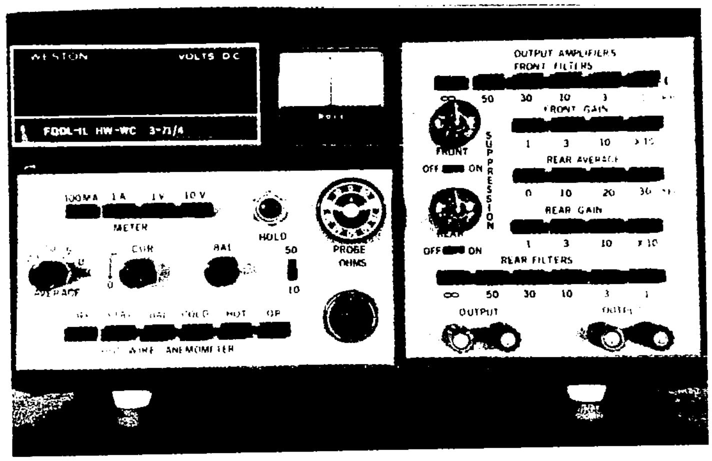

(a)

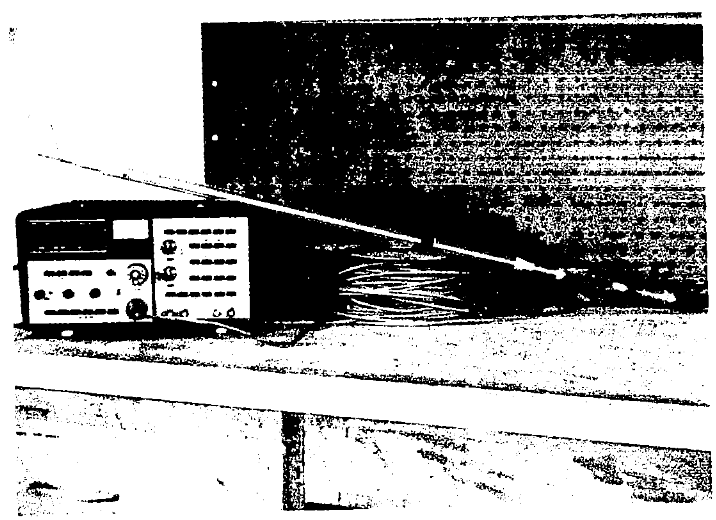

(b)

Fig. 5.2 View of the hot-wire unit including 150 m length of cables (a); and its front control panel (b).

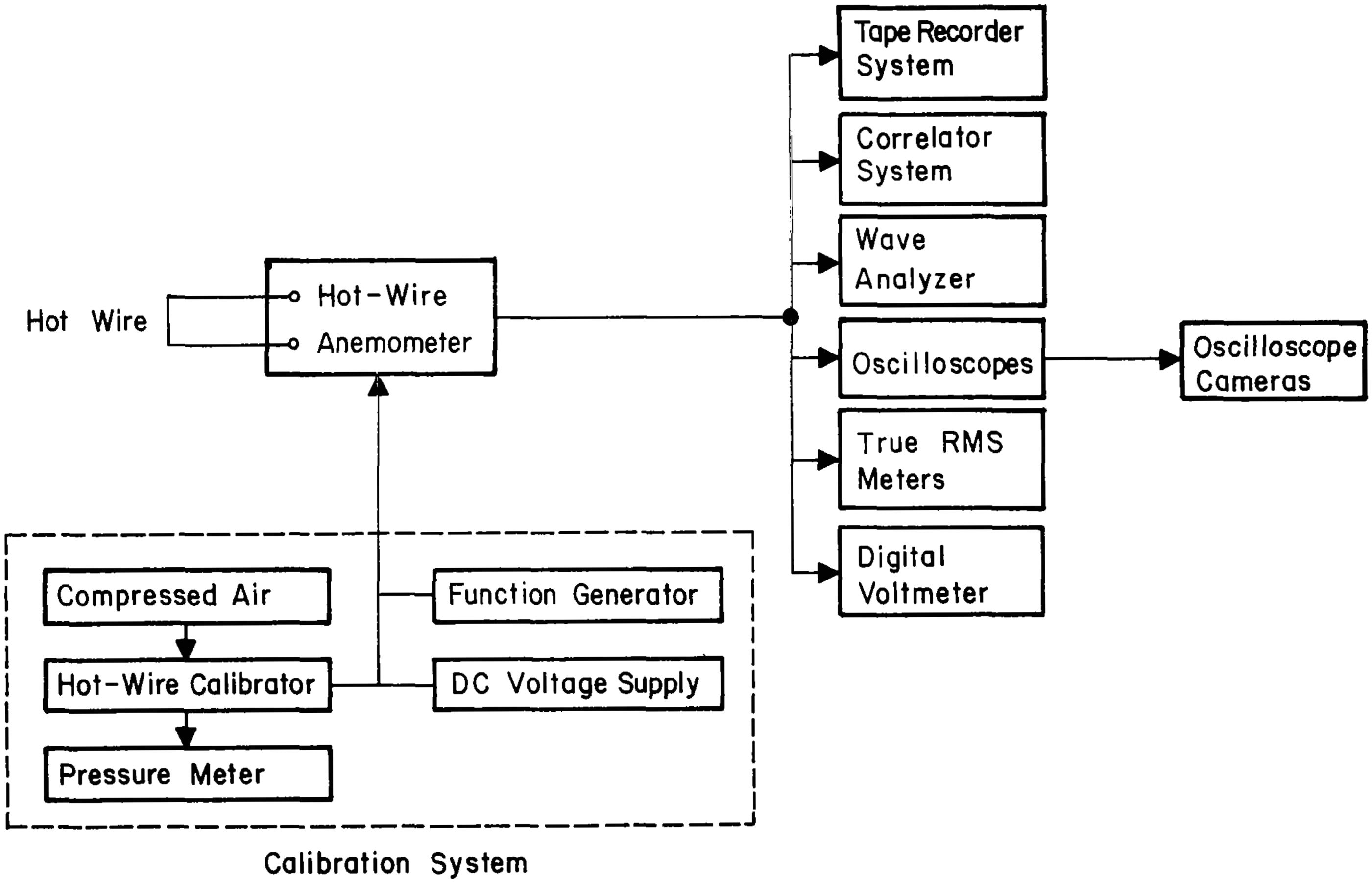

Fig. 5.3 Block diagram of the hot-wire anemometer unit and the Analog Data Acquisition System (ADAS), i.e., the hot-wire anemometer measuring system.

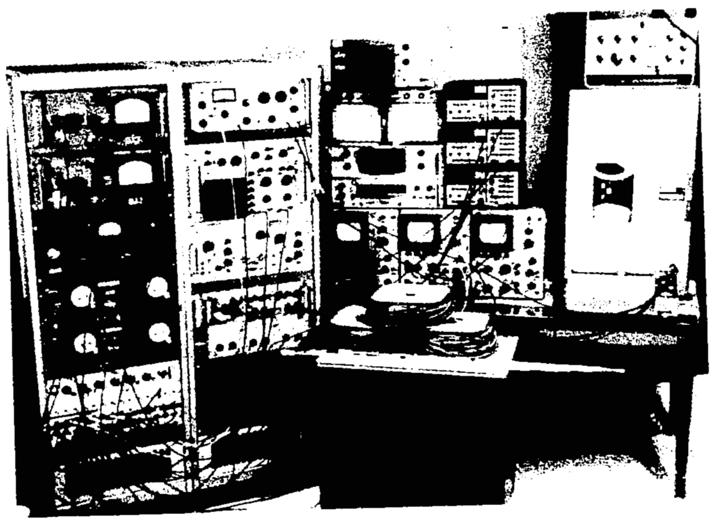

Fig. 5.4 Overall view of the Analog Data Acquisition Systems (ADAS).

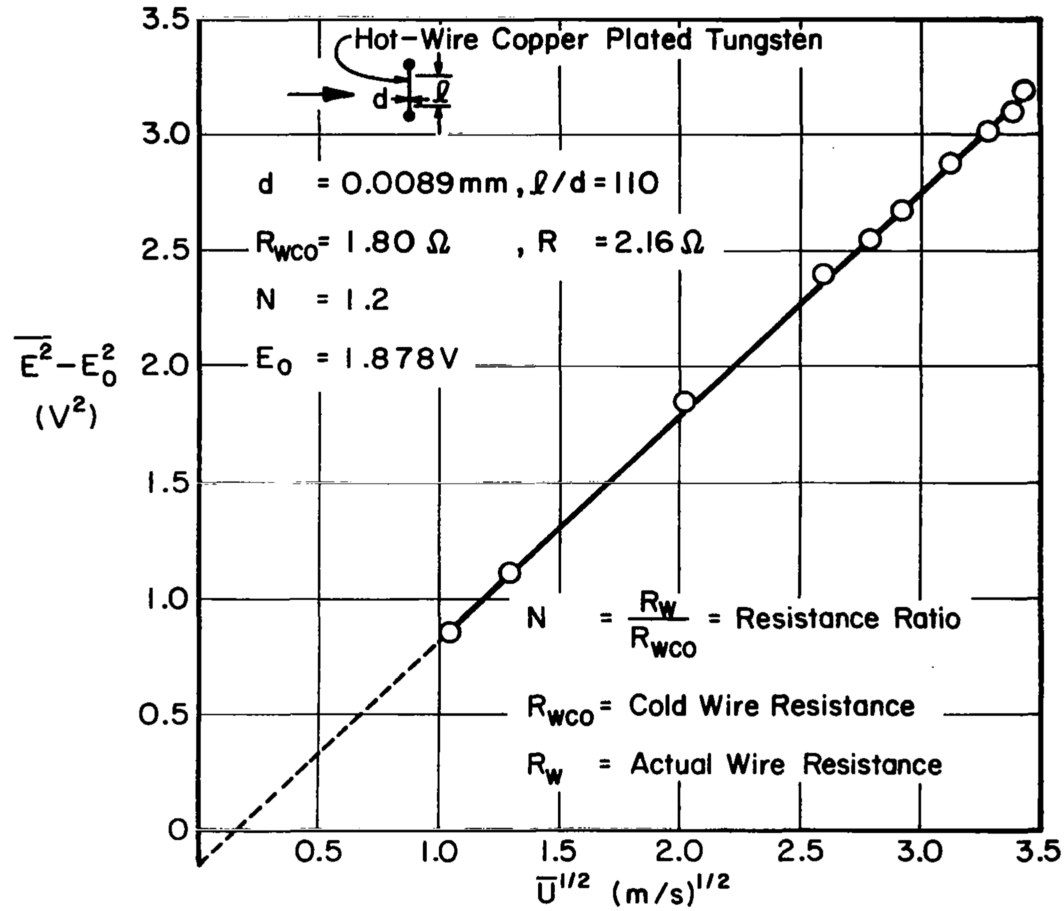

Fig. 5.5 Typical hot-wire calibration curve obtained by means of the calibrator.

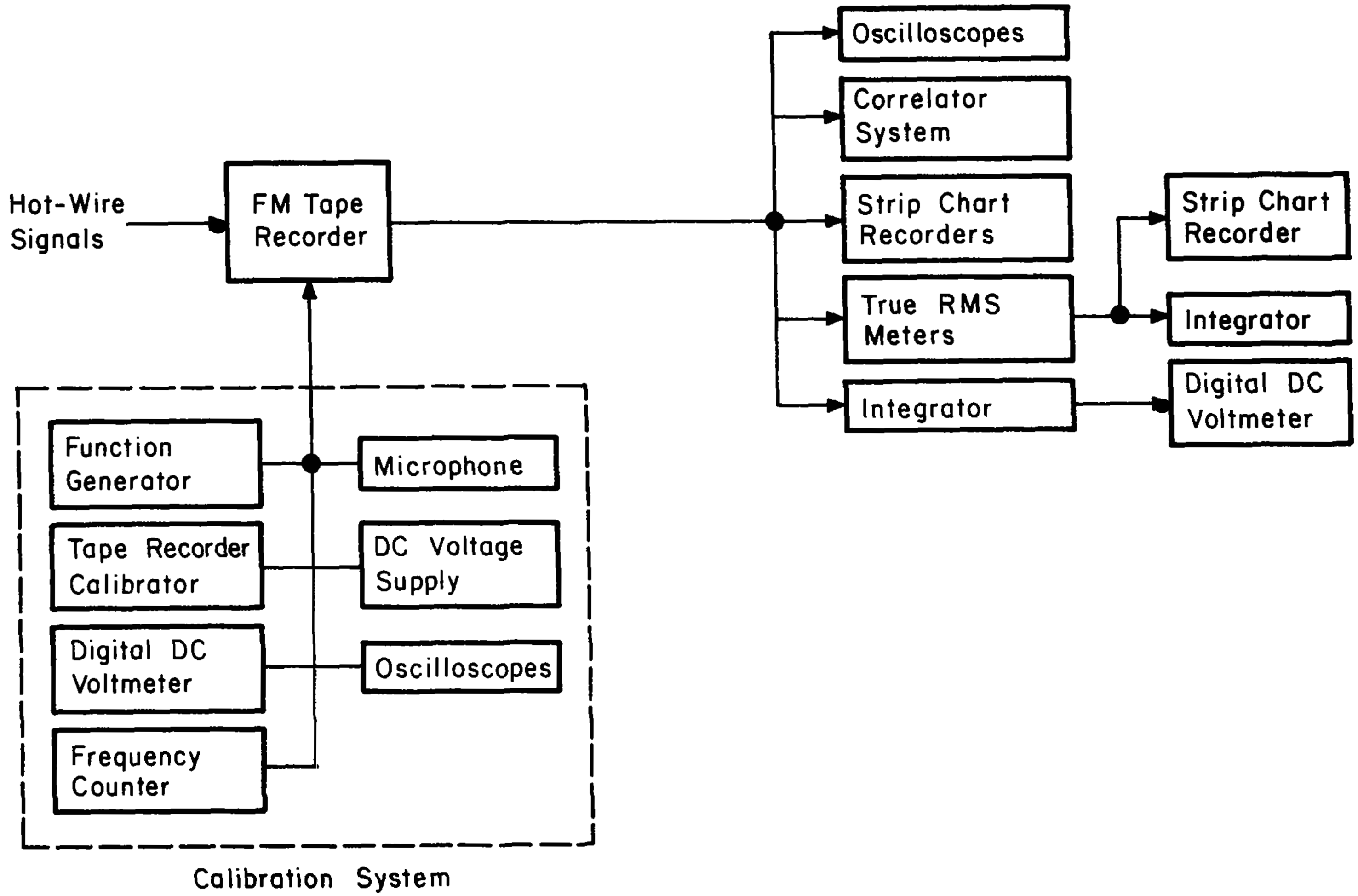

Fig. 5.6 Block diagram of the tape recorder system.

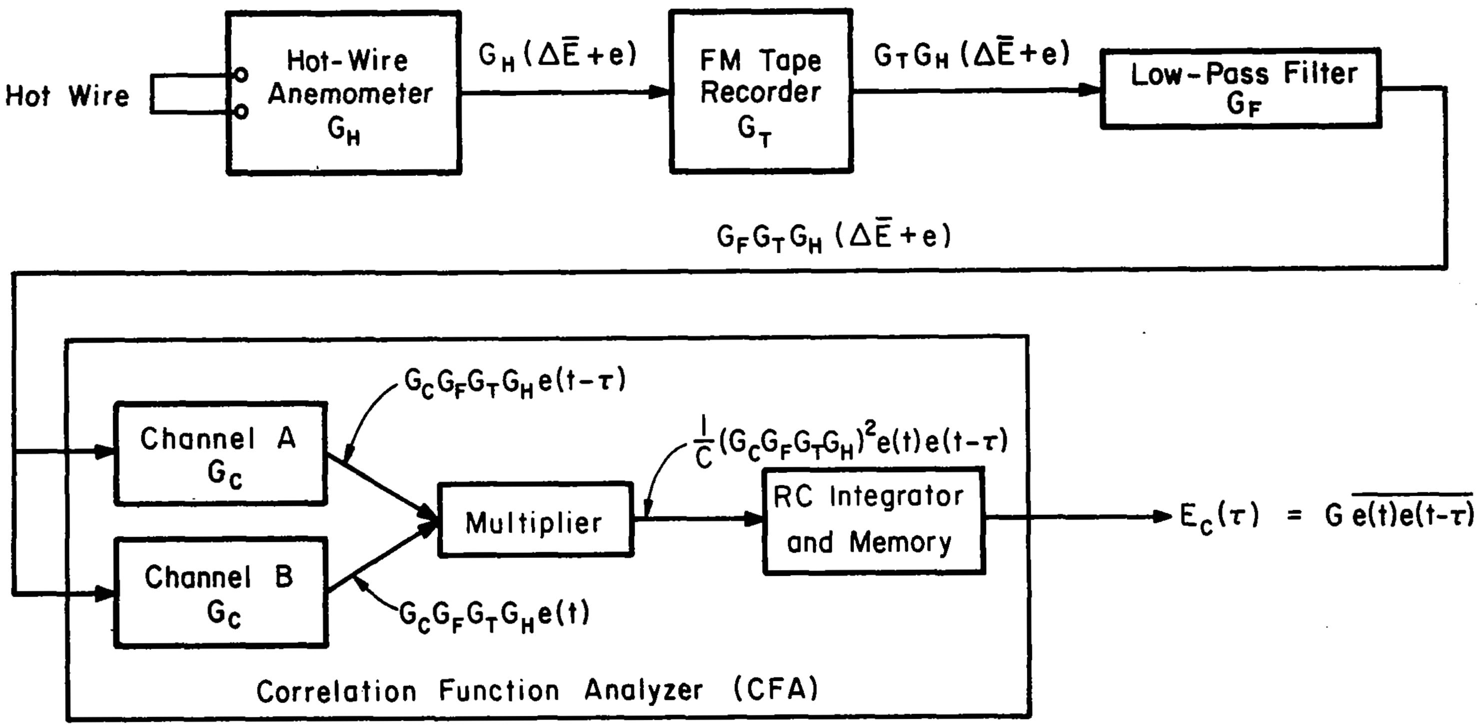

Fig. 5.7 Flow diagram of the autocorrelation computation.

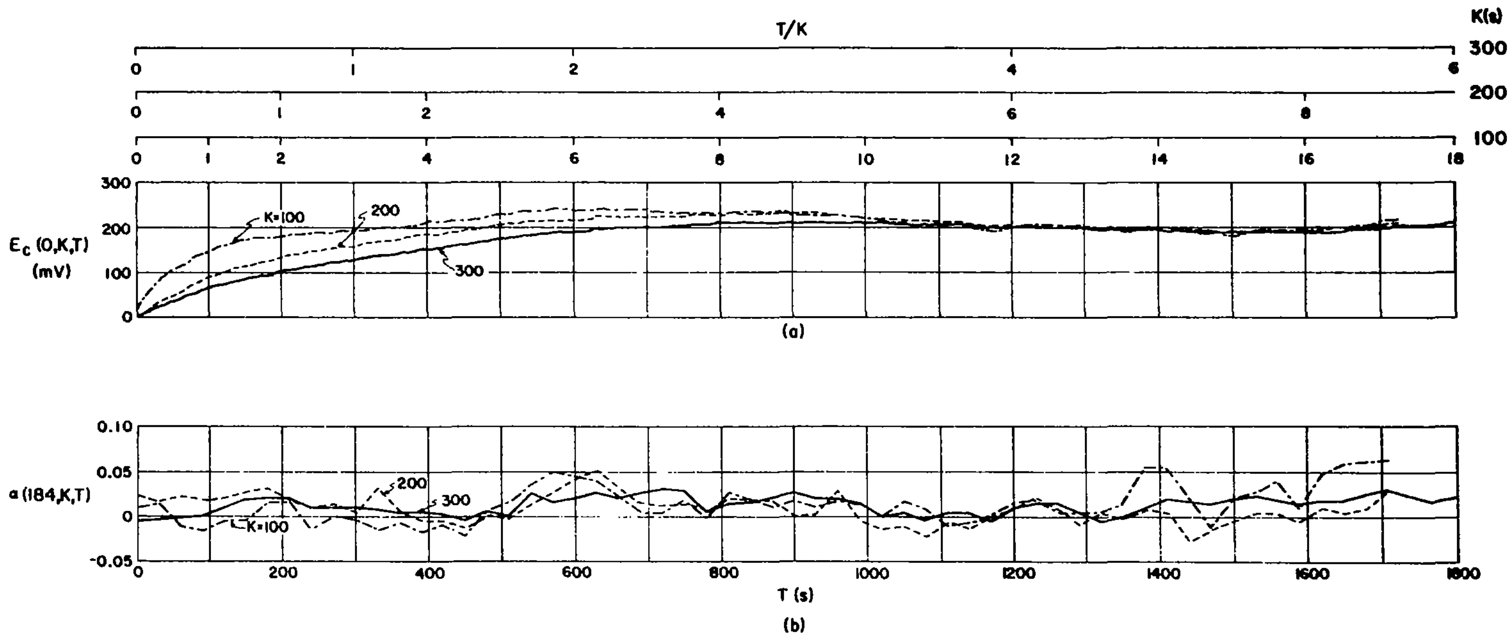

Fig. 5.8 Variations with increasing averaging time of: (a) the CFA output signal at zero time delay; and, (b) the autocorrelation running resolution coefficient when τ = 184 ms.

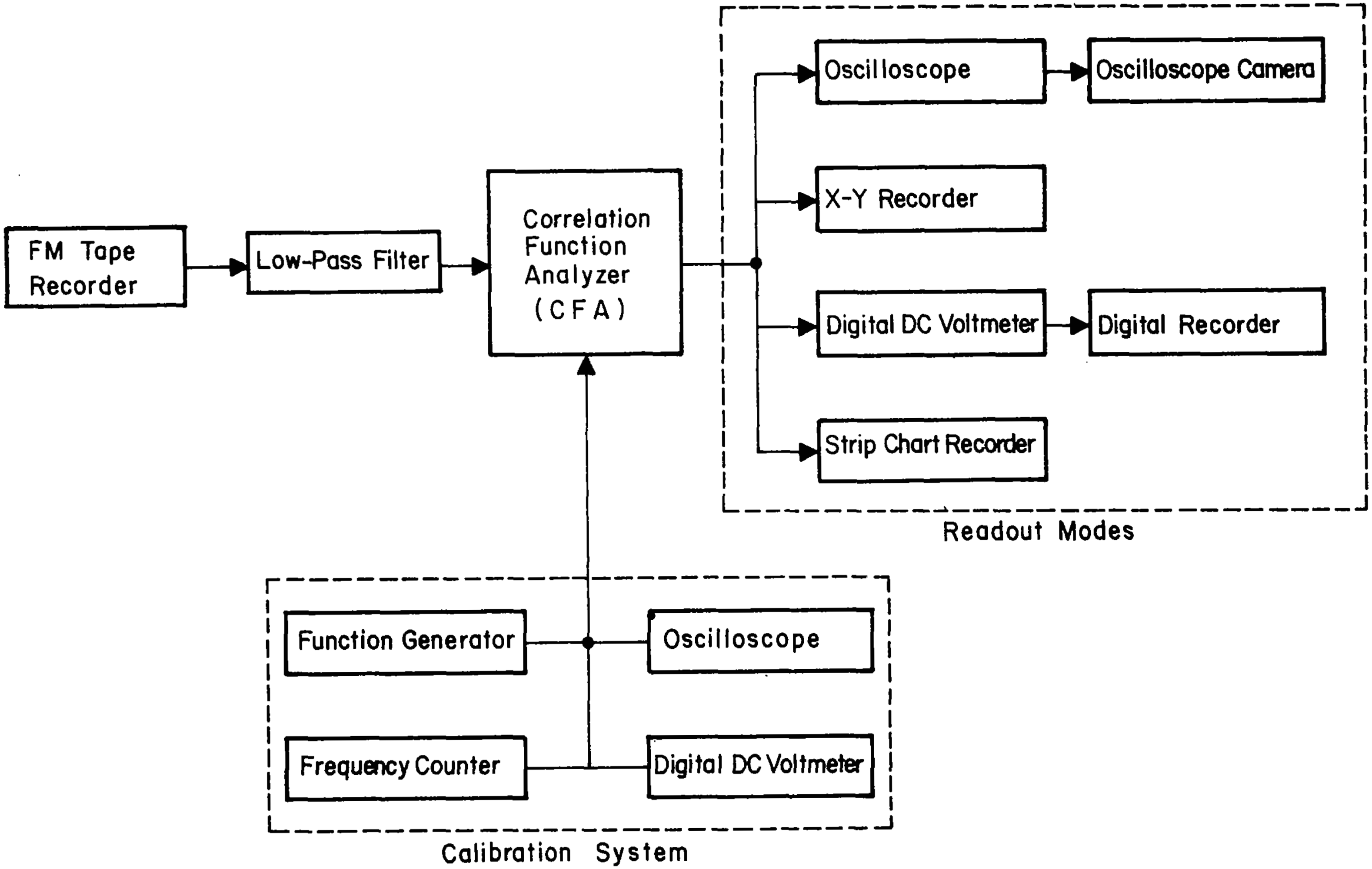

Fig. 5.9 Block diagram of the autocorrelation computation system.

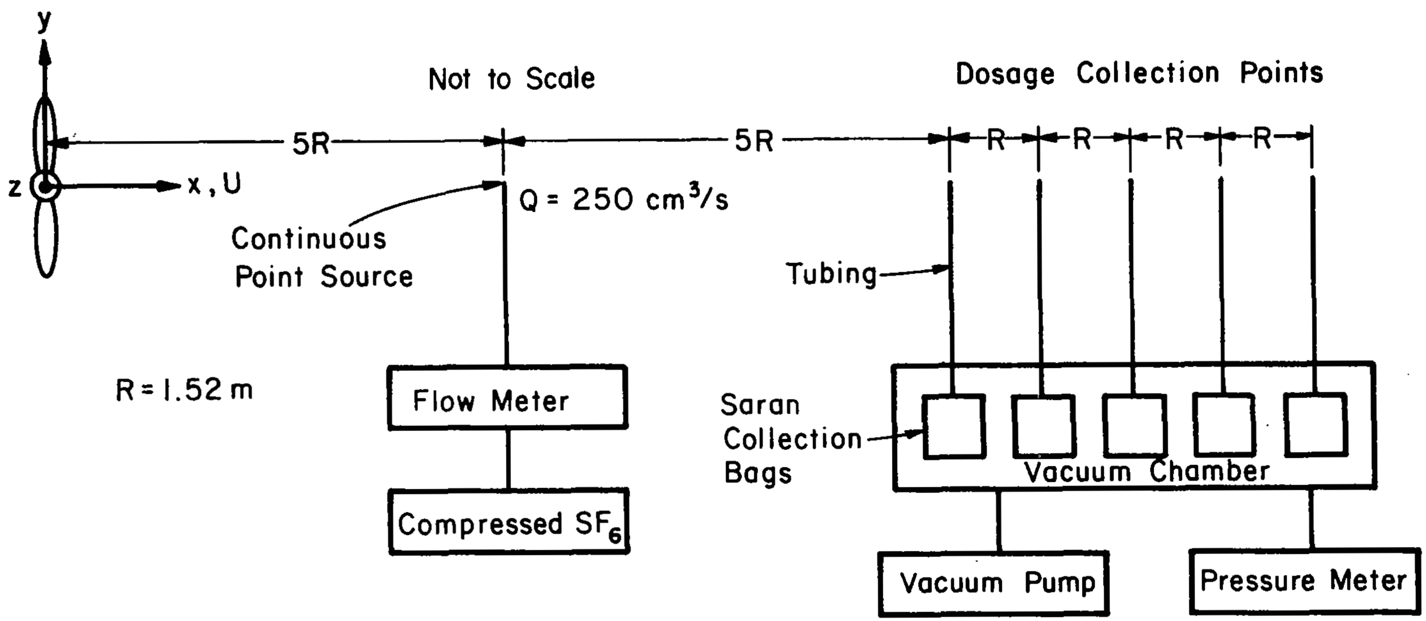

Fig. 5.10. Sketch of the sulfur hexaflouride SF_6 diffusion measurement arrangement.

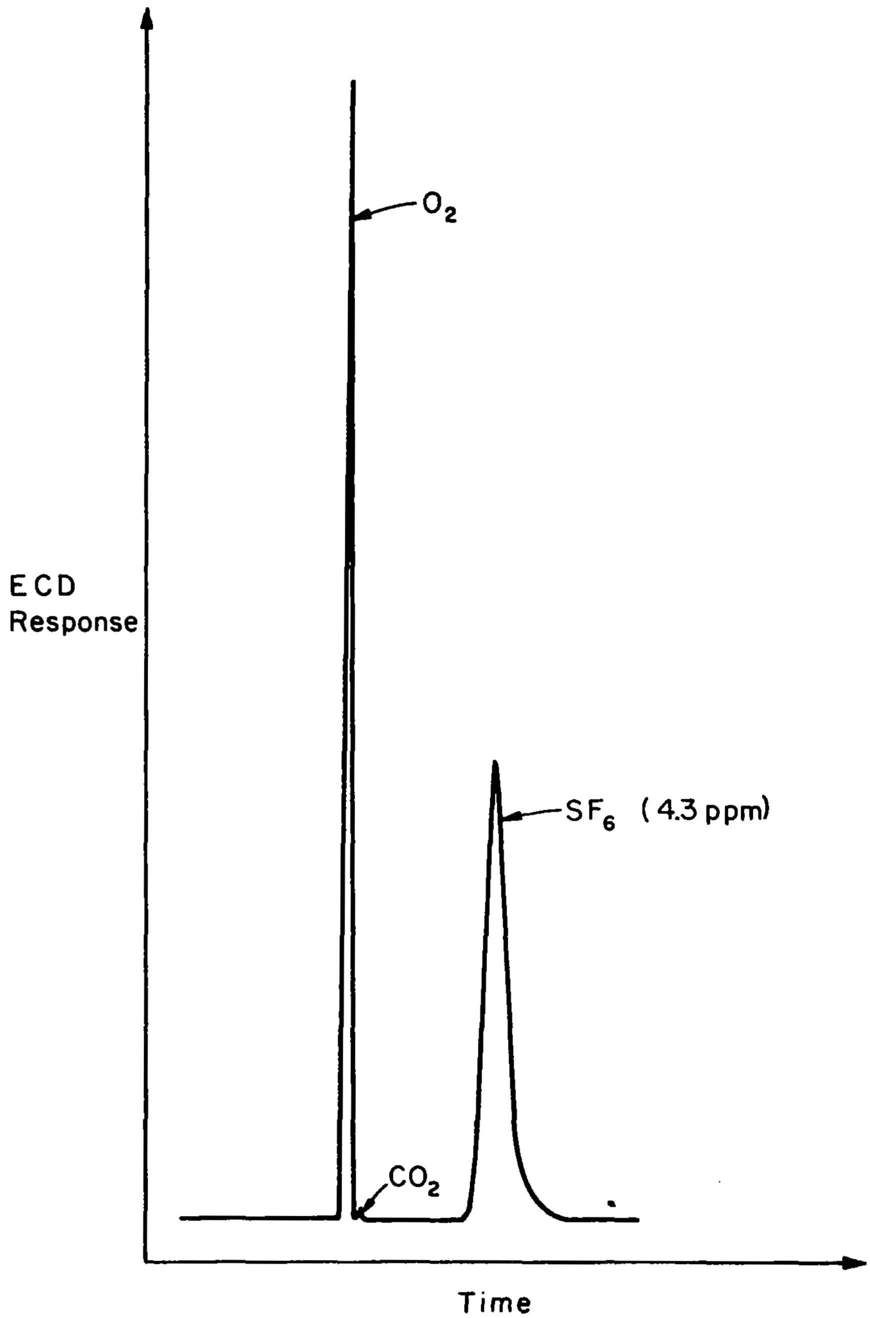

Fig. 5.11 Qualitative response of the electron capture dectector to a SF_6-air sample mixture.

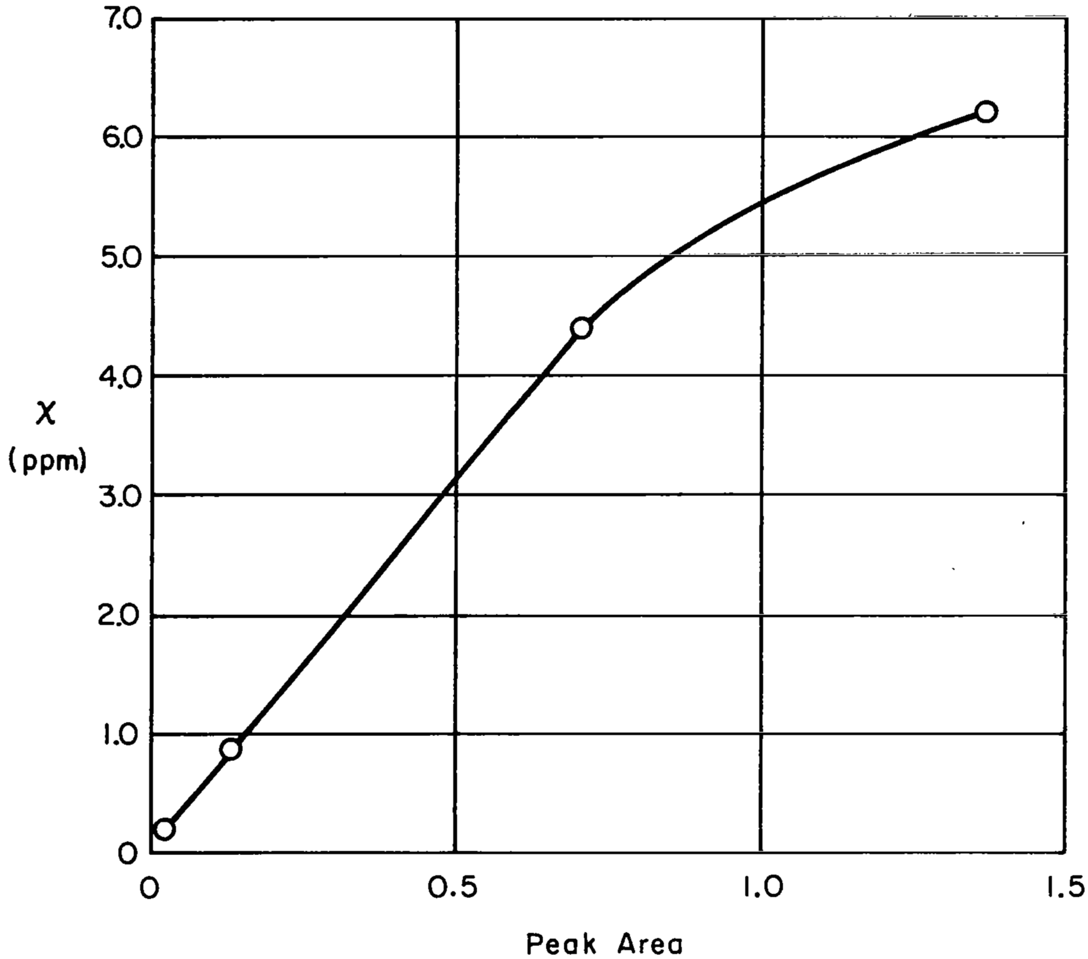

Fig. 5.12 Typical calibration curve of the electron capture detector (ECD) to known SF_6 concentrations χ in air mixtures.

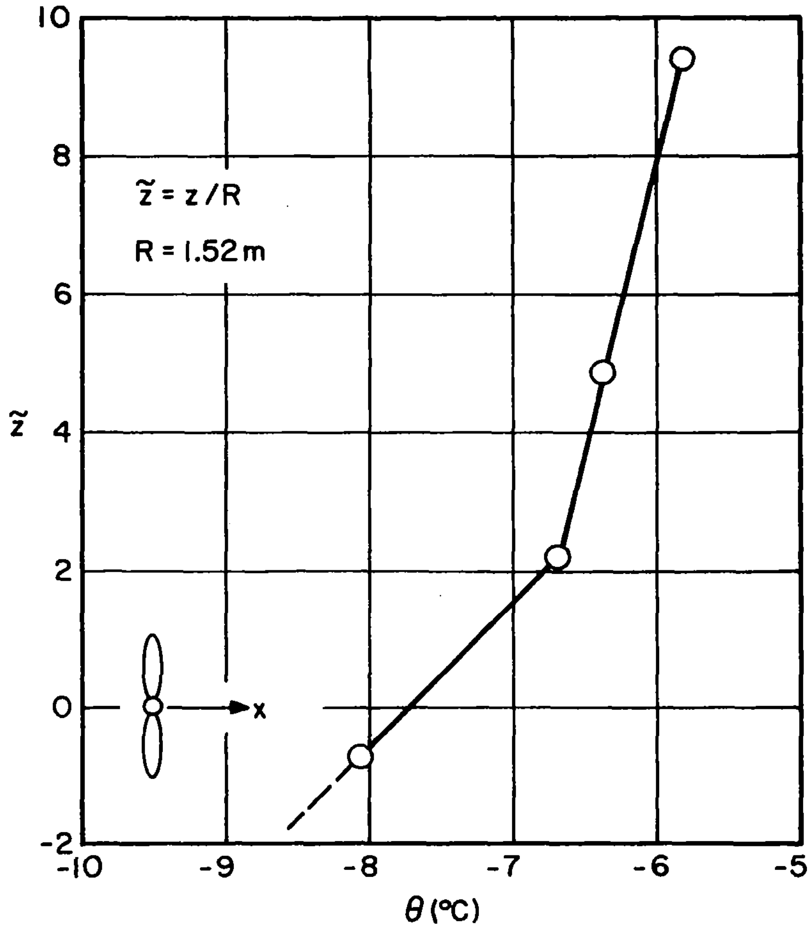

Fig. 6.1 Vertical temperature distribution.

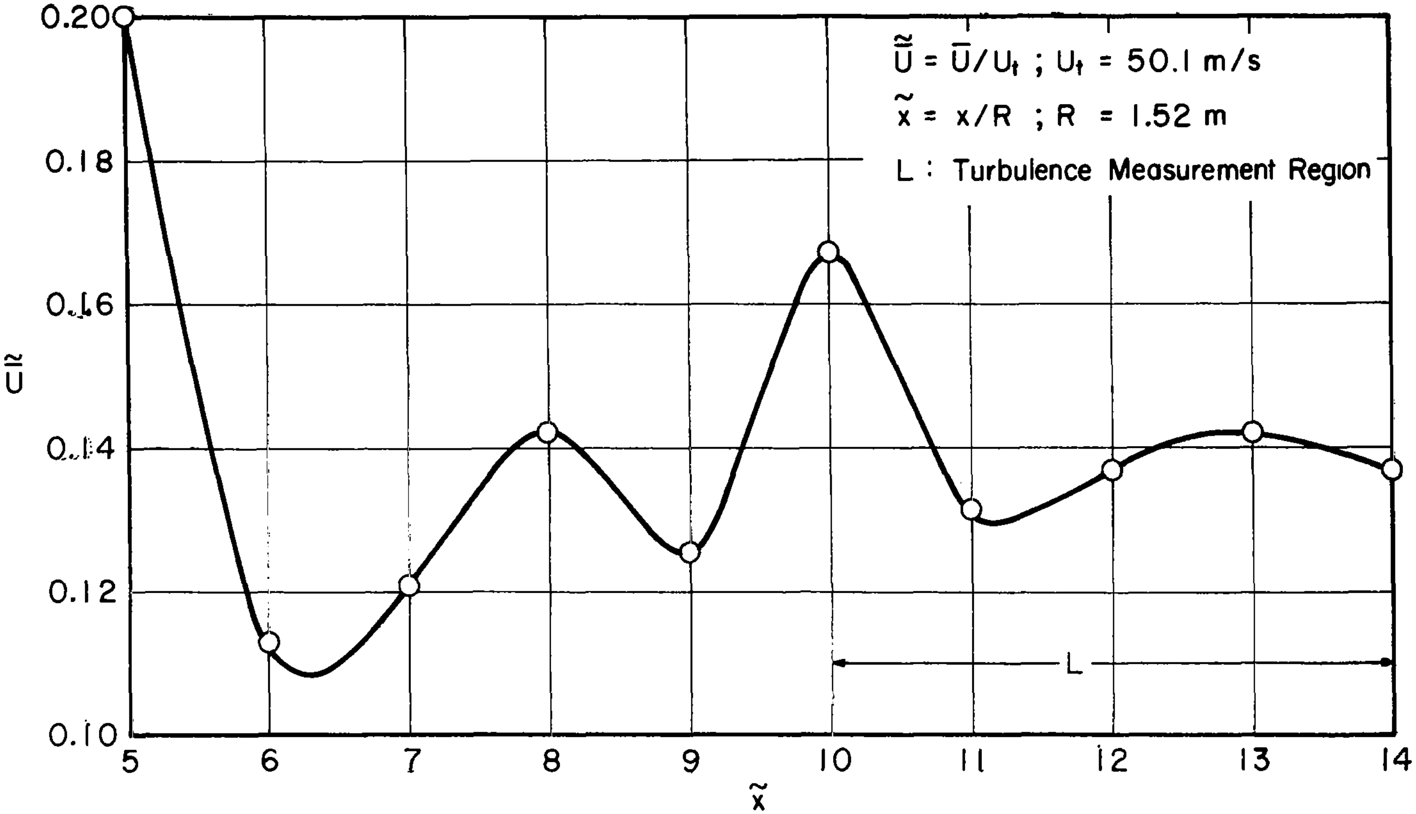

Fig. 6.2 Axial mean velocity distribution along the wake centerline.

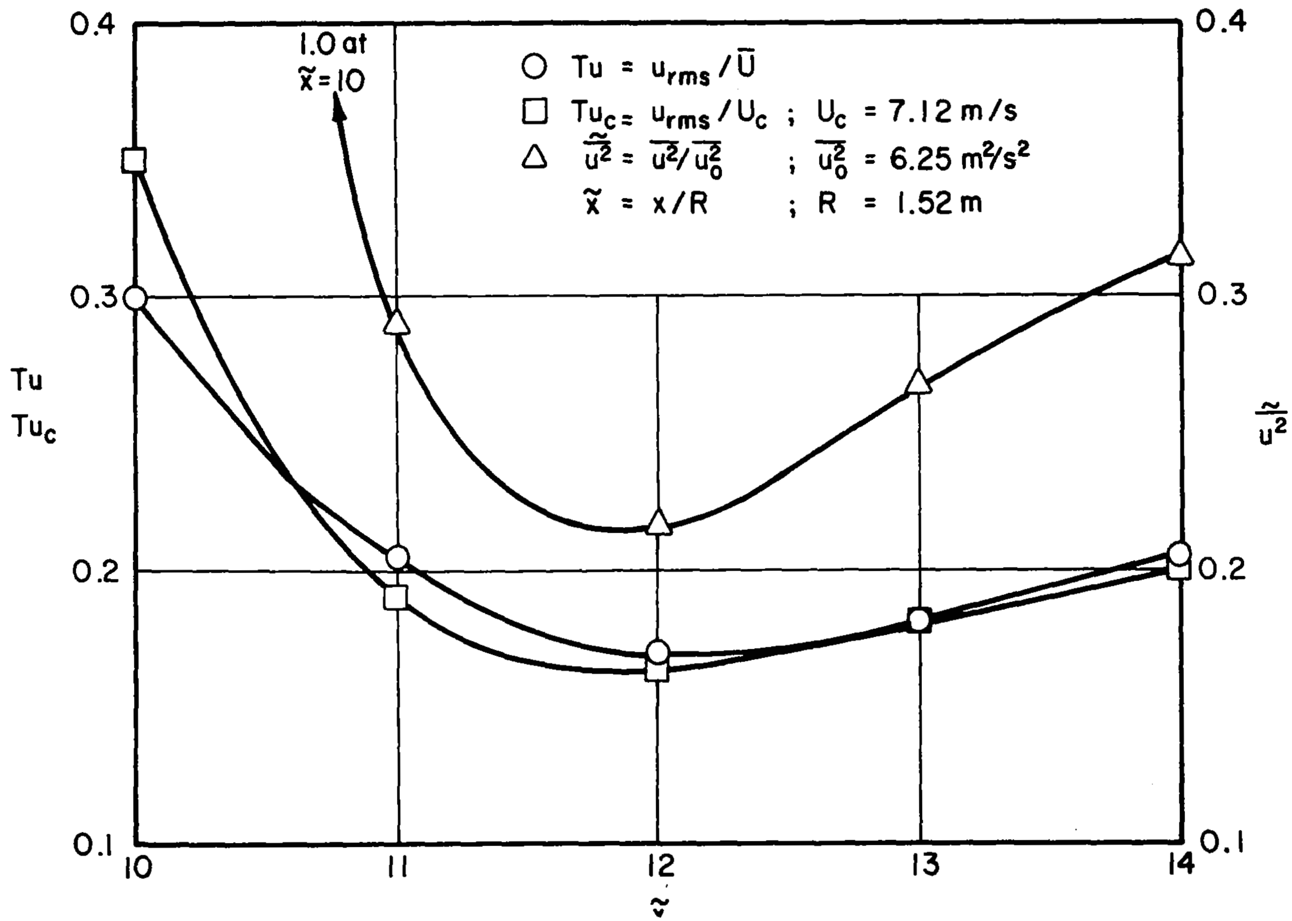

Fig. 6.3 Variation of the longitudinal turbulence intensities and normalized mean-square value of the longitudinal turbulent velocity along the turbulence line.

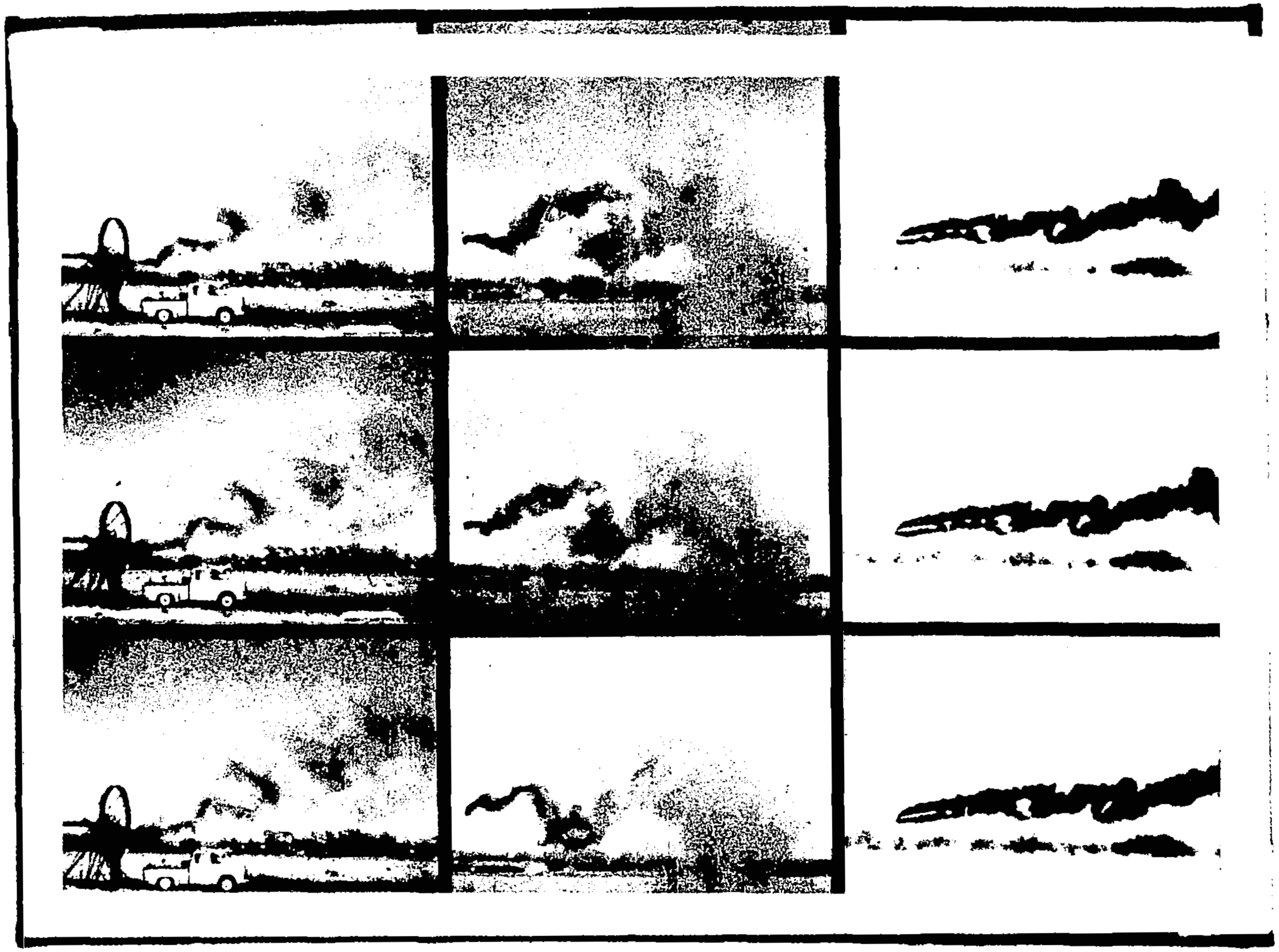

(a) (b) (c)

Fig. 6.4 Smoke plume circulation visualization: (1) unstable conditions (a) point source at $x = -0.5R$ and (b) point source at $x = 8R$; and, (2) under a temperature inversion (c) point source at $x = 30R$.

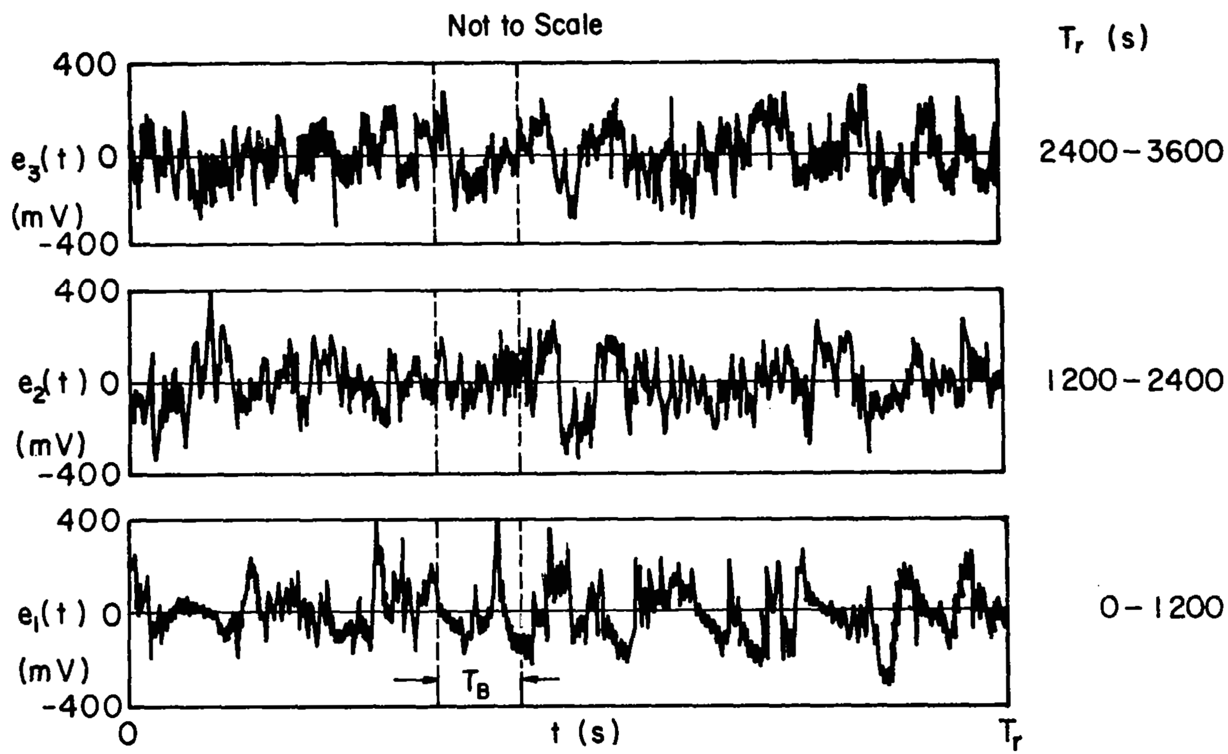

Fig. 6.5 Representation of the equivalent ensemble formed from the available record time history of the fluctuating voltage.

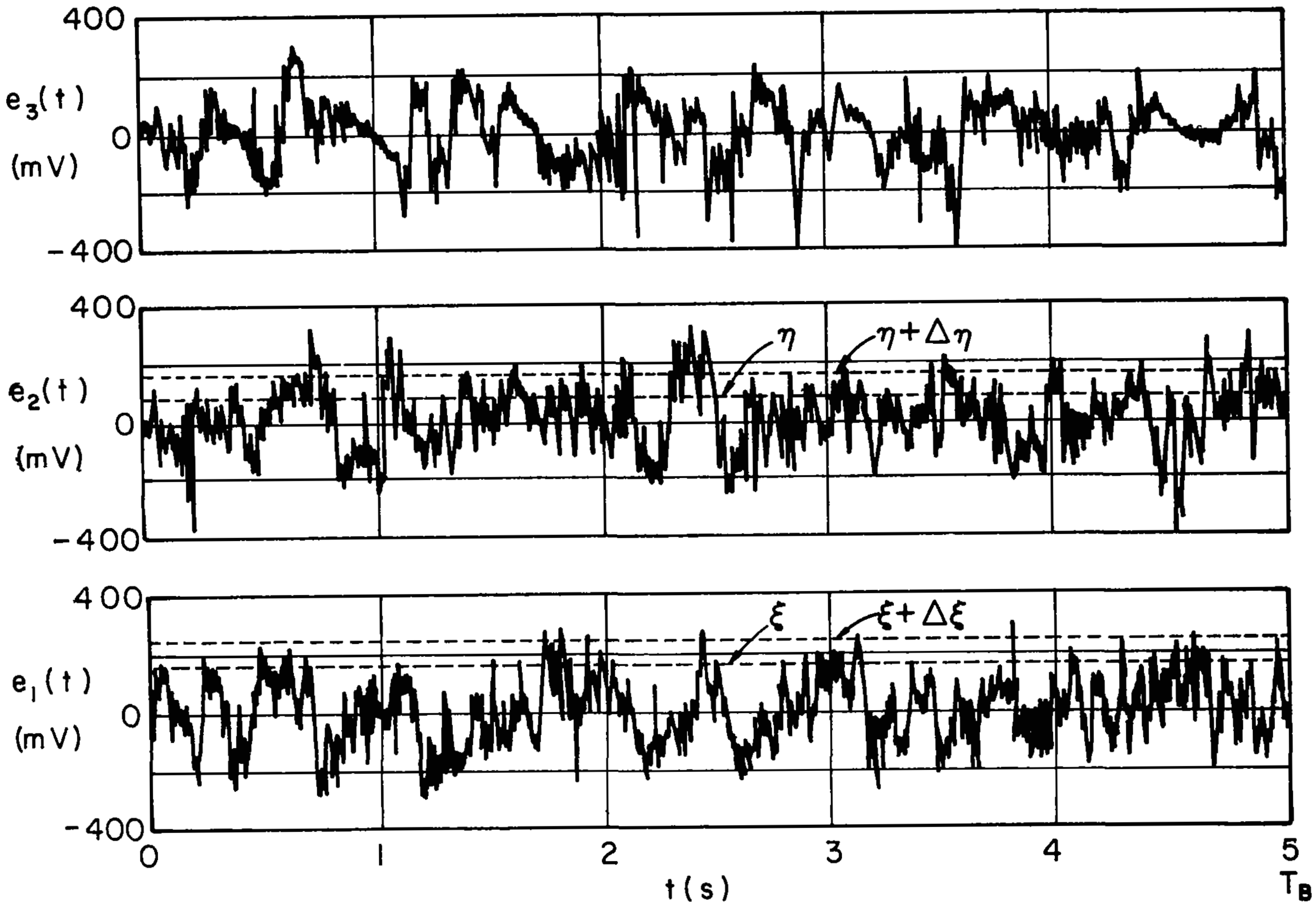

Fig. 6.6 Instantaneous fluctuating voltage during the observation time T_B of three sample records in the equivalent ensemble.

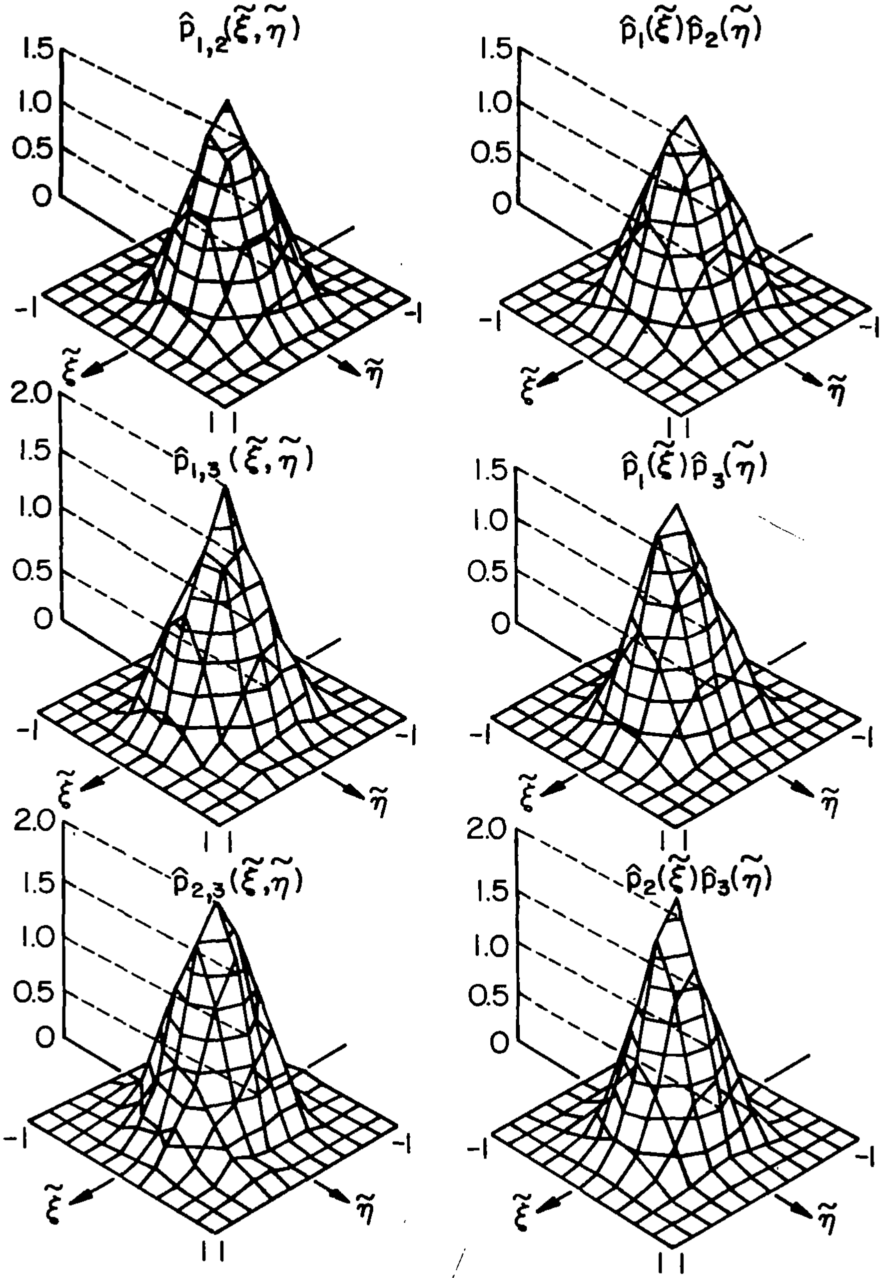

Fig. 6.7 Joint probability density functions and product of individual probability density functions of the three sample records constituting the equivalent ensemble.

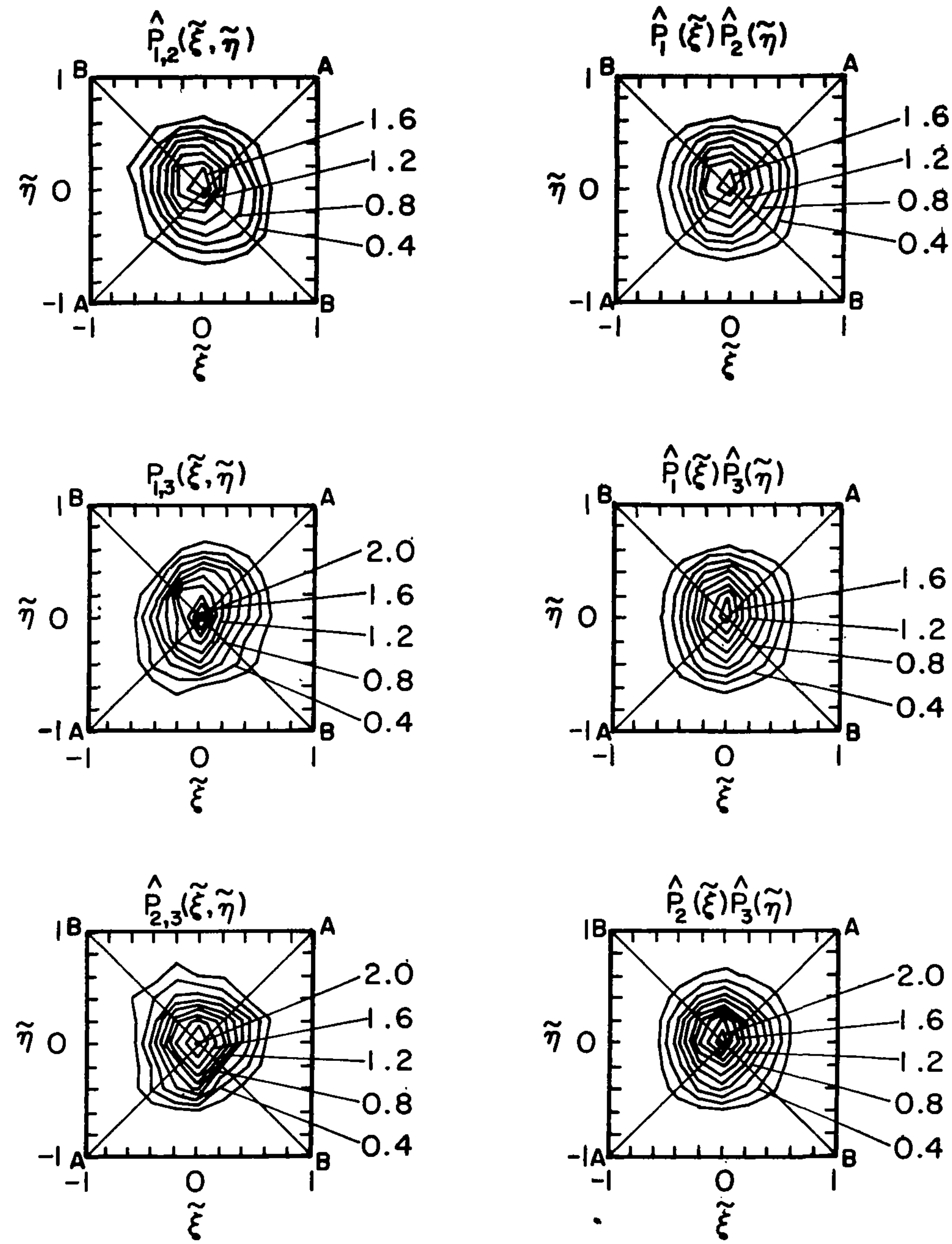

Fig. 6.8 Isoprobability curves of the joint probability density functions and products of individual probability density functions of the equivalent ensemble three sample records.

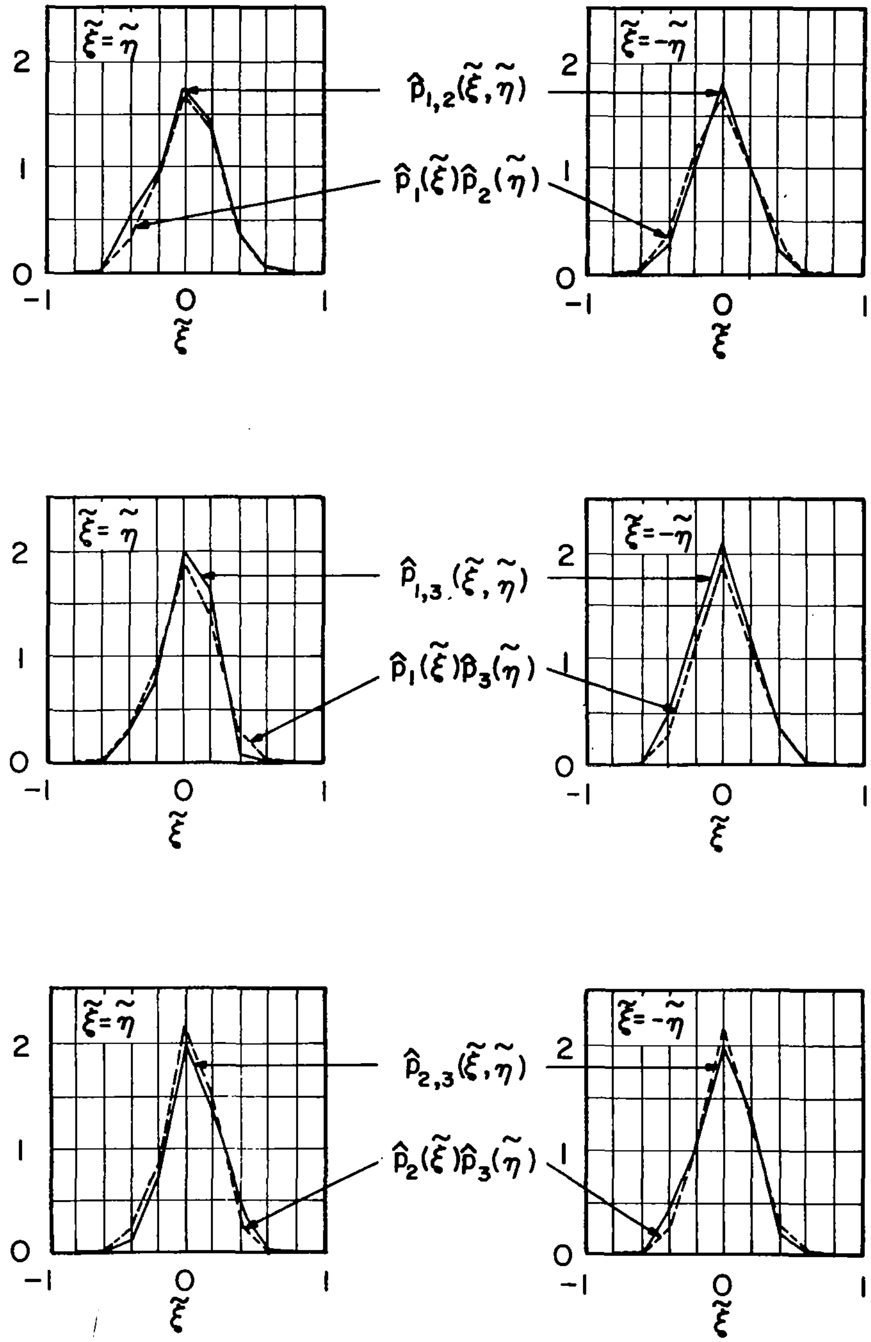

Fig. 6.9 Changes of the joint probability density functions and corresponding products of individual probability density functions for $\tilde{\xi} = \tilde{\eta}$ and $-\tilde{\eta}$.

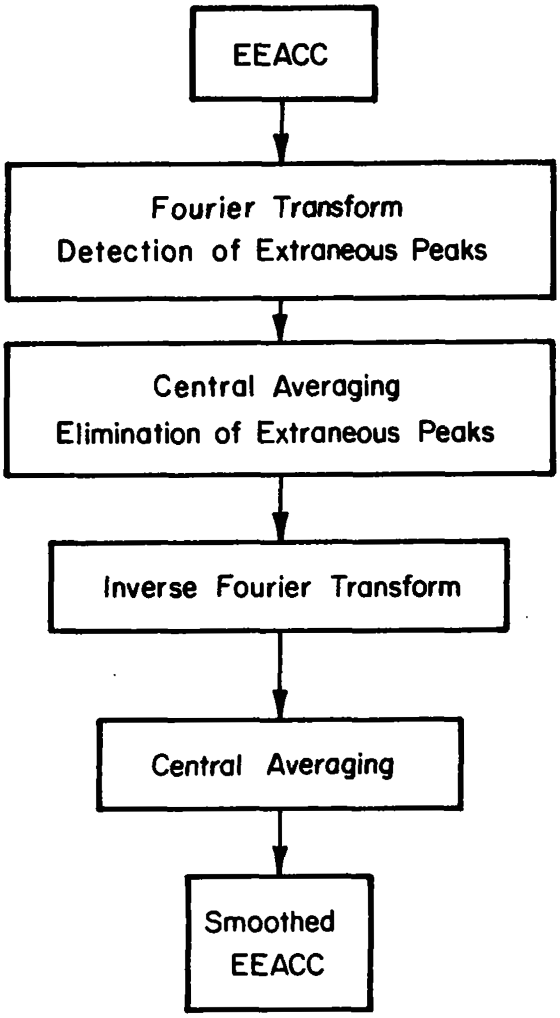

Fig. 6.10 Block diagram of the smoothing procedure for the equivalent ensemble autocorrelation coefficient (EEACC) computation.

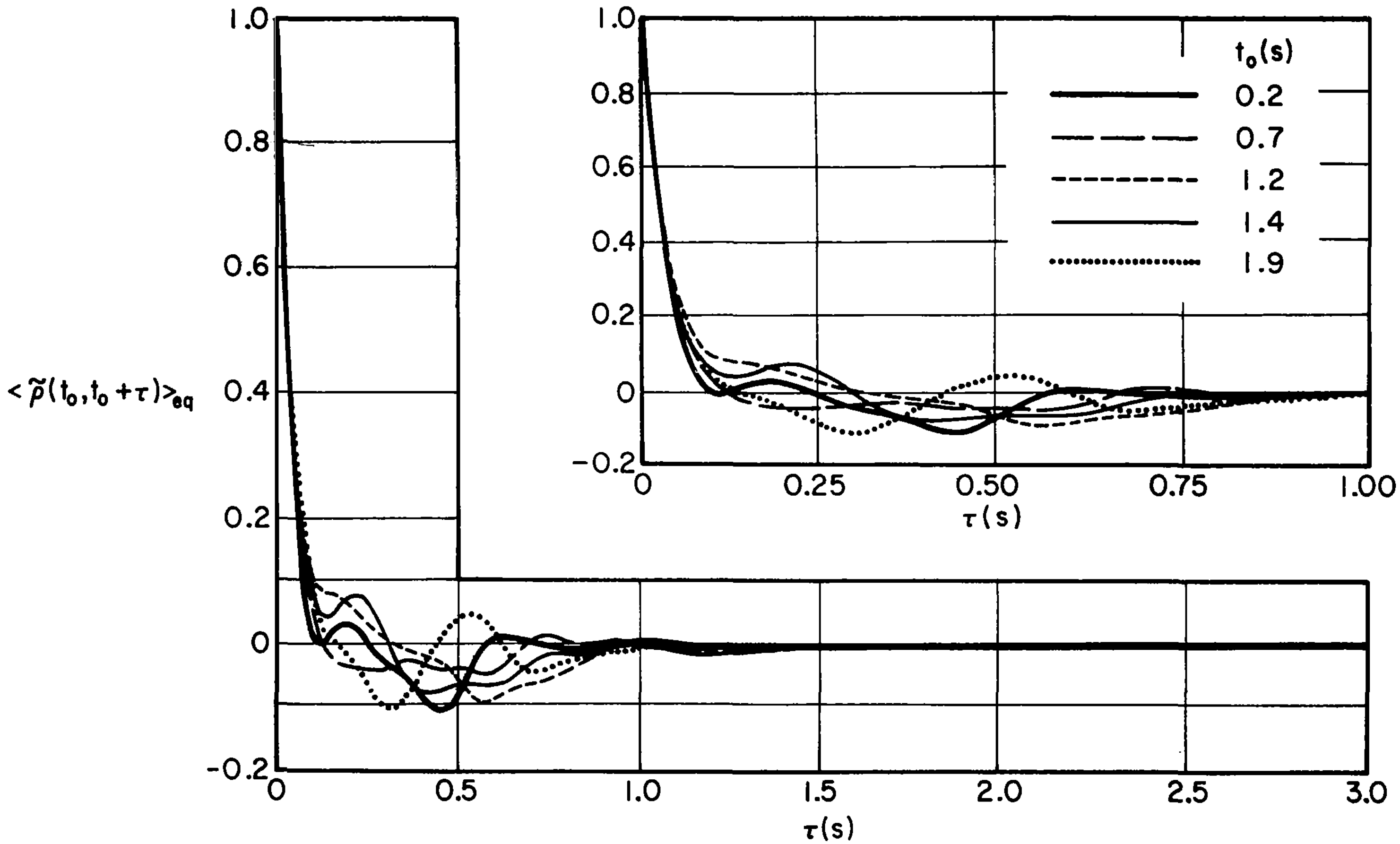

Fig. 6.11 Representative samples of the equivalent ensemble autocorrelation coefficients at five selected starting times t_o.

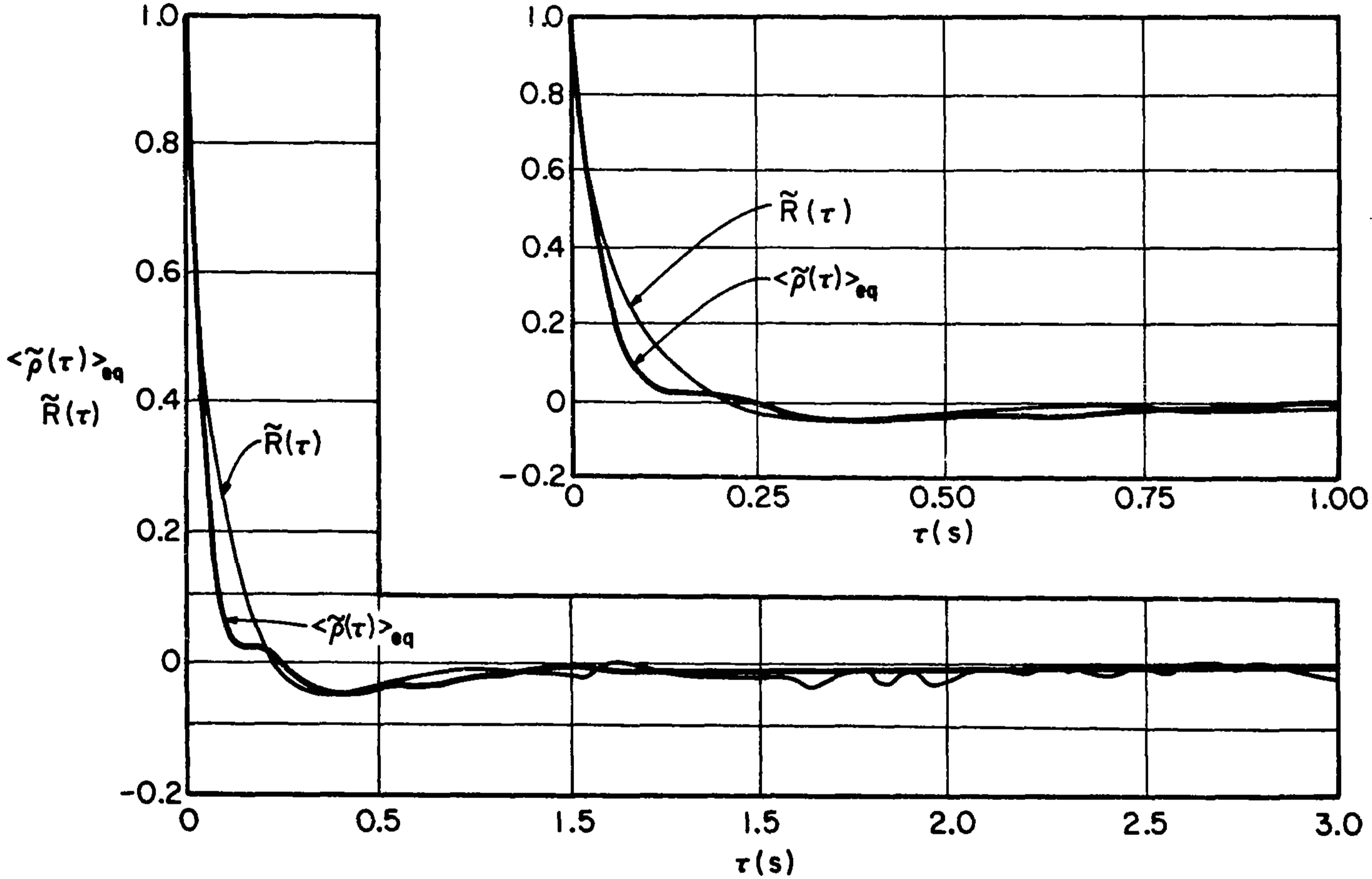

Fig. 6.12 Equivalent ensemble autocorrelation coefficient averaged over all starting times $<\tilde{\rho}(\tau)>_{eq}$ and time-averaged autocorrelation coefficient over a single sample record $\tilde{R}(\tau)$.

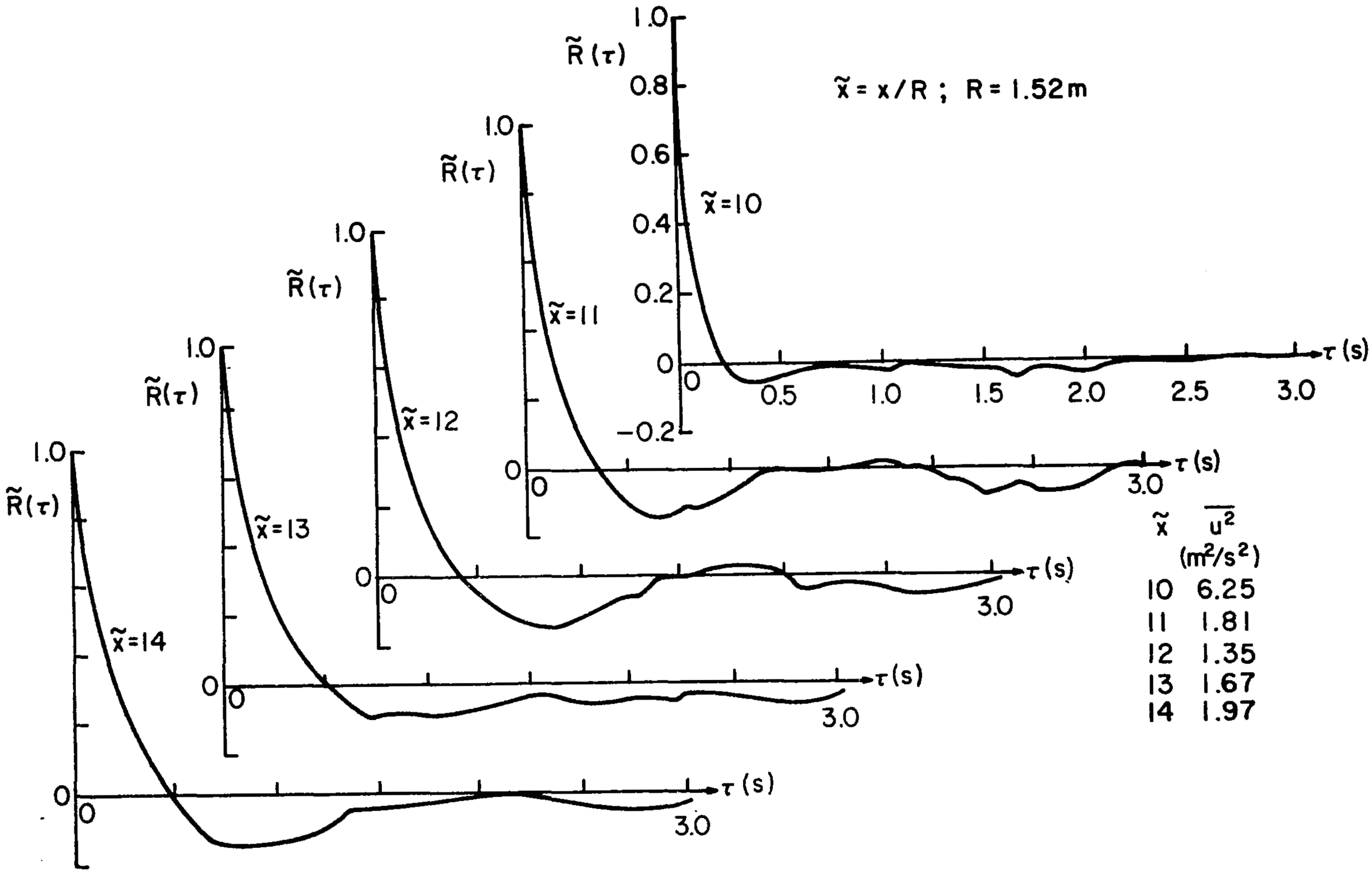

Fig. 6.13(a) Set of five Eulerian turbulent velocity autocorrelation coefficients obtained simultaneously within the turbulence measurement range, i.e., along the turbulence line.

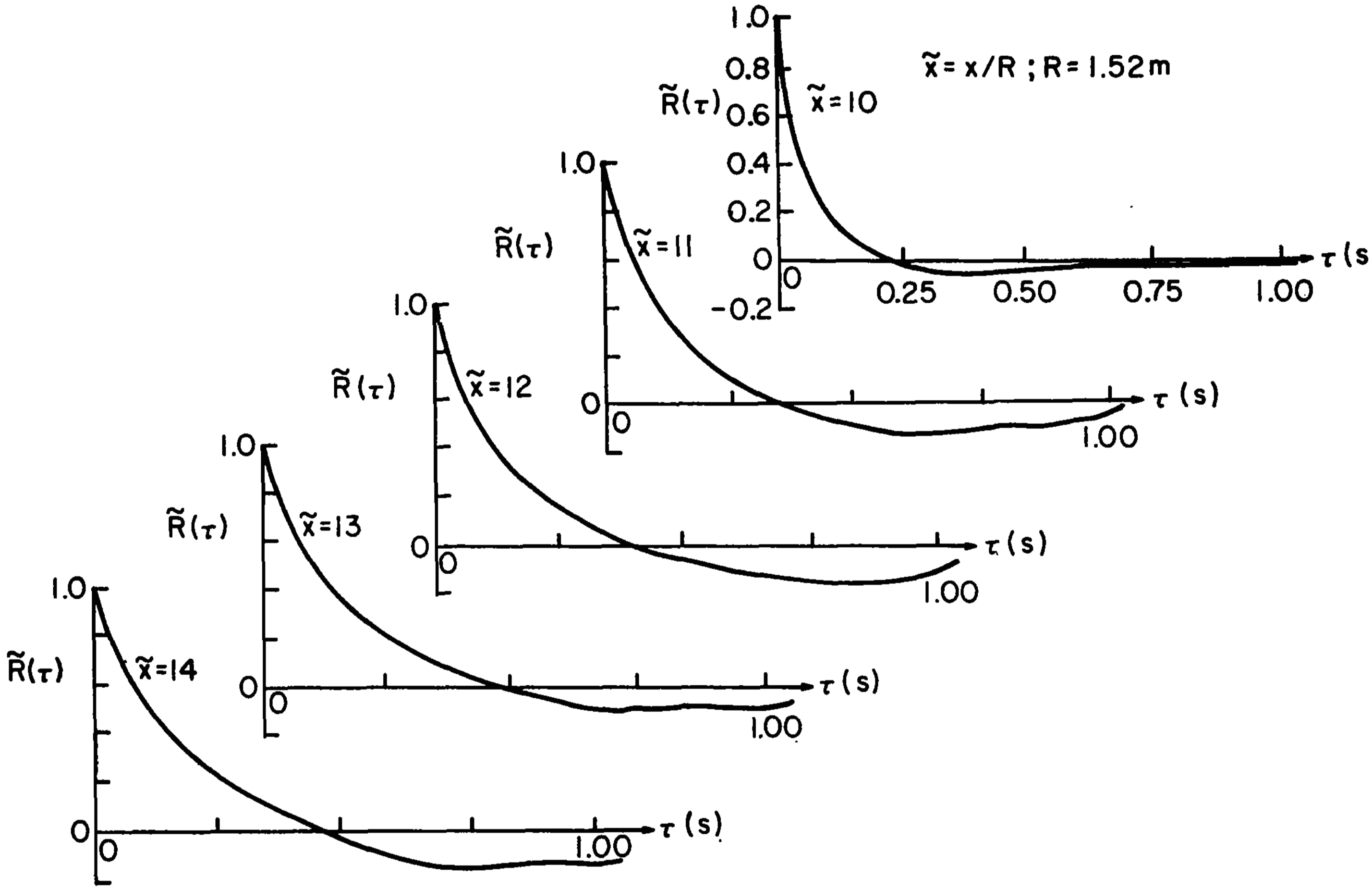

Fig. 6.13(b) Variation of the five Eulerian turbulent velocity autocorrelation coefficients during the first 1 s lag time.

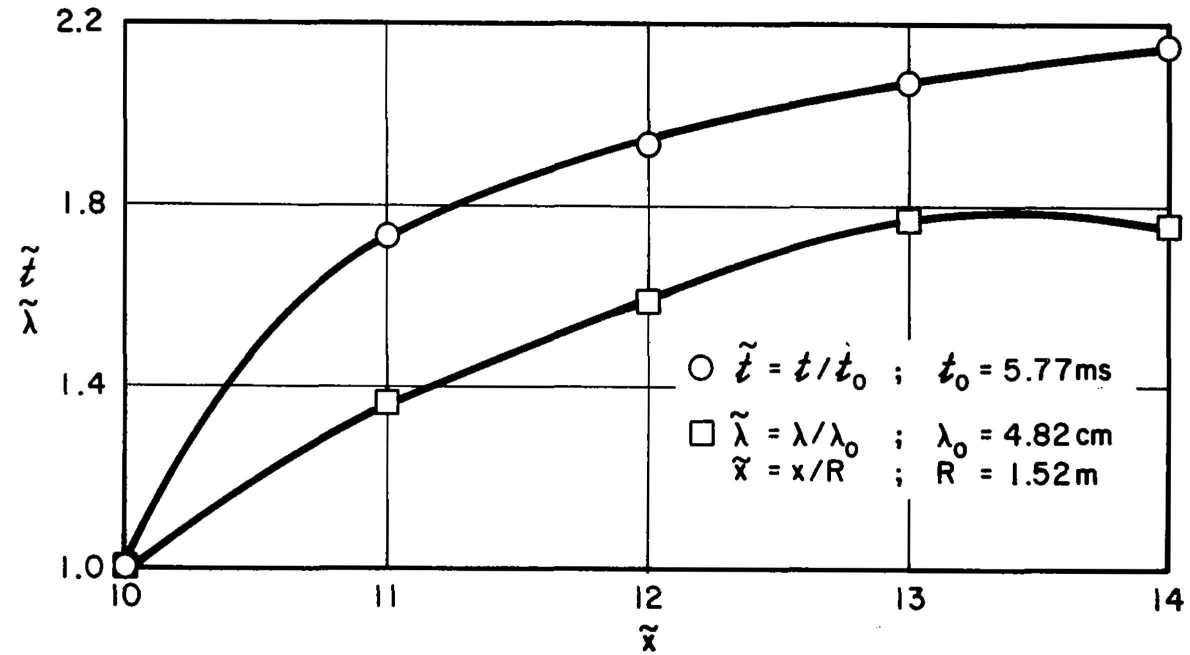

Fig. 6.14 Streamwise variation of the Eulerian micro time and length scales along the turbulence line.

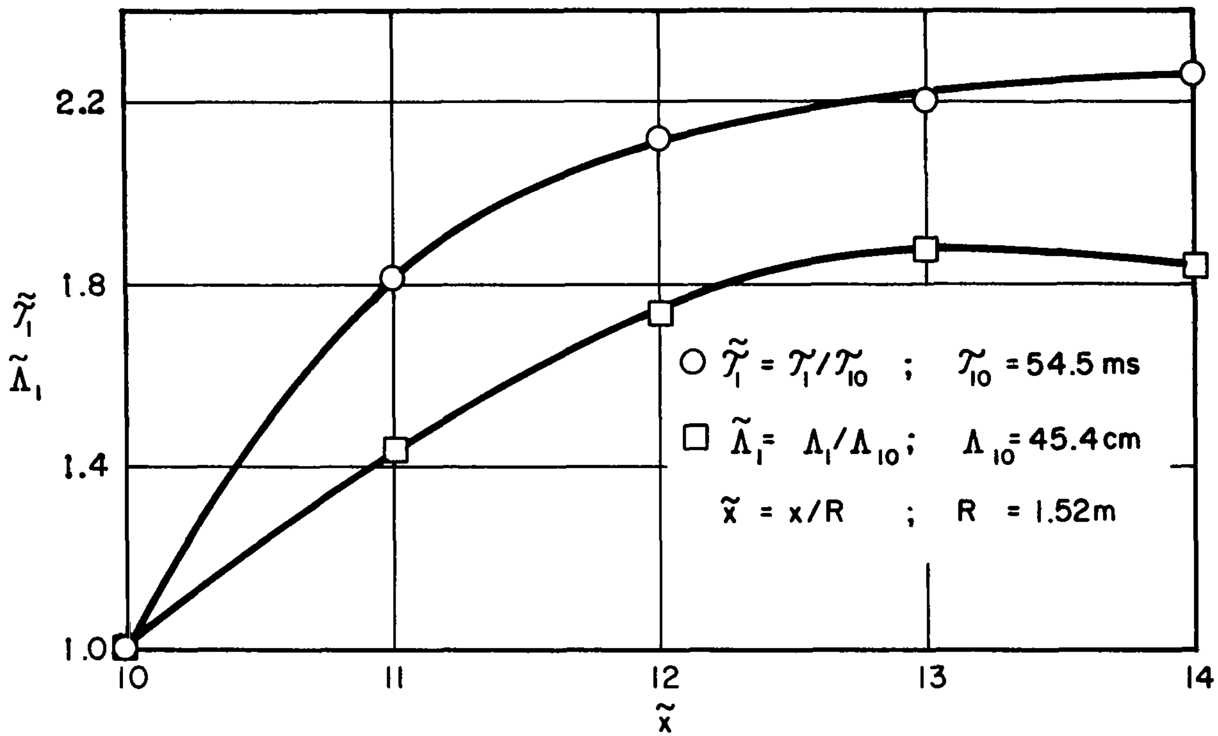

Fig. 6.15 Variation of the Eulerian first integral time and space scales along the turbulence line.

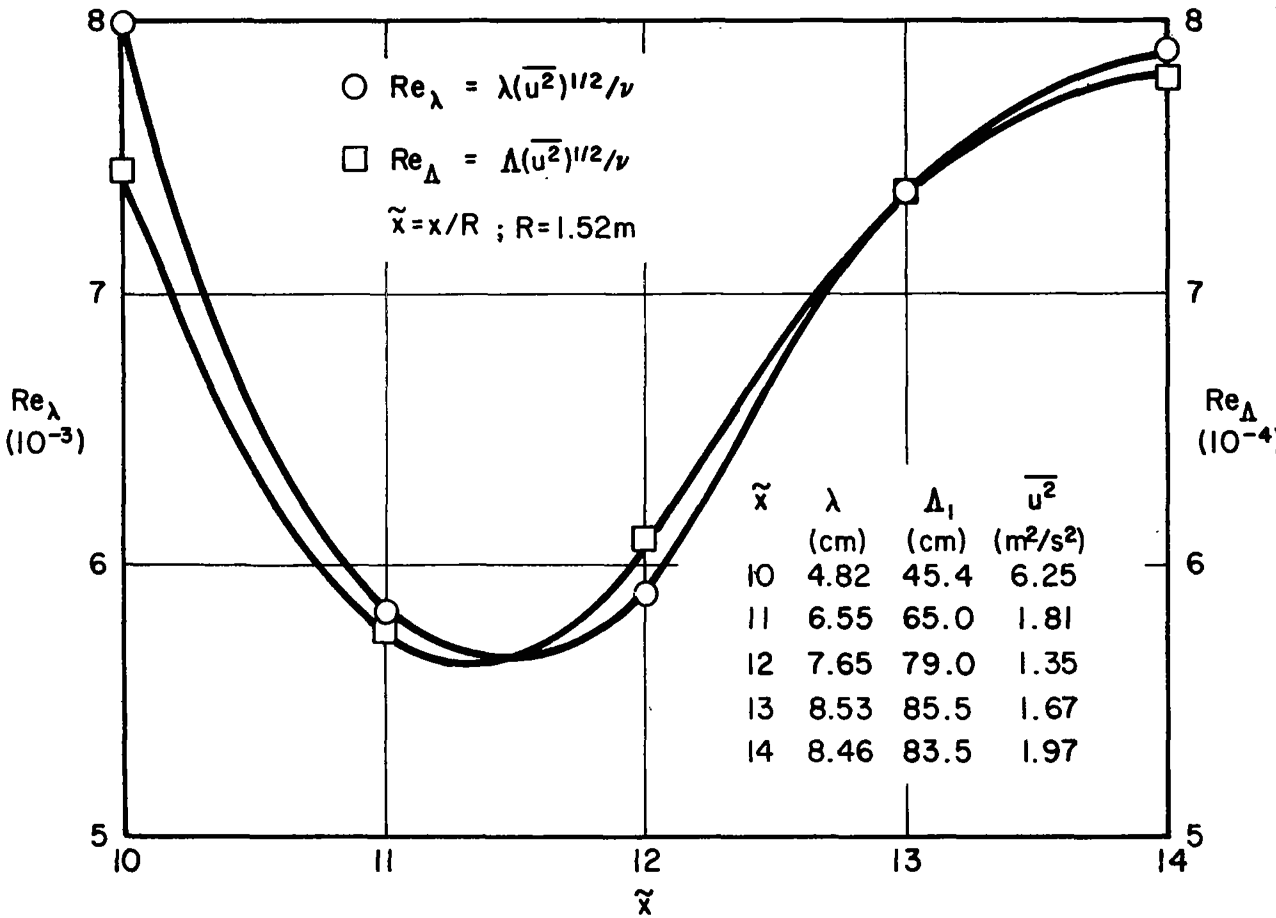

Fig. 6.16 Longitudinal variation of the micro and first integral scale Reynolds numbers along the turbulence line.

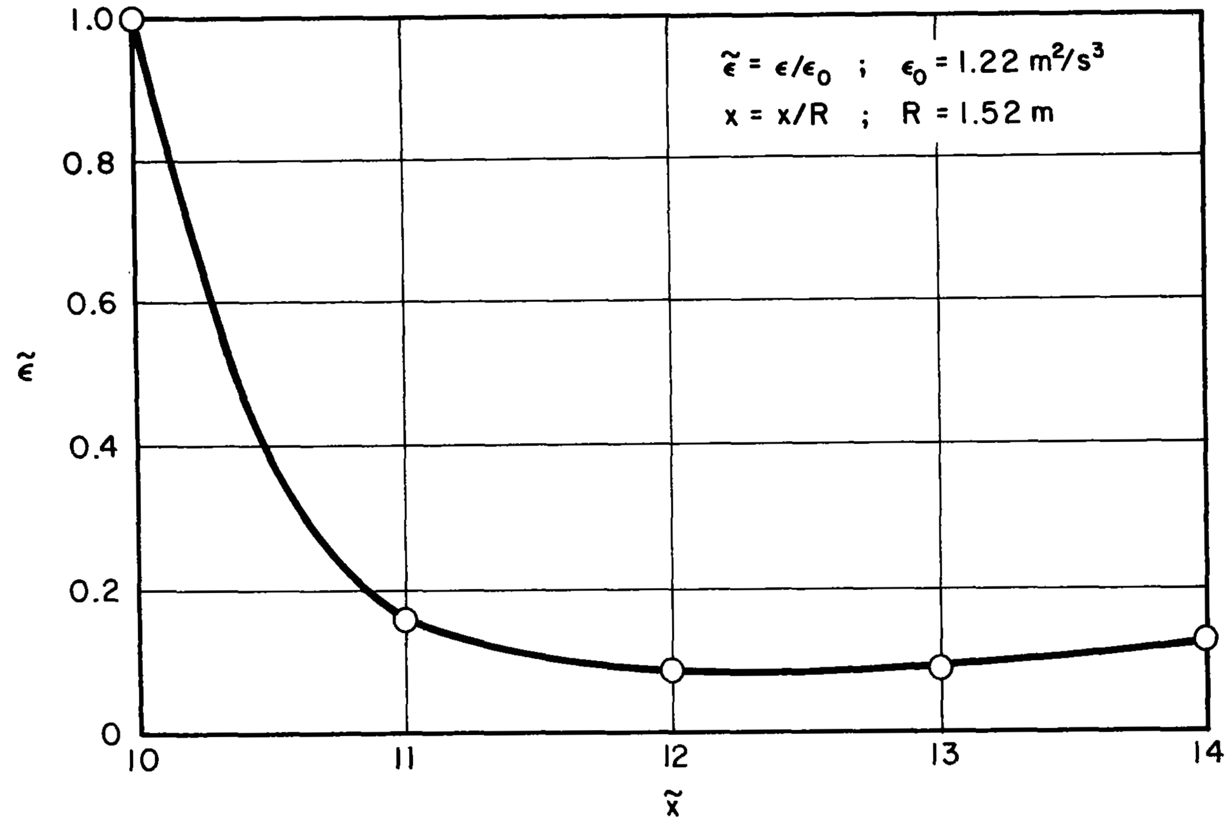

Fig. 6.17 Streamwise change of the dissipation along the turbulence line.

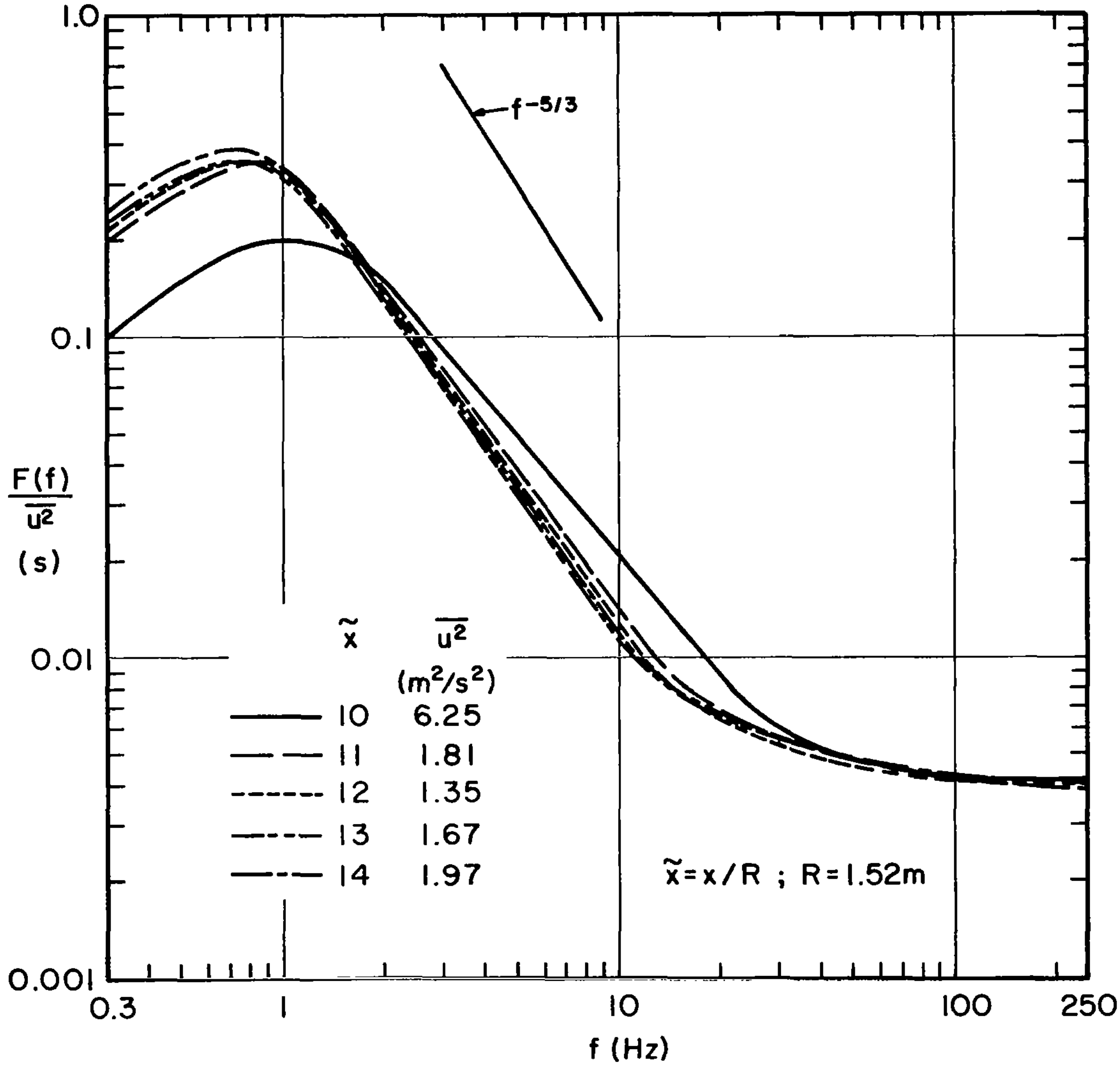

Fig. 6.18 Variation of the energy spectra of the longitudinal turbulent velocity along the turbulence line.

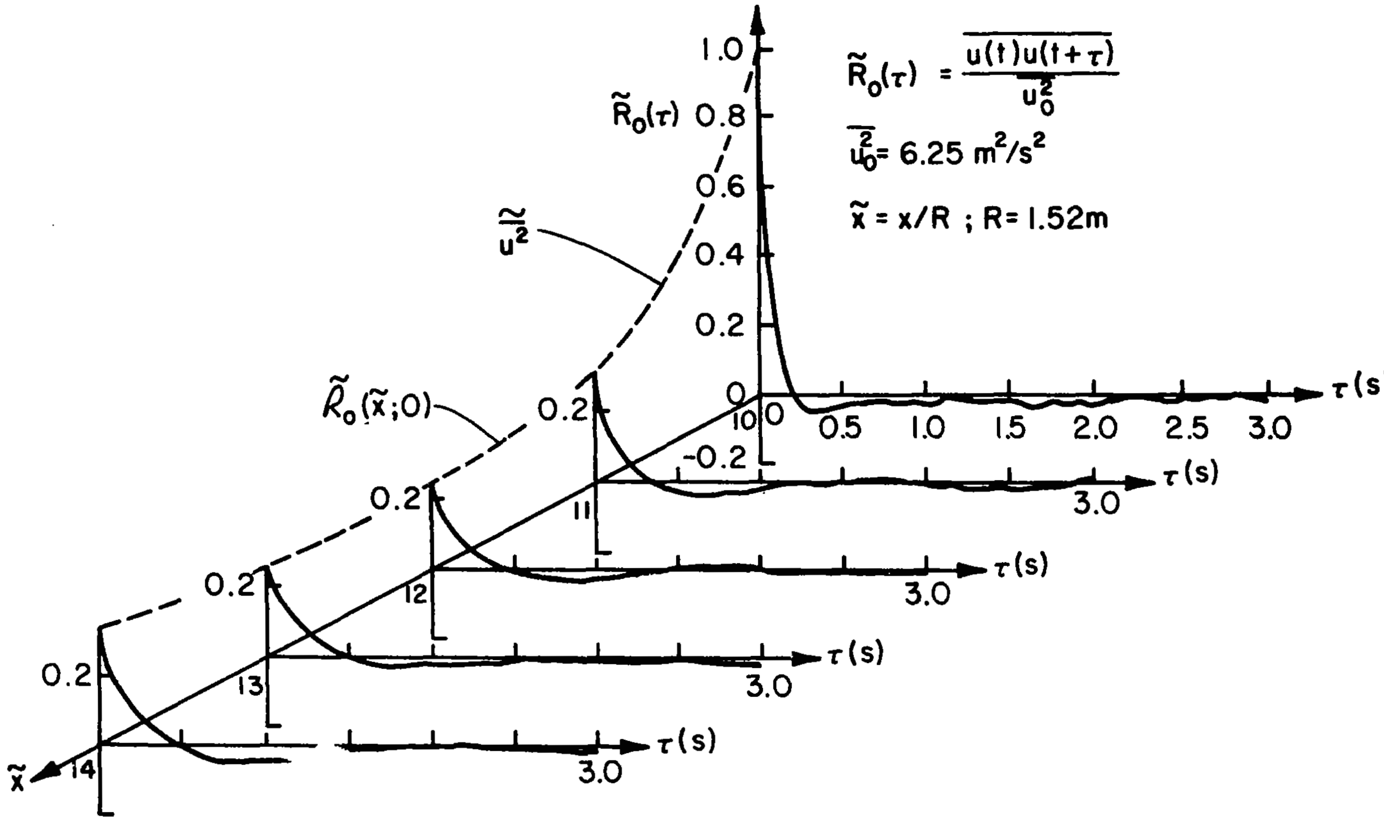

Fig. 6.19 Eulerian reference-point autocorrelation set $\tilde{R}_o(\tau)$ along the turbulence line and the autocorrelation envelope $\tilde{R}_o(\tilde{x};0)$.

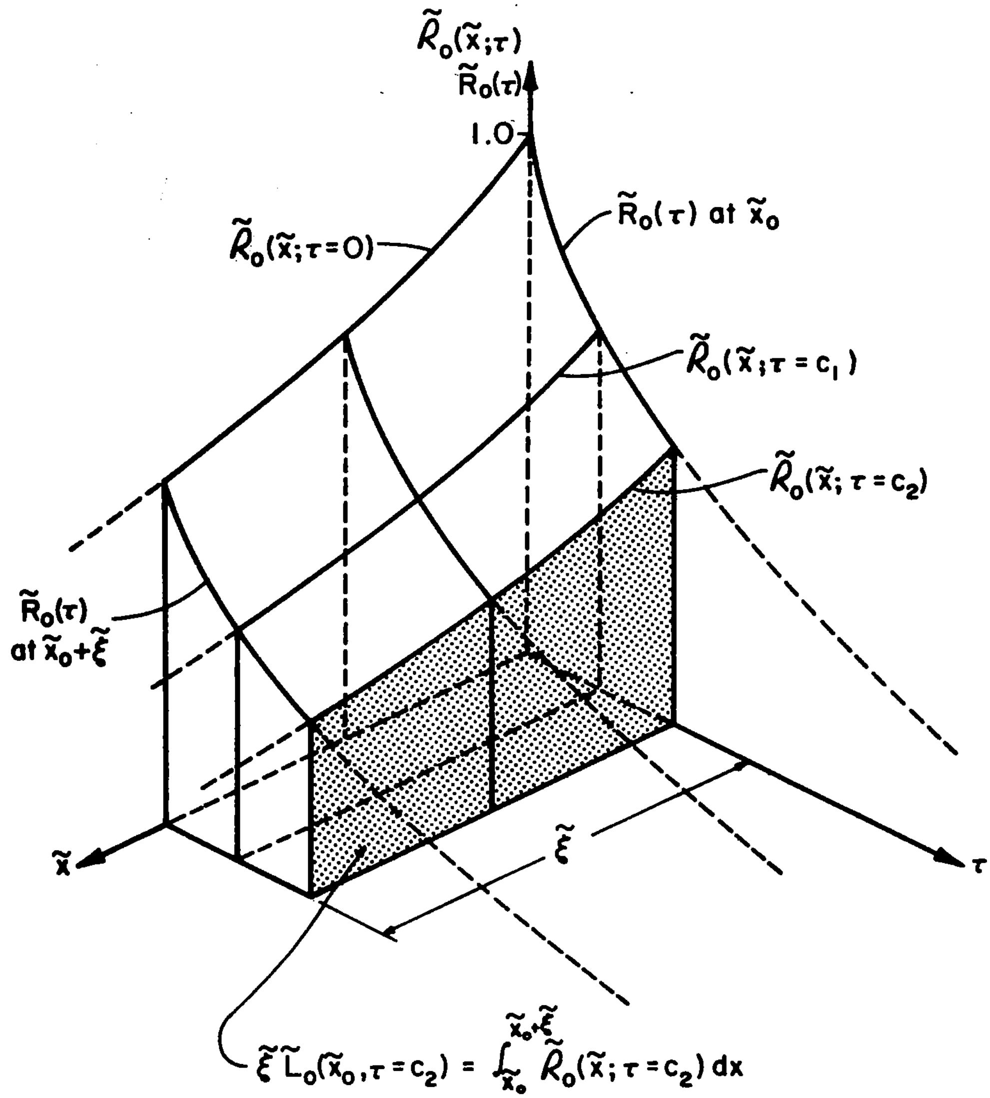

Fig. 6.20 Illustration of the dimensionless autocorrelation envelopes and of the Lagrangian autocorrelation coefficient evaluation at a particular lag time.

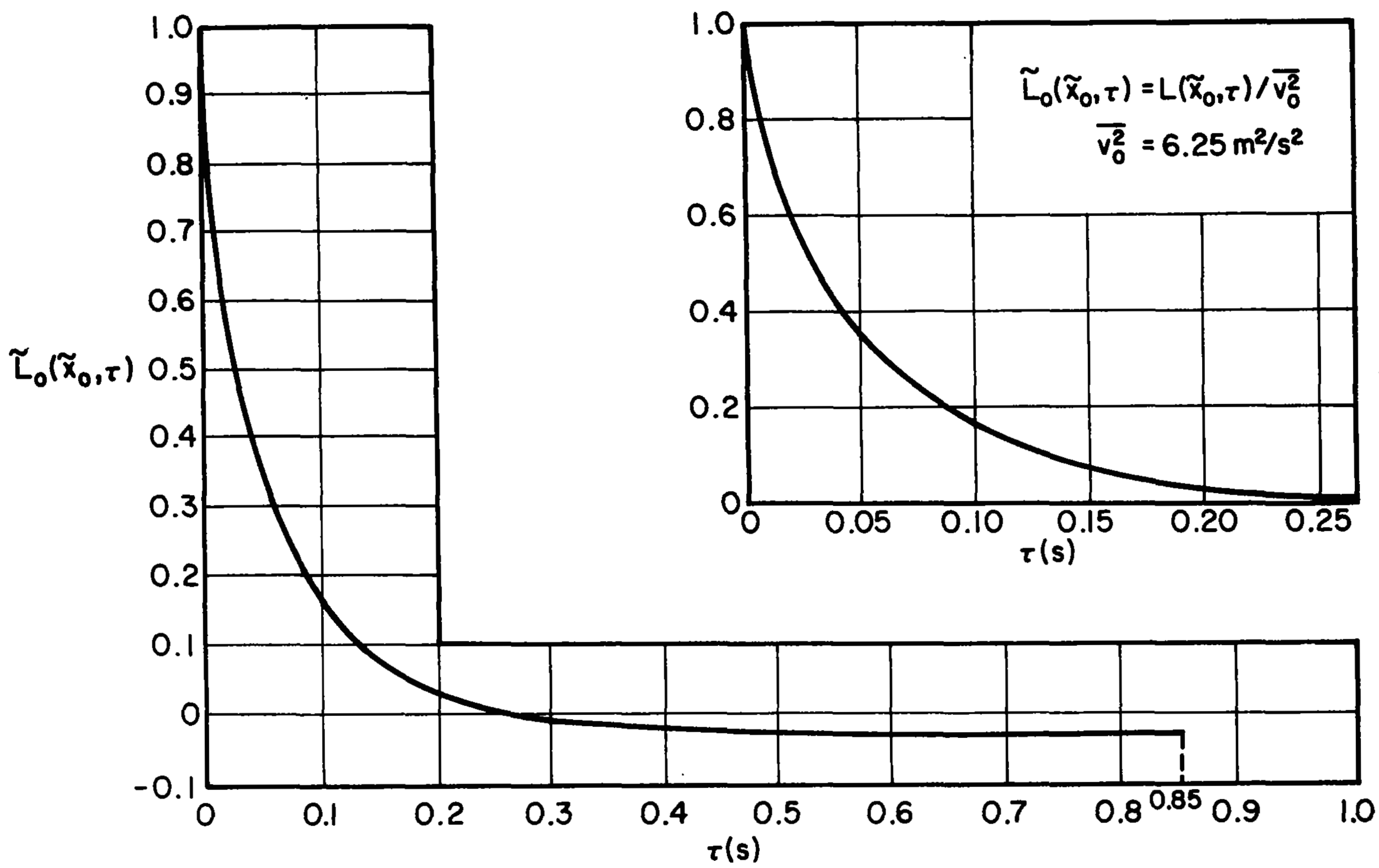

Fig. 6.21 Change of the Lagrangian autocorrelation coefficient with increasing time delay.

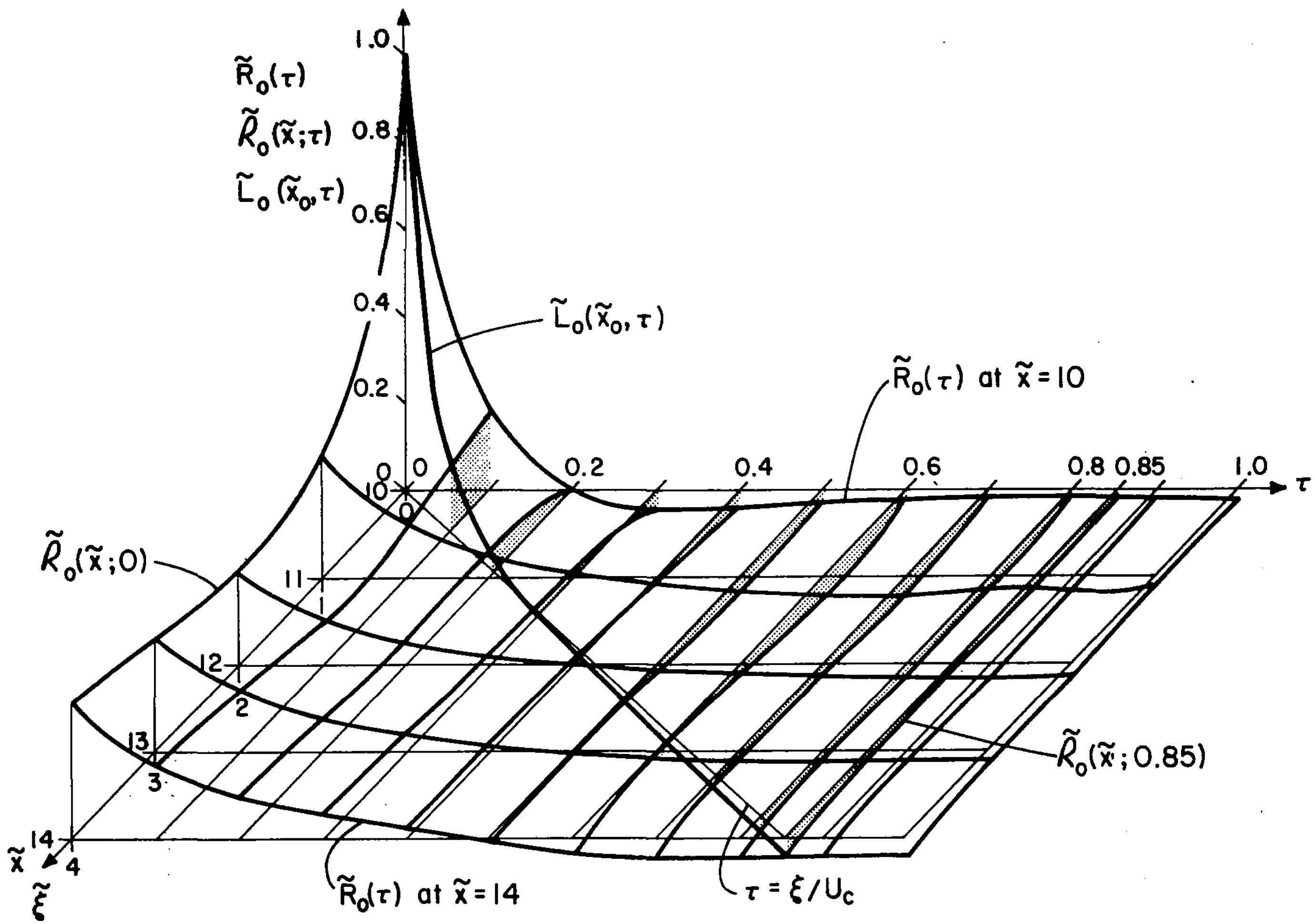

Fig. 6.22 Variations in time and space of the set of five Eulerian reference-point autocorrelation coefficients $\tilde{R}_0(\tau)$, of several envelopes $\tilde{\mathcal{R}}_0(\tilde{x};\tau)$ and of the Lagrangian autocorrelation coefficient $\tilde{L}_0(\tilde{x},\tau)$ for the turbulence line.

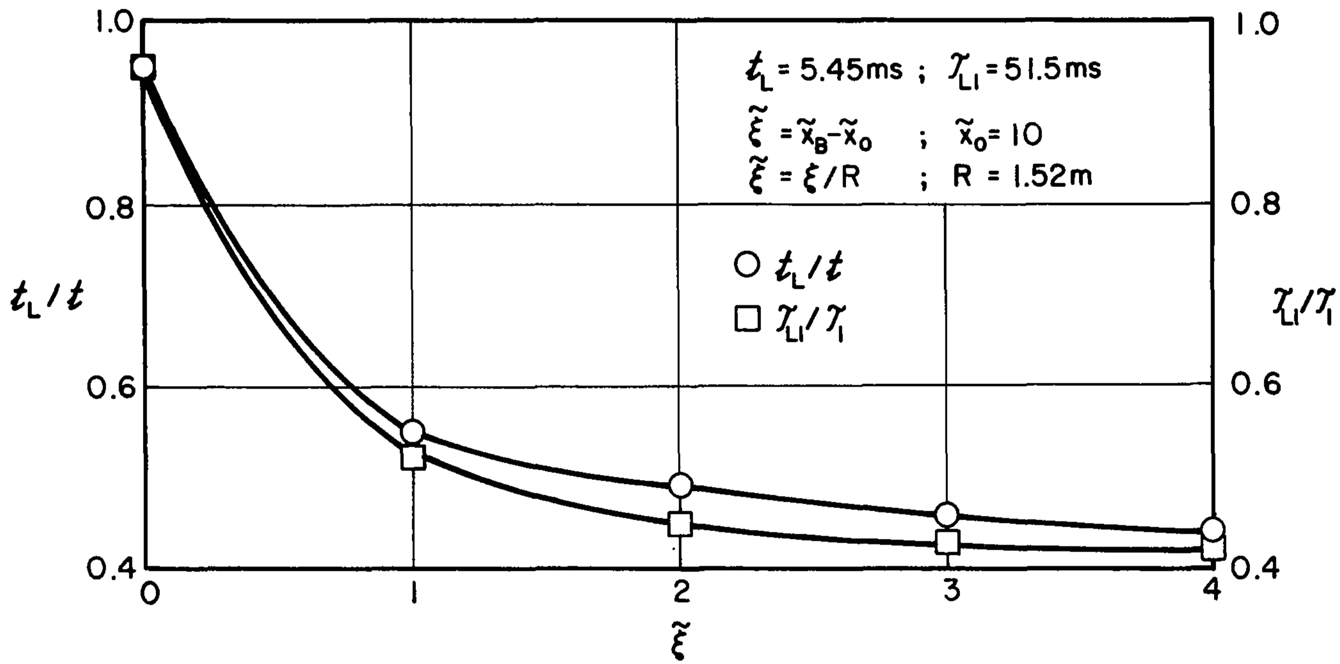

Fig. 6.23 Streamwise changes of the Lagrangian to Eulerian micro time scale and first integral time scale ratios along the turbulence line.

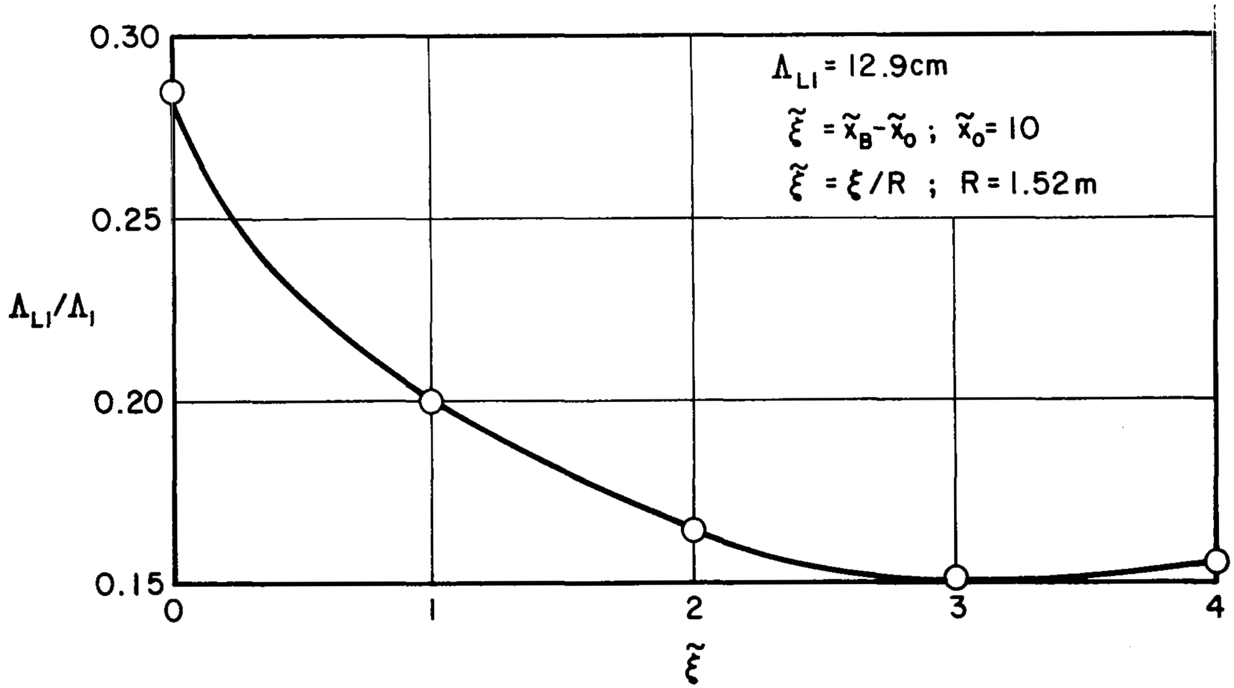

Fig. 6.24 Change of the Lagrangian to Eulerian first integral length scales ratio with increasing axial separation along the turbulence line.

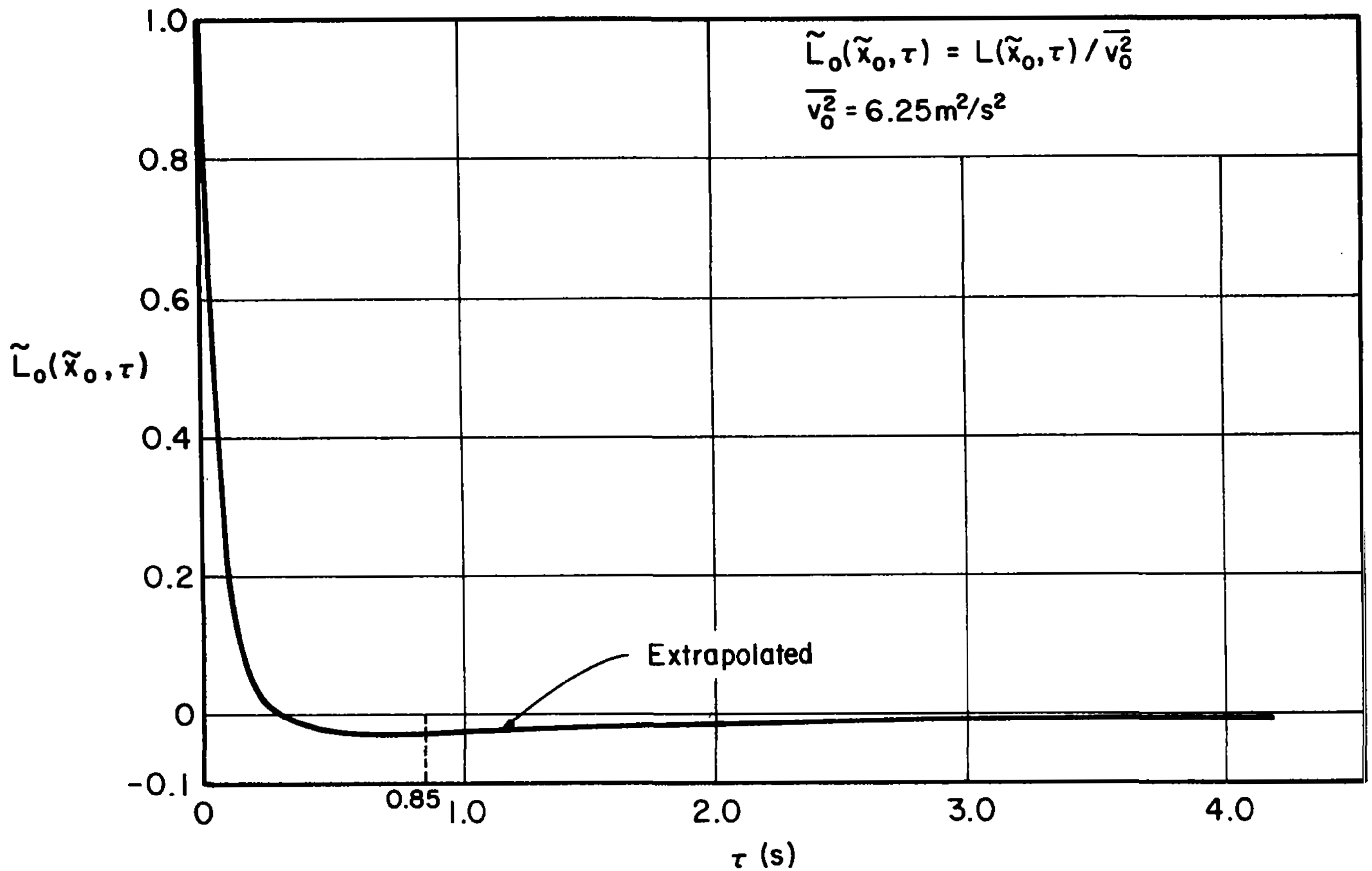

Fig. 6.25 Variation of the extended Lagrangian autocorrelation coefficient with increasing lag time.

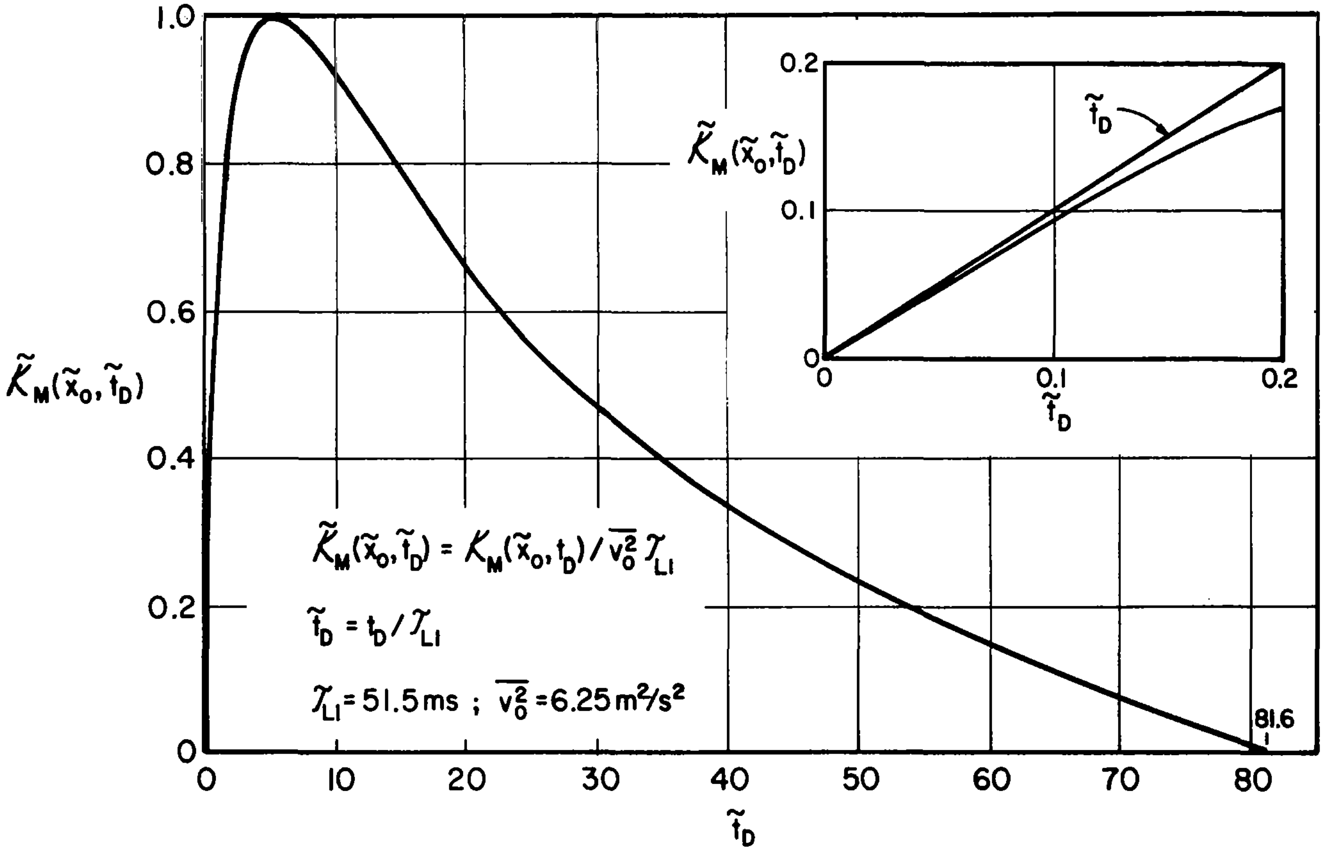

Fig. 6.26 Axial turbulent momentum exchange coefficient change with increasing diffusion time.

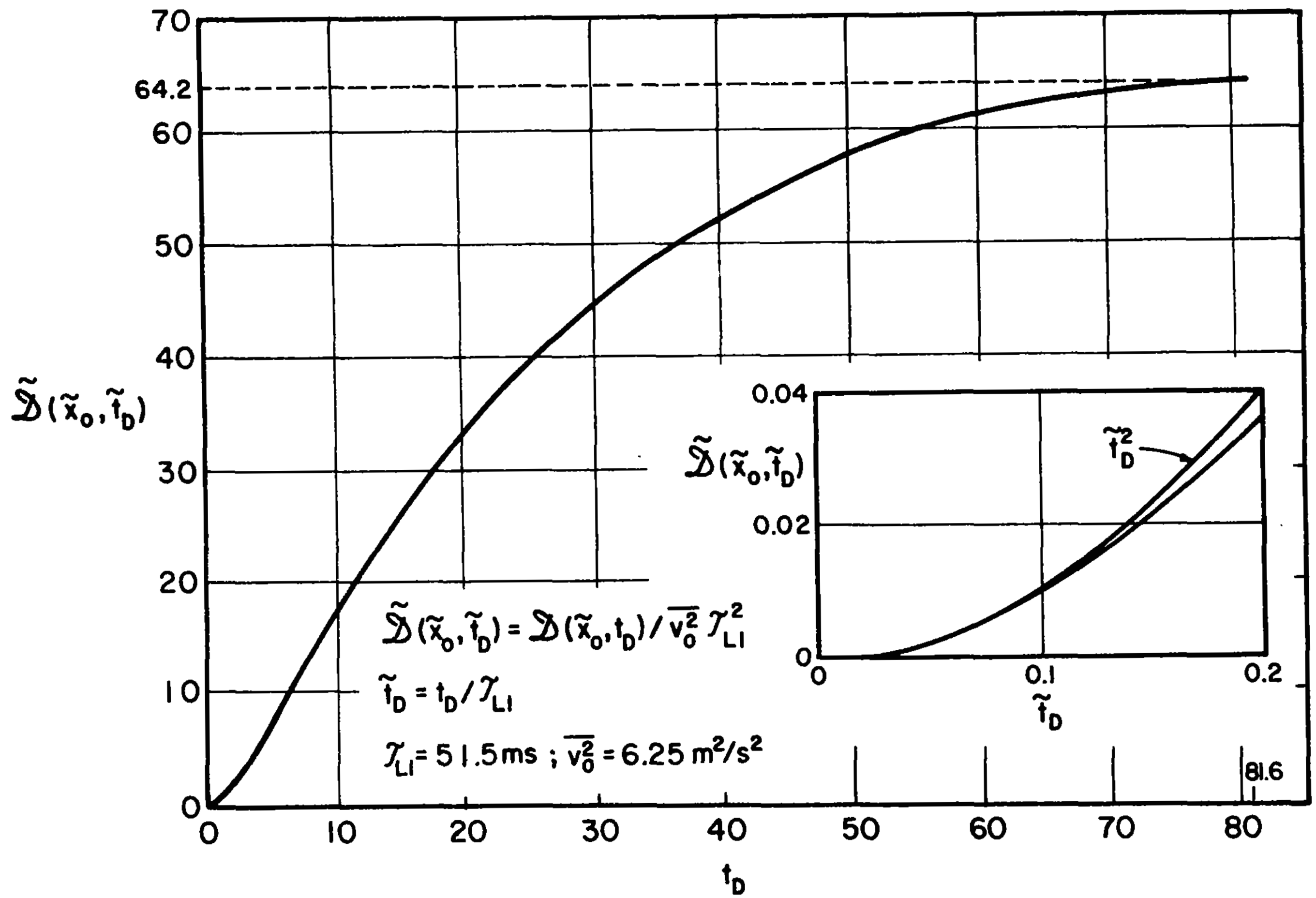

Fig. 6.27 Variation of the longitudinal dispersion coefficient with augmenting diffusion time.

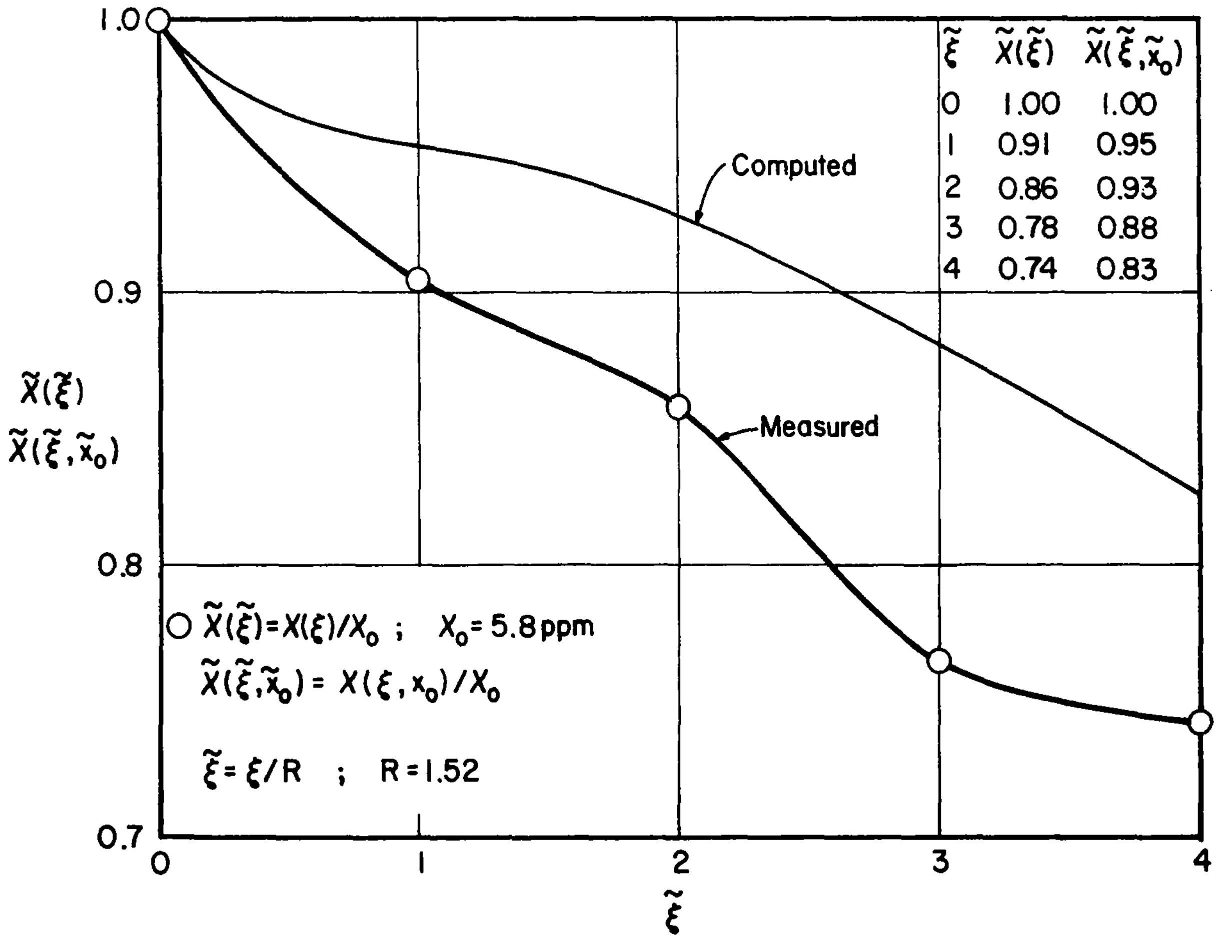

Fig. 6.28 Variation of the measured concentration $\tilde{\chi}(\tilde{\xi})$ and computed concentration $\tilde{\chi}(\tilde{\xi},\tilde{x}_0)$ along the turbulence line.

APPENDIX I

TRAJECTORY AVERAGING OF EULERIAN VELOCITY PRODUCT AND CROSS PRODUCTS

The Lagrangian velocity product obtained from Eq. (3.14) is

$$v_i(a_\ell, t_A^k) v_j(a_\ell, t_A^k+\tau) = r_{ij}(s^k; t_A^k, \tau) - \left[\sum_{m=1}^{\infty} \frac{(s^k)^m}{m!} c_{j,im}(s_B^k, 0, t_A^k+\tau, t_A^k) \right.$$

$$+ \sum_{n=1}^{\infty} \frac{(s^k - s_B^k)^n}{n!} c_{i,jn}(0, s_B^k, t_A^k, t_A^k+\tau)$$

$$\left. + \sum_{m=1}^{\infty} \sum_{n=1}^{\infty} \frac{(s^k)^m (s^k - s_B^k)}{m!n!} c_{im,jn}(0, s_B^k, t_A^k, t_A^k+\tau) \right], \qquad \text{(A.I.1)}$$

where $c_{j,im}$, $c_{i,jn}$ and $c_{im,jn}$ are given by Eqs. (3.15), (3.16) and (3.17), respectively. Trajectory averaging consists of line integration along each k-th path line from initial point $s^k = 0$ to point s_B^k of Eq. (A.I.1)

$$\frac{1}{s_B^k} \int_0^{s_B^k} v_i(a_\ell, t_A^k) v_j(a_\ell, t_A^k+\tau) ds^k = \frac{1}{s_B^k} \int_0^{s_B^k} r_{ij}(s^k; t_A^k, \tau) ds^k$$

$$- \left[\frac{1}{s_B^k} \int_0^{s_B^k} \sum_{m=1}^{\infty} \frac{(s^k)^m}{m!} c_{j,im}(s_B^k, 0, t_A^k+\tau, t_A^k) ds^k \right.$$

$$+ \frac{1}{s_B^k} \int_0^{s_B^k} \sum_{n=1}^{\infty} \frac{(s^k - s_B^k)^n}{n!} c_{i,jn}(0, s_B^k, t_A^k, t_A^k+\tau) ds^k$$

$$\left. + \frac{1}{s_B^k} \int_0^{s_B^k} \sum_{m=1}^{\infty} \sum_{n=1}^{\infty} \frac{(s^k)^m (s^k - s_B^k)^n}{m!n!} c_{im,jn}(0, s_B^k, t_A^k, t_A^k+\tau) ds^k \right]. \qquad \text{(A.I.2)}$$

The Lagrangian velocity product is independent of the s^k variable and, thus, its line integral leads to

$$\frac{1}{s_B^k}\int_0^{s_B^k} v_i(a_\ell,t_A^k)v_j(a_\ell,t_A^k+\tau)ds^k = v_i(a_\ell,t_A^k)v_j(a_\ell,t_A^k+\tau). \qquad \text{(A.I.3)}$$

Integration of the second, third and fourth terms on the right-hand side of Eq. (A.I.2) involves only $(s^k)^m$, $(s^k - s_B^k)^n$ and $(s^k)^m(s^k - s_B^k)^n$, respectively, inasmuch as $c_{j,im}$, $c_{i,jn}$ and $c_{im,jn}$ are constants. The order of integration and summation can be reversed in these terms since they are independent. Integration of the second and third terms for specific values of m and n yields

$$\frac{1}{s_B^k}\int_0^{s_B^k} (s^k)^m ds^k = \frac{(s^k)^{m+1}}{(m+1)s_B^k}\Bigg|_0^{s_B^k} = \frac{(s_B^k)^m}{(m+1)}, \qquad \text{(A.I.4)}$$

and

$$\frac{1}{s_B^k}\int_0^{s_B^k} (s^k - s_B^k)^n ds^k = \frac{(s^k - s_B^k)^{n+1}}{(n+1)s_B^k}\Bigg|_0^{s_B^k} = \frac{(-1)^n(s_B^k)^n}{(n+1)}. \qquad \text{(A.I.5)}$$

The fourth term in Eq. (A.I.2) is integrated by parts. One integration results in

$$\frac{1}{s_B^k}\int_0^{s^k_m} (s^k)^m(s^k - s_B^k)^n ds^k = \frac{(s^k)^{m+1}(s^k - s_B^k)^n}{(m+1)s_B^k}\Bigg|_0^{s_B^k}$$

$$- \frac{n}{(m+1)s_B^k}\int_0^{s_B^k} (s^k)^{m+1}(s^k - s_B^k)^{n-1} ds^k$$

$$= - \frac{n}{(m+1)s_B^k}\int_0^{s_B^k} (s^k)^{m+1}(s^k - s_B^k)^{n-1} ds^k. \qquad \text{(A.I.6)}$$

This integration by parts procedure is carried out n times consecutively yielding

$$\frac{(-1)^n \; n!}{(m+1)(m+2)\cdots(m+n)s_B^k} \int_0^{s_B^k} (s^k)^{m+n} ds^k. \qquad \text{(A.I.7)}$$

Finally, integration of Eq. (A.I.7) leads to

$$\frac{(-1)^n \; m!n!}{(m+n+1)!} (s_B^k)^{m+n} \qquad \text{(A.I.8)}$$

The results of this trajectory averaging are substituted into Eq. (A.I.2) which then becomes

$$\begin{aligned} v_i(a_\ell, t_A^k) v_j(a_\ell, t_A^k+\tau) &= \frac{1}{s_B^k} \int_0^{s_B^k} r_{ij}(s^k; t_A^k, \tau) ds^k \\ &- \left[\sum_{m=1}^{\infty} \frac{(s_B^k)^m}{(m+1)!} \; c_{j,im}(s_B^k, 0, t_A^k+\tau, t_A^k) \right. \\ &+ \sum_{n=1}^{\infty} \frac{(-1)^n (s_B^k)^n}{(n+1)!} \; c_{i,jn}(0, s_B^k, t_A^k, t_A^k, \tau) \\ &+ \left. \sum_{m=1}^{\infty} \sum_{n=1}^{\infty} \frac{(-1)^n (s_B^k)^{m+n}}{(m+n+1)!} \; c_{im,jn}(0, s_B^k, t_A^k, t_A^k+\tau) \right]. \qquad \text{(A.I.9)} \end{aligned}$$

The terms on the right-hand side of Eq. (A.I.9) are exactly the bracketed terms in Eqs. (3.19), (3.20), (3.21) and (3.22).

APPENDIX II

SIGNAL CHARACTERISTICS

Representative values of the signals generated by the five hot-wire probes prior to any amplification are summarized in Table A.II.1 In this table the following information is listed for each probe: (1) the location of the probe in dimensional and dimensionless coordinates, x and $\tilde{x}$, respectively (See Fig. 5.1); (2) the hot-wire anemometer voltage in still air E_o; (3) the DC voltage drop $\Delta\overline{E}$ caused by the mean velocity $\overline{U}$; and, (4) the rms value of the AC voltage e_{rms} arising from the fluctuating velocity u. Note that the dimensionless coordinate is $\tilde{x} = x/R$, where $R = 1.52$ m.

The total voltage drop induced by the flow $\Delta E = \Delta\overline{E} + e$ was recorded on FM magnetic tape and, therefore, the gains of the recorder data tracks are also tabulated in Table A.II.1. A 100 Hz frequency sine wave of 1 V peak (0.707 V rms) was recorded on each data track before the data recording as a calibration signal. The gain of each track $G_T = 1/A$, where A is the amplitude of the calibration sine wave after reproduction, is also tabulated in this table.

Table A.II.1

HOT-WIRE SIGNAL CHARACTERISTICS

Probe No.	Probe Location x (m)	$\tilde{x}$	E_o (V)	$\Delta\overline{E}$ (mV)	e_{rms} (mV)	Track No.	G_T
1	15.20	10	1.978	434	59.2	3	0.83
2	16.72	11	1.624	477	43.4	5	1.02
3	18.24	12	1.622	625	45.7	7	0.95
4	19.72	13	1.633	513	41.1	9	1.02
5	21.28	14	1.652	439	40.5	11	1.03

APPENDIX III

EULERIAN VELOCITY CROSS PRODUCTS ESTIMATION

The three Eulerian velocity cross products which were neglected in computing the Lagrangian autocorrelation are given by Eqs. (3.35), (3.36) and (3.37). Their longitudinal components, viz., $i = j = 1$ in these three equations, are

$$\Psi^2_{11}(x_o,\tau) = \sum_{m=1}^{\infty} \frac{(U_c\tau)^m}{(m+1)!} \frac{1}{S} \int_S C_{1,1m}(x_B,x_o,\tau)\, dS, \qquad \text{(A.III.1)}$$

$$\Psi^3_{11}(x_o,\tau) = \sum_{n=1}^{\infty} \frac{(-1)^n (U_c\tau)^n}{(n+1)!} \frac{1}{S} \int_S C_{1,1n}(x_o,x_B,\tau)\, dS, \qquad \text{(A.III.2)}$$

and

$$\Psi^4_{11}(x_o,\tau) = \sum_{m=1}^{\infty}\sum_{n=1}^{\infty} \frac{(-1)^n (U_c\tau)^{m+n}}{(m+n+1)!} \frac{1}{S} \int_S C_{1m,1n}(x_o,x_B,\tau)\, dS, \qquad \text{(A.III.3)}$$

in which x_o and x_B designate points in the reference and B-point planes viz., x_o and x_B are standing for x_ℓ and b_ℓ, respectively. In the foregoing equations the space-time cross-correlations are expressed by

$$C_{1,1m}(x_B,x_o,\tau) = \frac{1}{T} \int_0^T c_{1,1m}(x_B,x_o,t+\tau,t)\, dt, \qquad \text{(A.III.4)}$$

$$C_{1,1n}(x_o,x_B,\tau) = \frac{1}{T} \int_0^T c_{1,1n}(x_o,x_B,t,t+\tau)\, dt, \qquad \text{(A.III.5)}$$

and

$$C_{1m,1n}(x_o,x_B,\tau) = \frac{1}{T} \int_0^T c_{1m,1n}(x_o,x_B,t,t+\tau)\, dt, \qquad \text{(A.III.6)}$$

utilizing Eqs. (3.32), (3.33) and (3.34).

The integrands in these three equations are the longitudinal components of the Eulerian velocity cross products given by Eqs. (3.15), (3.16) and (3.17). These velocity cross products are expressed in Eqs. (A.III.4) to (A.III.6) in terms of spatial coordinates and time, In other words, x_o, x_B and t are superseding s = 0 and s_B^k and t_A^k, respectively. Next, the space-time cross-correlations are to be averaged over the reference plane $x_o = S =$ constant in Eqs. (A.III.1), (A.III.2) and (A.III.3). The cross-correlations at two points along the turbulence line can be essentially viewed as representative of all possible cross-correlations for any pair of points in the reference and B-point planes in a similar manner as for the Eulerian autocorrelation. Then the area integrals in three Ψ-terms reduce simply to evaluation of the cross-correlations at two points x_o and x_B on the turbulence line. The three sums in Eqs. (A.III.1), (A.III.2) and (A.III.3) are further dominated by their respective first-order space-time cross-correlation terms, viz., by the terms obtained when m = n = 1. Consequently, they are approximated by

$$\Psi_{11}^2(x_o,\tau) \approx \frac{U_c\tau}{2} \overline{u(x_B;t+\tau)\left[\frac{du(x;t)}{dx}\right]_{x=x_o}} , \qquad \text{(A.III.7)}$$

$$\Psi_{11}^3(x_o,\tau) \approx -\frac{U_c\tau}{2} \overline{u(x_o,t)\left[\frac{du(x;t+\tau)}{dx}\right]_{x=x_B}} , \qquad \text{(A.III.8)}$$

and

$$\Psi_{11}^4(x_o,\tau) \approx -\frac{(U_c\tau)^2}{6} \overline{\left[\frac{du(x;t)}{dx}\right]_{x=x_o}\left[\frac{du(x;t+\tau)}{dx}\right]_{x=x_B}} , \qquad \text{(A.III.9)}$$

where use was made of Eqs. (3.15), (3.16) and (3.17) in terms of spatial coordinates and time. The overbars in these equations denote time averaging according to Eqs. (A.III.4), (A.III.5) and (A.III.6).

The spatial derivatives which are evaluated at $x = x_o$ and x_B in the foregoing Ψ-terms were approximated by their corresponding time derivatives at the very same positions on the turbulent line in the usual manner. Thus, $d/dx = (1/U_c)(d/dt)$, where U_c is the characteristic mean velocity scale along the turbulence line. Then the three Eulerian velocity cross products are given by

$$\Psi^2_{11}(x_o,\tau) \approx \frac{\tau}{2}\ \overline{u(x_B,t+\tau)\ \frac{du(x_o,t)}{dt}}\ , \tag{A.III.10}$$

$$\Psi^3_{11}(x_o,\tau) \approx -\frac{\tau}{2}\ \overline{u(x_o,t)\ \frac{du(x_B,t+\tau)}{dt}}\ . \tag{A.III.11}$$

and

$$\Psi^4_{11}(x_o,\tau) \approx -\frac{\tau^2}{6}\ \overline{\frac{du(x_o,t)}{dt}\ \frac{du(x_B,t+\tau)}{dt}}\ . \tag{A.III.12}$$

The above three equations are furthermore expressed in terms of their respective dimensionless space-time cross-correlations according to

$$\Psi^2_{11}(x_o,\tau) \approx \frac{\tau}{2}\left\{\overline{[u(x_B,t)]^2}\ \overline{\left[\frac{du(x_o,t)}{dt}\right]^2}\right\}^{\frac{1}{2}} \tilde{C}_{1,11}(x_B,x_o,\tau), \tag{A.III.13}$$

$$\Psi^3_{11}(x_o,\tau) \approx -\frac{\tau}{2}\left\{\overline{[u(x_o,t)]^2}\ \overline{\left[\frac{du(x_B,t)}{dt}\right]^2}\right\}^{\frac{1}{2}} \tilde{C}_{1,11}(x_o,x_B,\tau), \tag{A.III.14}$$

and

$$\Psi^4_{11}(x_o,\tau) \approx -\frac{\tau^2}{6}\left\{\overline{\left[\frac{du(x_o,t)}{dt}\right]^2}\ \overline{\left[\frac{du(x_B,t)}{dt}\right]^2}\right\}^{\frac{1}{2}} \tilde{C}_{11,11}(x_o,x_B,\tau), \tag{A.III.15}$$

where the cross-correlation coefficients are

$$\tilde{C}_{1,11}(x_B,x_o,\tau) = \frac{\overline{u(x_B,t+\tau)\,\dfrac{du(x_o,t)}{dt}}}{\left\{\overline{[u(x_B,t)]^2}\;\overline{\left[\dfrac{du(x_o,t)}{dt}\right]^2}\right\}^{\frac{1}{2}}}, \qquad \text{(A.III.16)}$$

$$\tilde{C}_{1,11}(x_o,x_B,\tau) = \frac{\overline{u(x_o,t)\,\dfrac{du(x_B,t+\tau)}{dt}}}{\left\{\overline{[u(x_o,t]^2}\;\overline{\left[\dfrac{du(x_B,t)}{dt}\right]^2}\right\}^{\frac{1}{2}}}, \qquad \text{(A.III.17)}$$

and

$$\tilde{C}_{11,11}(x_o,x_B,\tau) = \frac{\overline{\dfrac{du(x_o,t)}{dt}\;\dfrac{du(x_B,t+\tau)}{dt}}}{\left\{\overline{\left[\dfrac{du(x_o,t)}{dt}\right]^2}\;\overline{\left[\dfrac{du(x_B,t)}{dt}\right]^2}\right\}^{\frac{1}{2}}}, \qquad \text{(A.III.18)}$$

and the averaging time T = 1200 s (see Sect. 5.5).

The cross-correlation coefficients were computed for the first two stations on the turbulence line, viz., at $\tilde{x}_o = 10$ and $\tilde{x}_B = 11$. Then the axial space separation $\tilde{\xi} = \tilde{x}_B - \tilde{x}_o = 1$ (1.52 m (5 ft)). Greater separation length would yield undoubtedly smaller cross-correlation values. The time lapse τ corresponding to this axial separation, i.e., $\tilde{\xi} = 1$ is about 0.21 s based on Eq. (3.23). For this lag time, the coefficients $\tau/2$, $-\tau/2$ and $-\tau^2/6$ in Eqs. (A.III.10), (A.III.11) and (A.III.12) are roughly 0.1 s, -0.1 s and -0.008 s^2, respectively.

The velocity-velocity derivative and double velocity derivative cross-correlation coefficients were estimated using the recorded hot-wire anemometer signals. These cross-correlation coefficients in terms of the fluctuating voltage $e(\tilde{x},t)$ are

$$\tilde{C}_{1,11}(11,10,\tau) = \frac{\overline{e(11,t+\tau)\,\frac{de(10,t)}{dt}}}{\left\{\overline{[e(11,t)]^2}\,\overline{\left[\frac{de(10,t)}{dt}\right]^2}\right\}^{\frac{1}{2}}}, \tag{A.III.19}$$

$$\tilde{C}_{1,11}(10,11,\tau) = \frac{\overline{e(10,t)\,\frac{de(11,t+\tau)}{dt}}}{\left\{\overline{[e(10,t)]^2}\,\overline{\left[\frac{de(11,t)}{dt}\right]^2}\right\}^{\frac{1}{2}}}, \tag{A.III.20}$$

and

$$\tilde{C}_{11,11}(10,11,\tau) = \frac{\overline{\frac{de(10,t)}{dt}\,\frac{de(11,t+\tau)}{dt}}}{\left\{\overline{\left[\frac{de(10,t)}{dt}\right]^2}\,\overline{\left[\frac{de(11,t)}{dt}\right]^2}\right\}^{\frac{1}{2}}}. \tag{A.III.21}$$

The preceding three cross-correlation coefficients were calculated in the very same manner as used in the autocorrelation computation. Each signal was fed concurrently to either channel A or B of the correlation function analyzer (see Sect. 5.5). A RC differentiating circuit was utilized to obtain the time derivative. In order to differentiate the signals up to their highest frequencies of interest $f_m = 250$ Hz, a RC time constant of 38 μs was used [A.III.1].

The resulting three first-order space-time cross-correlation coefficients are depicted in Figs. A.III.1(a), (b) and (c) up to a lag time of 1 s. This lag time range permits evaluation of the trends of the cross-correlations with increasing time delay in addition to furnishing their values at the lag time of interest $\tau = 0.21$ s. The magnitudes of the three cross-correlation coefficients are negligible as clearly indicated by their random variations shown in Figs. A.III.1. Their maximum values are at the most 0.02 which is smaller than the possible standard deviation of the correlation function analyzer output signal and the rms error of the autocorrelation estimator. *The three Eulerian velocity cross products can be disregarded.* Consequently, Eq. (3.38) or its axial component given by Eq. (6.39) supply an acceptable approximation for the Lagrangian autocorrelation.

REFERENCE

A.III.1. Magrab, E.B. and Bloomquist, D.S., The Measurement of Time-Varying Phenomena: Fundamentals and Applications, Wiley-Interscience, New York, N.Y., 1971.

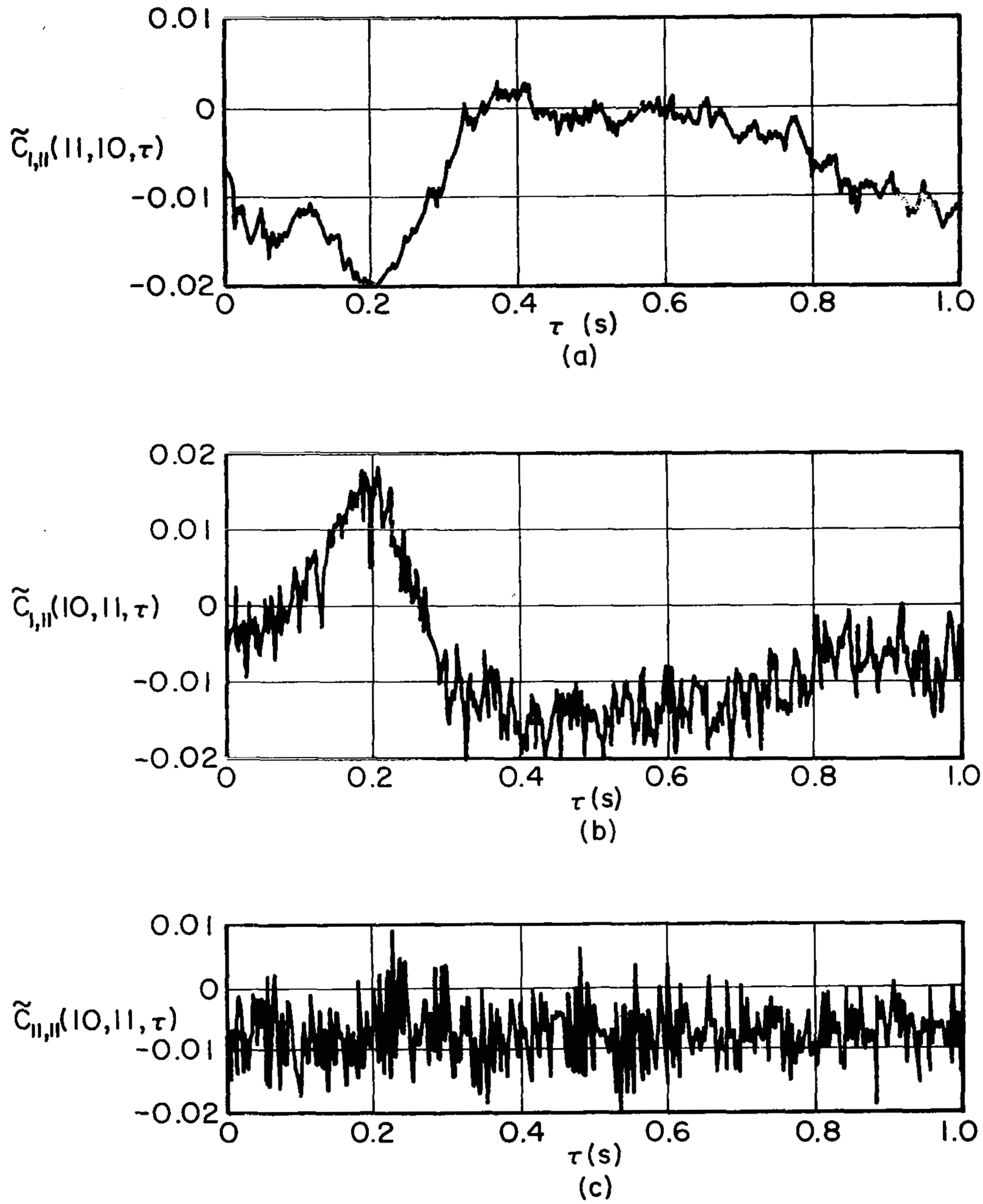

Fig. A.III.1 Variation with increasing time delay for an axial separation $\tilde{\xi} = 1$ of: (a) and (b) the velocity-velocity derivative cross-correlation coefficients; and, (c) the double velocity derivative cross-correlation coefficient.

APPENDIX IV

DATA TABLES

1. Eulerian autocorrelation coefficient

The five Eulerian autocorrelation coefficients data are summarized in Table A.IV.1. These Eulerian autocorrelations were obtained simultaneously at five stations on the turbulence line as described in Sect. 6.3 and their computation is outlined in Sect. 5.5. Variation of the set of five Eulerian autocorrelation coefficients with increasing time delay τ is portrayed in Fig. 6.13. The Eulerian autocorrelation coefficient is defined by Eq. (6.22)

$$\tilde{R}(\tau) = \overline{u(t)u(t+\tau)}/\overline{u^2},$$

where the total turbulent kinetic energy is $\overline{u^2} = R(0)$. In Table A.IV.1 the variation of the Eulerian autocorrelation coefficient at each station on the turbulence line with augmenting time displacement τ is tabulated.

The dimensionless axial position is defined by Eq. (6.1)

$$\tilde{x} = x/R,$$

where $R = 1.52$ m (5ft/s). The total turbulent kinetic energy at each station on the turbulence line is summarized below:

$\tilde{x}$	10	11	12	13	14
$\overline{u^2}$ (m^2/s^2)	6.25	1.81	1.35	1.67	1.97
$\overline{u^2}$ (ft^2/s^2)	67.2	19.5	14.5	18.0	21.2

Variation of the dimensionless mean-square value of the fluctuating velocity $\overline{\tilde{u}^2}$ along the turbulence line is shown in Fig. 6.3 and its computation is presented in Sect. 6.1.2.

TABLE A.IV.1

EULERIAN AUTOCORRELATION COEFFICIENT

$\tilde{x}$	10	11	12	13	14	$\tilde{x}$	10	11	12	13	14
τ (s)	$\tilde{R}$	$\tilde{R}$	$\tilde{R}$	$\tilde{R}$	$\tilde{R}$	τ (s)	$\tilde{R}$	$\tilde{R}$	$\tilde{R}$	$\tilde{R}$	$\tilde{R}$
0.000	1.000	1.000	1.000	1.000	1.000	.140	.091	.304	.349	.404	.419
.002	.926	.965	.977	.970	.985	.142	.087	.301	.346	.403	.419
.004	.870	.940	.952	.948	.963	.144	.087	.296	.341	.393	.407
.006	.824	.913	.931	.928	.943	.146	.082	.291	.336	.387	.401
.008	.782	.891	.912	.910	.925	.148	.077	.286	.336	.384	.397
.010	.791	.867	.893	.896	.903	.150	.077	.279	.332	.381	.391
.012	.745	.853	.876	.879	.885	.152	.077	.272	.328	.382	.387
.014	.689	.836	.859	.863	.873	.154	.077	.268	.323	.375	.382
.016	.666	.825	.842	.850	.856	.156	.073	.264	.315	.372	.377
.018	.638	.809	.826	.837	.841	.158	.073	.260	.312	.370	.379
.020	.620	.793	.815	.821	.836	.160	.068	.254	.306	.362	.371
.022	.592	.779	.802	.810	.822	.162	.063	.248	.302	.358	.367
.024	.578	.763	.785	.796	.807	.164	.059	.241	.299	.355	.364
.026	.555	.752	.772	.785	.798	.166	.059	.236	.296	.351	.360
.028	.536	.736	.756	.773	.786	.168	.059	.231	.292	.345	.361
.030	.527	.728	.744	.764	.775	.170	.050	.228	.290	.346	.349
.032	.504	.714	.733	.755	.766	.172	.045	.223	.288	.345	.346
.034	.495	.700	.724	.748	.759	.174	.040	.218	.283	.339	.342
.036	.476	.687	.712	.742	.755	.176	.036	.213	.277	.341	.336
.038	.462	.677	.703	.735	.742	.178	.036	.209	.274	.332	.332
.040	.448	.666	.693	.724	.731	.180	.040	.207	.271	.328	.331
.042	.434	.655	.684	.713	.725	.182	.031	.203	.266	.322	.324
.044	.411	.643	.673	.701	.713	.184	.031	.201	.263	.316	.320
.046	.402	.639	.662	.693	.706	.186	.036	.198	.262	.314	.321
.048	.397	.628	.652	.684	.696	.188	.031	.193	.255	.307	.308
.050	.388	.612	.640	.680	.691	.190	.026	.191	.249	.301	.302
.052	.370	.603	.632	.666	.677	.192	.013	.186	.252	.298	.302
.054	.360	.593	.621	.658	.670	.194	.026	.186	.252	.295	.302
.056	.356	.587	.611	.651	.660	.196	.003	.185	.252	.290	.302
.058	.374	.577	.604	.646	.653	.198	.003	.184	.245	.287	.302
.060	.374	.568	.594	.640	.646	.200	.003	.184	.245	.287	.302
.062	.319	.562	.588	.634	.638	.202	.003	.179	.235	.285	.302
.064	.309	.553	.581	.625	.632	.204	.003	.173	.228	.284	.299
.066	.305	.546	.574	.621	.627	.206	-.001	.170	.224	.281	.296
.068	.295	.535	.568	.617	.619	.208	-.001	.164	.221	.281	.291
.070	.300	.524	.557	.611	.614	.210	-.001	.159	.217	.282	.285
.072	.277	.513	.554	.601	.607	.212	-.006	.160	.217	.273	.284
.074	.272	.508	.541	.596	.601	.214	-.006	.160	.215	.269	.283
.076	.263	.496	.536	.587	.595	.216	-.006	.153	.210	.266	.277
.078	.258	.486	.528	.582	.585	.218	-.006	.153	.205	.265	.271
.080	.249	.475	.518	.576	.577	.220	-.015	.148	.200	.262	.266
.082	.254	.471	.510	.568	.573	.222	-.015	.143	.195	.259	.261
.084	.230	.467	.504	.558	.569	.224	-.020	.140	.192	.255	.258
.086	.226	.460	.498	.558	.570	.226	-.020	.136	.189	.251	.260
.088	.221	.451	.489	.552	.559	.228	-.025	.131	.188	.245	.256
.090	.216	.443	.481	.549	.549	.230	-.020	.125	.187	.240	.251
.092	212	.437	.474	.538	.543	.232	-.015	.120	.184	.240	.248
.094	.203	.431	.465	.530	.538	.234	-.020	.121	.180	.237	.245
.096	.198	.427	.458	.524	.532	.236	-.020	.121	.176	.232	.243
.098	.184	.424	.451	.520	.527	.238	-.020	.113	.171	.234	.243
.100	.179	.418	.442	.512	.519	.240	-.020	.115	.169	.226	.237
.102	.175	.414	.443	.505	.514	.242	-.020	.111	.164	.228	.233
.104	.165	.411	.429	.501	.511	.244	-.025	.112	.161	.221	.232
.106	.161	.401	.425	.492	.504	.246	-.025	.114	.159	.219	.232
.108	.156	.393	.419	.488	.497	.248	-.025	.112	.157	.213	.229
.110	.161	.386	.416	.482	.486	.250	-.020	.112	.154	.213	.226
.112	.161	.379	.407	.475	.489	.252	-.025	.106	.149	.208	.221
.114	.138	.374	.402	.469	.483	.254	-.025	.098	.147	.208	.220
.116	.138	.370	.402	.465	.475	.256	-.025	.099	.146	.204	.215
.118	.138	.365	.398	.458	.473	.258	-.025	.099	.148	.201	.214
.120	.133	.360	.394	.457	.463	.260	-.025	.092	.148	.197	.217
.122	.128	.356	.390	.452	.466	.262	-.025	.091	.148	.194	.210
.124	.124	.351	.384	.444	.457	.264	-.038	.089	.150	.191	.204
.126	.124	.343	.382	.440	.453	.266	-.048	.086	.141	.192	.205
.128	.142	.337	.378	.432	.452	.268	-.038	.084	.136	.195	.198
.130	.142	.338	.375	.426	.446	.270	-.038	.079	.135	.190	.199
.132	.142	.333	.373	.422	.440	.272	-.038	.075	.131	.186	.193
.134	.142	.323	.366	.419	.428	.274	-.038	.075	.133	.186	.191
.136	.110	.318	.360	.417	.428	.276	-.038	.074	.133	.180	.193
.138	.091	.309	.351	.408	.425	.278	-.043	.070	.128	.173	.189
.140	.091	.304	.349	.404	.419	.280	-.043	.067	.129	.173	.187

TABLE A.IV.1 (CONTINUED)

$\tilde{x}$	10	11	12	13	14	$\tilde{x}$	10	11	12	13	14
τ (s)	$\tilde{R}$	$\tilde{R}$	$\tilde{R}$	$\tilde{R}$	$\tilde{R}$	τ (s)	$\tilde{R}$	$\tilde{R}$	$\tilde{R}$	$\tilde{R}$	$\tilde{R}$
.280	-.043	.067	.129	.173	.187	.420	-.043	-.059	-.014	.049	.042
.282	-.043	.065	.126	.170	.184	.422	-.048	-.065	-.012	.048	.035
.284	-.048	.062	.123	.167	.181	.424	-.048	-.068	-.016	.042	.034
.286	-.043	.061	.122	.168	.182	.426	-.048	-.071	-.017	.042	.029
.288	-.043	.059	.120	.167	.182	.428	-.043	-.067	-.019	.046	.028
.290	-.043	.054	.119	.162	.182	.430	-.048	-.066	-.022	.042	.027
.292	-.043	.052	.119	.160	.171	.432	-.048	-.068	-.022	.045	.025
.294	-.038	.045	.116	.158	.170	.434	-.043	-.068	-.022	.047	.022
.296	-.048	.046	.113	.153	.170	.436	-.048	-.066	-.019	.046	.023
.298	-.038	.047	.112	.148	.170	.438	-.048	-.068	-.017	.042	.023
.300	-.048	.046	.112	.144	.173	.440	-.048	-.070	-.019	.037	.016
.302	-.038	.047	.106	.144	.164	.442	-.048	-.071	-.026	.033	.018
.304	-.043	.047	.100	.138	.163	.444	-.048	-.068	-.024	.033	.018
.306	-.048	.047	.097	.139	.163	.446	-.048	-.066	-.031	.030	.018
.308	-.048	.047	.095	.137	.162	.448	-.038	-.065	-.025	.028	.017
.310	-.048	.046	.091	.132	.156	.450	-.034	-.067	-.025	.025	.012
.312	-.048	.041	.090	.128	.157	.452	-.038	-.074	-.028	.025	.007
.314	-.052	.038	.088	.130	.156	.454	-.038	-.073	-.030	.024	.006
.316	-.052	.037	.083	.131	.151	.456	-.038	-.072	-.031	.024	.005
.318	-.052	.031	.079	.129	.146	.458	-.034	-.072	-.030	.027	.007
.320	-.052	.030	.078	.124	.145	.460	-.034	-.075	-.027	.020	.006
.322	-.057	.031	.073	.120	.142	.462	-.038	-.077	-.025	.022	.006
.324	-.057	.027	.070	.119	.138	.464	-.038	-.083	-.029	.021	.003
.326	-.057	.025	.071	.120	.137	.466	-.043	-.083	-.037	.023	.001
.328	-.057	.017	.067	.116	.133	.468	-.038	-.079	-.033	.021	-.005
.330	-.057	.018	.066	.112	.129	.470	-.038	-.082	-.034	.021	-.013
.332	-.057	.012	.065	.109	.127	.472	-.034	-.084	-.030	.022	-.006
.334	-.057	.013	.061	.107	.124	.474	-.038	-.084	-.030	.023	-.005
.336	-.057	.012	.058	.109	.123	.476	-.038	-.085	-.034	.019	-.006
.338	-.057	.007	.056	.099	.123	.478	-.038	-.084	-.033	.017	-.009
.340	-.057	.004	.058	.100	.119	.480	-.038	-.091	-.034	.008	-.012
.342	-.057	-.002	.054	.099	.116	.482	-.038	-.090	-.035	.007	-.015
.344	-.052	-.001	.054	.100	.115	.484	-.034	-.090	-.037	.005	-.017
.346	-.052	-.002	.051	.097	.111	.486	-.034	-.089	-.039	.006	-.021
.348	-.048	-.005	.049	.096	.112	.488	-.029	-.092	-.042	.007	-.022
.350	-.043	-.007	.042	.099	.105	.490	-.029	-.092	-.049	.006	-.023
.352	-.048	-.007	.036	.100	.107	.492	-.029	-.089	-.045	.010	-.026
.354	-.052	-.009	.033	.100	.100	.494	-.029	-.093	-.045	.004	-.027
.356	-.048	-.010	.028	.096	.098	.496	-.029	-.092	-.044	.004	-.032
.358	-.048	-.010	.025	.095	.094	.498	-.029	-.092	-.045	0.000	-.034
.360	-.043	-.015	.021	.095	.092	.500	-.025	-.095	-.046	-.001	-.034
.362	-.043	-.019	.020	.093	.093	.502	-.034	-.102	-.045	-.002	-.038
.364	-.043	-.027	.019	.089	.087	.504	-.034	-.106	-.048	-.010	-.039
.366	-.043	-.024	.016	.085	.089	.506	-.034	-.107	-.053	-.007	-.035
.368	-.048	-.025	.016	.087	.085	.508	-.038	-.104	-.054	-.009	-.035
.370	-.048	-.024	.015	.083	.083	.510	-.034	-.105	-.053	-.007	-.035
.372	-.052	-.026	.016	.083	.080	.512	-.034	-.110	-.054	-.008	-.038
.374	-.048	-.026	.016	.082	.076	.514	-.034	-.111	-.054	-.008	-.039
.376	-.048	-.027	.015	.083	.078	.516	-.029	-.114	-.052	-.006	-.045
.378	-.052	-.029	.012	.081	.074	.518	-.029	-.115	-.054	-.011	-.046
.380	-.052	-.031	.011	.077	.074	.520	-.025	-.116	-.056	-.011	-.047
.382	-.052	-.026	.010	.072	.071	.522	-.029	-.118	-.054	-.011	-.050
.384	-.052	-.030	.009	.072	.071	.524	-.029	-.121	-.056	-.013	-.050
.386	-.048	-.032	.008	.071	.070	.526	-.029	-.118	-.057	-.012	-.050
.388	-.048	-.044	.009	.064	.070	.528	-.029	-.118	-.059	-.012	-.049
.390	-.052	-.044	.008	.064	.060	.530	-.034	-.116	-.062	-.013	-.049
.392	-.048	-.043	.008	.065	.053	.532	-.034	-.118	-.063	-.013	-.049
.394	-.048	-.045	.006	.066	.053	.534	-.034	-.118	-.065	-.013	-.055
.396	-.043	-.048	.005	.064	.053	.536	-.034	-.116	-.065	-.011	-.054
.398	-.038	-.048	.005	.063	.053	.538	-.029	-.118	-.066	-.014	-.053
.400	-.038	-.048	.005	.063	.053	.540	-.034	-.116	-.065	-.014	-.058
.402	-.038	-.049	.002	.057	.053	.542	-.034	-.118	-.068	-.014	-.062
.404	-.038	-.049	-.001	.052	.054	.544	-.029	-.120	-.070	-.017	-.064
.406	-.038	-.054	-.004	.050	.046	.546	-.029	-.120	-.070	-.020	-.071
.408	-.043	-.054	-.006	.054	.047	.548	-.029	-.116	-.071	-.019	-.068
.410	-.038	-.053	-.008	.054	.046	.550	-.029	-.120	-.078	-.021	-.068
.412	-.043	-.051	-.008	.054	.042	.552	-.029	-.120	-.084	-.024	-.072
.414	-.043	-.051	-.011	.054	.040	.554	-.029	-.121	-.084	-.024	-.074
.416	-.043	-.055	-.008	.050	.042	.556	-.025	-.120	-.081	-.026	-.075
.418	-.048	-.057	-.007	.050	.044	.558	-.020	-.118	-.082	-.024	-.078
.420	-.043	-.059	-.014	.049	.042	.560	-.020	-.121	-.083	-.024	-.079

TABLE A.IV.1 (CONTINUED)

$\tilde{x}$	10	11	12	13	14	$\tilde{x}$	10	11	12	13	14
τ (s)	$\tilde{R}$	$\tilde{R}$	$\tilde{R}$	$\tilde{R}$	$\tilde{R}$	τ (s)	$\tilde{R}$	$\tilde{R}$	$\tilde{R}$	$\tilde{R}$	$\tilde{R}$
.560	-.020	-.121	-.083	-.024	-.079	.700	-.013	-.133	-.122	-.086	-.134
.562	-.025	-.120	-.082	-.026	-.080	.702	-.016	-.132	-.123	-.084	-.137
.564	-.025	-.123	-.081	-.030	-.078	.704	-.017	-.133	-.127	-.092	-.138
.566	-.025	-.127	-.081	-.036	-.079	.706	-.017	-.134	-.128	-.092	-.138
.568	-.025	-.127	-.081	-.032	-.080	.708	-.013	-.131	-.128	-.090	-.138
.570	-.029	-.127	-.081	-.039	-.084	.710	-.012	-.131	-.128	-.089	-.146
.572	-.029	-.128	-.083	-.039	-.084	.712	-.017	-.126	-.128	-.091	-.146
.574	-.025	-.128	-.083	-.036	-.084	.714	-.017	-.125	-.130	-.090	-.146
.576	-.029	-.132	-.083	-.038	-.087	.716	-.013	-.126	-.130	-.093	-.145
.578	-.029	-.131	-.083	-.038	-.087	.718	-.016	-.125	-.130	-.092	-.145
.580	-.006	-.132	-.087	-.042	-.094	.720	-.015	-.127	-.127	-.091	-.145
.582	-.020	-.135	-.091	-.042	-.093	.722	-.011	-.134	-.127	-.094	-.145
.584	-.020	-.138	-.091	-.042	-.093	.724	-.011	-.131	-.130	-.095	-.145
.586	-.025	-.134	-.087	-.039	-.092	.726	-.007	-.127	-.131	-.090	-.148
.588	-.025	-.141	-.092	-.043	-.093	.728	-.006	-.125	-.130	-.095	-.148
.590	-.029	-.135	-.094	-.046	-.097	.730	-.008	-.124	-.134	-.098	-.149
.592	-.029	-.132	-.095	-.048	-.098	.732	-.012	-.125	-.138	-.101	-.147
.594	-.025	-.129	-.095	-.043	-.098	.734	-.012	-.121	-.139	-.098	-.148
.596	-.025	-.128	-.098	-.043	-.098	.736	-.008	-.120	-.135	-.095	-.147
.598	-.025	-.129	-.098	-.048	-.098	.738	-.013	-.122	-.138	-.096	-.148
.600	-.025	-.129	-.098	-.048	-.098	.740	-.012	-.119	-.135	-.092	-.148
.602	-.025	-.132	-.098	-.050	-.098	.742	-.013	-.121	-.133	-.090	-.148
.604	-.026	-.132	-.099	-.050	-.103	.744	-.013	-.121	-.133	-.088	-.148
.606	-.025	-.133	-.102	-.050	-.103	.746	-.013	-.122	-.134	-.084	-.148
.608	-.026	-.133	-.098	-.054	-.098	.748	-.012	-.121	-.133	-.084	-.147
.610	-.026	-.136	-.098	-.054	-.099	.750	-.013	-.119	-.135	-.091	-.144
.612	-.026	-.137	-.103	-.054	-.098	.752	-.015	-.119	-.135	-.086	-.148
.614	-.026	-.136	-.106	-.055	-.101	.754	-.018	-.115	-.135	-.083	-.143
.616	-.026	-.132	-.106	-.056	-.102	.756	-.022	-.114	-.142	-.080	-.142
.618	-.027	-.130	-.105	-.056	-.102	.758	-.021	-.119	-.138	-.080	-.144
.620	-.029	-.127	-.113	-.061	-.103	.760	-.020	-.116	-.138	-.084	-.145
.622	-.029	-.127	-.109	-.065	-.107	.762	-.022	-.114	-.140	-.084	-.145
.624	-.026	-.134	-.110	-.066	-.108	.764	-.013	-.113	-.141	-.084	-.144
.626	-.026	-.134	-.109	-.068	-.108	.766	-.013	-.114	-.141	-.084	-.145
.628	-.027	-.127	-.105	-.071	-.108	.768	-.008	-.114	-.142	-.084	-.144
.630	-.022	-.126	-.107	-.073	-.110	.770	-.008	-.111	-.138	-.086	-.145
.632	-.022	-.127	-.099	-.073	-.111	.772	-.013	-.109	-.141	-.089	-.145
.634	-.030	-.134	-.102	-.071	-.111	.774	-.018	-.110	-.138	-.089	-.147
.636	-.026	-.133	-.101	-.071	-.114	.776	-.018	-.110	-.135	-.089	-.148
.638	-.020	-.131	-.101	-.072	-.115	.778	-.017	-.109	-.133	-.083	-.149
.640	-.018	-.133	-.104	-.073	-.116	.780	-.018	-.109	-.133	-.086	-.150
.642	-.020	-.137	-.106	-.074	-.118	.782	-.017	-.109	-.136	-.086	-.153
.644	-.022	-.139	-.107	-.076	-.116	.784	-.012	-.104	-.138	-.093	-.155
.646	-.021	-.139	-.106	-.078	-.120	.786	-.012	-.104	-.136	-.086	-.151
.648	-.023	-.135	-.105	-.074	-.120	.788	-.016	-.104	-.139	-.090	-.150
.650	-.017	-.136	-.107	-.074	-.122	.790	-.020	-.106	-.135	-.086	-.151
.652	-.023	-.138	-.109	-.076	-.125	.792	-.020	-.100	-.135	-.083	-.149
.654	-.026	-.145	-.110	-.077	-.126	.794	-.016	-.100	-.142	-.083	-.149
.656	-.025	-.137	-.110	-.079	-.126	.796	-.016	-.099	-.141	-.083	-.149
.658	-.022	-.138	-.112	-.079	-.127	.798	-.013	-.099	-.144	-.083	-.149
.660	-.022	-.136	-.119	-.077	-.127	.800	-.013	-.099	-.144	-.083	-.146
.662	-.026	-.133	-.115	-.078	-.131	.802	-.011	-.100	-.144	-.083	-.146
.664	-.026	-.136	-.116	-.080	-.133	.804	-.014	-.100	-.145	-.084	-.145
.666	-.025	-.136	-.116	-.080	-.134	.806	-.021	-.101	-.144	-.083	-.146
.668	-.022	-.136	-.116	-.080	-.128	.808	-.020	-.100	-.146	-.084	-.146
.670	-.020	-.136	-.117	-.083	-.132	.810	-.016	-.101	-.144	-.084	-.146
.672	-.017	-.137	-.117	-.083	-.134	.812	-.010	-.100	-.144	-.079	-.153
.674	-.021	-.137	-.116	-.080	-.134	.814	-.013	-.104	-.144	-.080	-.149
.676	-.020	-.132	-.117	-.083	-.138	.816	-.015	-.101	-.140	-.079	-.149
.678	-.013	-.131	-.117	-.083	-.133	.818	-.018	-.101	-.137	-.083	-.149
.680	-.010	-.131	-.121	-.086	-.134	.820	-.019	-.104	-.136	-.080	-.144
.682	-.008	-.132	-.123	-.083	-.133	.822	-.018	-.105	-.137	-.083	-.145
.684	-.011	-.136	-.118	-.084	-.131	.824	-.019	-.105	-.138	-.083	-.144
.686	-.010	-.138	-.112	-.079	-.131	.826	-.018	-.106	-.139	-.084	-.141
.688	-.006	-.135	-.119	-.080	-.132	.828	-.020	-.105	-.138	-.079	-.142
.690	-.009	-.138	-.116	-.083	-.132	.830	-.025	-.104	-.139	-.079	-.138
.692	-.012	-.139	-.117	-.086	-.132	.832	-.021	-.101	-.140	-.076	-.138
.694	-.013	-.138	-.118	-.084	-.134	.834	-.016	-.104	-.137	-.077	-.139
.696	-.011	-.132	-.117	-.087	-.134	.836	-.018	-.103	-.137	-.077	-.138
.698	-.007	-.131	-.119	-.085	-.133	.838	-.018	-.106	-.143	-.074	-.139
.700	-.013	-.133	-.122	-.086	-.134	.840	-.017	-.107	-.145	-.074	-.137

TABLE A.IV.1 (CONTINUED)

$\tilde{x}$	10	11	12	13	14	$\tilde{x}$	10	11	12	13	14
τ (s)	$\tilde{R}$	$\tilde{R}$	$\tilde{R}$	$\tilde{R}$	$\tilde{R}$	τ (s)	$\tilde{R}$	$\tilde{R}$	$\tilde{R}$	$\tilde{R}$	$\tilde{R}$
.840	-.017	-.107	-.145	-.074	-.137	.980	-.021	-.076	-.116	-.086	-.138
.842	-.013	-.109	-.145	-.081	-.135	.982	-.021	-.077	-.116	-.085	-.138
.844	-.011	-.110	-.146	-.081	-.133	.984	-.018	-.076	-.123	-.088	-.138
.846	-.017	-.112	-.146	-.081	-.133	.986	-.015	-.072	-.117	-.086	-.138
.848	-.018	-.119	-.138	-.074	-.133	.988	-.015	-.070	-.117	-.093	-.134
.850	-.020	-.115	-.138	-.073	-.134	.990	-.016	-.071	-.116	-.090	-.139
.852	-.019	-.114	-.139	-.072	-.135	.992	-.021	-.067	-.117	-.085	-.137
.854	-.019	-.111	-.144	-.072	-.135	.994	-.022	-.065	-.119	-.084	-.137
.856	-.019	-.111	-.148	-.072	-.134	.996	-.024	-.062	-.116	-.089	-.137
.858	-.019	-.111	-.148	-.072	-.139	.998	-.021	-.062	-.115	-.089	-.138
.860	-.020	-.112	-.145	-.072	-.143	1.000	-.021	-.062	-.115	-.089	-.138
.862	-.020	-.109	-.148	-.071	-.139	1.002	-.022	-.063	-.117	-.090	-.138
.864	-.015	-.111	-.148	-.073	-.143	1.004	-.018	-.065	-.117	-.089	-.139
.866	-.019	-.107	-.151	-.074	-.143	1.006	-.016	-.062	-.112	-.090	-.134
.868	-.016	-.105	-.150	-.076	-.140	1.008	-.022	-.062	-.110	-.087	-.132
.870	-.015	-.106	-.150	-.083	-.141	1.010	-.023	-.063	-.109	-.086	-.131
.872	-.021	-.101	-.150	-.080	-.141	1.012	-.024	-.057	-.110	-.087	-.128
.874	-.019	-.100	-.152	-.085	-.141	1.014	-.018	-.059	-.110	-.083	-.126
.876	-.020	-.101	-.152	-.084	-.138	1.016	-.020	-.063	-.110	-.084	-.127
.878	-.024	-.101	-.149	-.084	-.137	1.018	-.016	-.061	-.110	-.087	-.128
.880	-.024	-.105	-.149	-.084	-.138	1.020	-.022	-.062	-.111	-.090	-.127
.882	-.025	-.110	-.149	-.086	-.137	1.022	-.022	-.062	-.113	-.090	-.136
.884	-.018	-.109	-.145	-.086	-.138	1.024	-.020	-.061	-.106	-.092	-.131
.886	-.013	-.105	-.145	-.083	-.135	1.026	-.022	-.061	-.106	-.092	-.135
.888	-.013	-.113	-.146	-.083	-.134	1.028	-.023	-.063	-.107	-.093	-.135
.890	-.011	-.113	-.141	-.080	-.128	1.030	-.026	-.062	-.110	-.092	-.134
.892	-.007	-.100	-.139	-.083	-.128	1.032	-.027	-.057	-.109	-.090	-.134
.894	-.013	-.101	-.139	-.085	-.131	1.034	-.033	-.057	-.110	-.090	-.131
.896	-.011	-.104	-.146	-.083	-.132	1.036	-.033	-.056	-.107	-.091	-.131
.898	-.010	-.104	-.146	-.079	-.128	1.038	-.030	-.056	-.110	-.089	-.133
.900	-.012	-.105	-.142	-.083	-.127	1.040	-.025	-.053	-.109	-.090	-.134
.902	-.014	-.100	-.139	-.083	-.128	1.042	-.027	-.054	-.106	-.089	-.141
.904	-.024	-.101	-.138	-.086	-.126	1.044	-.027	-.052	-.107	-.090	-.139
.906	-.024	-.100	-.146	-.085	-.126	1.046	-.026	-.055	-.110	-.087	-.137
.908	-.025	-.099	-.146	-.077	-.127	1.048	-.028	-.048	-.106	-.090	-.133
.910	-.024	-.098	-.138	-.074	-.129	1.050	-.025	-.046	-.104	-.084	-.133
.912	-.024	-.095	-.136	-.081	-.131	1.052	-.021	-.048	-.103	-.084	-.133
.914	-.025	-.096	-.136	-.079	-.133	1.054	-.017	-.048	-.104	-.084	-.134
.916	-.020	-.091	-.137	-.080	-.134	1.056	-.017	-.049	-.103	-.083	-.133
.918	-.021	-.089	-.134	-.087	-.133	1.058	-.017	-.042	-.104	-.084	-.135
.920	-.014	-.089	-.134	-.084	-.133	1.060	-.019	-.041	-.104	-.086	-.139
.922	-.011	-.089	-.133	-.084	-.136	1.062	-.019	-.041	-.098	-.093	-.138
.924	-.018	-.088	-.132	-.086	-.128	1.064	-.024	-.046	-.095	-.092	-.137
.926	-.024	-.087	-.131	-.080	-.127	1.066	-.024	-.040	-.095	-.089	-.134
.928	-.024	-.087	-.128	-.082	-.128	1.068	-.021	-.041	-.099	-.086	-.136
.930	-.024	-.084	-.126	-.083	-.127	1.070	-.020	-.041	-.098	-.089	-.136
.932	-.020	-.087	-.125	-.083	-.128	1.072	-.016	-.036	-.094	-.089	-.129
.934	-.018	-.084	-.127	-.083	-.134	1.074	-.013	-.034	-.095	-.092	-.132
.936	-.020	-.083	-.126	-.083	-.134	1.076	-.012	-.034	-.094	-.092	-.128
.938	-.023	-.085	-.127	-.090	-.134	1.078	-.007	-.028	-.096	-.086	-.130
.940	-.018	-.079	-.130	-.088	-.134	1.080	-.008	-.030	-.095	-.087	-.127
.942	-.018	-.077	-.127	-.089	-.137	1.082	-.009	-.032	-.098	-.086	-.129
.944	-.018	-.077	-.128	-.089	-.138	1.084	-.014	-.029	-.098	-.086	-.132
.946	-.019	-.077	-.128	-.085	-.139	1.086	-.007	-.029	-.095	-.083	-.133
.948	-.018	-.077	-.126	-.083	-.139	1.088	-.011	-.029	-.093	-.084	-.133
.950	-.017	-.078	-.125	-.084	-.139	1.090	-.013	-.031	-.089	-.080	-.129
.952	-.015	-.077	-.125	-.084	-.140	1.092	-.013	-.031	-.086	-.079	-.128
.954	-.013	-.076	-.125	-.080	-.140	1.094	-.013	-.038	-.088	-.080	-.128
.956	-.017	-.079	-.121	-.080	-.141	1.096	-.010	-.030	-.087	-.080	-.131
.958	-.018	-.079	-.120	-.080	-.140	1.098	-.003	-.032	-.089	-.083	-.131
.960	-.019	-.079	-.121	-.084	-.139	1.100	-.005	-.032	-.087	-.079	-.128
.962	-.022	-.077	-.121	-.083	-.139	1.102	-.002	-.031	-.087	-.077	-.132
.964	-.019	-.076	-.123	-.084	-.141	1.104	-.007	-.038	-.089	-.078	-.133
.966	-.019	-.077	-.125	-.083	-.141	1.106	-.002	-.031	-.088	-.077	-.133
.968	-.025	-.079	-.125	-.083	-.140	1.108	-.002	-.025	-.087	-.074	-.136
.970	-.019	-.079	-.123	-.083	-.139	1.110	-.002	-.025	-.087	-.074	-.131
.972	-.020	-.080	-.122	-.084	-.140	1.112	0.000	-.025	-.085	-.077	-.132
.974	-.018	-.080	-.121	-.084	-.139	1.114	-.002	-.025	-.087	-.080	-.127
.976	-.020	-.077	-.123	-.087	-.139	1.116	.002	-.022	-.087	-.080	-.127
.978	-.021	-.076	-.117	-.084	-.139	1.118	-.004	-.024	-.086	-.080	-.127
.980	-.021	-.076	-.116	-.086	-.138	1.120	-.001	-.027	-.086	-.080	-.128

TABLE A.IV.1 (CONTINUED)

$\tilde{x}$	10	11	12	13	14
τ (s)	$\tilde{R}$	$\tilde{R}$	$\tilde{R}$	$\tilde{R}$	$\tilde{R}$
1.120	-.001	-.027	-.086	-.080	-.128
1.122	.003	-.019	-.087	-.079	-.128
1.124	.001	-.019	-.087	-.082	-.130
1.126	.005	-.014	-.087	-.073	-.126
1.128	.003	-.012	-.083	-.074	-.123
1.130	.005	-.009	-.090	-.072	-.124
1.132	.006	-.010	-.083	-.071	-.117
1.134	.005	-.012	-.080	-.068	-.120
1.136	.004	-.009	-.078	-.065	-.116
1.138	.001	-.012	-.083	-.071	-.115
1.140	-.001	-.006	-.081	-.069	-.112
1.142	-.002	-.004	-.077	-.072	-.109
1.144	-.007	-.007	-.078	-.074	-.112
1.146	-.004	-.004	-.078	-.071	-.117
1.148	-.004	-.002	-.071	-.067	-.116
1.150	-.004	-.007	-.078	-.068	-.114
1.152	-.003	-.008	-.072	-.072	-.116
1.154	-.004	-.008	-.071	-.072	-.116
1.156	-.008	-.008	-.072	-.077	-.115
1.158	-.009	-.009	-.075	-.079	-.110
1.160	-.019	-.016	-.070	-.079	-.108
1.162	-.019	-.015	-.069	-.077	-.105
1.164	-.018	-.014	-.069	-.077	-.103
1.166	-.013	-.015	-.070	-.078	-.103
1.168	-.013	-.015	-.073	-.077	-.100
1.170	-.011	-.015	-.073	-.079	-.098
1.172	-.012	-.015	-.073	-.075	-.098
1.174	-.007	-.017	-.067	-.078	-.100
1.176	-.008	-.018	-.060	-.080	-.103
1.178	-.007	-.015	-.067	-.077	-.100
1.180	-.003	-.012	-.063	-.079	-.094
1.182	-.010	-.012	-.065	-.079	-.097
1.184	-.007	-.009	-.063	-.077	-.098
1.186	-.003	-.004	-.063	-.074	-.101
1.188	-.002	-.008	-.064	-.077	-.093
1.190	-.004	-.008	-.067	-.081	-.097
1.192	-.007	-.004	-.059	-.077	-.097
1.194	-.005	-.003	-.059	-.072	-.097
1.196	-.009	-.006	-.063	-.074	-.097
1.198	-.012	-.006	-.058	-.079	-.097
1.200	-.012	-.006	-.058	-.079	-.097
1.202	-.008	-.005	-.058	-.083	-.096
1.204	-.007	-.003	-.055	-.080	-.095
1.206	-.008	-.006	-.054	-.080	-.096
1.208	-.009	-.004	-.054	-.081	-.098
1.210	-.008	-.001	-.058	-.084	-.099
1.212	-.014	.001	-.057	-.080	-.099
1.214	-.014	.001	-.054	-.078	-.098
1.216	-.007	-.002	-.052	-.078	-.097
1.218	-.009	-.002	-.054	-.077	-.097
1.220	-.007	.005	-.054	-.079	-.093
1.222	-.007	.005	-.055	-.075	-.100
1.224	-.007	.002	-.059	-.078	-.095
1.226	-.008	.002	-.060	-.080	-.093
1.228	-.009	.001	-.060	-.080	-.092
1.230	-.013	.002	-.059	-.075	-.092
1.232	-.013	.002	-.061	-.078	-.090
1.234	-.013	.001	-.058	-.078	-.087
1.236	-.017	-.001	-.059	-.074	-.094
1.238	-.016	-.001	-.059	-.073	-.091
1.240	-.013	0.000	-.058	-.073	-.093
1.242	-.009	.001	-.058	-.075	-.092
1.244	-.011	0.000	-.058	-.073	-.095
1.246	-.012	.001	-.055	-.073	-.095
1.248	-.016	-.001	-.058	-.071	-.096
1.250	-.015	-.005	-.058	-.074	-.092
1.252	-.017	-.005	-.052	-.073	-.086
1.254	-.016	-.010	-.051	-.071	-.084
1.256	-.012	-.006	-.052	-.071	-.084
1.258	-.011	-.007	-.054	-.072	-.085
1.260	-.013	-.010	-.058	-.067	-.086

$\tilde{x}$	10	11	12	13	14
τ (s)	$\tilde{R}$	$\tilde{R}$	$\tilde{R}$	$\tilde{R}$	$\tilde{R}$
1.260	-.013	-.010	-.058	-.067	-.086
1.262	-.015	-.009	-.053	-.066	-.081
1.264	-.018	-.010	-.061	-.071	-.087
1.266	-.021	-.007	-.054	-.067	-.087
1.268	-.023	-.010	-.053	-.070	-.086
1.270	-.018	-.009	-.053	-.065	-.086
1.272	-.021	-.006	-.053	-.063	-.086
1.274	-.021	-.009	-.057	-.065	-.081
1.276	-.020	-.011	-.059	-.063	-.081
1.278	-.018	-.013	-.058	-.062	-.082
1.280	-.020	-.009	-.056	-.067	-.078
1.282	-.023	-.011	-.053	-.067	-.079
1.284	-.022	-.017	-.054	-.068	-.079
1.286	-.021	-.012	-.051	-.067	-.075
1.288	-.022	-.012	-.048	-.067	-.075
1.290	-.021	-.015	-.049	-.067	-.074
1.292	-.017	-.016	-.051	-.066	-.074
1.294	-.018	-.016	-.051	-.068	-.075
1.296	-.017	-.012	-.051	-.065	-.072
1.298	-.019	-.006	-.051	-.066	-.072
1.300	-.017	-.006	-.052	-.066	-.072
1.302	-.013	-.009	-.051	-.063	-.073
1.304	-.016	-.011	-.053	-.066	-.073
1.306	-.015	-.016	-.055	-.062	-.069
1.308	-.012	-.010	-.049	-.064	-.067
1.310	-.012	-.006	-.045	-.064	-.068
1.312	-.016	-.006	-.042	-.061	-.071
1.314	-.020	-.005	-.049	-.061	-.064
1.316	-.020	-.005	-.042	-.056	-.068
1.318	-.016	-.006	-.042	-.064	-.071
1.320	-.013	-.006	-.044	-.056	-.071
1.322	-.015	-.005	-.044	-.056	-.068
1.324	-.012	-.005	-.043	-.061	-.063
1.326	-.009	-.001	-.042	-.064	-.071
1.328	-.008	.001	-.042	-.062	-.067
1.330	-.014	0.000	-.042	-.070	-.066
1.332	-.013	0.000	-.037	-.068	-.067
1.334	-.015	.001	-.035	-.071	-.068
1.336	-.012	.002	-.033	-.071	-.064
1.338	-.018	-.005	-.034	-.079	-.063
1.340	-.018	0.000	-.031	-.074	-.061
1.342	-.017	-.003	-.030	-.073	-.058
1.344	-.023	-.010	-.030	-.074	-.058
1.346	-.027	-.006	-.031	-.072	-.056
1.348	-.023	-.007	-.031	-.073	-.052
1.350	-.021	-.010	-.035	-.075	-.052
1.352	-.026	-.009	-.034	-.069	-.052
1.354	-.032	-.004	-.029	-.067	-.049
1.356	-.027	-.004	-.028	-.075	-.049
1.358	-.025	-.003	-.024	-.068	-.050
1.360	-.020	-.006	-.024	-.068	-.049
1.362	-.021	-.007	-.022	-.068	-.044
1.364	-.017	-.005	-.023	-.067	-.040
1.366	-.023	-.001	-.020	-.067	-.039
1.368	-.023	-.005	-.017	-.068	-.039
1.370	-.022	-.006	-.016	-.068	-.041
1.372	-.021	-.006	-.013	-.067	-.041
1.374	-.020	-.013	-.011	-.067	-.040
1.376	-.020	-.011	-.008	-.067	-.043
1.378	-.018	-.018	-.008	-.070	-.045
1.380	-.017	-.016	-.007	-.061	-.048
1.382	-.013	-.016	-.008	-.064	-.046
1.384	-.011	-.017	-.010	-.057	-.046
1.386	-.008	-.016	-.006	-.055	-.045
1.388	-.012	-.016	-.008	-.056	-.040
1.390	-.013	-.018	-.008	-.055	-.041
1.392	-.012	-.015	-.006	-.055	-.044
1.394	-.015	-.016	-.005	-.050	-.044
1.396	-.013	-.016	-.006	-.058	-.044
1.398	-.013	-.003	-.006	-.055	-.044
1.400	-.013	-.003	-.006	-.055	-.044

TABLE A.IV.1 (CONTINUED)

$\tilde{x}$	10	11	12	13	14
τ (s)	$\tilde{R}$	$\tilde{R}$	$\tilde{R}$	$\tilde{R}$	$\tilde{R}$
1.400	-.013	-.003	-.006	-.055	-.044
1.402	-.016	-.005	-.006	-.055	-.044
1.404	-.015	-.008	-.003	-.052	-.045
1.406	-.018	-.004	-.004	-.050	-.050
1.408	-.021	-.004	-.007	-.050	-.049
1.410	-.024	-.024	-.013	-.051	-.052
1.412	-.020	-.021	-.013	-.051	-.052
1.414	-.021	-.018	-.016	-.060	-.047
1.416	-.024	-.016	-.009	-.056	-.048
1.418	-.025	-.013	-.012	-.055	-.045
1.420	-.028	-.006	-.013	-.053	-.045
1.422	-.023	-.006	-.012	-.055	-.048
1.424	-.023	-.005	-.012	-.056	-.043
1.426	-.020	-.003	-.009	-.052	-.045
1.428	-.018	-.004	-.008	-.052	-.049
1.430	-.015	-.005	-.012	-.050	-.050
1.432	-.015	-.004	-.012	-.052	-.048
1.434	-.015	-.005	-.012	-.052	-.048
1.436	-.018	-.006	-.011	-.049	-.048
1.438	-.018	.001	-.012	-.050	-.049
1.440	-.015	-.006	-.009	-.046	-.049
1.442	-.018	-.002	-.007	-.046	-.049
1.444	-.023	.001	-.006	-.044	-.048
1.446	-.021	-.001	-.006	-.044	-.045
1.448	-.018	.001	-.007	-.043	-.048
1.450	-.018	.001	-.004	-.040	-.044
1.452	-.020	.002	-.005	-.039	-.045
1.454	-.020	-.001	-.006	-.039	-.048
1.456	-.022	.006	-.004	-.039	-.048
1.458	-.023	.007	-.002	-.039	-.048
1.460	-.021	.006	-.004	-.043	-.049
1.462	-.020	-.001	-.001	-.044	-.049
1.464	-.022	.002	-.001	-.045	-.050
1.466	-.021	.002	-.004	-.048	-.048
1.468	-.016	-.006	-.002	-.040	-.045
1.470	-.023	-.005	-.002	-.043	-.049
1.472	-.027	-.003	-.004	-.044	-.049
1.474	-.025	-.004	-.008	-.044	-.050
1.476	-.025	-.006	-.009	-.039	-.049
1.478	-.025	0.000	-.008	-.039	-.048
1.480	-.028	-.002	-.008	-.039	-.044
1.482	-.025	.001	-.010	-.039	-.044
1.484	-.027	.004	-.008	-.038	-.045
1.486	-.024	.007	-.008	-.038	-.045
1.488	-.020	.006	-.008	-.038	-.052
1.490	-.018	.006	-.006	-.040	-.052
1.492	-.015	.006	-.004	-.039	-.052
1.494	-.016	.001	-.008	-.035	-.047
1.496	-.015	0.000	-.007	-.033	-.044
1.498	-.016	.001	-.008	-.034	-.043
1.500	-.014	.001	-.007	-.035	-.046
1.502	-.013	-.001	-.006	-.033	-.045
1.504	-.016	.001	-.009	-.036	-.043
1.506	-.016	-.003	-.009	-.027	-.039
1.508	-.021	.001	-.008	-.027	-.042
1.510	-.020	.001	-.007	-.026	-.047
1.512	-.025	-.005	-.008	-.029	-.048
1.514	-.023	-.008	-.009	-.029	-.045
1.516	-.023	-.006	-.010	-.028	-.044
1.518	-.028	-.009	-.008	-.028	-.043
1.520	-.025	-.008	-.008	-.029	-.042
1.522	-.019	-.005	-.010	-.029	-.043
1.524	-.020	-.008	-.010	-.032	-.043
1.526	-.024	-.008	-.002	-.029	-.045
1.528	-.022	-.009	-.002	-.031	-.044
1.530	-.019	-.007	-.003	-.029	-.045
1.532	-.023	-.008	-.010	-.028	-.048
1.534	-.023	-.008	-.003	-.029	-.049
1.536	-.020	-.008	-.002	-.028	-.044
1.538	-.019	-.011	-.004	-.032	-.045
1.540	-.013	-.012	.004	-.028	-.044

$\tilde{x}$	10	11	12	13	14
τ (s)	$\tilde{R}$	$\tilde{R}$	$\tilde{R}$	$\tilde{R}$	$\tilde{R}$
1.540	-.013	-.012	.004	-.028	-.044
1.542	-.015	-.010	.006	-.027	-.044
1.544	-.014	-.007	.009	-.029	-.048
1.546	-.019	-.006	.009	-.027	-.048
1.548	-.019	-.005	.010	-.027	-.047
1.550	-.016	-.005	.008	-.027	-.047
1.552	-.021	-.004	.009	-.028	-.049
1.554	-.023	.001	.002	-.027	-.045
1.556	-.023	-.001	.004	-.027	-.043
1.558	-.023	.006	.002	-.027	-.043
1.560	-.025	.007	0.000	-.026	-.043
1.562	-.024	.006	.003	-.026	-.043
1.564	-.026	.006	.004	-.026	-.046
1.566	-.021	.006	0.000	-.026	-.043
1.568	-.018	.003	-.002	-.026	-.043
1.570	-.019	.001	-.002	-.026	-.043
1.572	-.020	.001	-.001	-.026	-.043
1.574	-.024	.001	-.001	-.023	-.042
1.576	-.019	.002	-.001	-.023	-.041
1.578	-.018	.007	.002	-.030	-.041
1.580	-.015	.009	.005	-.027	-.039
1.582	-.014	.007	.010	-.036	-.042
1.584	-.016	.007	.010	-.039	-.042
1.586	-.015	.008	.008	-.039	-.039
1.588	-.021	.008	.008	-.040	-.036
1.590	-.023	.013	.004	-.041	-.038
1.592	-.025	.017	.006	-.040	-.038
1.594	-.031	.017	.009	-.038	-.038
1.596	-.025	.019	.009	-.034	-.038
1.598	-.024	.021	.009	-.042	-.038
1.600	-.024	.021	.009	-.042	-.038
1.602	-.022	.021	.009	-.038	-.038
1.604	-.020	.023	.012	-.036	-.038
1.606	-.019	.023	.014	-.034	-.035
1.608	-.021	.024	.014	-.032	-.029
1.610	-.021	.024	.016	-.035	-.027
1.612	-.021	.017	.018	-.036	-.028
1.614	-.025	.018	.017	-.038	-.026
1.616	-.026	.018	.018	-.037	-.027
1.618	-.030	.021	.019	-.041	-.028
1.620	-.030	.023	.019	-.041	-.032
1.622	-.029	.021	.019	-.040	-.028
1.624	-.030	.021	.017	-.042	-.025
1.626	-.035	.021	.021	-.042	-.027
1.628	-.034	.018	.021	-.042	-.023
1.630	-.035	.015	.020	-.042	-.022
1.632	-.035	.018	.019	-.041	-.022
1.634	-.036	.012	.021	-.041	-.026
1.636	-.034	.015	.020	-.040	-.025
1.638	-.035	.014	.020	-.038	-.026
1.640	-.036	.006	.021	-.042	-.025
1.642	-.040	.008	.021	-.042	-.025
1.644	-.044	.007	.020	-.038	-.027
1.646	-.044	.008	.024	-.036	-.028
1.648	-.044	.007	.025	-.035	-.029
1.650	-.043	.007	.025	-.036	-.032
1.652	-.043	.009	.024	-.040	-.034
1.654	-.043	.010	.023	-.042	-.038
1.656	-.043	.010	.024	-.038	-.038
1.658	-.042	.011	.021	-.037	-.033
1.660	-.043	.010	.020	-.034	-.033
1.662	-.040	.013	.023	-.032	-.033
1.664	-.040	.007	.023	-.036	-.034
1.666	-.038	.007	.021	-.038	-.035
1.668	-.036	.012	.021	-.036	-.034
1.670	-.038	.010	.020	-.036	-.029
1.672	-.036	.010	.020	-.035	-.027
1.674	-.032	.010	.020	-.036	-.027
1.676	-.031	.012	.019	-.038	-.028
1.678	-.030	.018	.016	-.042	-.027
1.680	-.032	.018	.020	-.047	-.029

TABLE A.IV.1 (CONTINUED)

$\tilde{x}$	10	11	12	13	14	$\tilde{x}$	10	11	12	13	14
τ (s)	$\tilde{R}$	$\tilde{R}$	$\tilde{R}$	$\tilde{R}$	$\tilde{R}$	τ (s)	$\tilde{R}$	$\tilde{R}$	$\tilde{R}$	$\tilde{R}$	$\tilde{R}$
1.680	-.032	.018	.020	-.047	-.029	1.820	-.030	.017	.021	-.054	-.019
1.682	-.026	.018	.020	-.043	-.027	1.822	-.030	.016	.017	-.055	-.024
1.684	-.027	.016	.015	-.050	-.028	1.824	-.033	.015	.018	-.065	-.024
1.686	-.024	.016	.015	-.044	-.028	1.826	-.032	.016	.017	-.064	-.024
1.688	-.025	.015	.018	-.042	-.031	1.828	-.029	.017	.017	-.060	-.022
1.690	-.025	.015	.011	-.044	-.028	1.830	-.030	.015	.017	-.059	-.025
1.692	-.026	.015	.015	-.044	-.028	1.832	-.029	.015	.018	-.058	-.024
1.694	-.027	.015	.015	-.044	-.027	1.834	-.028	.016	.016	-.058	-.027
1.696	-.029	.014	.020	-.046	-.027	1.836	-.025	.017	.015	-.055	-.027
1.698	-.029	.013	.020	-.049	-.028	1.838	-.028	.019	.008	-.056	-.027
1.700	-.027	.014	.015	-.048	-.028	1.840	-.030	.016	.014	-.058	-.027
1.702	-.029	.019	.017	-.049	-.031	1.842	-.031	.015	.016	-.060	-.028
1.704	-.029	.015	.015	-.050	-.032	1.844	-.031	.015	.017	-.058	-.024
1.706	-.029	.018	.016	-.052	-.032	1.846	-.025	.014	.017	-.056	-.024
1.708	-.030	.017	.016	-.054	-.032	1.848	-.027	.010	.020	-.052	-.022
1.710	-.034	.021	.018	-.056	-.034	1.850	-.024	.010	.020	-.055	-.024
1.712	-.035	.021	.018	-.058	-.035	1.852	-.023	.012	.021	-.055	-.027
1.714	-.031	.024	.019	-.059	-.035	1.854	-.025	.006	.021	-.062	-.029
1.716	-.031	.021	.021	-.054	-.028	1.856	-.028	.005	.022	-.054	-.029
1.718	-.029	.022	.020	-.054	-.027	1.858	-.033	.003	.020	-.055	-.027
1.720	-.025	.025	.021	-.054	-.025	1.860	-.033	.003	.020	-.059	-.032
1.722	-.027	.025	.023	-.054	-.025	1.862	-.032	.004	.017	-.059	-.032
1.724	-.021	.021	.024	-.054	-.027	1.864	-.029	.003	.020	-.060	-.032
1.726	-.019	.025	.025	-.049	-.026	1.866	-.024	.005	.020	-.058	-.034
1.728	-.019	.024	.023	-.056	-.026	1.868	-.024	.002	.021	-.055	-.030
1.730	-.020	.023	.021	-.054	-.027	1.870	-.028	.002	.021	-.054	-.029
1.732	-.015	.025	.019	-.052	-.023	1.872	-.028	.009	.022	-.054	-.027
1.734	-.015	.023	.018	-.053	-.025	1.874	-.025	.010	.021	-.055	-.028
1.736	-.013	.023	.020	-.047	-.025	1.876	-.023	.003	.021	-.058	-.027
1.738	-.015	.017	.014	-.049	-.025	1.878	-.020	.005	.021	-.059	-.026
1.740	-.016	.023	.018	-.048	-.023	1.880	-.020	.005	.022	-.055	-.027
1.742	-.020	.029	.025	-.049	-.023	1.882	-.020	.004	.023	-.056	-.027
1.744	-.022	.029	.023	-.054	-.028	1.884	-.020	.003	.027	-.055	-.027
1.746	-.020	.026	.029	-.055	-.025	1.886	-.024	-.001	.027	-.054	-.029
1.748	-.015	.024	.029	-.055	-.025	1.888	-.023	.001	.026	-.052	-.027
1.750	-.015	.019	.029	-.054	-.023	1.890	-.019	.001	.023	-.052	-.026
1.752	-.016	.019	.031	-.054	-.023	1.892	-.019	-.001	.021	-.052	-.034
1.754	-.016	.020	.028	-.052	-.026	1.894	-.020	-.002	.019	-.054	-.030
1.756	-.017	.024	.035	-.048	-.026	1.896	-.016	0.000	.021	-.049	-.031
1.758	-.023	.018	.035	-.056	-.026	1.898	-.016	.001	.013	-.048	-.028
1.760	-.021	.012	.032	-.054	-.026	1.900	-.015	.003	.013	-.047	-.027
1.762	-.021	.019	.031	-.054	-.023	1.902	-.017	0.000	.014	-.046	-.030
1.764	-.018	.017	.030	-.055	-.026	1.904	-.018	-.002	.015	-.049	-.027
1.766	-.015	.017	.027	-.055	-.027	1.906	-.018	-.006	.017	-.053	-.025
1.768	-.012	.020	.026	-.059	-.029	1.908	-.023	-.001	.021	-.050	-.025
1.770	-.013	.019	.026	-.061	-.023	1.910	-.025	.003	.023	-.052	-.028
1.772	-.013	.018	.030	-.058	-.022	1.912	-.024	-.001	.026	-.052	-.025
1.774	-.013	.016	.027	-.058	-.023	1.914	-.019	-.009	.025	-.049	-.021
1.776	-.013	.016	.026	-.058	-.023	1.916	-.015	-.009	.027	-.056	-.026
1.778	-.013	.019	.024	-.059	-.025	1.918	-.018	-.006	.027	-.056	-.026
1.780	-.012	.015	.023	-.059	-.021	1.920	-.020	-.002	.025	-.054	-.025
1.782	-.010	.012	.019	-.059	-.029	1.922	-.019	-.003	.025	-.056	-.025
1.784	-.012	.013	.017	-.056	-.025	1.924	-.020	-.005	.025	-.060	-.022
1.786	-.012	.018	.020	-.054	-.023	1.926	-.016	-.005	.026	-.060	-.021
1.788	-.010	.018	.021	-.058	-.025	1.928	-.020	-.007	.021	-.060	-.021
1.790	-.011	.018	.020	-.055	-.027	1.930	-.023	-.007	.020	-.058	-.025
1.792	-.013	.021	.021	-.054	-.021	1.932	-.024	-.007	.021	-.058	-.025
1.794	-.013	.024	.024	-.052	-.021	1.934	-.028	-.007	.021	-.058	-.026
1.796	-.015	.023	.021	-.052	-.021	1.936	-.021	-.008	.017	-.055	-.021
1.798	-.015	.019	.024	-.055	-.021	1.938	-.025	-.013	.020	-.058	-.022
1.800	-.015	.019	.024	-.055	-.021	1.940	-.026	-.015	.021	-.054	-.026
1.802	-.016	.020	.026	-.062	-.021	1.942	-.020	-.007	.020	-.054	-.028
1.804	-.022	.017	.026	-.062	-.018	1.944	-.026	-.009	.013	-.054	-.022
1.806	-.023	.017	.021	-.056	-.018	1.946	-.028	-.002	.013	-.056	-.020
1.808	-.018	.017	.020	-.055	-.018	1.948	-.027	-.001	.016	-.056	-.021
1.810	-.018	.017	.019	-.056	-.019	1.950	-.032	-.002	.016	-.052	-.023
1.812	-.023	.016	.019	-.056	-.016	1.952	-.038	-.005	.016	-.052	-.021
1.814	-.025	.016	.022	-.059	-.015	1.954	-.034	-.002	.015	-.054	-.021
1.816	-.028	.017	.021	-.060	-.018	1.956	-.033	-.001	.015	-.054	-.021
1.818	-.032	.017	.020	-.059	-.019	1.958	-.034	-.001	.015	-.054	-.019
1.820	-.030	.017	.021	-.054	-.019	1.960	-.034	-.002	.016	-.055	-.020

TABLE A.IV.1 (CONTINUED)

$\tilde{x}$	10	11	12	13	14	$\tilde{x}$	10	11	12	13	14
τ (s)	$\tilde{R}$	$\tilde{R}$	$\tilde{R}$	$\tilde{R}$	$\tilde{R}$	τ (s)	$\tilde{R}$	$\tilde{R}$	$\tilde{R}$	$\tilde{R}$	$\tilde{R}$
1.960	-.034	-.002	.016	-.055	-.020	2.100	-.013	-.031	-.037	-.050	-.005
1.962	-.030	-.002	.015	-.052	-.018	2.102	-.013	-.026	-.035	-.050	-.006
1.964	-.032	-.005	.014	-.049	-.015	2.104	-.015	-.032	-.036	-.057	-.008
1.966	-.037	-.007	.014	-.048	-.016	2.106	-.014	-.030	-.040	-.050	-.008
1.968	-.038	-.006	.011	-.046	-.016	2.108	-.014	-.031	-.041	-.048	-.001
1.970	-.034	-.005	.012	-.048	-.015	2.110	-.013	-.031	-.040	-.048	-.004
1.972	-.030	-.002	.011	-.048	-.014	2.112	-.015	-.036	-.041	-.050	-.003
1.974	-.029	-.002	.011	-.049	-.015	2.114	-.019	-.033	-.042	-.054	.001
1.976	-.035	0.000	.012	-.049	-.019	2.116	-.022	-.030	-.042	-.047	-.008
1.978	-.035	0.000	.014	-.044	-.019	2.118	-.023	-.029	-.041	-.048	-.003
1.980	-.037	0.000	.011	-.043	-.014	2.120	-.025	-.026	-.040	-.048	-.001
1.982	-.039	0.000	.011	-.042	-.014	2.122	-.026	-.026	-.036	-.042	-.003
1.984	-.044	.005	.016	-.045	-.013	2.124	-.027	-.025	-.041	-.042	-.004
1.986	-.038	.006	.016	-.038	-.010	2.126	-.023	-.024	-.044	-.038	-.005
1.988	-.039	.004	.015	-.038	-.009	2.128	-.019	-.024	-.044	-.039	-.001
1.990	-.038	.005	.015	-.038	-.009	2.130	-.018	-.026	-.044	-.039	.001
1.992	-.035	.006	.016	-.038	-.010	2.132	-.018	-.025	-.044	-.037	.002
1.994	-.034	.005	.014	-.036	-.010	2.134	-.018	-.026	-.044	-.045	.001
1.996	-.035	.003	.012	-.040	-.010	2.136	-.018	-.022	-.037	-.043	.002
1.998	-.032	0.000	.010	-.042	-.010	2.138	-.018	-.027	-.044	-.048	.003
2.000	-.032	0.000	.010	-.042	-.010	2.140	-.018	-.028	-.040	-.042	0.000
2.002	-.028	-.003	.008	-.042	-.009	2.142	-.015	-.027	-.037	-.040	.002
2.004	-.026	-.005	.008	-.037	-.009	2.144	-.016	-.027	-.035	-.036	.005
2.006	-.026	-.003	.009	-.036	-.006	2.146	-.011	-.027	-.033	-.036	.005
2.008	-.027	-.003	.006	-.036	-.005	2.148	-.011	-.026	-.034	-.040	.006
2.010	-.024	-.003	.009	-.037	-.001	2.150	-.013	-.026	-.033	-.044	.006
2.012	-.027	-.003	.011	-.039	.001	2.152	-.014	-.029	-.031	-.044	-.002
2.014	-.032	-.008	.003	-.038	-.002	2.154	-.011	-.027	-.031	-.045	.005
2.016	-.032	-.010	.007	-.039	0.000	2.156	-.011	-.030	-.035	-.047	.005
2.018	-.029	-.011	.006	-.039	-.003	2.158	-.010	-.027	-.035	-.047	.006
2.020	-.032	-.014	.001	-.035	-.004	2.160	-.011	-.030	-.036	-.050	.005
2.022	-.030	-.011	.001	-.032	-.004	2.162	-.013	-.033	-.035	-.053	.005
2.024	-.028	-.016	-.001	-.039	-.004	2.164	-.014	-.037	-.035	-.054	-.002
2.026	-.028	-.016	-.001	-.039	-.009	2.166	-.011	-.038	-.036	-.053	.001
2.028	-.022	-.016	-.002	-.037	-.010	2.168	-.016	-.041	-.040	-.052	.001
2.030	-.020	-.015	-.005	-.038	-.010	2.170	-.010	-.044	-.039	-.054	-.001
2.032	-.020	-.023	-.005	-.036	-.005	2.172	-.006	-.038	-.037	-.048	0.000
2.034	-.020	-.023	-.005	-.041	-.004	2.174	-.004	-.045	-.037	-.048	0.000
2.036	-.019	-.024	-.005	-.043	-.004	2.176	-.002	-.045	-.034	-.048	-.001
2.038	-.018	-.026	-.008	-.043	-.001	2.178	-.007	-.041	-.029	-.049	-.005
2.040	-.019	-.022	-.011	-.046	.001	2.180	-.007	-.041	-.028	-.050	-.005
2.042	-.019	-.022	-.012	-.048	-.002	2.182	-.007	-.042	-.030	-.050	-.006
2.044	-.020	-.024	-.014	-.048	-.001	2.184	-.011	-.045	-.031	-.050	-.009
2.046	-.025	-.026	-.014	-.049	-.004	2.186	-.010	-.042	-.030	-.050	-.006
2.048	-.029	-.026	-.013	-.050	-.005	2.188	-.011	-.047	-.031	-.049	-.003
2.050	-.028	-.025	-.020	-.049	-.005	2.190	-.011	-.049	-.033	-.051	-.004
2.052	-.028	-.026	-.018	-.048	-.008	2.192	-.013	-.047	-.034	-.047	-.005
2.054	-.027	-.034	-.026	-.049	-.003	2.194	-.016	-.044	-.030	-.045	-.005
2.056	-.023	-.030	-.026	-.048	-.004	2.196	-.016	-.045	-.028	-.047	-.005
2.058	-.015	-.028	-.024	-.050	-.004	2.198	-.010	-.047	-.029	-.047	-.005
2.060	-.018	-.031	-.029	-.049	-.006	2.200	-.010	-.047	-.029	-.047	-.005
2.062	-.023	-.027	-.028	-.049	-.006	2.202	-.008	-.052	-.027	-.048	-.005
2.064	-.027	-.028	-.029	-.049	-.009	2.204	-.014	-.059	-.027	-.049	-.004
2.066	-.024	-.028	-.027	-.051	-.010	2.206	-.015	-.055	-.024	-.049	-.005
2.068	-.025	-.027	-.025	-.047	-.009	2.208	-.021	-.055	-.024	-.056	-.005
2.070	-.025	-.028	-.031	-.048	-.012	2.210	-.016	-.056	-.023	-.054	-.005
2.072	-.018	-.031	-.035	-.048	-.010	2.212	-.015	-.056	-.026	-.055	-.006
2.074	-.015	-.035	-.037	-.049	-.011	2.214	-.018	-.061	-.025	-.053	-.013
2.076	-.021	-.036	-.040	-.049	-.012	2.216	-.018	-.061	-.022	-.052	-.013
2.078	-.021	-.035	-.040	-.048	-.012	2.218	-.015	-.057	-.022	-.054	-.007
2.080	-.018	-.037	-.040	-.048	-.015	2.220	-.016	-.064	-.026	-.055	-.007
2.082	-.019	-.036	-.040	-.047	-.016	2.222	-.019	-.062	-.025	-.055	-.007
2.084	-.017	-.033	-.040	-.048	-.012	2.224	-.019	-.061	-.023	-.055	-.006
2.086	-.015	-.033	-.037	-.047	-.011	2.226	-.018	-.058	-.023	-.058	-.013
2.088	-.014	-.035	-.036	-.048	-.007	2.228	-.018	-.067	-.026	-.060	-.013
2.090	-.001	-.031	-.035	-.048	-.005	2.230	-.016	-.072	-.026	-.058	-.009
2.092	-.004	-.029	-.035	-.049	-.005	2.232	-.016	-.068	-.026	-.056	-.007
2.094	-.013	-.033	-.037	-.052	-.005	2.234	-.013	-.067	-.026	-.055	-.006
2.096	-.013	-.030	-.038	-.054	-.005	2.236	-.011	-.068	-.022	-.053	-.006
2.098	-.013	-.030	-.036	-.050	-.006	2.238	-.013	-.067	-.029	-.050	-.004
2.100	-.013	-.031	-.037	-.050	-.005	2.240	-.014	-.070	-.021	-.049	-.007

TABLE A.IV.1 (CONTINUED)

$\tilde{x}$	10	11	12	13	14
τ (s)	$\tilde{R}$	$\tilde{R}$	$\tilde{R}$	$\tilde{R}$	$\tilde{R}$
2.240	-.014	-.070	-.021	-.049	-.007
2.242	-.012	-.068	-.026	-.047	-.007
2.244	-.011	-.070	-.028	-.046	-.009
2.246	-.011	-.067	-.028	-.043	-.011
2.248	-.011	-.067	-.029	-.042	-.013
2.250	-.011	-.068	-.029	-.040	-.006
2.252	-.011	-.076	-.027	-.040	-.013
2.254	-.010	-.070	-.028	-.041	-.013
2.256	-.009	-.067	-.028	-.041	-.019
2.258	-.005	-.067	-.028	-.041	-.016
2.260	-.002	-.067	-.021	-.041	-.017
2.262	-.002	-.066	-.026	-.041	-.018
2.264	-.001	-.067	-.028	-.040	-.018
2.266	.002	-.067	-.028	-.037	-.018
2.268	0.000	-.064	-.029	-.037	-.017
2.270	.001	-.063	-.029	-.040	-.021
2.272	0.000	-.063	-.027	-.038	-.021
2.274	.001	-.062	-.028	-.040	-.021
2.276	.005	-.057	-.028	-.038	-.016
2.278	.004	-.057	-.028	-.037	-.017
2.280	-.001	-.062	-.026	-.037	-.018
2.282	-.004	-.063	-.025	-.037	-.018
2.284	-.006	-.064	-.023	-.034	-.021
2.286	-.007	-.063	-.023	-.029	-.018
2.288	-.006	-.062	-.026	-.026	-.025
2.290	-.005	-.063	-.026	-.026	-.022
2.292	-.005	-.064	-.026	-.028	-.021
2.294	-.005	-.067	-.026	-.032	-.023
2.296	-.007	-.062	-.022	-.032	-.023
2.298	-.009	-.058	-.029	-.031	-.018
2.300	-.006	-.062	-.029	-.031	-.018
2.302	-.005	-.062	-.027	-.032	-.018
2.304	-.007	-.066	-.027	-.039	-.023
2.306	-.012	-.067	-.024	-.034	-.025
2.308	-.005	-.067	-.024	-.031	-.025
2.310	-.004	-.066	-.023	-.032	-.021
2.312	-.004	-.068	-.026	-.037	-.021
2.314	-.002	-.068	-.025	-.034	-.016
2.316	-.001	-.067	-.022	-.031	-.017
2.318	-.002	-.068	-.022	-.034	-.018
2.320	-.006	-.063	-.021	-.032	-.018
2.322	-.009	-.068	-.021	-.035	-.017
2.324	-.009	-.073	-.021	-.036	-.017
2.326	-.007	-.068	-.021	-.039	-.017
2.328	-.007	-.068	-.020	-.034	-.017
2.330	-.007	-.068	-.020	-.035	-.017
2.332	-.011	-.066	-.020	-.036	-.018
2.334	-.017	-.062	-.021	-.036	-.017
2.336	-.015	-.062	-.019	-.030	-.021
2.338	-.016	-.064	-.026	-.035	-.017
2.340	-.018	-.062	-.026	-.032	-.016
2.342	-.015	-.062	-.026	-.035	-.017
2.344	-.013	-.061	-.028	-.035	-.018
2.346	-.011	-.058	-.027	-.032	-.017
2.348	-.005	-.058	-.027	-.039	-.018
2.350	-.007	-.058	-.035	-.034	-.018
2.352	-.009	-.055	-.034	-.035	-.017
2.354	-.011	-.055	-.033	-.032	-.017
2.356	-.010	-.055	-.034	-.033	-.018
2.358	-.005	-.053	-.041	-.030	-.018
2.360	-.004	-.056	-.040	-.039	-.025
2.362	-.007	-.058	-.046	-.032	-.025
2.364	-.011	-.056	-.046	-.039	-.023
2.366	-.011	-.056	-.040	-.038	-.023
2.368	-.012	-.055	-.041	-.032	-.021
2.370	-.011	-.053	-.041	-.031	-.018
2.372	-.010	-.055	-.032	-.029	-.025
2.374	-.012	-.057	-.031	-.030	-.018
2.376	-.011	-.057	-.031	-.039	-.018
2.378	-.017	-.056	-.032	-.031	-.025
2.380	-.017	-.056	-.034	-.035	-.023

$\tilde{x}$	10	11	12	13	14
τ (s)	$\tilde{R}$	$\tilde{R}$	$\tilde{R}$	$\tilde{R}$	$\tilde{R}$
2.380	-.017	-.056	-.034	-.035	-.023
2.382	-.016	-.057	-.034	-.034	-.022
2.384	-.015	-.056	-.036	-.035	-.023
2.386	-.016	-.053	-.032	-.035	-.022
2.388	-.011	-.055	-.032	-.034	-.024
2.390	-.014	-.056	-.034	-.036	-.024
2.392	-.018	-.056	-.036	-.034	-.024
2.394	-.010	-.057	-.034	-.031	-.024
2.396	-.012	-.058	-.036	-.036	-.024
2.398	-.013	-.047	-.034	-.035	-.024
2.400	-.013	-.047	-.034	-.035	-.027
2.402	-.018	-.047	-.034	-.036	-.026
2.404	-.020	-.048	-.034	-.036	-.028
2.406	-.019	-.048	-.034	-.036	-.030
2.408	-.023	-.048	-.041	-.031	-.030
2.410	-.023	-.048	-.037	-.028	-.029
2.412	-.024	-.049	-.037	-.028	-.029
2.414	-.023	-.043	-.037	-.028	-.036
2.416	-.019	-.043	-.037	-.031	-.028
2.418	-.019	-.041	-.034	-.034	-.027
2.420	-.019	-.042	-.034	-.035	-.028
2.422	-.019	-.041	-.037	-.036	-.029
2.424	-.019	-.041	-.034	-.043	-.024
2.426	-.016	-.049	-.037	-.041	-.024
2.428	-.016	-.042	-.032	-.042	-.024
2.430	-.019	-.049	-.031	-.042	-.024
2.432	-.023	-.049	-.031	-.049	-.024
2.434	-.024	-.043	-.031	-.043	-.027
2.436	-.025	-.042	-.031	-.042	-.024
2.438	-.024	-.043	-.034	-.042	-.027
2.440	-.024	-.045	-.034	-.043	-.029
2.442	-.023	-.046	-.034	-.040	-.032
2.444	-.020	-.047	-.032	-.040	-.033
2.446	-.018	-.045	-.032	-.040	-.035
2.448	-.015	-.041	-.032	-.040	-.036
2.450	-.011	-.047	-.032	-.040	-.035
2.452	-.013	-.042	-.033	-.034	-.036
2.454	-.016	-.044	-.036	-.040	-.035
2.456	-.016	-.040	-.038	-.041	-.036
2.458	-.016	-.040	-.038	-.036	-.039
2.460	-.016	-.041	-.046	-.033	-.039
2.462	-.014	-.041	-.044	-.035	-.040
2.464	-.015	-.042	-.044	-.035	-.045
2.466	-.021	-.042	-.044	-.036	-.041
2.468	-.021	-.042	-.044	-.030	-.041
2.470	-.019	-.041	-.043	-.031	-.040
2.472	-.015	-.041	-.043	-.031	-.038
2.474	-.012	-.041	-.043	-.030	-.039
2.476	-.011	-.046	-.039	-.029	-.038
2.478	-.011	-.051	-.037	-.031	-.040
2.480	-.011	-.053	-.032	-.034	-.048
2.482	-.009	-.051	-.028	-.028	-.042
2.484	-.009	-.048	-.030	-.028	-.040
2.486	-.011	-.052	-.031	-.030	-.042
2.488	-.009	-.052	-.026	-.029	-.042
2.490	-.009	-.054	-.026	-.030	-.039
2.492	-.007	-.060	-.028	-.030	-.041
2.494	-.006	-.056	-.028	-.030	-.042
2.496	-.005	-.052	-.031	-.034	-.040
2.498	-.004	-.054	-.031	-.028	-.044
2.500	-.005	-.054	-.028	-.028	-.041
2.502	-.001	-.056	-.032	-.024	-.042
2.504	-.005	-.057	-.034	-.025	-.040
2.506	-.005	-.061	-.038	-.031	-.039
2.508	-.001	-.063	-.038	-.030	-.036
2.510	-.004	-.062	-.038	-.034	-.039
2.512	-.005	-.068	-.039	-.035	-.039
2.514	-.002	-.070	-.040	-.043	-.038
2.516	-.002	-.071	-.040	-.043	-.040
2.518	-.004	-.063	-.040	-.043	-.042
2.520	-.001	-.065	-.040	-.043	-.041

TABLE A.IV.1 (CONTINUED)

$\tilde{x}$	10	11	12	13	14	$\tilde{x}$	10	11	12	13	14
τ (s)	$\tilde{R}$	$\tilde{R}$	$\tilde{R}$	$\tilde{R}$	$\tilde{R}$	τ (s)	$\tilde{R}$	$\tilde{R}$	$\tilde{R}$	$\tilde{R}$	$\tilde{R}$
2.520	-.001	-.065	-.040	-.043	-.041	2.660	-.009	-.047	-.055	-.060	-.053
2.522	-.003	-.063	-.040	-.040	-.041	2.662	-.005	-.051	-.057	-.062	-.053
2.524	-.001	-.065	-.046	-.040	-.039	2.664	-.002	-.052	-.061	-.065	-.055
2.526	-.002	-.068	-.040	-.042	-.039	2.666	-.004	-.054	-.058	-.065	-.052
2.528	-.006	-.067	-.038	-.036	-.039	2.668	-.001	-.050	-.056	-.065	-.049
2.530	-.002	-.067	-.040	-.040	-.039	2.670	.002	-.056	-.054	-.073	-.049
2.532	0.000	-.070	-.042	-.040	-.038	2.672	.002	-.056	-.054	-.066	-.047
2.534	-.001	-.069	-.049	-.040	-.040	2.674	.003	-.056	-.055	-.067	-.043
2.536	-.003	-.065	-.048	-.040	-.039	2.676	.004	-.056	-.055	-.065	-.046
2.538	-.004	-.071	-.044	-.040	-.040	2.678	.001	-.056	-.056	-.065	-.042
2.540	-.002	-.065	-.049	-.042	-.040	2.680	.003	-.056	-.058	-.067	-.040
2.542	-.005	-.064	-.051	-.042	-.040	2.682	.003	-.055	-.058	-.063	-.041
2.544	-.006	-.065	-.051	-.048	-.041	2.684	-.001	-.052	-.058	-.061	-.041
2.546	-.007	-.067	-.050	-.049	-.040	2.686	-.003	-.051	-.058	-.063	-.038
2.548	-.012	-.062	-.051	-.047	-.038	2.688	-.003	-.053	-.056	-.064	-.036
2.550	-.013	-.064	-.050	-.045	-.039	2.690	-.003	-.054	-.064	-.060	-.036
2.552	-.018	-.062	-.051	-.045	-.040	2.692	.001	-.046	-.062	-.059	-.040
2.554	-.016	-.061	-.058	-.045	-.041	2.694	-.001	-.046	-.057	-.057	-.038
2.556	-.015	-.062	-.058	-.046	-.045	2.696	-.001	-.042	-.058	-.059	-.037
2.558	-.012	-.059	-.052	-.052	-.041	2.698	-.002	-.044	-.052	-.060	-.044
2.560	-.014	-.059	-.052	-.052	-.039	2.700	-.007	-.041	-.052	-.055	-.044
2.562	-.011	-.058	-.055	-.049	-.040	2.702	-.002	-.041	-.054	-.056	-.044
2.564	-.011	-.060	-.054	-.050	-.040	2.704	-.007	-.045	-.054	-.060	-.042
2.566	-.013	-.058	-.055	-.048	-.040	2.706	-.003	-.045	-.051	-.059	-.042
2.568	-.015	-.059	-.054	-.048	-.040	2.708	.005	-.041	-.050	-.059	-.043
2.570	-.014	-.060	-.055	-.047	-.040	2.710	.004	-.041	-.045	-.060	-.043
2.572	-.018	-.057	-.054	-.049	-.042	2.712	-.007	-.048	-.048	-.061	-.042
2.574	-.018	-.057	-.054	-.045	-.040	2.714	-.012	-.042	-.050	-.057	-.040
2.576	-.014	-.054	-.054	-.045	-.041	2.716	-.007	-.045	-.052	-.058	-.043
2.578	-.013	-.051	-.050	-.043	-.044	2.718	-.006	-.051	-.050	-.054	-.042
2.580	-.011	-.051	-.046	-.042	-.040	2.720	-.004	-.050	-.051	-.052	-.042
2.582	-.013	-.053	-.045	-.045	-.040	2.722	-.005	-.047	-.051	-.056	-.042
2.584	-.010	-.051	-.048	-.046	-.044	2.724	-.006	-.046	-.055	-.055	-.041
2.586	-.007	-.051	-.049	-.046	-.043	2.726	-.006	-.046	-.055	-.058	-.045
2.588	-.006	-.056	-.048	-.051	-.039	2.728	-.009	-.046	-.052	-.059	-.043
2.590	-.007	-.057	-.049	.001	-.041	2.730	-.008	-.042	-.055	-.061	-.044
2.592	-.010	-.056	-.048	-.049	-.048	2.732	-.006	-.043	-.054	-.058	-.039
2.594	-.017	-.058	-.044	-.046	-.048	2.734	-.005	-.040	-.051	-.060	-.043
2.596	-.012	-.053	-.045	-.047	-.048	2.736	.001	-.040	-.050	-.058	-.043
2.598	-.011	-.050	-.046	-.048	-.048	2.738	-.001	-.045	-.058	-.058	-.046
2.600	-.011	-.050	-.046	-.048	-.048	2.740	-.002	-.045	-.056	-.058	-.048
2.602	-.012	-.047	-.050	-.048	-.049	2.742	-.004	-.045	-.055	-.054	-.046
2.604	-.011	-.048	-.050	-.048	-.049	2.744	-.004	-.044	-.054	-.061	-.048
2.606	-.010	-.046	-.050	-.048	-.047	2.746	-.005	-.045	-.054	-.059	-.051
2.608	-.010	-.047	-.052	-.048	-.048	2.748	-.007	-.042	-.051	-.058	-.052
2.610	-.009	-.052	-.051	-.048	-.049	2.750	-.008	-.041	-.052	-.060	-.049
2.612	-.005	-.054	-.052	-.047	-.056	2.752	-.007	-.041	-.050	-.060	-.049
2.614	-.007	-.053	-.049	-.042	-.049	2.754	-.009	-.041	-.054	-.061	-.048
2.616	-.007	-.054	-.049	-.049	-.048	2.756	-.010	-.042	-.055	-.059	-.049
2.618	-.006	-.055	-.049	-.042	-.049	2.758	-.010	-.048	-.056	-.061	-.049
2.620	-.001	-.055	-.051	-.043	-.049	2.760	-.010	-.048	-.060	-.064	-.048
2.622	-.003	-.053	-.051	-.048	-.049	2.762	-.009	-.047	-.063	-.061	-.052
2.624	-.002	-.053	-.054	-.047	-.048	2.764	-.009	-.047	-.067	-.060	-.052
2.626	-.001	-.060	-.055	-.049	-.049	2.766	-.014	-.045	-.070	-.058	-.052
2.628	-.005	-.053	-.056	-.048	-.048	2.768	-.014	-.042	-.064	-.059	-.052
2.630	-.005	-.052	-.056	-.046	-.049	2.770	-.014	-.040	-.058	-.058	-.051
2.632	-.007	-.051	-.058	-.051	-.049	2.772	-.014	-.036	-.055	-.061	-.052
2.634	-.007	-.050	-.051	-.054	-.048	2.774	-.013	-.035	-.051	-.059	-.053
2.636	-.006	-.052	-.058	-.052	-.048	2.776	-.013	-.035	-.050	-.057	-.052
2.638	-.006	-.052	-.054	-.052	-.048	2.778	-.014	-.033	-.048	-.055	-.052
2.640	-.002	-.056	-.051	-.054	-.048	2.780	-.011	-.034	-.046	-.055	-.052
2.642	-.004	-.057	-.052	-.057	-.056	2.782	-.012	-.030	-.051	-.054	-.053
2.644	-.005	-.054	-.054	-.055	-.052	2.784	-.007	-.029	-.049	-.052	-.052
2.646	-.004	-.051	-.054	-.058	-.049	2.786	-.007	-.028	-.045	-.052	-.049
2.648	-.001	-.050	-.051	-.060	-.048	2.788	-.002	-.026	-.052	-.052	-.043
2.650	-.001	-.050	-.051	-.060	-.050	2.790	0.000	-.025	-.052	-.054	-.046
2.652	-.001	-.051	-.054	-.067	-.047	2.792	0.000	-.026	-.052	-.053	-.047
2.654	-.001	-.048	-.055	-.061	-.048	2.794	.001	-.026	-.051	-.048	-.047
2.656	-.002	-.046	-.055	-.061	-.048	2.796	.002	-.026	-.051	-.054	-.047
2.658	-.007	-.045	-.051	-.061	-.052	2.798	.004	-.023	-.058	-.054	-.047
2.660	-.009	-.047	-.055	-.060	-.053	2.800	.004	-.023	-.058	-.054	-.047

TABLE A.IV.1 (CONTINUED)

$\tilde{x}$	10	11	12	13	14	$\tilde{x}$	10	11	12	13	14
τ (s)	$\tilde{R}$	$\tilde{R}$	$\tilde{R}$	$\tilde{R}$	$\tilde{R}$	τ (s)	$\tilde{R}$	$\tilde{R}$	$\tilde{R}$	$\tilde{R}$	$\tilde{R}$
2.800	.004	-.023	-.058	-.054	-.047	2.940	-.016	.015	-.059	-.089	-.061
2.802	-.002	-.021	-.065	-.056	-.047	2.942	-.019	.013	-.058	-.088	-.059
2.804	.003	-.018	-.062	-.056	-.050	2.944	-.020	.010	-.056	-.086	-.059
2.806	.003	-.017	-.061	-.062	-.050	2.946	-.021	.010	-.052	-.086	-.062
2.808	.008	-.023	-.062	-.062	-.047	2.948	-.018	.010	-.053	-.083	-.063
2.810	.008	-.023	-.059	-.068	-.047	2.950	-.013	.005	-.052	-.084	-.065
2.812	.003	-.021	-.057	-.068	-.054	2.952	-.011	.008	-.051	-.077	-.064
2.814	.001	-.021	-.059	-.068	-.052	2.954	-.015	.011	-.051	-.077	-.063
2.816	-.001	-.019	-.052	-.064	-.053	2.956	-.021	.009	-.051	-.084	-.065
2.818	-.001	-.018	-.050	-.063	-.060	2.958	-.021	.010	-.049	-.081	-.067
2.820	-.001	-.019	-.049	-.064	-.060	2.960	-.021	.008	-.049	-.080	-.068
2.822	-.007	-.017	-.047	-.062	-.057	2.962	-.021	.011	-.049	-.077	-.068
2.824	-.007	-.018	-.046	-.067	-.060	2.964	-.020	.011	-.047	-.080	-.065
2.826	-.004	-.019	-.046	-.068	-.060	2.966	-.019	.010	-.049	-.085	-.068
2.828	-.002	-.019	-.054	-.070	-.060	2.968	-.018	.015	-.049	-.086	-.067
2.830	-.001	-.023	-.049	-.070	-.058	2.970	-.019	.015	-.050	-.082	-.070
2.832	-.004	-.022	-.049	-.070	-.061	2.972	-.019	.016	-.050	-.081	-.069
2.834	-.004	-.023	-.051	-.072	-.056	2.974	-.021	.016	-.050	-.080	-.067
2.836	.001	-.022	-.059	-.070	-.056	2.976	-.019	.019	-.050	-.080	-.069
2.838	.005	-.023	-.055	-.071	-.056	2.978	-.020	.021	-.051	-.080	-.069
2.840	.001	-.019	-.056	-.071	-.056	2.980	-.022	.019	-.050	-.077	-.069
2.842	.001	-.021	-.056	-.071	-.056	2.982	-.022	.018	-.052	-.080	-.073
2.844	.001	-.021	-.058	-.078	-.057	2.984	-.023	.018	-.052	-.082	-.074
2.846	0.000	-.017	-.062	-.075	-.058	2.986	-.020	.021	-.050	-.080	-.074
2.848	-.003	-.013	-.057	-.075	-.058	2.988	-.022	.019	-.051	-.080	-.074
2.850	-.003	-.010	-.059	-.073	-.059	2.990	-.023	.022	-.049	-.077	-.074
2.852	-.004	-.012	-.055	-.074	-.062	2.992	-.019	.026	-.050	-.075	-.069
2.854	-.004	-.012	-.058	-.075	-.062	2.994	-.023	.026	-.046	-.074	-.067
2.856	-.003	-.009	-.057	-.074	-.061	2.996	-.029	.023	-.045	-.080	-.065
2.858	-.004	-.013	-.058	-.071	-.057	2.998	-.030	.018	-.041	-.080	-.063

2. Lagrangian autocorrelation coefficient, turbulent momentum exchange coefficient and dispersion coefficient

The axial Lagrangian autocorrelation coefficient, the dimensionless longitudinal turbulent momentum exchange coefficient and the normalized axial dispersion coefficient data are summarized in Table A.IV.2 Computation of the Lagrangian autocorrelation is described in Sect. 6.2 whereas calculation of the latter two coefficients is outlined in Sect. 6.5.

The axial Lagrangian autocorrelation coefficient is portrayed in Figs. 6.21 and 6.25. In the latter figure the extended Lagrangian autocorrelation coefficient is depicted. The axial Lagrangian autocorrelation coefficient is defined by Eq. (6.40)

$$\tilde{L}_o(\tilde{x}_o,\tau) = L(x_o,\tau)/\overline{v_o^2}$$

where the axial Lagrangian autocorrelation $L(x_o,\tau)$ is given in terms of the Eulerian autocorrelation $R(x;\tau)$ by Eq. (6.39). Computation of the longitudinal Lagrangian autocorrelation coefficient was carried out utilizing Eq. (6.42)

$$\tilde{L}_o(\tilde{x}_o,\tau) = \frac{1}{\tilde{\xi}} \int_{x_o}^{\tilde{x}_o+\tilde{\xi}} \tilde{R}_o(\tilde{x};\tau)\, d\tilde{x},$$

where $\tilde{R}_o(\tilde{x};\tau)$ is the dimensionless envelope of the Eulerian reference-point autocorrelation coefficients defined by Eq. (6.41).

The dimensionless axial turbulent momentum exchange coefficient (dimensionless eddy diffusivity) is expressed by Eq. (6.47)

$$\tilde{K}_M(\tilde{x}_o,\tilde{t}_D) = K_M(\tilde{x}_o,t_D)/\overline{v_o^2}\, T_{L1},$$

in which the turbulent momentum exchange coefficient $\tilde{K}_M(\tilde{x}_o, t_D)$ is defined in terms of the axial Lagrangian autocorrelation coefficient by Eq. (6.46). In the foregoing equation the dimensionless diffusion time is given by Eq. (6.48)

$$\tilde{t}_D = t_D/T_{L1}.$$

Variation of the axial eddy diffusivity with increasing diffusion time is displayed in Fig. 6.26.

The normalized longitudinal dispersion coefficient (dimensionless longitudinal mean-square displacement) is defined by Eq. (6.51)

$$\tilde{D}(\tilde{x}_o, \tilde{t}_D) = D(\tilde{x}_o, t_D)/\overline{v_o^2}\; T_{L1}^2,$$

where the axial dispersion coefficient is expressed in terms of the longitudinal Lagrangian autocorrelation coefficients by Eq. (6.50). Change of the longitudinal dispersion coefficient with increasing diffusion time is portrayed in Fig. 6.27. In all foregoing equations $\overline{v_o^2} = 6.25\ m^2/s^2$ ($67.2\ ft^2/s^2$; see Sect. 6.4) and $T_{L1} = 51.5$ ms (see Sect. 6.4). In Table A.IV.2 the variations of $\tilde{L}(\tilde{x}_o, \tau)$ with increasing time delay τ, and the changes of $\tilde{K}_M(\tilde{x}_o, \tilde{t}_D)$ and $\tilde{D}(\tilde{x}_o, \tilde{t}_D)$ with augmenting dimensionless diffusion time $\tilde{t}_D$ are tabulated.

TABLE A.IV.2

LAGRANGIAN AUTOCORRELATION COEFFICIENT, TURBULENT MOMENTUM EXCHANGE COEFFICIENT AND DISPERSION COEFFICIENT

τ (s)	$\tilde{L}_o$	$\tilde{t}_D$	$\tilde{K}_M$	$\tilde{D}$	τ (s)	$\tilde{L}_o$	$\tilde{t}_D$	$\tilde{K}_M$	$\tilde{D}$
0.000	1.000	0.00	0.000	0.00	.140	.090	2.72	.917	3.37
.002	.923	.04	.037	.00	.142	.087	2.76	.921	3.44
.004	.865	.08	.072	.01	.144	.086	2.80	.924	3.52
.006	.816	.12	.105	.01	.146	.083	2.84	.927	3.59
.008	.772	.16	.136	.02	.148	.079	2.88	.930	3.66
.010	.779	.19	.166	.03	.150	.078	2.92	.933	3.73
.012	.731	.23	.195	.05	.152	.078	2.95	.936	3.80
.014	.675	.27	.222	.06	.154	.077	2.99	.939	3.88
.016	.650	.31	.248	.08	.156	.074	3.03	.942	3.95
.018	.621	.35	.273	.10	.158	.073	3.07	.945	4.02
.020	.601	.39	.297	.12	.160	.070	3.11	.948	4.10
.022	.573	.43	.320	.15	.162	.066	3.15	.951	4.17
.024	.558	.47	.341	.17	.164	.063	3.19	.953	4.25
.026	.534	.51	.363	.20	.166	.062	3.23	.956	4.32
.028	.515	.54	.383	.23	.168	.062	3.27	.958	4.39
.030	.505	.58	.403	.26	.170	.056	3.30	.960	4.47
.032	.482	.62	.422	.29	.172	.053	3.34	.962	4.54
.034	.471	.66	.441	.33	.174	.049	3.38	.964	4.62
.036	.453	.70	.459	.36	.176	.046	3.42	.966	4.69
.038	.438	.74	.476	.40	.178	.046	3.46	.968	4.77
.040	.424	.78	.493	.44	.180	.048	3.50	.970	4.84
.042	.410	.82	.509	.48	.182	.043	3.54	.972	4.92
.044	.388	.86	.524	.52	.184	.042	3.58	.973	4.99
.046	.378	.89	.539	.56	.186	.045	3.62	.975	5.07
.048	.373	.93	.554	.60	.188	.042	3.65	.977	5.15
.050	.363	.97	.568	.64	.190	.039	3.69	.978	5.22
.052	.346	1.01	.582	.69	.192	.031	3.73	.980	5.30
.054	.336	1.05	.595	.73	.194	.039	3.77	.981	5.37
.056	.331	1.09	.608	.78	.196	.026	3.81	.982	5.45
.058	.346	1.13	.621	.83	.198	.026	3.85	.983	5.53
.060	.344	1.17	.635	.88	.200	.026	3.89	.984	5.60
.062	.296	1.21	.647	.93	.202	.026	3.93	.985	5.68
.064	.287	1.24	.659	.98	.204	.025	3.97	.986	5.76
.066	.282	1.28	.670	1.03	.206	.023	4.00	.987	5.83
.068	.273	1.32	.680	1.08	.208	.022	4.04	.988	5.91
.070	.276	1.36	.691	1.13	.210	.022	4.08	.989	5.99
.072	.255	1.40	.701	1.19	.212	.020	4.12	.990	6.06
.074	.250	1.44	.711	1.24	.214	.020	4.16	.990	6.14
.076	.241	1.48	.721	1.30	.216	.019	4.20	.991	6.22
.078	.237	1.52	.730	1.36	.218	.019	4.24	.992	6.30
.080	.228	1.55	.739	1.41	.220	.014	4.28	.993	6.37
.082	.231	1.59	.748	1.47	.222	.014	4.31	.993	6.45
.084	.211	1.63	.757	1.53	.224	.011	4.35	.994	6.53
.086	.207	1.67	.765	1.59	.226	.011	4.39	.994	6.60
.088	.202	1.71	.773	1.65	.228	.009	4.43	.995	6.68
.090	.194	1.75	.780	1.71	.230	.010	4.47	.995	6.76
.092	.193	1.79	.788	1.77	.232	.012	4.51	.995	6.84
.094	.185	1.83	.795	1.83	.234	.010	4.55	.996	6.91
.096	.181	1.87	.802	1.89	.236	.010	4.59	.996	6.99
.098	.170	1.90	.809	1.96	.238	.009	4.63	.996	7.07
.100	.165	1.94	.816	2.02	.240	.010	4.66	.997	7.15
.102	.161	1.98	.822	2.08	.242	.009	4.70	.997	7.22
.104	.154	2.02	.828	2.15	.244	.007	4.74	.947	7.30
.106	.150	2.06	.834	2.21	.246	.008	4.78	.998	7.38
.108	.145	2.10	.840	2.28	.248	.008	4.82	.998	7.46
.110	.148	2.14	.846	2.34	.250	.010	4.86	.998	7.53
.112	.147	2.18	.851	2.41	.252	.007	4.90	.999	7.61
.114	.130	2.22	.857	2.47	.254	.006	4.94	.999	7.69
.116	.129	2.25	.862	2.54	.256	.006	4.98	.999	7.77
.118	.129	2.29	.867	2.61	.258	.006	5.01	1.000	7.84
.120	.125	2.33	.872	2.68	.260	.006	5.05	1.000	7.92
.122	.121	2.37	.876	2.74	.262	.006	5.09	1.000	8.00
.124	.117	2.41	.881	2.81	.264	-.000	5.13	1.000	8.08
.126	.116	2.45	.886	2.88	.266	-.004	5.17	1.000	8.16
.128	.124	2.49	.890	2.95	.268	-.001	5.21	1.000	8.23
.130	.129	2.53	.895	3.02	.270	-.001	5.25	1.000	8.31
.132	.128	2.57	.900	3.09	.272	-.002	5.29	1.000	8.39
.134	.127	2.60	.905	3.16	.274	-.002	5.33	1.000	8.47
.136	.104	2.64	.910	3.23	.276	-.002	5.36	1.000	8.54
.138	.090	2.68	.914	3.30	.278	-.004	5.40	1.000	8.62
.140	.090	2.72	.917	3.37	.260	-.004	5.44	.999	8.70

TABLE A.IV.2 (CONTINUED)

τ (s)	$\tilde{L}_o$	$\tilde{t}_D$	$\tilde{K}_M$	$\tilde{D}$	τ (s)	$\tilde{L}_o$	$\tilde{t}_D$	$\tilde{K}_M$	$\tilde{D}$
.280	-.004	5.44	.999	8.70	.420	-.020	8.16	.961	14.05
.282	-.004	5.48	.999	8.78	.422	-.022	8.20	.961	14.13
.284	-.006	5.52	.999	8.85	.424	-.023	8.24	.960	14.20
.286	-.005	5.56	.999	8.93	.426	-.023	8.28	.959	14.28
.288	-.005	5.60	.999	9.01	.428	-.021	8.32	.958	14.35
.290	-.006	5.64	.998	9.09	.430	-.023	8.36	.957	14.43
.292	-.006	5.68	.998	9.17	.432	-.023	8.40	.956	14.50
.294	-.005	5.71	.998	9.24	.434	-.022	8.44	.955	14.58
.296	-.008	5.75	.998	9.32	.436	-.022	8.47	.954	14.65
.298	-.004	5.79	.997	9.40	.438	-.022	8.51	.954	14.72
.300	-.008	5.83	.997	9.48	.440	-.022	8.55	.953	14.80
.302	-.004	5.87	.997	9.55	.442	-.023	8.59	.952	14.87
.304	-.006	5.91	.997	9.63	.444	-.022	8.63	.951	14.95
.306	-.007	5.95	.996	9.71	.446	-.022	8.67	.950	15.02
.308	-.007	5.99	.996	9.79	.448	-.020	8.71	.949	15.09
.310	-.007	6.03	.996	9.86	.450	-.019	8.75	.949	15.17
.312	-.008	6.06	.996	9.94	.452	-.021	8.79	.948	15.24
.314	-.010	6.10	.995	10.02	.454	-.021	8.82	.947	15.32
.316	-.010	6.14	.995	10.10	.456	-.021	8.86	.946	15.39
.318	-.011	6.18	.994	10.17	.458	-.019	8.90	.945	15.46
.320	-.011	6.22	.994	10.25	.460	-.020	8.94	.945	15.54
.322	-.012	6.26	.994	10.33	.462	-.021	8.98	.944	15.61
.324	-.013	6.30	.993	10.40	.464	-.022	9.02	.943	15.68
.326	-.013	6.34	.993	10.48	.466	-.023	9.06	.942	15.76
.328	-.014	6.38	.992	10.56	.468	-.021	9.10	.941	15.83
.330	-.014	6.41	.991	10.64	.470	-.022	9.14	.940	15.90
.332	-.015	6.45	.991	10.71	.472	-.020	9.17	.940	15.98
.334	-.015	6.49	.990	10.79	.474	-.021	9.21	.939	16.05
.336	-.015	6.53	.990	10.87	.476	-.022	9.25	.938	16.12
.338	-.016	6.57	.989	10.94	.478	-.022	9.29	.937	16.19
.340	-.016	6.61	.989	11.02	.480	-.022	9.33	.936	16.27
.342	-.017	6.65	.988	11.10	.482	-.022	9.37	.935	16.34
.344	-.015	6.69	.987	11.17	.484	-.021	9.41	.935	16.41
.346	-.015	6.72	.987	11.25	.486	-.021	9.45	.934	16.49
.348	-.014	6.76	.986	11.33	.488	-.021	9.48	.933	16.56
.350	-.013	6.80	.986	11.40	.490	-.021	9.52	.932	16.63
.352	-.015	6.84	.985	11.48	.492	-.021	9.56	.931	16.70
.354	-.016	6.88	.984	11.56	.494	-.021	9.60	.930	16.78
.356	-.015	6.92	.984	11.63	.496	-.021	9.64	.930	16.85
.358	-.015	6.96	.983	11.71	.498	-.021	9.68	.929	16.92
.360	-.015	7.00	.983	11.79	.500	-.020	9.72	.928	16.99
.362	-.015	7.04	.982	11.86	.502	-.023	9.76	.927	17.06
.364	-.016	7.07	.982	11.94	.504	-.024	9.80	.926	17.14
.366	-.016	7.11	.981	12.02	.506	-.024	9.83	.925	17.21
.368	-.017	7.15	.980	12.09	.508	-.025	9.87	.924	17.28
.370	-.017	7.19	.980	12.17	.510	-.024	9.91	.923	17.35
.372	-.019	7.23	.979	12.24	.512	-.024	9.95	.923	17.42
.374	-.017	7.27	.978	12.32	.514	-.024	9.99	.922	17.50
.376	-.017	7.31	.977	12.40	.516	-.023	10.03	.921	17.57
.378	-.019	7.35	.977	12.47	.518	-.024	10.07	.920	17.64
.380	-.019	7.39	.976	12.55	.520	-.023	10.11	.919	17.71
.382	-.018	7.42	.975	12.62	.522	-.024	10.15	.918	17.78
.384	-.019	7.46	.975	12.70	.524	-.024	10.18	.917	17.85
.386	-.018	7.50	.974	12.78	.526	-.024	10.22	.916	17.92
.388	-.020	7.54	.973	12.85	.528	-.024	10.26	.915	18.00
.390	-.021	7.58	.972	12.93	.530	-.025	10.30	.914	18.07
.392	-.019	7.62	.972	13.00	.532	-.025	10.34	.913	18.14
.394	-.020	7.66	.971	13.08	.534	-.025	10.38	.912	18.21
.396	-.019	7.70	.970	13.15	.536	-.025	10.42	.911	18.28
.398	-.018	7.74	.969	13.23	.538	-.024	10.46	.910	18.35
.400	-.017	7.77	.969	13.30	.540	-.025	10.50	.909	18.42
.402	-.018	7.81	.968	13.38	.542	-.025	10.53	.908	18.49
.404	-.018	7.85	.967	13.45	.544	-.025	10.57	.907	18.56
.406	-.018	7.89	.967	13.53	.546	-.025	10.61	.906	18.63
.408	-.020	7.93	.966	13.61	.548	-.024	10.65	.905	18.70
.410	-.018	7.97	.965	13.68	.550	-.025	10.69	.904	18.77
.412	-.019	8.01	.964	13.76	.552	-.026	10.73	.903	18.84
.414	-.019	8.05	.964	13.83	.554	-.026	10.77	.902	18.91
.416	-.019	8.09	.963	13.91	.556	-.025	10.81	.901	18.98
.418	-.021	8.12	.962	13.98	.558	-.023	10.85	.901	19.05
.420	-.020	8.16	.961	14.05	.560	-.024	10.88	.900	19.12

TABLE A.IV.2 (CONTINUED)

τ (s)	$\tilde{L}_o$	$\bar{t}_D$	$\tilde{K}_M$	$\tilde{D}$	τ (s)	$\tilde{L}_o$	$\bar{t}_D$	$\tilde{K}_M$	$\tilde{D}$
.560	-.024	10.88	.900	19.12	.700	-.027	13.61	.826	23.82
.562	-.025	10.92	.899	19.19	.702	-.028	13.64	.825	23.89
.564	-.025	10.96	.898	19.26	.704	-.029	13.68	.824	23.95
.566	-.025	11.00	.897	19.33	.706	-.029	13.72	.823	24.01
.568	-.025	11.04	.896	19.40	.708	-.028	13.76	.822	24.08
.570	-.026	11.08	.895	19.47	.710	-.028	13.80	.821	24.14
.572	-.026	11.12	.894	19.54	.712	-.028	13.84	.820	24.21
.574	-.025	11.16	.893	19.61	.714	-.028	13.88	.818	24.27
.576	-.027	11.20	.892	19.68	.716	-.028	13.92	.817	24.33
.578	-.027	11.23	.891	19.75	.718	-.028	13.96	.816	24.40
.580	-.023	11.27	.890	19.82	.720	-.028	13.99	.815	24.46
.582	-.026	11.31	.889	19.89	.722	-.028	14.03	.814	24.52
.584	-.026	11.35	.888	19.96	.724	-.028	14.07	.813	24.59
.586	-.026	11.39	.887	20.03	.726	-.027	14.11	.812	24.65
.588	-.027	11.43	.886	20.10	.728	-.027	14.15	.811	24.71
.590	-.028	11.47	.885	20.16	.730	-.028	14.19	.810	24.78
.592	-.027	11.51	.884	20.23	.732	-.029	14.23	.809	24.84
.594	-.026	11.55	.883	20.30	.734	-.028	14.27	.808	24.90
.596	-.026	11.58	.882	20.37	.736	-.027	14.31	.807	24.96
.598	-.026	11.62	.881	20.44	.738	-.028	14.34	.806	25.03
.600	-.026	11.66	.879	20.51	.740	-.027	14.38	.804	25.09
.602	-.027	11.70	.878	20.58	.742	-.028	14.42	.803	25.15
.604	-.027	11.74	.877	20.64	.744	-.027	14.46	.802	25.21
.606	-.027	11.78	.876	20.71	.746	-.027	14.50	.801	25.28
.608	-.027	11.82	.875	20.78	.748	-.027	14.54	.800	25.34
.610	-.027	11.86	.874	20.85	.750	-.028	14.58	.799	25.40
.612	-.028	11.90	.873	20.92	.752	-.028	14.62	.798	25.46
.614	-.028	11.94	.872	20.98	.754	-.027	14.66	.797	25.53
.616	-.028	11.97	.871	21.05	.756	-.028	14.69	.796	25.59
.618	-.027	12.01	.870	21.12	.758	-.028	14.73	.795	25.65
.620	-.028	12.05	.869	21.19	.760	-.028	14.77	.794	25.71
.622	-.028	12.09	.868	21.25	.762	-.028	14.81	.793	25.77
.624	-.028	12.13	.867	21.32	.764	-.027	14.85	.792	25.83
.626	-.028	12.17	.866	21.39	.766	-.027	14.89	.790	25.90
.628	-.028	12.21	.864	21.46	.768	-.027	14.93	.789	25.96
.630	-.027	12.24	.863	21.52	.770	-.026	14.97	.788	26.02
.632	-.026	12.28	.862	21.59	.772	-.027	15.00	.787	26.08
.634	-.028	12.32	.861	21.66	.774	-.028	15.04	.786	26.14
.636	-.028	12.36	.860	21.72	.776	-.028	15.08	.785	26.20
.638	-.026	12.40	.859	21.79	.778	-.027	15.12	.784	26.26
.640	-.026	12.44	.858	21.86	.780	-.027	15.16	.783	26.32
.642	-.027	12.48	.857	21.92	.782	-.027	15.20	.782	26.38
.644	-.028	12.52	.856	21.99	.784	-.027	15.24	.781	26.45
.646	-.028	12.56	.855	22.06	.786	-.026	15.28	.780	26.51
.648	-.028	12.59	.854	22.12	.788	-.028	15.32	.779	26.57
.650	-.027	12.63	.853	22.19	.790	-.028	15.35	.778	26.63
.652	-.028	12.67	.852	22.26	.792	-.027	15.39	.777	26.69
.654	-.029	12.71	.851	22.32	.794	-.027	15.43	.776	26.75
.656	-.029	12.75	.850	22.39	.796	-.027	15.47	.775	26.81
.658	-.028	12.79	.848	22.46	.798	-.027	15.51	.774	26.87
.660	-.028	12.83	.847	22.52	.800	-.027	15.55	.773	26.93
.662	-.029	12.87	.846	22.59	.802	-.027	15.59	.772	26.99
.664	-.029	12.91	.845	22.65	.804	-.027	15.63	.770	27.05
.666	-.029	12.94	.844	22.72	.806	-.028	15.67	.769	27.11
.668	-.028	12.98	.843	22.78	.808	-.028	15.70	.768	27.17
.670	-.028	13.02	.842	22.85	.810	-.027	15.74	.767	27.23
.672	-.028	13.06	.841	22.91	.812	-.026	15.78	.766	27.29
.674	-.028	13.10	.840	22.98	.814	-.027	15.82	.765	27.35
.676	-.028	13.14	.839	23.05	.816	-.027	15.86	.764	27.41
.678	-.027	13.18	.837	23.11	.818	-.028	15.90	.763	27.47
.680	-.027	13.22	.836	23.18	.820	-.028	15.94	.762	27.53
.682	-.026	13.26	.835	23.24	.822	-.028	15.98	.761	27.58
.684	-.027	13.29	.834	23.31	.824	-.028	16.02	.760	27.64
.686	-.026	13.33	.833	23.37	.826	-.028	16.05	.759	27.70
.688	-.026	13.37	.832	23.44	.828	-.028	16.09	.758	27.76
.690	-.026	13.41	.831	23.50	.830	-.029	16.13	.757	27.82
.692	-.027	13.45	.830	23.56	.832	-.028	16.17	.755	27.88
.694	-.027	13.49	.829	23.63	.834	-.027	16.21	.754	27.94
.696	-.027	13.53	.828	23.69	.836	-.027	16.25	.753	28.00
.698	-.026	13.57	.827	23.76	.838	-.028	16.29	.752	28.05
.700	-.027	13.61	.826	23.82	.840	-.028	16.33	.751	28.11

TABLE A.IV.2 (CONTINUED)

τ (s)	$\tilde{L}_o$	$\tilde{t}_D$	$\tilde{K}_M$	$\tilde{D}$	τ (s)	$\tilde{L}_o$	$\tilde{t}_D$	$\tilde{K}_M$	$\tilde{D}$
.840	-.028	16.33	.751	28.11	.980	-.025	19.05	.679	32.00
.842	-.028	16.37	.750	28.17	.982	-.024	19.09	.678	32.05
.844	-.028	16.40	.749	28.23	.984	-.024	19.13	.677	32.11
.846	-.029	16.44	.748	28.29	.986	-.024	19.16	.676	32.16
.848	-.028	16.48	.747	28.35	.988	-.024	19.20	.675	32.21
.850	-.028	16.52	.746	28.40	.990	-.024	19.24	.674	32.26
.852	-.028	16.56	.745	28.46	.992	-.024	19.28	.674	32.32
.854	-.028	16.60	.744	28.52	.994	-.024	19.32	.673	32.37
.856	-.028	16.64	.742	28.58	.996	-.024	19.36	.672	32.42
.858	-.028	16.68	.741	28.64	.998	-.024	19.40	.671	32.47
.860	-.028	16.72	.740	28.69	1.000	-.024	19.44	.670	32.52
.862	-.028	16.75	.739	28.75	1.002	-.024	19.48	.669	32.58
.864	-.028	16.79	.738	28.81	1.004	-.024	19.51	.668	32.63
.866	-.028	16.83	.737	28.87	1.006	-.024	19.55	.667	32.68
.868	-.028	16.87	.736	28.92	1.008	-.024	19.59	.666	32.73
.870	-.028	16.91	.735	28.98	1.010	-.024	19.63	.665	32.78
.872	-.028	16.95	.734	29.04	1.012	-.024	19.67	.664	32.84
.874	-.028	16.99	.733	29.09	1.014	-.024	19.71	.663	32.89
.876	-.027	17.03	.732	29.15	1.016	-.024	19.75	.662	32.94
.878	-.027	17.07	.731	29.21	1.018	-.024	19.79	.661	32.99
.880	-.027	17.10	.729	29.26	1.020	-.024	19.83	.660	33.04
.882	-.027	17.14	.728	29.32	1.022	-.024	19.86	.660	33.09
.884	-.027	17.18	.727	29.38	1.024	-.023	19.90	.659	33.14
.886	-.027	17.22	.726	29.43	1.026	-.023	19.94	.658	33.20
.888	-.027	17.26	.725	29.49	1.028	-.023	19.98	.657	33.25
.890	-.027	17.30	.724	29.55	1.030	-.023	20.02	.656	33.30
.892	-.027	17.34	.723	29.60	1.032	-.023	20.06	.655	33.35
.894	-.027	17.38	.722	29.66	1.034	-.023	20.10	.654	33.40
.896	-.027	17.41	.721	29.72	1.036	-.023	20.14	.653	33.45
.898	-.027	17.45	.720	29.77	1.038	-.023	20.17	.652	33.50
.900	-.027	17.49	.719	29.83	1.040	-.023	20.21	.651	33.55
.902	-.027	17.53	.718	29.88	1.042	-.023	20.25	.651	33.60
.904	-.027	17.57	.717	29.94	1.044	-.023	20.29	.650	33.65
.906	-.027	17.61	.716	29.99	1.046	-.023	20.33	.649	33.70
.908	-.026	17.65	.715	30.05	1.048	-.023	20.37	.648	33.75
.910	-.026	17.69	.714	30.11	1.050	-.023	20.41	.647	33.80
.912	-.026	17.73	.713	30.16	1.052	-.023	20.45	.646	33.85
.914	-.026	17.76	.712	30.22	1.054	-.023	20.49	.645	33.90
.916	-.026	17.80	.711	30.27	1.056	-.023	20.52	.644	33.95
.918	-.026	17.84	.710	30.33	1.058	-.023	20.56	.643	34.00
.920	-.026	17.88	.709	30.38	1.060	-.023	20.60	.643	34.05
.922	-.026	17.92	.708	30.44	1.062	-.023	20.64	.642	34.10
.924	-.026	17.96	.707	30.49	1.064	-.023	20.68	.641	34.15
.926	-.026	18.00	.706	30.55	1.066	-.023	20.72	.640	34.20
.928	-.026	18.04	.705	30.60	1.068	-.023	20.76	.639	34.25
.930	-.026	18.08	.704	30.66	1.070	-.022	20.80	.638	34.30
.932	-.026	18.11	.703	30.71	1.072	-.022	20.84	.637	34.35
.934	-.026	18.15	.702	30.77	1.074	-.022	20.87	.636	34.40
.936	-.026	18.19	.701	30.82	1.076	-.022	20.91	.636	34.45
.938	-.026	18.23	.700	30.88	1.078	-.022	20.95	.635	34.50
.940	-.026	18.27	.699	30.93	1.080	-.022	20.99	.634	34.55
.942	-.026	18.31	.698	30.98	1.082	-.022	21.03	.633	34.60
.944	-.025	18.35	.697	31.04	1.084	-.022	21.07	.632	34.65
.946	-.025	18.39	.696	31.09	1.086	-.022	21.11	.631	34.70
.948	-.025	18.43	.695	31.15	1.088	-.022	21.15	.630	34.75
.950	-.025	18.46	.694	31.20	1.090	-.022	21.19	.629	34.80
.952	-.025	18.50	.693	31.25	1.092	-.022	21.22	.629	34.85
.954	-.025	18.54	.692	31.31	1.094	-.022	21.26	.628	34.89
.956	-.025	18.58	.691	31.36	1.096	-.022	21.30	.627	34.94
.958	-.025	18.62	.690	31.42	1.098	-.022	21.34	.626	34.99
.960	-.025	18.66	.689	31.47	1.100	-.022	21.38	.625	35.04
.962	-.025	18.70	.688	31.52	1.102	-.022	21.42	.624	35.09
.964	-.025	18.74	.687	31.58	1.104	-.022	21.46	.624	35.14
.966	-.025	18.78	.686	31.63	1.106	-.022	21.50	.623	35.19
.968	-.025	18.81	.685	31.68	1.108	-.022	21.54	.622	35.23
.970	-.025	18.85	.684	31.74	1.110	-.022	21.57	.621	35.28
.972	-.025	18.89	.683	31.79	1.112	-.022	21.61	.620	35.33
.974	-.025	18.93	.682	31.84	1.114	-.022	21.65	.619	35.38
.976	-.025	18.97	.681	31.89	1.116	-.022	21.69	.618	35.43
.978	-.025	19.01	.680	31.95	1.118	-.022	21.73	.618	35.48
.980	-.025	19.05	.679	32.00	1.120	-.021	21.77	.617	35.52

TABLE A.IV.2 (CONTINUED)

τ (s)	$\tilde{L}_o$	$\tilde{\tau}_D$	$\tilde{K}_M$	$\tilde{D}$	τ (s)	$\tilde{L}_o$	$\tilde{\tau}_D$	$\tilde{K}_M$	$\tilde{D}$
1.120	-.021	21.77	.617	35.52	1.260	-.019	24.49	.562	38.73
1.122	-.021	21.81	.616	35.57	1.262	-.019	24.53	.561	38.77
1.124	-.021	21.85	.615	35.62	1.264	-.019	24.57	.560	38.81
1.126	-.021	21.89	.614	35.67	1.266	-.019	24.61	.560	38.86
1.128	-.021	21.92	.613	35.71	1.268	-.019	24.65	.559	38.90
1.130	-.021	21.96	.613	35.76	1.270	-.019	24.68	.558	38.94
1.132	-.021	22.00	.612	35.81	1.272	-.019	24.72	.557	38.99
1.134	-.021	22.04	.611	35.86	1.274	-.019	24.76	.557	39.03
1.136	-.021	22.08	.610	35.90	1.276	-.019	24.80	.556	39.07
1.138	-.021	22.12	.609	35.95	1.278	-.019	24.84	.555	39.12
1.140	-.021	22.16	.609	36.00	1.280	-.019	24.88	.554	39.16
1.142	-.021	22.20	.608	36.05	1.282	-.019	24.92	.554	39.20
1.144	-.021	22.24	.607	36.09	1.284	-.019	24.96	.553	39.25
1.146	-.021	22.27	.606	36.14	1.286	-.019	25.00	.552	39.29
1.148	-.021	22.31	.605	36.19	1.288	-.019	25.03	.551	39.33
1.150	-.021	22.35	.604	36.24	1.290	-.019	25.07	.551	39.38
1.152	-.021	22.39	.604	36.28	1.292	-.019	25.11	.550	39.42
1.154	-.021	22.43	.603	36.33	1.294	-.019	25.15	.549	39.46
1.156	-.021	22.47	.602	36.38	1.296	-.019	25.19	.549	39.50
1.158	-.021	22.51	.601	36.42	1.298	-.019	25.23	.548	39.55
1.160	-.021	22.55	.600	36.47	1.300	-.018	25.27	.547	39.59
1.162	-.021	22.59	.600	36.52	1.302	-.018	25.31	.546	39.63
1.164	-.021	22.62	.599	36.56	1.304	-.018	25.34	.546	39.67
1.166	-.021	22.66	.598	36.61	1.306	-.018	25.38	.545	39.72
1.168	-.021	22.70	.597	36.66	1.308	-.018	25.42	.544	39.76
1.170	-.021	22.74	.596	36.70	1.310	-.018	25.46	.544	39.80
1.172	-.021	22.78	.596	36.75	1.312	-.018	25.50	.543	39.84
1.174	-.020	22.82	.595	36.79	1.314	-.018	25.54	.542	39.89
1.176	-.020	22.86	.594	36.84	1.316	-.018	25.58	.541	39.93
1.178	-.020	22.90	.593	36.89	1.318	-.018	25.62	.541	39.97
1.180	-.020	22.93	.592	36.93	1.320	-.018	25.66	.540	40.01
1.182	-.020	22.97	.592	36.98	1.322	-.018	25.69	.539	40.05
1.184	-.020	23.01	.591	37.03	1.324	-.018	25.73	.539	40.10
1.186	-.020	23.05	.590	37.07	1.326	-.018	25.77	.538	40.14
1.188	-.020	23.09	.589	37.12	1.328	-.018	25.81	.537	40.18
1.190	-.020	23.13	.588	37.16	1.330	-.018	25.85	.536	40.22
1.192	-.020	23.17	.588	37.21	1.332	-.018	25.89	.536	40.26
1.194	-.020	23.21	.587	37.25	1.334	-.018	25.93	.535	40.30
1.196	-.020	23.25	.586	37.30	1.336	-.018	25.97	.534	40.35
1.198	-.020	23.28	.585	37.35	1.338	-.018	26.01	.534	40.39
1.200	-.020	23.32	.585	37.39	1.340	-.018	26.04	.533	40.43
1.202	-.020	23.36	.584	37.44	1.342	-.018	26.08	.532	40.47
1.204	-.020	23.40	.583	37.48	1.344	-.018	26.12	.532	40.51
1.206	-.020	23.44	.582	37.53	1.346	-.018	26.16	.531	40.55
1.208	-.020	23.48	.581	37.57	1.348	-.018	26.20	.530	40.59
1.210	-.020	23.52	.581	37.62	1.350	-.018	26.24	.529	40.64
1.212	-.020	23.56	.580	37.66	1.352	-.018	26.28	.529	40.68
1.214	-.020	23.60	.579	37.71	1.354	-.018	26.32	.528	40.72
1.216	-.020	23.63	.578	37.75	1.356	-.018	26.36	.527	40.76
1.218	-.020	23.67	.578	37.80	1.358	-.018	26.39	.527	40.80
1.220	-.020	23.71	.577	37.84	1.360	-.018	26.43	.526	40.84
1.222	-.020	23.75	.576	37.89	1.362	-.018	26.47	.525	40.88
1.224	-.020	23.79	.575	37.93	1.364	-.018	26.51	.525	40.92
1.226	-.020	23.83	.575	37.98	1.366	-.018	26.55	.524	40.96
1.228	-.020	23.87	.574	38.02	1.368	-.018	26.59	.523	41.00
1.230	-.020	23.91	.573	38.07	1.370	-.018	26.63	.523	41.04
1.232	-.020	23.95	.572	38.11	1.372	-.018	26.67	.522	41.08
1.234	-.019	23.98	.571	38.15	1.374	-.018	26.71	.521	41.13
1.236	-.019	24.02	.571	38.20	1.376	-.017	26.74	.521	41.17
1.238	-.019	24.06	.570	38.24	1.378	-.017	26.78	.520	41.21
1.240	-.019	24.10	.569	38.29	1.380	-.017	26.82	.519	41.25
1.242	-.019	24.14	.568	38.33	1.382	-.017	26.86	.519	41.29
1.244	-.019	24.18	.568	38.38	1.384	-.017	26.90	.518	41.33
1.246	-.019	24.22	.567	38.42	1.386	-.017	26.94	.517	41.37
1.248	-.019	24.26	.566	38.46	1.388	-.017	26.98	.517	41.41
1.250	-.019	24.30	.565	38.51	1.390	-.017	27.02	.516	41.45
1.252	-.019	24.33	.565	38.55	1.392	-.017	27.06	.515	41.49
1.254	-.019	24.37	.564	38.60	1.394	-.017	27.09	.515	41.53
1.256	-.019	24.41	.563	38.64	1.396	-.017	27.13	.514	41.57
1.258	-.019	24.45	.562	38.68	1.398	-.017	27.17	.513	41.61
1.260	-.019	24.49	.562	38.73	1.400	-.017	27.21	.512	41.65

TABLE A.IV.2 (CONTINUED)

τ (s)	$\tilde{L}_o$	$\tilde{t}_D$	$\tilde{K}_M$	$\tilde{D}$	τ (s)	$\tilde{L}_o$	$\tilde{t}_D$	$\tilde{K}_M$	$\tilde{D}$
1.400	-.017	27.21	.512	41.65	1.540	-.016	29.93	.468	44.31
1.402	-.017	27.25	.512	41.69	1.542	-.016	29.97	.467	44.35
1.404	-.017	27.29	.511	41.73	1.544	-.016	30.01	.467	44.39
1.406	-.017	27.33	.511	41.77	1.546	-.016	30.05	.466	44.42
1.408	-.017	27.37	.510	41.81	1.548	-.016	30.09	.466	44.46
1.410	-.017	27.41	.509	41.85	1.550	-.016	30.13	.465	44.50
1.412	-.017	27.44	.509	41.89	1.552	-.015	30.17	.464	44.53
1.414	-.017	27.48	.508	41.93	1.554	-.015	30.20	.464	44.57
1.416	-.017	27.52	.507	41.96	1.556	-.015	30.24	.463	44.60
1.418	-.017	27.56	.507	42.00	1.558	-.015	30.28	.463	44.64
1.420	-.017	27.60	.506	42.04	1.560	-.015	30.32	.462	44.68
1.422	-.017	27.64	.505	42.08	1.562	-.015	30.36	.461	44.71
1.424	-.017	27.68	.505	42.12	1.564	-.015	30.40	.461	44.75
1.426	-.017	27.72	.504	42.16	1.566	-.015	30.44	.460	44.78
1.428	-.017	27.76	.503	42.20	1.568	-.015	30.48	.460	44.82
1.430	-.017	27.79	.503	42.24	1.570	-.015	30.52	.459	44.85
1.432	-.017	27.83	.502	42.28	1.572	-.015	30.55	.458	44.89
1.434	-.017	27.87	.501	42.32	1.574	-.015	30.59	.458	44.93
1.436	-.017	27.91	.501	42.36	1.576	-.015	30.63	.457	44.96
1.438	-.017	27.95	.500	42.40	1.578	-.015	30.67	.457	45.00
1.440	-.017	27.99	.499	42.43	1.580	-.015	30.71	.456	45.03
1.442	-.017	28.03	.499	42.47	1.582	-.015	30.75	.455	45.07
1.444	-.017	28.07	.498	42.51	1.584	-.015	30.79	.455	45.10
1.446	-.017	28.10	.497	42.55	1.586	-.015	30.83	.454	45.14
1.448	-.017	28.14	.497	42.59	1.588	-.015	30.86	.454	45.17
1.450	-.017	28.18	.496	42.63	1.590	-.015	30.90	.453	45.21
1.452	-.017	28.22	.495	42.67	1.592	-.015	30.94	.452	45.24
1.454	-.017	28.26	.495	42.70	1.594	-.015	30.98	.452	45.28
1.456	-.017	28.30	.494	42.74	1.596	-.015	31.02	.451	45.31
1.458	-.016	28.34	.494	42.78	1.598	-.015	31.06	.451	45.35
1.460	-.016	28.38	.493	42.82	1.600	-.015	31.10	.450	45.38
1.462	-.016	28.42	.492	42.86	1.602	-.015	31.14	.450	45.42
1.464	-.016	28.45	.492	42.90	1.604	-.015	31.18	.449	45.45
1.466	-.016	28.49	.491	42.93	1.606	-.015	31.21	.448	45.49
1.468	-.016	28.53	.490	42.97	1.608	-.015	31.25	.448	45.52
1.470	-.016	28.57	.490	43.01	1.610	-.015	31.29	.447	45.56
1.472	-.016	28.61	.489	43.05	1.612	-.015	31.33	.447	45.59
1.474	-.016	28.65	.498	43.09	1.614	-.015	31.37	.446	45.63
1.476	-.016	28.69	.488	43.13	1.616	-.015	31.41	.445	45.66
1.478	-.016	28.73	.487	43.16	1.618	-.015	31.45	.445	45.70
1.480	-.016	28.77	.487	43.20	1.620	-.015	31.49	.444	45.73
1.482	-.016	28.80	.486	43.24	1.622	-.015	31.53	.444	45.77
1.484	-.016	28.84	.485	43.28	1.624	-.015	31.56	.443	45.80
1.486	-.016	28.88	.485	43.31	1.626	-.015	31.60	.443	45.84
1.488	-.016	28.92	.484	43.35	1.628	-.015	31.64	.442	45.87
1.490	-.016	28.96	.483	43.39	1.630	-.015	31.68	.441	45.90
1.492	-.016	29.00	.483	43.43	1.632	-.015	31.72	.441	45.94
1.494	-.016	29.04	.482	43.46	1.634	-.015	31.76	.440	45.97
1.496	-.016	29.08	.482	43.50	1.636	-.015	31.80	.440	46.01
1.498	-.016	29.12	.481	43.54	1.638	-.015	31.84	.439	46.04
1.500	-.016	29.15	.480	43.58	1.640	-.015	31.88	.439	46.08
1.502	-.016	29.19	.480	43.61	1.642	-.015	31.91	.438	46.11
1.504	-.016	29.23	.479	43.65	1.644	-.015	31.95	.437	46.14
1.506	-.016	29.27	.478	43.69	1.646	-.015	31.99	.437	46.18
1.508	-.016	29.31	.478	43.73	1.648	-.015	32.03	.436	46.21
1.510	-.016	29.35	.477	43.76	1.650	-.015	32.07	.436	46.25
1.512	-.016	29.39	.477	43.80	1.652	-.015	32.11	.435	46.28
1.514	-.016	29.43	.476	43.84	1.654	-.015	32.15	.435	46.31
1.516	-.016	29.47	.475	43.87	1.656	-.015	32.19	.434	46.35
1.518	-.016	29.50	.475	43.91	1.658	-.015	32.23	.433	46.38
1.520	-.016	29.54	.474	43.95	1.660	-.014	32.26	.433	46.41
1.522	-.016	29.58	.473	43.98	1.662	-.014	32.30	.432	46.45
1.524	-.016	29.62	.473	44.02	1.664	-.014	32.34	.432	46.48
1.526	-.016	29.66	.472	44.06	1.666	-.014	32.38	.431	46.51
1.528	-.016	29.70	.472	44.09	1.668	-.014	32.42	.431	46.55
1.530	-.016	29.74	.471	44.13	1.670	-.014	32.46	.430	46.58
1.532	-.016	29.78	.470	44.17	1.672	-.014	32.50	.430	46.62
1.534	-.016	29.82	.470	44.20	1.674	-.014	32.54	.429	46.65
1.536	-.016	29.85	.469	44.24	1.676	-.014	32.58	.428	46.68
1.538	-.016	29.89	.469	44.28	1.678	-.014	32.61	.428	46.72
1.540	-.016	29.93	.468	44.31	1.680	-.014	32.65	.427	46.75

TABLE A.IV.2 (CONTINUED)

τ (s)	$\tilde{L}_c$	$\tilde{t}_D$	$\tilde{K}_M$	$\tilde{D}$	τ (s)	$\tilde{L}_o$	$\tilde{t}_D$	$\tilde{K}_M$	$\tilde{D}$
1.680	-.014	32.65	.427	46.75	1.820	-.013	35.37	.390	48.97
1.682	-.014	32.69	.427	46.78	1.822	-.013	35.41	.389	49.00
1.684	-.014	32.73	.426	46.81	1.824	-.013	35.45	.389	49.03
1.686	-.014	32.77	.426	46.85	1.826	-.013	35.49	.388	49.06
1.688	-.014	32.81	.425	46.88	1.828	-.013	35.53	.388	49.09
1.690	-.014	32.85	.425	46.91	1.830	-.013	35.57	.387	49.12
1.692	-.014	32.89	.424	46.95	1.832	-.013	35.61	.387	49.15
1.694	-.014	32.93	.423	46.98	1.834	-.013	35.65	.386	49.18
1.696	-.014	32.96	.423	47.01	1.836	-.013	35.69	.386	49.21
1.698	-.014	33.00	.422	47.05	1.838	-.013	35.72	.385	49.24
1.700	-.014	33.04	.422	47.08	1.840	-.013	35.76	.385	49.27
1.702	-.014	33.08	.421	47.11	1.842	-.013	35.80	.384	49.30
1.704	-.014	33.12	.421	47.14	1.844	-.013	35.84	.384	49.33
1.706	-.014	33.16	.420	47.18	1.846	-.013	35.88	.383	49.36
1.708	-.014	33.20	.420	47.21	1.848	-.013	35.92	.383	49.39
1.710	-.014	33.24	.419	47.24	1.850	-.013	35.96	.382	49.42
1.712	-.014	33.28	.418	47.27	1.852	-.013	36.00	.382	49.45
1.714	-.014	33.31	.418	47.31	1.854	-.013	36.03	.381	49.48
1.716	-.014	33.35	.417	47.34	1.856	-.013	36.07	.381	49.51
1.718	-.014	33.39	.417	47.37	1.858	-.013	36.11	.380	49.54
1.720	-.014	33.43	.416	47.40	1.860	-.013	36.15	.380	49.57
1.722	-.014	33.47	.416	47.44	1.862	-.013	36.19	.379	49.60
1.724	-.014	33.51	.415	47.47	1.864	-.013	36.23	.379	49.63
1.726	-.014	33.55	.415	47.50	1.866	-.013	36.27	.378	49.66
1.728	-.014	33.59	.414	47.53	1.868	-.013	36.31	.378	49.69
1.730	-.014	33.62	.414	47.57	1.870	-.013	36.35	.377	49.72
1.732	-.014	33.66	.413	47.60	1.872	-.013	36.38	.377	49.75
1.734	-.014	33.70	.413	47.63	1.874	-.013	36.42	.376	49.77
1.736	-.014	33.74	.412	47.66	1.876	-.013	36.46	.376	49.80
1.738	-.014	33.78	.411	47.69	1.878	-.013	36.50	.375	49.83
1.740	-.014	33.82	.411	47.73	1.880	-.013	36.54	.375	49.86
1.742	-.014	33.86	.410	47.76	1.882	-.013	36.58	.374	49.89
1.744	-.014	33.90	.410	47.79	1.884	-.013	36.62	.374	49.92
1.746	-.014	33.94	.409	47.82	1.886	-.013	36.66	.373	49.95
1.748	-.014	33.97	.409	47.85	1.888	-.013	36.70	.373	49.98
1.750	-.014	34.01	.408	47.88	1.890	-.013	36.73	.372	50.01
1.752	-.014	34.05	.408	47.92	1.892	-.013	36.77	.372	50.04
1.754	-.014	34.09	.407	47.95	1.894	-.013	36.81	.371	50.07
1.756	-.014	34.13	.407	47.98	1.896	-.013	36.85	.371	50.09
1.758	-.014	34.17	.406	48.01	1.898	-.013	36.89	.370	50.12
1.760	-.014	34.21	.406	48.04	1.900	-.013	36.93	.370	50.15
1.762	-.014	34.25	.405	48.07	1.902	-.013	36.97	.369	50.18
1.764	-.014	34.29	.404	48.11	1.904	-.013	37.01	.369	50.21
1.766	-.014	34.32	.404	48.14	1.906	-.013	37.05	.368	50.24
1.768	-.014	34.36	.403	48.17	1.908	-.013	37.08	.368	50.27
1.770	-.014	34.40	.403	48.20	1.910	-.013	37.12	.367	50.29
1.772	-.014	34.44	.402	48.23	1.912	-.013	37.16	.367	50.32
1.774	-.014	34.48	.402	48.26	1.914	-.013	37.20	.366	50.35
1.776	-.014	34.52	.401	48.29	1.916	-.013	37.24	.366	50.38
1.778	-.014	34.56	.401	48.33	1.918	-.013	37.28	.365	50.41
1.780	-.014	34.60	.400	48.36	1.920	-.013	37.32	.365	50.44
1.782	-.013	34.64	.400	48.39	1.922	-.013	37.36	.364	50.47
1.784	-.013	34.67	.399	48.42	1.924	-.012	37.40	.364	50.49
1.786	-.013	34.71	.399	48.45	1.926	-.012	37.43	.363	50.52
1.788	-.013	34.75	.398	48.48	1.928	-.012	37.47	.363	50.55
1.790	-.013	34.79	.398	48.51	1.930	-.012	37.51	.362	50.58
1.792	-.013	34.83	.397	48.54	1.932	-.012	37.55	.362	50.61
1.794	-.013	34.87	.397	48.57	1.934	-.012	37.59	.361	50.63
1.796	-.013	34.91	.396	48.60	1.936	-.012	37.63	.361	50.66
1.798	-.013	34.95	.396	48.63	1.938	-.012	37.67	.361	50.69
1.800	-.013	34.99	.395	48.67	1.940	-.012	37.71	.360	50.72
1.802	-.013	35.02	.395	48.70	1.942	-.012	37.75	.360	50.75
1.804	-.013	35.06	.394	48.73	1.944	-.012	37.78	.359	50.77
1.806	-.013	35.10	.393	48.76	1.946	-.012	37.82	.359	50.80
1.808	-.013	35.14	.393	48.79	1.948	-.012	37.86	.358	50.83
1.810	-.013	35.18	.392	48.82	1.950	-.012	37.90	.358	50.86
1.812	-.013	35.22	.392	48.85	1.952	-.012	37.94	.357	50.89
1.814	-.013	35.26	.391	48.88	1.954	-.012	37.98	.357	50.91
1.816	-.013	35.30	.391	48.91	1.956	-.012	38.02	.356	50.94
1.818	-.013	35.34	.390	48.94	1.958	-.012	38.06	.356	50.97
1.820	-.013	35.37	.390	48.97	1.960	-.012	38.10	.355	51.00

TABLE A.IV.2 (CONTINUED)

τ (s)	$\tilde{L}_o$	$\tilde{t}_D$	$\tilde{K}_M$	$\tilde{D}$	τ (s)	$\tilde{L}_o$	$\tilde{t}_D$	$\tilde{K}_M$	$\tilde{D}$
1.960	-.012	38.10	.355	51.00	2.100	-.011	40.82	.323	52.84
1.962	-.012	38.13	.355	51.02	2.102	-.011	40.86	.323	52.87
1.964	-.012	38.17	.354	51.05	2.104	-.011	40.89	.322	52.89
1.966	-.012	38.21	.354	51.08	2.106	-.011	40.93	.322	52.92
1.968	-.012	38.25	.353	51.11	2.108	-.011	40.97	.321	52.94
1.970	-.012	38.29	.353	51.13	2.110	-.011	41.01	.321	52.97
1.972	-.012	38.33	.352	51.16	2.112	-.011	41.05	.320	52.99
1.974	-.012	38.37	.352	51.19	2.114	-.011	41.09	.320	53.02
1.976	-.012	38.41	.351	51.22	2.116	-.011	41.13	.319	53.04
1.978	-.012	38.45	.351	51.24	2.118	-.011	41.17	.319	53.07
1.980	-.012	38.48	.351	51.27	2.120	-.011	41.21	.319	53.09
1.982	-.012	38.52	.350	51.30	2.122	-.011	41.24	.318	53.12
1.984	-.012	38.56	.350	51.33	2.124	-.011	41.28	.318	53.14
1.986	-.012	38.60	.349	51.35	2.126	-.011	41.32	.317	53.17
1.988	-.012	38.64	.349	51.38	2.128	-.011	41.36	.317	53.19
1.990	-.012	38.68	.348	51.41	2.130	-.011	41.40	.316	53.21
1.992	-.012	38.72	.348	51.43	2.132	-.011	41.44	.316	53.24
1.994	-.012	38.76	.347	51.46	2.134	-.011	41.48	.316	53.26
1.996	-.012	38.79	.347	51.49	2.136	-.011	41.52	.315	53.29
1.998	-.012	38.83	.346	51.52	2.138	-.011	41.55	.315	53.31
2.000	-.012	38.87	.346	51.54	2.140	-.011	41.59	.314	53.34
2.002	-.012	38.91	.345	51.57	2.142	-.011	41.63	.314	53.36
2.004	-.012	38.95	.345	51.60	2.144	-.011	41.67	.313	53.39
2.006	-.012	38.99	.344	51.62	2.146	-.011	41.71	.313	53.41
2.008	-.012	39.03	.344	51.65	2.148	-.011	41.75	.312	53.43
2.010	-.012	39.07	.343	51.68	2.150	-.011	41.79	.312	53.46
2.012	-.012	39.11	.343	51.70	2.152	-.011	41.83	.312	53.48
2.014	-.012	39.14	.343	51.73	2.154	-.011	41.87	.311	53.51
2.016	-.012	39.18	.342	51.76	2.156	-.011	41.90	.311	53.53
2.018	-.012	39.22	.342	51.78	2.158	-.011	41.94	.310	53.56
2.020	-.012	39.26	.341	51.81	2.160	-.011	41.98	.310	53.58
2.022	-.012	39.30	.341	51.84	2.162	-.011	42.02	.309	53.60
2.024	-.012	39.34	.340	51.86	2.164	-.011	42.06	.309	53.63
2.026	-.012	39.38	.340	51.89	2.166	-.011	42.10	.309	53.65
2.028	-.012	39.42	.339	51.91	2.168	-.011	42.14	.308	53.68
2.030	-.012	39.46	.339	51.94	2.170	-.011	42.18	.308	53.70
2.032	-.012	39.49	.338	51.97	2.172	-.011	42.22	.307	53.72
2.034	-.012	39.53	.338	51.99	2.174	-.011	42.25	.307	53.75
2.036	-.012	39.57	.337	52.02	2.176	-.011	42.29	.306	53.77
2.038	-.012	39.61	.337	52.05	2.178	-.011	42.33	.306	53.79
2.040	-.012	39.65	.337	52.07	2.180	-.011	42.37	.306	53.82
2.042	-.012	39.69	.336	52.10	2.182	-.011	42.41	.305	53.84
2.044	-.012	39.73	.336	52.12	2.184	-.011	42.45	.305	53.87
2.046	-.012	39.77	.335	52.15	2.186	-.011	42.49	.304	53.89
2.048	-.012	39.81	.335	52.18	2.188	-.011	42.53	.304	53.91
2.050	-.012	39.84	.334	52.20	2.190	-.011	42.57	.303	53.94
2.052	-.012	39.88	.334	52.23	2.192	-.011	42.60	.303	53.96
2.054	-.012	39.92	.333	52.25	2.194	-.011	42.64	.303	53.98
2.056	-.012	39.96	.333	52.28	2.196	-.011	42.68	.302	54.01
2.058	-.012	40.00	.332	52.31	2.198	-.011	42.72	.302	54.03
2.060	-.012	40.04	.332	52.33	2.200	-.011	42.76	.301	54.05
2.062	-.012	40.08	.332	52.36	2.202	-.011	42.80	.301	54.08
2.064	-.012	40.12	.331	52.38	2.204	-.011	42.84	.300	54.10
2.066	-.012	40.16	.331	52.41	2.206	-.011	42.88	.300	54.12
2.068	-.012	40.19	.330	52.44	2.208	-.011	42.92	.300	54.15
2.070	-.012	40.23	.330	52.46	2.210	-.011	42.95	.299	54.17
2.072	-.012	40.27	.329	52.49	2.212	-.011	42.99	.299	54.19
2.074	-.012	40.31	.329	52.51	2.214	-.011	43.03	.298	54.22
2.076	-.012	40.35	.328	52.54	2.216	-.011	43.07	.298	54.24
2.078	-.012	40.39	.328	52.56	2.218	-.011	43.11	.297	54.26
2.080	-.012	40.43	.327	52.59	2.220	-.011	43.15	.297	54.29
2.082	-.012	40.47	.327	52.61	2.222	-.011	43.19	.297	54.31
2.084	-.012	40.51	.327	52.64	2.224	-.011	43.23	.296	54.33
2.086	-.012	40.54	.326	52.66	2.226	-.011	43.27	.296	54.36
2.088	-.012	40.58	.326	52.69	2.228	-.011	43.30	.295	54.38
2.090	-.012	40.62	.325	52.72	2.230	-.011	43.34	.295	54.40
2.092	-.011	40.66	.325	52.74	2.232	-.011	43.38	.295	54.43
2.094	-.011	40.70	.324	52.77	2.234	-.011	43.42	.294	54.45
2.096	-.011	40.74	.324	52.79	2.236	-.011	43.46	.294	54.47
2.098	-.011	40.78	.323	52.82	2.238	-.011	43.50	.293	54.49
2.100	-.011	40.82	.323	52.84	2.240	-.011	43.54	.293	54.52

TABLE A.IV.2 (CONTINUED)

τ (s)	$\tilde{L}_o$	$\tilde{t}_D$	$\tilde{K}_M$	$\tilde{D}$	τ (s)	$\tilde{L}_o$	$\tilde{t}_D$	$\tilde{K}_M$	$\tilde{D}$
2.240	-.011	43.54	.293	54.52	2.380	-.010	46.26	.265	56.03
2.242	-.011	43.58	.292	54.54	2.382	-.010	46.30	.264	56.05
2.244	-.011	43.62	.292	54.56	2.384	-.010	46.34	.264	56.07
2.246	-.011	43.65	.292	54.58	2.386	-.010	46.38	.263	56.09
2.248	-.011	43.69	.291	54.61	2.388	-.010	46.41	.263	56.11
2.250	-.011	43.73	.291	54.63	2.390	-.010	46.45	.263	56.13
2.252	-.011	43.77	.290	54.65	2.392	-.010	46.49	.262	56.16
2.254	-.011	43.81	.290	54.68	2.394	-.010	46.53	.262	56.18
2.256	-.011	43.85	.290	54.70	2.396	-.010	46.57	.261	56.20
2.258	-.011	43.89	.289	54.72	2.398	-.010	46.61	.261	56.22
2.260	-.011	43.93	.289	54.74	2.400	-.010	46.65	.261	56.24
2.262	-.011	43.97	.288	54.76	2.402	-.010	46.69	.260	56.26
2.264	-.011	44.00	.288	54.79	2.404	-.010	46.72	.260	56.28
2.266	-.011	44.04	.287	54.81	2.406	-.010	46.76	.259	56.30
2.268	-.011	44.08	.287	54.83	2.408	-.010	46.80	.259	56.32
2.270	-.011	44.12	.287	54.85	2.410	-.010	46.84	.259	56.34
2.272	-.011	44.16	.286	54.88	2.412	-.010	46.88	.258	56.36
2.274	-.011	44.20	.286	54.90	2.414	-.010	46.92	.258	56.38
2.276	-.011	44.24	.285	54.92	2.416	-.010	46.96	.257	56.40
2.278	-.011	44.28	.285	54.94	2.418	-.010	47.00	.257	56.42
2.280	-.011	44.31	.285	54.97	2.420	-.010	47.04	.257	56.44
2.282	-.011	44.35	.284	54.99	2.422	-.010	47.07	.256	56.46
2.284	-.011	44.39	.284	55.01	2.424	-.010	47.11	.256	56.48
2.286	-.011	44.43	.283	55.03	2.426	-.010	47.15	.256	56.50
2.288	-.011	44.47	.283	55.05	2.428	-.010	47.19	.255	56.52
2.290	-.011	44.51	.283	55.08	2.430	-.010	47.23	.255	56.54
2.292	-.010	44.55	.282	55.10	2.432	-.010	47.27	.254	56.56
2.294	-.010	44.59	.282	55.12	2.434	-.010	47.31	.254	56.58
2.296	-.010	44.63	.281	55.14	2.436	-.010	47.35	.254	56.60
2.298	-.010	44.66	.281	55.16	2.438	-.010	47.39	.253	56.62
2.300	-.010	44.70	.280	55.18	2.440	-.010	47.42	.253	56.64
2.302	-.010	44.74	.280	55.21	2.442	-.010	47.46	.252	56.66
2.304	-.010	44.78	.280	55.23	2.444	-.010	47.50	.252	56.67
2.306	-.010	44.82	.279	55.25	2.446	-.010	47.54	.252	56.69
2.308	-.010	44.86	.279	55.27	2.448	-.010	47.58	.251	56.71
2.310	-.010	44.90	.278	55.29	2.450	-.010	47.62	.251	56.73
2.312	-.010	44.94	.278	55.32	2.452	-.010	47.66	.251	56.75
2.314	-.010	44.98	.278	55.34	2.454	-.010	47.70	.250	56.77
2.316	-.010	45.01	.277	55.36	2.456	-.010	47.74	.250	56.79
2.318	-.010	45.05	.277	55.38	2.458	-.010	47.77	.249	56.81
2.320	-.010	45.09	.276	55.40	2.460	-.010	47.81	.249	56.83
2.322	-.010	45.13	.276	55.42	2.462	-.010	47.85	.249	56.85
2.324	-.010	45.17	.276	55.44	2.464	-.010	47.89	.248	56.87
2.326	-.010	45.21	.275	55.47	2.466	-.010	47.93	.248	56.89
2.328	-.010	45.25	.275	55.49	2.468	-.010	47.97	.248	56.91
2.330	-.010	45.29	.274	55.51	2.470	-.010	48.01	.247	56.93
2.332	-.010	45.33	.274	55.53	2.472	-.010	48.05	.247	56.95
2.334	-.010	45.36	.274	55.55	2.474	-.010	48.09	.246	56.97
2.336	-.010	45.40	.273	55.57	2.476	-.010	48.12	.246	56.98
2.338	-.010	45.44	.273	55.59	2.478	-.010	48.16	.246	57.00
2.340	-.010	45.48	.272	55.61	2.480	-.010	48.20	.245	57.02
2.342	-.010	45.52	.272	55.64	2.482	-.010	48.24	.245	57.04
2.344	-.010	45.56	.272	55.66	2.484	-.010	48.28	.245	57.06
2.346	-.010	45.60	.271	55.68	2.486	-.010	48.32	.244	57.08
2.348	-.010	45.64	.271	55.70	2.488	-.010	48.36	.244	57.10
2.350	-.010	45.68	.270	55.72	2.490	-.010	48.40	.243	57.12
2.352	-.010	45.71	.270	55.74	2.492	-.010	48.44	.243	57.14
2.354	-.010	45.75	.270	55.76	2.494	-.010	48.47	.243	57.16
2.356	-.010	45.79	.269	55.78	2.496	-.010	48.51	.242	57.17
2.358	-.010	45.83	.269	55.80	2.498	-.010	48.55	.242	57.19
2.360	-.010	45.87	.268	55.83	2.500	-.010	48.59	.242	57.21
2.362	-.010	45.91	.268	55.85	2.502	-.010	48.63	.241	57.23
2.364	-.010	45.95	.268	55.87	2.504	-.010	48.67	.241	57.25
2.366	-.010	45.99	.267	55.89	2.506	-.010	48.71	.240	57.27
2.368	-.010	46.03	.267	55.91	2.508	-.010	48.75	.240	57.29
2.370	-.010	46.06	.266	55.93	2.510	-.010	48.79	.240	57.31
2.372	-.010	46.10	.266	55.95	2.512	-.010	48.82	.239	57.32
2.374	-.010	46.14	.266	55.97	2.514	-.010	48.86	.239	57.34
2.376	-.010	46.18	.265	55.99	2.516	-.010	48.90	.239	57.36
2.378	-.010	46.22	.265	56.01	2.518	-.010	48.94	.238	57.38
2.380	-.010	46.26	.265	56.03	2.520	-.010	48.98	.238	57.40

TABLE A.IV.2 (CONTINUED)

τ (s)	$\tilde{L}_o$	$\tilde{t}_D$	$\tilde{K}_M$	$\tilde{D}$	τ (s)	$\tilde{L}_o$	$\tilde{t}_D$	$\tilde{K}_M$	$\tilde{D}$
2.520	-.010	48.98	.238	57.40	2.660	-.009	51.70	.213	58.62
2.522	-.010	49.02	.237	57.42	2.662	-.009	51.74	.212	58.64
2.524	-.010	49.06	.237	57.44	2.664	-.009	51.78	.212	58.66
2.526	-.010	49.10	.237	57.45	2.666	-.009	51.82	.211	58.67
2.528	-.010	49.14	.236	57.47	2.668	-.009	51.86	.211	58.69
2.530	-.010	49.17	.236	57.49	2.670	-.009	51.90	.211	58.71
2.532	-.009	49.21	.236	57.51	2.672	-.009	51.93	.210	58.72
2.534	-.009	49.25	.235	57.53	2.674	-.009	51.97	.210	58.74
2.536	-.009	49.29	.235	57.55	2.676	-.009	52.01	.210	58.75
2.538	-.009	49.33	.234	57.56	2.678	-.009	52.05	.209	58.77
2.540	-.009	49.37	.234	57.58	2.680	-.009	52.09	.209	58.79
2.542	-.009	49.41	.234	57.60	2.682	-.009	52.13	.209	58.80
2.544	-.009	49.45	.233	57.62	2.684	-.009	52.17	.208	58.82
2.546	-.009	49.48	.233	57.64	2.686	-.009	52.21	.208	58.84
2.548	-.009	49.52	.233	57.65	2.688	-.009	52.24	.208	58.85
2.550	-.009	49.56	.232	57.67	2.690	-.009	52.28	.207	58.87
2.552	-.009	49.60	.232	57.69	2.692	-.009	52.32	.207	58.88
2.554	-.009	49.64	.232	57.71	2.694	-.009	52.36	.207	58.90
2.556	-.009	49.68	.231	57.73	2.696	-.009	52.40	.206	58.92
2.558	-.009	49.72	.231	57.74	2.698	-.009	52.44	.206	58.93
2.560	-.009	49.76	.230	57.76	2.700	-.009	52.48	.206	58.95
2.562	-.009	49.80	.230	57.78	2.702	-.009	52.52	.205	58.96
2.564	-.009	49.83	.230	57.80	2.704	-.009	52.56	.205	58.98
2.566	-.009	49.87	.229	57.82	2.706	-.009	52.59	.205	59.00
2.568	-.009	49.91	.229	57.83	2.708	-.009	52.63	.204	59.01
2.570	-.009	49.95	.229	57.85	2.710	-.009	52.67	.204	59.03
2.572	-.009	49.99	.228	57.87	2.712	-.009	52.71	.203	59.04
2.574	-.009	50.03	.228	57.89	2.714	-.009	52.75	.203	59.06
2.576	-.009	50.07	.228	57.90	2.716	-.009	52.79	.203	59.08
2.578	-.009	50.11	.227	57.92	2.718	-.009	52.83	.202	59.09
2.580	-.009	50.15	.227	57.94	2.720	-.009	52.87	.202	59.11
2.582	-.009	50.18	.226	57.96	2.722	-.009	52.91	.202	59.12
2.584	-.009	50.22	.226	57.98	2.724	-.009	52.94	.201	59.14
2.586	-.009	50.26	.226	57.99	2.726	-.009	52.98	.201	59.15
2.588	-.009	50.30	.225	58.01	2.728	-.009	53.02	.201	59.17
2.590	-.009	50.34	.225	58.03	2.730	-.009	53.06	.200	59.18
2.592	-.009	50.38	.225	58.05	2.732	-.009	53.10	.200	59.20
2.594	-.009	50.42	.224	58.06	2.734	-.009	53.14	.200	59.22
2.596	-.009	50.46	.224	58.08	2.736	-.009	53.18	.199	59.23
2.598	-.009	50.50	.224	58.10	2.738	-.009	53.22	.199	59.25
2.600	-.009	50.53	.223	58.12	2.740	-.009	53.26	.199	59.26
2.602	-.009	50.57	.223	58.13	2.742	-.009	53.29	.198	59.28
2.604	-.009	50.61	.222	58.15	2.744	-.009	53.33	.198	59.29
2.606	-.009	50.65	.222	58.17	2.746	-.009	53.37	.198	59.31
2.608	-.009	50.69	.222	58.18	2.748	-.009	53.41	.197	59.32
2.610	-.009	50.73	.221	58.20	2.750	-.009	53.45	.197	59.34
2.612	-.009	50.77	.221	58.22	2.752	-.009	53.49	.197	59.35
2.614	-.009	50.81	.221	58.24	2.754	-.009	53.53	.196	59.37
2.616	-.009	50.85	.220	58.25	2.756	-.009	53.57	.196	59.39
2.618	-.009	50.88	.220	58.27	2.758	-.009	53.61	.196	59.40
2.620	-.009	50.92	.220	58.29	2.760	-.009	53.64	.195	59.42
2.622	-.009	50.96	.219	58.30	2.762	-.009	53.68	.195	59.43
2.624	-.009	51.00	.219	58.32	2.764	-.009	53.72	.195	59.45
2.626	-.009	51.04	.219	58.34	2.766	-.009	53.76	.194	59.46
2.628	-.009	51.08	.218	58.36	2.768	-.009	53.80	.194	59.48
2.630	-.009	51.12	.218	58.37	2.770	-.009	53.84	.194	59.49
2.632	-.009	51.16	.217	58.39	2.772	-.009	53.88	.193	59.51
2.634	-.009	51.20	.217	58.41	2.774	-.009	53.92	.193	59.52
2.636	-.009	51.23	.217	58.42	2.776	-.009	53.96	.193	59.54
2.638	-.009	51.27	.216	58.44	2.778	-.009	53.99	.192	59.55
2.640	-.009	51.31	.216	58.46	2.780	-.009	54.03	.192	59.57
2.642	-.009	51.35	.216	58.47	2.782	-.009	54.07	.192	59.58
2.644	-.009	51.39	.215	58.49	2.784	-.009	54.11	.191	59.60
2.646	-.009	51.43	.215	58.51	2.786	-.009	54.15	.191	59.61
2.648	-.009	51.47	.215	58.52	2.788	-.009	54.19	.191	59.63
2.650	-.009	51.51	.214	58.54	2.790	-.009	54.23	.190	59.64
2.652	-.009	51.55	.214	58.56	2.792	-.009	54.27	.190	59.66
2.654	-.009	51.58	.214	58.57	2.794	-.009	54.31	.190	59.67
2.656	-.009	51.62	.213	58.59	2.796	-.009	54.34	.189	59.68
2.658	-.009	51.66	.213	58.61	2.798	-.009	54.38	.189	59.70
2.660	-.009	51.70	.213	58.62	2.800	-.009	54.42	.189	59.71

TABLE A.IV.2 (CONTINUED)

τ (s)	$\tilde{L}_o$	$\tilde{t}_D$	$\tilde{K}_M$	$\tilde{D}$	τ (s)	$\tilde{L}_o$	$\tilde{t}_D$	$\tilde{K}_M$	$\tilde{D}$
2.800	-.009	54.42	.189	59.71	2.940	-.008	57.14	.166	60.68
2.802	-.009	54.46	.188	59.73	2.942	-.008	57.18	.165	60.69
2.804	-.009	54.50	.188	59.74	2.944	-.008	57.22	.165	60.70
2.806	-.009	54.54	.188	59.76	2.946	-.008	57.26	.165	60.72
2.808	-.009	54.58	.187	59.77	2.948	-.008	57.30	.164	60.73
2.810	-.009	54.62	.187	59.79	2.950	-.008	57.34	.164	60.74
2.812	-.009	54.66	.187	59.80	2.952	-.008	57.38	.164	60.75
2.814	-.009	54.69	.186	59.82	2.954	-.008	57.41	.164	60.77
2.816	-.009	54.73	.186	59.83	2.956	-.008	57.45	.163	60.78
2.818	-.009	54.77	.186	59.84	2.958	-.008	57.49	.163	60.79
2.820	-.009	54.81	.185	59.86	2.960	-.008	57.53	.163	60.81
2.822	-.009	54.85	.185	59.87	2.962	-.008	57.57	.162	60.82
2.824	-.009	54.89	.185	59.89	2.964	-.008	57.61	.162	60.83
2.826	-.009	54.93	.184	59.90	2.966	-.008	57.65	.162	60.84
2.828	-.009	54.97	.184	59.92	2.968	-.008	57.69	.161	60.86
2.830	-.008	55.00	.184	59.93	2.970	-.008	57.73	.161	60.87
2.832	-.008	55.04	.183	59.95	2.972	-.008	57.76	.161	60.88
2.834	-.008	55.08	.183	59.96	2.974	-.008	57.80	.160	60.89
2.836	-.008	55.12	.183	59.97	2.976	-.008	57.84	.160	60.91
2.838	-.008	55.16	.182	59.99	2.978	-.008	57.88	.160	60.92
2.840	-.008	55.20	.182	60.00	2.980	-.008	57.92	.159	60.93
2.842	-.008	55.24	.182	60.02	2.982	-.008	57.96	.159	60.94
2.844	-.008	55.28	.181	60.03	2.984	-.008	58.00	.159	60.96
2.846	-.008	55.32	.181	60.04	2.986	-.008	58.04	.159	60.97
2.848	-.008	55.35	.181	60.06	2.988	-.008	58.08	.158	60.98
2.850	-.008	55.39	.180	60.07	2.990	-.008	58.11	.158	60.99
2.852	-.008	55.43	.180	60.09	2.992	-.008	58.15	.158	61.00
2.854	-.008	55.47	.180	60.10	2.994	-.008	58.19	.157	61.02
2.856	-.008	55.51	.179	60.11	2.996	-.008	58.23	.157	61.03
2.858	-.008	55.55	.179	60.13	2.998	-.008	58.27	.157	61.04
2.860	-.008	55.59	.179	60.14	3.000	-.008	58.31	.156	61.05
2.862	-.008	55.63	.178	60.16	3.002	-.008	58.35	.156	61.07
2.864	-.008	55.67	.178	60.17	3.004	-.008	58.39	.156	61.08
2.866	-.008	55.70	.178	60.18	3.006	-.008	58.43	.155	61.09
2.868	-.008	55.74	.177	60.20	3.008	-.008	58.46	.155	61.10
2.870	-.008	55.78	.177	60.21	3.010	-.008	58.50	.155	61.11
2.872	-.008	55.82	.177	60.23	3.012	-.008	58.54	.154	61.13
2.874	-.008	55.86	.176	60.24	3.014	-.008	58.58	.154	61.14
2.876	-.008	55.90	.176	60.25	3.016	-.008	58.62	.154	61.15
2.878	-.008	55.94	.176	60.27	3.018	-.008	58.66	.154	61.16
2.880	-.008	55.98	.175	60.28	3.020	-.008	58.70	.153	61.17
2.882	-.008	56.02	.175	60.29	3.022	-.008	58.74	.153	61.19
2.884	-.008	56.05	.175	60.31	3.024	-.008	58.78	.153	61.20
2.886	-.008	56.09	.174	60.32	3.026	-.008	58.81	.152	61.21
2.888	-.008	56.13	.174	60.33	3.028	-.008	58.85	.152	61.22
2.890	-.008	56.17	.174	60.35	3.030	-.008	58.89	.152	61.23
2.892	-.008	56.21	.173	60.36	3.032	-.008	58.93	.151	61.24
2.894	-.008	56.25	.173	60.37	3.034	-.008	58.97	.151	61.26
2.896	-.008	56.29	.173	60.39	3.036	-.008	59.01	.151	61.27
2.898	-.008	56.33	.172	60.40	3.038	-.008	59.05	.150	61.28
2.900	-.008	56.37	.172	60.41	3.040	-.008	59.09	.150	61.29
2.902	-.008	56.40	.172	60.43	3.042	-.008	59.13	.150	61.30
2.904	-.008	56.44	.172	60.44	3.044	-.008	59.16	.150	61.31
2.906	-.008	56.48	.171	60.45	3.046	-.008	59.20	.149	61.33
2.908	-.008	56.52	.171	60.47	3.048	-.008	59.24	.149	61.34
2.910	-.008	56.56	.171	60.48	3.050	-.008	59.28	.149	61.35
2.912	-.008	56.60	.170	60.49	3.052	-.008	59.32	.148	61.36
2.914	-.008	56.64	.170	60.51	3.054	-.008	59.36	.148	61.37
2.916	-.008	56.68	.170	60.52	3.056	-.008	59.40	.148	61.38
2.918	-.008	56.72	.169	60.53	3.058	-.008	59.44	.147	61.40
2.920	-.008	56.75	.169	60.55	3.060	-.008	59.48	.147	61.41
2.922	-.008	56.79	.169	60.56	3.062	-.008	59.51	.147	61.42
2.924	-.008	56.83	.168	60.57	3.064	-.008	59.55	.146	61.43
2.926	-.008	56.87	.168	60.59	3.066	-.008	59.59	.146	61.44
2.928	-.008	56.91	.168	60.60	3.068	-.008	59.63	.146	61.45
2.930	-.008	56.95	.167	60.61	3.070	-.008	59.67	.146	61.46
2.932	-.008	56.99	.167	60.63	3.072	-.008	59.71	.145	61.48
2.934	-.008	57.03	.167	60.64	3.074	-.008	59.75	.145	61.49
2.936	-.008	57.07	.166	60.65	3.076	-.008	59.79	.145	61.50
2.938	-.008	57.10	.166	60.66	3.078	-.008	59.83	.144	61.51
2.940	-.008	57.14	.166	60.68	3.080	-.008	59.86	.144	61.52

TABLE A.IV.2 (CONTINUED)

τ (s)	$\tilde{L}_o$	$\tilde{t}_D$	$\tilde{K}_M$	$\tilde{D}$	τ (s)	$\tilde{L}_o$	$\tilde{t}_d$	$\tilde{K}_M$	$\tilde{D}$
3.080	-.008	59.86	.144	61.52	3.220	-.007	62.59	.123	62.25
3.082	-.008	59.90	.144	61.53	3.222	-.007	62.62	.123	62.26
3.084	-.008	59.94	.143	61.54	3.224	-.007	62.66	.123	62.27
3.086	-.008	59.98	.143	61.55	3.226	-.007	62.70	.122	62.28
3.088	-.008	60.02	.143	61.56	3.228	-.007	62.74	.122	62.29
3.090	-.008	60.06	.143	61.58	3.230	-.007	62.78	.122	62.29
3.092	-.008	60.10	.142	61.59	3.232	-.007	62.82	.122	62.30
3.094	-.008	60.14	.142	61.60	3.234	-.007	62.86	.121	62.31
3.096	-.008	60.17	.142	61.61	3.236	-.007	62.90	.121	62.32
3.098	-.008	60.21	.141	61.62	3.238	-.007	62.93	.121	62.33
3.100	-.008	60.25	.141	61.63	3.240	-.007	62.97	.120	62.34
3.102	-.008	60.29	.141	61.64	3.242	-.007	63.01	.120	62.35
3.104	-.008	60.33	.140	61.65	3.244	-.007	63.05	.120	62.36
3.106	-.008	60.37	.140	61.66	3.246	-.007	63.09	.119	62.37
3.108	-.008	60.41	.140	61.67	3.248	-.007	63.13	.119	62.38
3.110	-.008	60.45	.139	61.69	3.250	-.007	63.17	.119	62.39
3.112	-.008	60.49	.139	61.70	3.252	-.007	63.21	.119	62.40
3.114	-.008	60.52	.139	61.71	3.254	-.007	63.25	.118	62.41
3.116	-.008	60.56	.139	61.72	3.256	-.007	63.28	.118	62.42
3.118	-.008	60.60	.138	61.73	3.258	-.007	63.32	.118	62.42
3.120	-.008	60.64	.138	61.74	3.260	-.007	63.36	.117	62.43
3.122	-.008	60.68	.138	61.75	3.262	-.007	63.40	.117	62.44
3.124	-.008	60.72	.137	61.76	3.264	-.007	63.44	.117	62.45
3.126	-.008	60.76	.137	61.77	3.266	-.007	63.48	.117	62.46
3.128	-.008	60.80	.137	61.78	3.268	-.007	63.52	.116	62.47
3.130	-.008	60.84	.136	61.79	3.270	-.007	63.56	.116	62.48
3.132	-.008	60.87	.136	61.80	3.272	-.007	63.60	.116	62.49
3.134	-.008	60.91	.136	61.81	3.274	-.007	63.63	.115	62.50
3.136	-.008	60.95	.136	61.82	3.276	-.007	63.67	.115	62.51
3.138	-.008	60.99	.135	61.83	3.278	-.007	63.71	.115	62.52
3.140	-.008	61.03	.135	61.85	3.280	-.007	63.75	.115	62.52
3.142	-.008	61.07	.135	61.86	3.282	-.007	63.79	.114	62.53
3.144	-.008	61.11	.134	61.87	3.284	-.007	63.83	.114	62.54
3.146	-.008	61.15	.134	61.88	3.286	-.007	63.87	.114	62.55
3.148	-.008	61.19	.134	61.89	3.288	-.007	63.91	.113	62.56
3.150	-.008	61.22	.134	61.90	3.290	-.007	63.95	.113	62.57
3.152	-.008	61.26	.133	61.91	3.292	-.007	63.98	.113	62.58
3.154	-.008	61.30	.133	61.92	3.294	-.007	64.02	.113	62.59
3.156	-.008	61.34	.133	61.93	3.296	-.007	64.06	.112	62.59
3.158	-.008	61.38	.132	61.94	3.298	-.007	64.10	.112	62.60
3.160	-.008	61.42	.132	61.95	3.300	-.007	64.14	.112	62.61
3.162	-.008	61.46	.132	61.96	3.302	-.007	64.18	.111	62.62
3.164	-.008	61.50	.131	61.97	3.304	-.007	64.22	.111	62.63
3.166	-.008	61.54	.131	61.98	3.306	-.007	64.26	.111	62.64
3.168	-.008	61.57	.131	61.99	3.308	-.007	64.30	.111	62.65
3.170	-.008	61.61	.131	62.00	3.310	-.007	64.33	.110	62.66
3.172	-.008	61.65	.130	62.01	3.312	-.007	64.37	.110	62.66
3.174	-.008	61.69	.130	62.02	3.314	-.007	64.41	.110	62.67
3.176	-.008	61.73	.130	62.03	3.316	-.007	64.45	.110	62.68
3.178	-.008	61.77	.129	62.04	3.318	-.007	64.49	.109	62.69
3.180	-.008	61.81	.129	62.05	3.320	-.007	64.53	.109	62.70
3.182	-.008	61.85	.129	62.06	3.322	-.007	64.57	.109	62.71
3.184	-.008	61.89	.128	62.07	3.324	-.007	64.61	.108	62.71
3.186	-.008	61.92	.128	62.08	3.326	-.007	64.65	.108	62.72
3.188	-.008	61.96	.128	62.09	3.328	-.007	64.68	.108	62.73
3.190	-.008	62.00	.128	62.10	3.330	-.007	64.72	.108	62.74
3.192	-.008	62.04	.127	62.11	3.332	-.007	64.76	.107	62.75
3.194	-.008	62.08	.127	62.12	3.334	-.007	64.80	.107	62.76
3.196	-.008	62.12	.127	62.13	3.336	-.007	64.84	.107	62.77
3.198	-.008	62.16	.126	62.14	3.338	-.007	64.88	.106	62.77
3.200	-.008	62.20	.126	62.15	3.340	-.007	64.92	.106	62.78
3.202	-.008	62.24	.126	62.16	3.342	-.007	64.96	.106	62.79
3.204	-.008	62.27	.126	62.17	3.344	-.007	65.00	.106	62.80
3.206	-.008	62.31	.125	62.18	3.346	-.007	65.03	.105	62.81
3.208	-.007	62.35	.125	62.19	3.348	-.007	65.07	.105	62.81
3.210	-.007	62.39	.125	62.20	3.350	-.007	65.11	.105	62.82
3.212	-.007	62.43	.124	62.21	3.352	-.007	65.15	.104	62.83
3.214	-.007	62.47	.124	62.22	3.354	-.007	65.19	.104	62.84
3.216	-.007	62.51	.124	62.23	3.356	-.007	65.23	.104	62.85
3.218	-.007	62.55	.124	62.24	3.358	-.007	65.27	.104	62.86
3.220	-.007	62.59	.123	62.25	3.360	-.007	65.31	.103	62.86

TABLE A.IV.2 (CONTINUED)

τ (s)	$\tilde{L}_o$	$\tilde{t}_D$	$\tilde{K}_M$	D	τ (s)	$\tilde{L}_o$	$\tilde{t}_D$	$\tilde{K}_M$	$\tilde{D}$
3.360	-.007	65.31	.103	62.86	3.500	-.007	68.03	.084	63.37
3.362	-.007	65.34	.103	62.87	3.502	-.007	68.07	.084	63.38
3.364	-.007	65.38	.103	62.88	3.504	-.007	68.10	.084	63.39
3.366	-.007	65.42	.103	62.89	3.506	-.007	68.14	.083	63.39
3.368	-.007	65.46	.102	62.90	3.508	-.007	68.18	.083	63.40
3.370	-.007	65.50	.102	62.90	3.510	-.007	68.22	.083	63.41
3.372	-.007	65.54	.102	62.91	3.512	-.007	68.26	.083	63.41
3.374	-.007	65.58	.101	62.92	3.514	-.007	68.30	.082	63.42
3.376	-.007	65.62	.101	62.93	3.516	-.007	68.34	.082	63.43
3.378	-.007	65.66	.101	62.93	3.518	-.007	68.38	.082	63.43
3.380	-.007	65.69	.101	62.94	3.520	-.007	68.42	.082	63.44
3.382	-.007	65.73	.100	62.95	3.522	-.007	68.45	.081	63.44
3.384	-.007	65.77	.100	62.96	3.524	-.007	68.49	.081	63.45
3.386	-.007	65.81	.100	62.97	3.526	-.007	68.53	.081	63.46
3.388	-.007	65.85	.099	62.97	3.528	-.007	68.57	.081	63.46
3.390	-.007	65.89	.099	62.98	3.530	-.007	68.61	.080	63.47
3.392	-.007	65.93	.099	62.99	3.532	-.007	68.65	.080	63.48
3.394	-.007	65.97	.099	63.00	3.534	-.007	68.69	.080	63.48
3.396	-.007	66.01	.098	63.00	3.536	-.007	68.73	.079	63.49
3.398	-.007	66.04	.098	63.01	3.538	-.007	68.77	.079	63.49
3.400	-.007	66.08	.098	63.02	3.540	-.007	68.80	.079	63.50
3.402	-.007	66.12	.098	63.03	3.542	-.007	68.84	.079	63.51
3.404	-.007	66.16	.097	63.03	3.544	-.007	68.88	.078	63.51
3.406	-.007	66.20	.097	63.04	3.546	-.007	68.92	.078	63.52
3.408	-.007	66.24	.097	63.05	3.548	-.007	68.96	.078	63.52
3.410	-.007	66.28	.096	63.06	3.550	-.007	69.00	.078	63.53
3.412	-.007	66.32	.096	63.06	3.552	-.007	69.04	.077	63.54
3.414	-.007	66.36	.096	63.07	3.554	-.007	69.08	.077	63.54
3.416	-.007	66.39	.096	63.08	3.556	-.007	69.12	.077	63.55
3.418	-.007	66.43	.095	63.09	3.558	-.007	69.15	.077	63.55
3.420	-.007	66.47	.095	63.09	3.560	-.007	69.19	.076	63.56
3.422	-.007	66.51	.095	63.10	3.562	-.007	69.23	.076	63.57
3.424	-.007	66.55	.095	63.11	3.564	-.007	69.27	.076	63.57
3.426	-.007	66.59	.094	63.12	3.566	-.007	69.31	.076	63.58
3.428	-.007	66.63	.094	63.12	3.568	-.007	69.35	.075	63.58
3.430	-.007	66.67	.094	63.13	3.570	-.007	69.39	.075	63.59
3.432	-.007	66.71	.093	63.14	3.572	-.007	69.43	.075	63.60
3.434	-.007	66.74	.093	63.15	3.574	-.007	69.47	.074	63.60
3.436	-.007	66.78	.093	63.15	3.576	-.007	69.50	.074	63.61
3.438	-.007	66.82	.093	63.16	3.578	-.007	69.54	.074	63.61
3.440	-.007	66.86	.092	63.17	3.580	-.007	69.58	.074	63.62
3.442	-.007	66.90	.092	63.17	3.582	-.007	69.62	.073	63.62
3.444	-.007	66.94	.092	63.18	3.584	-.007	69.66	.073	63.63
3.446	-.007	66.98	.092	63.19	3.586	-.007	69.70	.073	63.64
3.448	-.007	67.02	.091	63.20	3.588	-.007	69.74	.073	63.64
3.450	-.007	67.06	.091	63.20	3.590	-.007	69.78	.072	63.65
3.452	-.007	67.09	.091	63.21	3.592	-.007	69.82	.072	63.65
3.454	-.007	67.13	.090	63.22	3.594	-.007	69.85	.072	63.66
3.456	-.007	67.17	.090	63.22	3.596	-.007	69.89	.072	63.66
3.458	-.007	67.21	.090	63.23	3.598	-.007	69.93	.071	63.67
3.460	-.007	67.25	.090	63.24	3.600	-.007	69.97	.071	63.68
3.462	-.007	67.29	.089	63.25	3.602	-.007	70.01	.071	63.68
3.464	-.007	67.33	.089	63.25	3.604	-.007	70.05	.071	63.69
3.466	-.007	67.37	.089	63.26	3.606	-.007	70.09	.070	63.69
3.468	-.007	67.41	.089	63.27	3.608	-.007	70.13	.070	63.70
3.470	-.007	67.44	.088	63.27	3.610	-.007	70.17	.070	63.70
3.472	-.007	67.48	.088	63.28	3.612	-.007	70.20	.070	63.71
3.474	-.007	67.52	.088	63.29	3.614	-.007	70.24	.069	63.71
3.476	-.007	67.56	.087	63.29	3.616	-.007	70.28	.069	63.72
3.478	-.007	67.60	.087	63.30	3.618	-.007	70.32	.069	63.72
3.480	-.007	67.64	.087	63.31	3.620	-.007	70.36	.069	63.73
3.482	-.007	67.68	.087	63.31	3.622	-.007	70.40	.068	63.73
3.484	-.007	67.72	.086	63.32	3.624	-.007	70.44	.068	63.74
3.486	-.007	67.76	.086	63.33	3.626	-.007	70.48	.068	63.75
3.488	-.007	67.79	.086	63.33	3.628	-.007	70.52	.067	63.75
3.490	-.007	67.83	.086	63.34	3.630	-.007	70.55	.067	63.76
3.492	-.007	67.87	.085	63.35	3.632	-.007	70.59	.067	63.76
3.494	-.007	67.91	.085	63.35	3.634	-.007	70.63	.067	63.77
3.496	-.007	67.95	.085	63.36	3.636	-.007	70.67	.066	63.77
3.498	-.007	67.99	.085	63.37	3.638	-.007	70.71	.066	63.78
3.500	-.007	68.03	.084	63.37	3.640	-.007	70.75	.066	63.78

TABLE A.IV.2 (CONTINUED)

τ (s)	$\tilde{L}_o$	$\tilde{t}_D$	$\tilde{K}_M$	$\tilde{D}$	τ (s)	$\tilde{L}_o$	$\tilde{t}_D$	$\tilde{K}_M$	$\tilde{D}$
3.640	-.007	70.75	.066	63.78	3.780	-.006	73.47	.048	64.09
3.642	-.007	70.79	.066	63.79	3.782	-.006	73.51	.048	64.10
3.644	-.007	70.83	.065	63.79	3.784	-.006	73.55	.048	64.10
3.646	-.007	70.86	.065	63.80	3.786	-.006	73.59	.048	64.10
3.648	-.007	70.90	.065	63.80	3.788	-.006	73.62	.047	64.11
3.650	-.007	70.94	.065	63.81	3.790	-.006	73.66	.047	64.11
3.652	-.007	70.98	.064	63.81	3.792	-.006	73.70	.047	64.11
3.654	-.007	71.02	.064	63.82	3.794	-.006	73.74	.047	64.12
3.656	-.007	71.06	.064	63.82	3.796	-.006	73.78	.046	64.12
3.658	-.007	71.10	.064	63.83	3.798	-.006	73.82	.046	64.13
3.660	-.007	71.14	.063	63.83	3.800	-.006	73.86	.046	64.13
3.662	-.007	71.18	.063	63.84	3.802	-.006	73.90	.046	64.13
3.664	-.007	71.21	.063	63.84	3.804	-.006	73.94	.045	64.14
3.666	-.007	71.25	.063	63.85	3.806	-.006	73.97	.045	64.14
3.668	-.007	71.29	.062	63.85	3.808	-.006	74.01	.045	64.14
3.670	-.007	71.33	.062	63.86	3.810	-.006	74.05	.045	64.15
3.672	-.007	71.37	.062	63.86	3.812	-.006	74.09	.044	64.15
3.674	-.007	71.41	.062	63.87	3.814	-.006	74.13	.044	64.15
3.676	-.007	71.45	.061	63.87	3.816	-.006	74.17	.044	64.16
3.678	-.007	71.49	.061	63.88	3.818	-.006	74.21	.044	64.16
3.680	-.007	71.53	.061	63.88	3.820	-.006	74.25	.043	64.16
3.682	-.007	71.56	.061	63.88	3.822	-.006	74.29	.043	64.17
3.684	-.007	71.60	.060	63.89	3.824	-.006	74.32	.043	64.17
3.686	-.007	71.64	.060	63.89	3.826	-.006	74.36	.043	64.17
3.688	-.007	71.68	.060	63.90	3.828	-.006	74.40	.042	64.18
3.690	-.007	71.72	.060	63.90	3.830	-.006	74.44	.042	64.18
3.692	-.007	71.76	.059	63.91	3.832	-.006	74.48	.042	64.18
3.694	-.007	71.80	.059	63.91	3.834	-.006	74.52	.042	64.19
3.696	-.007	71.84	.059	63.92	3.836	-.006	74.56	.041	64.19
3.698	-.007	71.88	.059	63.92	3.838	-.006	74.60	.041	64.19
3.700	-.006	71.91	.058	63.93	3.840	-.006	74.64	.041	64.20
3.702	-.006	71.95	.058	63.93	3.842	-.006	74.67	.041	64.20
3.704	-.006	71.99	.058	63.94	3.844	-.006	74.71	.040	64.20
3.706	-.006	72.03	.058	63.94	3.846	-.006	74.75	.040	64.21
3.708	-.006	72.07	.057	63.94	3.848	-.006	74.79	.040	64.21
3.710	-.006	72.11	.057	63.95	3.850	-.006	74.83	.040	64.21
3.712	-.006	72.15	.057	63.95	3.852	-.006	74.87	.039	64.22
3.714	-.006	72.19	.057	63.96	3.854	-.006	74.91	.039	64.22
3.716	-.006	72.23	.056	63.96	3.856	-.006	74.95	.039	64.22
3.718	-.006	72.26	.056	63.97	3.858	-.006	74.99	.039	64.22
3.720	-.006	72.30	.056	63.97	3.860	-.006	75.02	.039	64.23
3.722	-.006	72.34	.056	63.98	3.862	-.006	75.06	.038	64.23
3.724	-.006	72.38	.055	63.98	3.864	-.006	75.10	.038	64.23
3.726	-.006	72.42	.055	63.98	3.866	-.006	75.14	.038	64.24
3.728	-.006	72.46	.055	63.99	3.868	-.006	75.18	.038	64.24
3.730	-.006	72.50	.055	63.99	3.870	-.006	75.22	.037	64.24
3.732	-.006	72.54	.054	64.00	3.872	-.006	75.26	.037	64.24
3.734	-.006	72.58	.054	64.00	3.874	-.006	75.30	.037	64.25
3.736	-.006	72.61	.054	64.00	3.876	-.006	75.34	.037	64.25
3.738	-.006	72.65	.054	64.01	3.878	-.006	75.37	.036	64.25
3.740	-.006	72.69	.053	64.01	3.880	-.006	75.41	.036	64.26
3.742	-.006	72.73	.053	64.02	3.882	-.006	75.45	.036	64.26
3.744	-.006	72.77	.053	64.02	3.884	-.006	75.49	.036	64.26
3.746	-.006	72.81	.053	64.03	3.886	-.006	75.53	.035	64.26
3.748	-.006	72.85	.052	64.03	3.888	-.006	75.57	.035	64.27
3.750	-.006	72.89	.052	64.03	3.890	-.006	75.61	.035	64.27
3.752	-.006	72.93	.052	64.04	3.892	-.006	75.65	.035	64.27
3.754	-.006	72.96	.052	64.04	3.894	-.006	75.69	.034	64.28
3.756	-.006	73.00	.051	64.05	3.896	-.006	75.72	.034	64.28
3.758	-.006	73.04	.051	64.05	3.898	-.006	75.76	.034	64.28
3.760	-.006	73.08	.051	64.05	3.900	-.006	75.80	.034	64.28
3.762	-.006	73.12	.051	64.06	3.902	-.006	75.84	.033	64.29
3.764	-.006	73.16	.050	64.06	3.904	-.006	75.88	.033	64.29
3.766	-.006	73.20	.050	64.07	3.906	-.006	75.92	.033	64.29
3.768	-.006	73.24	.050	64.07	3.908	-.006	75.96	.033	64.29
3.770	-.006	73.28	.050	64.07	3.910	-.006	76.00	.033	64.30
3.772	-.006	73.31	.049	64.08	3.912	-.006	76.03	.032	64.30
3.774	-.006	73.35	.049	64.08	3.914	-.006	76.07	.032	64.30
3.776	-.006	73.39	.049	64.08	3.916	-.006	76.11	.032	64.30
3.778	-.006	73.43	.049	64.09	3.918	-.006	76.15	.032	64.31
3.780	-.006	73.47	.048	64.09	3.920	-.006	76.19	.031	64.31

TABLE A.IV.2 (CONTINUED)

τ (s)	$\tilde{L}_o$	$\tilde{t}_D$	$\tilde{K}_M$	$\tilde{D}$	τ (s)	$\tilde{L}_o$	$\tilde{t}_D$	$\tilde{K}_M$	$\tilde{D}$
3.918	-.006	76.15	.032	64.31	4.058	-.006	78.87	.015	64.43
3.920	-.006	76.19	.031	64.31	4.060	-.006	78.91	.015	64.43
3.922	-.006	76.23	.031	64.31	4.062	-.006	78.95	.015	64.44
3.924	-.006	76.27	.031	64.31	4.064	-.006	78.99	.014	64.44
3.926	-.006	76.31	.031	64.32	4.066	-.006	79.03	.014	64.44
3.928	-.006	76.35	.030	64.32	4.068	-.006	79.07	.014	64.44
3.930	-.006	76.38	.030	64.32	4.070	-.006	79.11	.014	64.44
3.932	-.006	76.42	.030	64.32	4.072	-.006	79.14	.014	64.44
3.934	-.006	76.46	.030	64.33	4.074	-.006	79.18	.013	64.44
3.936	-.006	76.50	.029	64.33	4.076	-.006	79.22	.013	64.44
3.938	-.006	76.54	.029	64.33	4.078	-.006	79.26	.013	64.44
3.940	-.006	76.58	.029	64.33	4.080	-.006	79.30	.013	64.44
3.942	-.006	76.62	.029	64.33	4.082	-.006	79.34	.012	64.45
3.944	-.006	76.66	.028	64.34	4.084	-.006	79.38	.012	64.45
3.946	-.006	76.70	.028	64.34	4.086	-.006	79.42	.012	64.45
3.948	-.006	76.73	.028	64.34	4.088	-.006	79.46	.012	64.45
3.950	-.006	76.77	.028	64.34	4.090	-.006	79.49	.011	64.45
3.952	-.006	76.81	.028	64.35	4.092	-.006	79.53	.011	64.45
3.954	-.006	76.85	.027	64.35	4.094	-.006	79.57	.011	64.45
3.956	-.006	76.89	.027	64.35	4.096	-.006	79.61	.011	64.45
3.958	-.006	76.93	.027	64.35	4.098	-.006	79.65	.011	64.45
3.960	-.006	76.97	.027	64.35	4.100	-.006	79.69	.010	64.45
3.962	-.006	77.01	.026	64.36	4.102	-.006	79.73	.010	64.45
3.964	-.006	77.05	.026	64.36	4.104	-.006	79.77	.010	64.46
3.966	-.006	77.08	.026	64.36	4.106	-.006	79.61	.010	64.46
3.968	-.006	77.12	.026	64.36	4.108	-.006	79.84	.009	64.46
3.970	-.006	77.16	.025	64.36	4.110	-.006	79.88	.009	64.46
3.972	-.006	77.20	.025	64.37	4.112	-.006	79.92	.009	64.46
3.974	-.006	77.24	.025	64.37	4.114	-.006	79.96	.009	64.46
3.976	-.006	77.28	.025	64.37	4.116	-.006	80.00	.009	64.46
3.978	-.006	77.32	.024	64.37	4.118	-.006	80.04	.008	64.46
3.980	-.006	77.36	.024	64.37	4.120	-.006	80.08	.008	64.46
3.982	-.006	77.40	.024	64.38	4.122	-.006	80.12	.008	64.46
3.984	-.006	77.43	.024	64.38	4.124	-.006	80.16	.008	64.46
3.986	-.006	77.47	.024	64.38	4.126	-.006	80.19	.007	64.46
3.988	-.006	77.51	.023	64.38	4.128	-.006	80.23	.007	64.46
3.990	-.006	77.55	.023	64.38	4.130	-.006	80.27	.007	64.45
3.992	-.006	77.59	.023	64.38	4.132	-.006	80.31	.007	64.46
3.994	-.006	77.63	.023	64.39	4.134	-.006	80.35	.006	64.46
3.996	-.006	77.67	.022	64.39	4.136	-.006	80.39	.006	64.47
3.998	-.006	77.71	.022	64.39	4.138	-.006	80.43	.006	64.47
4.000	-.006	77.75	.022	64.39	4.140	-.006	80.47	.006	64.47
4.002	-.006	77.78	.022	64.39	4.142	-.006	80.51	.006	64.47
4.004	-.006	77.82	.021	64.39	4.144	-.006	80.54	.005	64.47
4.006	-.006	77.86	.021	64.40	4.146	-.006	80.58	.005	64.47
4.008	-.006	77.90	.021	64.40	4.148	-.006	80.62	.005	64.47
4.010	-.006	77.94	.021	64.40	4.150	-.006	80.66	.005	64.47
4.012	-.006	77.98	.020	64.40	4.152	-.006	80.70	.004	64.47
4.014	-.006	78.02	.020	64.40	4.154	-.006	80.74	.004	64.47
4.016	-.006	78.06	.020	64.40	4.156	-.006	80.78	.004	64.47
4.018	-.006	78.10	.020	64.41	4.158	-.006	80.82	.004	64.47
4.020	-.006	78.13	.020	64.41	4.160	-.006	80.86	.004	64.47
4.022	-.006	78.17	.019	64.41	4.162	-.006	80.89	.003	64.47
4.024	-.006	78.21	.019	64.41	4.164	-.006	80.93	.003	64.47
4.026	-.006	78.25	.019	64.41	4.166	-.006	80.97	.003	64.47
4.028	-.006	78.29	.019	64.41	4.168	-.006	81.01	.003	64.47
4.030	-.006	78.33	.018	64.41	4.170	-.006	81.05	.002	64.47
4.032	-.006	78.37	.018	64.42	4.172	-.006	81.09	.002	64.47
4.034	-.006	78.41	.018	64.42	4.174	-.006	81.13	.002	64.47
4.036	-.006	78.45	.018	64.42	4.176	-.006	81.17	.002	64.47
4.038	-.006	78.48	.017	64.42	4.178	-.006	81.21	.002	64.47
4.040	-.006	78.52	.017	64.42	4.180	-.006	81.24	.001	64.47
4.042	-.006	78.56	.017	64.42	4.182	-.006	81.28	.001	64.47
4.044	-.006	78.60	.017	64.42	4.184	-.006	81.32	.001	64.47
4.184	-.006	81.32	.001	64.47					

*U.S. GOVERNMENT PRINTING OFFICE: 1975 - 635-275/15